



**Universitat Ramon Llull**

## **DOCTORAL THESIS**

<b>Title</b>	<b>New functionalization methodologies of mesoporous silica nanoparticles (MSNs) for biomedical applications.</b>
<b>Presented by</b>	<b>Maria del Carme Llinàs Riera</b>
<b>Centre</b>	<b>IQS school of Engineering</b>
<b>Department</b>	<b>Organic Chemistry</b>
<b>Directed by</b>	<b>Dr. David Sánchez García</b>

C. Claravall, 1-3  
08022 Barcelona  
Tel. 936 022 200  
Fax 936 022 249  
E-mail: [urisc@sec.url.es](mailto:urisc@sec.url.es)  
[www.url.es](http://www.url.es)



Al Gonzalo i a la meva família per no haver deixat mai d'estimar-me i creure en mi.



“Now, the name of this talk is “**There is plenty of room at the bottom**” not just “There is room at the bottom.” What I have demonstrated is that, there is room, that you can decrease the size of things in a practical way. I, now, want to show that there is **plenty of room**. I will not now discuss how we are going to do it, but only what is possible in principle, in other words, what is possible according to the laws of physics. I am not inventing anti-gravity, which is possible someday, only if the laws are not what we think. I am telling you what could be done if the laws are what we think; we are not doing it simply because we haven't yet gotten around to it”.

Transcript of the talk that Richard Feynman gave on December 29th 1959 at the annual meeting of the American Physical Society at the California Institute of Technology (Caltech).



**Alfred Pennyworth:** Why do we fall sir?  
So that we can learn to pick ourselves up.

**Bruce Wayne:** You still haven't given  
up on me?

**Alfred Pennyworth:** Never

Batman Begins (2005)





## Agraïments

Voldria en primer lloc donar les gràcies al IQS per haver-me donat l'oportunitat de cursar aquesta tesi i haver-me concedit la beca salari IQS. Des de ben petita que volia convertir-me en doctora en aquest centre.

No puc deixar d'agrair al meu Director de Tesi, el Dr. David Sánchez, per haver-me brindat l'oportunitat de treballar amb nanopartícules. Tot i que hem començat des de zero i amb tots els inconvenients i dificultats que te obrir una nova línia d' investigació, crec que finalment ens en hem sortit prou bé. Em aprés molt i em trobat un nínxol en aquest gran mon que és la nanotecnologia. Llàstima que els millors resultats sempre arribin al final!

Seguidament, voldria agrair al Dr. Salvador Borròs per haver posat al nostre abast tots els medis i haver-nos brindat tota l'ajuda del món. Mil gràcies Chicho per el teu suport i per animar-me a seguir endavant.

I would like to thank Dr. Ivan Huc for the collaboration and for providing us with the alkyne functionalized quinolin foldamer.

Voldria també donar les gràcies al equip de la doctora Francina Munell de l' *Hospital de la Vall Hebron* per la seva col·laboració en el projecte conjunt sobre la distròfia muscular de Duchenne (DMD).

Gràcies també al Dr. Borrell i tota la gent del laboratori de Síntesi per animar els llargs dies de laboratori: Maia, Gemma, Montse, Marta, Xavi, Rai, Albert, Senyor, Anna, Joan, Claudi, Eli, Alba, Gonzalo i en especial al Gabi perquè gràcies al seu bon caràcter i a la seva bona feina va fer que tornés a creure en el meu treball.

Gràcies al laboratori de Bioquímica I i II, Bioenginyeria, Teixits, Materials vells i Materials nous per deixar-me utilitzar sempre els equips i respondre amablement a totes les meves preguntes. Gràcies Cristina, Amanda, Hugo, Victoria, Estela, Cate, Lurdes, Robert, Pri, Maria, Joan, Ingrid, Pau, Miguel Angel, Sei Jin i Victor Ramos. Sense oblidar a la Marina, Ana Ramos i Bernat Sempere que han patit amb escriu la meva tossuderia. En especial, també voldria agrair a la Irene Porcar i a la Dra. Ana Cascante per ajudar-me amb els assajos cel·lulars. A la Dra. Magda Faijes i a la Patricia Turrueuella per deixar-me fer servir l'espectrofotòmetre, el fluorímetre i les centrífugues de màster. Al Dr. Martorell per haver-me deixat la seva microcentrífuga i haver-me donat ànims en la recta final.

També voldria agrair al Dr. Uwe Pischel i Vania Païs per la meva estada a Huelva i per ajudar-me en l'estudi de les naftalimides com a sensors.

No voldria oblidar-me de la meva estimada amiga Merimer perquè encara que estigui a 1000 km de distància està sempre al meu costat. A l'Ana i la Miriam per haver-me suportat aquests anys difícils i no haver-se enfadat gaire quan anul·lava casi tots els seus plans. Gràcies per haver insistit i continuar al meu costat.

Als meus pares per el seu suport incondicional. No podré donar mai als meus fills ni la meitat del que ells han donat i fet per mi. Sou el meu suport més ferm. Al meu germà, Ferran, per ensenyar-me que tots els problemes tenen solució i que les situacions s'afronten amb el cap ben alt. A les meves precioses nebodes Marina i Alexandra que sempre estan presents en els meus pensaments. Espero que algun dia es sentin orgulloses de la seva tieta i escullin el camí de la llum. A la meva padrina, Yais, per estar al meu costat i entendre que no pogués passar més temps amb ella. I finalment al Gonzalo per haver pintat de colors la meva vida grisosa. Per haver fet que tornés a ser jo mateixa i estimar-me tal com sóc.





# Summary

In this PhD dissertation, a general procedure for the obtaining of different regioselective orthogonal bifunctionalized mesoporous silica nanoparticles (MSNs) has been carried out. The strategy consists of a covalent functionalization of co-condensed monodispersed and uniform aminated-MSNs, where tensioactive is still present in its structure. Three bifunctionalized MSNs, amine-azide ( $\text{MSN}-(\text{NH}_2)_i(\text{N}_3)_o$ ), amine-isothiocyanate ( $\text{MSN}-(\text{NH}_2)_i(\text{NCS})_o$ ) and amine-aldehyde ( $\text{MSN}-(\text{NH}_2)_i(\text{CHO})_o$ ), with efficient “click” reactions, have been synthesized for its use in biomedical applications.

First, a well characterized batch of precursor aminated-MSNs ( $\text{MSN}-(\text{NH}_2)$ ) has been prepared. The best conditions for the synthesis of homogenous and reproducible  $\text{MSN}-(\text{NH}_2)$  with a size between 50-100 nm have been studied.

These aminated-MSNs have been used for the synthesis of naphthalimide sensors where a general procedure for the introduction of 4-amine-1,8-naphthalimides has been developed. These naphthalimides have been tested as potential logic gates for the detection of  $\text{H}^+$  and  $\text{F}^-$ .

A straightforward protocol to prepare amine-azide MSNs has been described. These MSNs have been functionalized with quinoline cationic foldamers for the first time. The ability of these foldamer-MSNs to cross cytoplasmic membranes and its viability has been studied. The penetrating capacity of foldamer-MSNs have been used for intracellular delivery of Doxorubicin (DOX).

A new protocol to prepare isothiocyanate functionalized MSNs is described. The synthetic methodology is general and can be applied, in principle, to all type of aminated MSNs. The efficiency of the functionalization is comparable to the copper cycloaddition (CuAAC) avoiding isolation and copper removal protocols. Following this methodology, new amino-isothiocyanate-MSNs have been prepared for the design of a nano-container able to release the drug Ataluren in a controlled manner, for the treatment of Duchenne muscular dystrophy (DMD).

Regioselective bifunctionalized amine-aldehyde-MSNs have been synthesized. These MSNs have been applied as a versatile nanoplatform able to release dual synergistic CPT/DOX mixture for cancer treatment only by using pH stimuli. While CPT is absorbed at the inner surface, DOX is covalently linked to the external surface acting both as an active and a capping agent (pH=4).



# Resumen

En la presente tesis doctoral se describe un procedimiento general para la obtención de nanopartículas mesoporosas de sílice (MSNs) regioselectivamente bifuncionalizadas de forma ortogonal con distintos grupos funcionales. La estrategia sintética consiste en la preparación de MSNs mediante co-condensación, seguido de una posterior funcionalización covalente, mientras el tensioactivo se encuentra todavía presente en la estructura de las MSNs. Siguiendo esta metodología, se han sintetizado las nanopartículas bifuncionalizadas amina-azida ( $(\text{NH}_2)_i(\text{N}_3)_o$ ), amina-isotiocianato ( $(\text{MSN}-(\text{NH}_2)_i(\text{NCS})_o)$ ) y amina-aldehído ( $(\text{MSN}-(\text{NH}_2)_i(\text{CHO})_o)$ ), para su uso en aplicaciones biomédicas.

En primer lugar, se han sintetizado y caracterizado de forma homogénea y reproducible las nanopartículas aminadas de referencia ( $\text{MSN-NH}_2$ ) que permitirán las sucesivas funcionalizaciones, con un tamaño de 50 nm y 100 nm aproximadamente.

Estas nanopartículas aminadas se han usado posteriormente para la síntesis de sensores de naftalimida. Se ha conseguido desarrollar un procedimiento general para la introducción de 4-amino-1,8 naftalimidias. Estas naftalimidias han sido probadas como sensores y puertas lógicas para la detección de  $\text{H}^+$  y  $\text{F}^-$ .

Por otra parte, se ha descrito un protocolo para preparar amino-azida-MSNs de forma regioselectiva. Estas MSNs han sido funcionalizadas por primera vez con foldámeros catiónicos y su capacidad para cruzar membranas citoplasmáticas y viabilidad ha sido estudiada, así como el uso de estos sistemas para la liberación intracelular de doxorubicina (DOX) de forma controlada.

También se ha realizado un nuevo protocolo para preparar MSNs con isotiocianato en su estructura. La metodología sintética es general y puede aplicarse, en principio, a todo tipo de MSNs aminadas. La eficiencia de la funcionalización es comparable a la cicloadición de cobre (CuAAC) evitando los protocolos de aislamiento y de eliminación del metal. Siguiendo esta metodología, se han preparado unas nuevas amino-isotiocianato-MSNs para el diseño de un nano-contenedor capaz de liberar el fármaco Ataluren de forma controlada.

Se ha logrado sintetizar amina-aldehído-MSN. Estas MSNs se han aplicado como una nanoplataforma simple y versátil capaz de liberar de forma dual una mezcla CPT/DOX para el tratamiento del cáncer, mediante el uso de estímulos de pH. Mientras un fármaco es absorbido dentro de la superficie interior, el otro está unido covalentemente a la superficie externa, actuando así como fármaco y como agente bloqueante de poro. Este sistema responde a los estímulos de pH y ambos fármacos son solamente liberados en un medio ácido.





# Resum

En la present tesi doctoral es descriu un procediment general per a l'obtenció de nanopartícules mesoporoses de sílice (MSNs) regioselectivament bifuncionalitzades de forma ortogonal amb diferents grups funcionals. L'estratègia sintètica consisteix en la preparació de MSNs mitjançant co-condensació, seguit d'una posterior funcionalització covalent, mentre el tensioactiu es troba encara present en l'estructura de les MSNs. Seguint aquesta metodologia, s'han sintetitzat les nanopartícules bifuncionalitzades amina-azida ( $\text{MSN}-(\text{NH}_2)_i(\text{N}_3)_o$ ), amina-isotiocianat ( $\text{MSN}-(\text{NH}_2)_i(\text{NCS})_o$ ) i amina-aldehid ( $\text{MSN}-(\text{NH}_2)_i(\text{CHO})_o$ ), per al seu ús en aplicacions biomèdiques.

En primer lloc, s'han sintetitzat i caracteritzat de forma homogènia i reproducible les nanopartícules de referència ( $\text{MSN-NH}_2$ ) que permetran les successives funcionalitzacions. Aquestes nanopartícules aminades s'han fet servir posteriorment per a la síntesi de sensors de naftalimida. S'ha aconseguit desenvolupar un procediment general per a la introducció de 4-amino-1,8 naftalimides. Aquestes naftalimides han estat provades com a sensor i portes lògiques per a la detecció de  $\text{H}^+$  i  $\text{F}^-$ .

D'altra banda, s'ha descrit un protocol per preparar amino-azida-MSNs de forma regioselectiva. Aquestes MSNs han estat funcionalitzades per primera vegada amb foldàmers catiónics i la seva capacitat per creuar membranes citoplasmàtiques i viabilitat ha estat estudiada, així com l'ús d'aquests sistemes per a l'alliberament intracel·lular de Doxorubicina (DOX) de forma controlada.

També s'ha realitzat un nou protocol per preparar MSNs amb isotiocianat en la seva estructura. La metodologia sintètica és general i es pot aplicar, en principi, a qualsevol MSNs aminada. L'eficiència de la funcionalització és comparable a la cicloadició de coure (CuAAC) evitant els protocols d'aïllament i d'eliminació del metall. Seguint aquesta metodologia, s'han preparat unes noves amino-isotiocianat-MSNs per al disseny d'un nano-contenedor capaç d'alliberar el fàrmac Ataluren de forma controlada, per el seu us en la distròfia muscular de Duchenne (DMD).

S'han aconseguit sintetitzar amina-aldehid-MSNs. Aquestes MSNs s'han aplicat com una nanoplataforma simple i versàtil capaç d'alliberar de forma dual una barreja CPT/DOX per al tractament del càncer, mitjançant l'ús d'estímuls de pH. Mentre un fàrmac és absorbit dins de la superfície interior, l'altre està unit covalentment a la superfície externa, actuant així, a la vegada, com a fàrmac i com agent bloquejant de porus. Aquest sistema respon als estímuls de pH i tots dos fàrmacs són només alliberats en un medi àcid.



## List of figures

<b>Figure 1.1.</b> Size scale.....	3
<b>Figure 1.2.</b> Nanotechnology applications in biomedicine. ....	5
<b>Figure 1.3.</b> Schematic representation of MSNs channels and TEM micrograph. ....	5
<b>Figure 1.4.</b> Theranostic concept. ....	7
<b>Figure 1.5.</b> Example of nanoplatform.....	8
<b>Figure 1.6.</b> Nanogate triggered release by external or internal stimulus. ....	9
<b>Figure 1.7.</b> Relevant strategies for controlled release systems. ....	11
<b>Figure 1.8.</b> Advances in MSNs clinical applications. ....	12
<b>Figure 1.9.</b> Image probe anchored in MSNs matrix. ....	14
<b>Figure 1.10.</b> Post-synthetic grafting functionalization. ....	14
<b>Figure 1.11.</b> One-pot co-condensation process. ....	15
<b>Figure 1.12.</b> Non regioselective bifunctionalization . ....	16
<b>Figure 1.13.</b> Amide bond formation. ....	17
<b>Figure 1.14.</b> 1,2,3-triazol formation. ....	17
<b>Figure 1.15.</b> Selective reaction between a thiol and a maleimide. ....	18
<b>Figure 1.16.</b> Disulfide formation from two dithiols. ....	18
<b>Figure 1.17.</b> Disulfide formation with pyridine-2-thione. ....	19
<b>Figure 1.18.</b> Urea, urethane and amide formation. ....	19
<b>Figure 1.19.</b> Thiourea formation. ....	19
<b>Figure 1.20.</b> Imine formation. ....	20
<b>Figure 1.21.</b> Hydrazone formation. ....	20
<b>Figure 1.22.</b> Complete regioselective bifunctionalization.....	21
<b>Figure 1.23.</b> Schematic representation of the thesis aims. ....	22
<b>Figure 2.1.</b> Mechanism of silica condensation. ....	31
<b>Figure 2.2.</b> Preparation of MSNs scheme.....	31
<b>Figure 2.3.</b> Formation of spherical MSNs. ....	32
<b>Figure 2.4.</b> Tyndall effect. ....	32
<b>Figure 2.5.</b> APTES intercalation in tensioactive micelles. ....	34
<b>Figure 2.6.</b> Length diagram effects of temperature and stirring rate.....	36
<b>Figure 2.7.</b> Length diagram effects of temperature and [NH <sub>4</sub> OH]. ....	37
<b>Figure 2.8.</b> FTIR spectra of CTAB removal in MSNs. ....	40
<b>Figure 2.9.</b> TEM micrographs of MSN-(NH <sub>2</sub> ). ....	41
<b>Figure 2.10.</b> TEM micrographs showing monodispersed MSN-(NH <sub>2</sub> ) of 100 nm. ....	41
<b>Figure 2.11.</b> N <sub>2</sub> adsorption-desorption and BJH pore size distribution plots of MSN-(NH <sub>2</sub> )....	42
<b>Figure 2.12.</b> SXRD of MSN-(NH <sub>2</sub> ).....	43
<b>Figure 3.1.</b> Chemosensor scheme.....	49
<b>Figure 3.2.</b> Naphtalimide functionalization points. ....	50
<b>Figure 3.3.</b> Fluoride-Proton sensor.....	52
<b>Figure 3.4.</b> Global scheme of isothiocyanate synthetic approach. ....	53
<b>Figure 3.5.</b> Normalized absorption and fluorescence spectra of MSN-(NaphBr). ....	53
<b>Figure 3.6.</b> Direct bromo substitution in MSNs. ....	53
<b>Figure 3.7.</b> Global scheme for the conjugation of 4-amino-1,8-naphtalimides in MSNs. ....	54
<b>Figure 3.8.</b> FTIR of functionalized MSN-(NaphPIP).....	55
<b>Figure 3.9.</b> Normalized absorption and fluorescence spectra of MSN-(NaphPIP).....	55

<b>Figure 3.10.</b> Normalized absorption and fluorescence spectra of MSN-(NaphBut) .....	55
<b>Figure 3.11.</b> Normalized absorption and fluorescence spectra of MSN-(NaphMetProp) .....	56
<b>Figure 3.12.</b> TEM micrographs MSN(NaphtPIP), MSN(NaphhBut), MSN(NaphhMetProp)...	56
<b>Figure 3.13.</b> Absorption spectra of different samples of MSN-(NaphPIP).....	57
<b>Figure 3.14.</b> Last synthetic step of reference model molecules.....	57
<b>Figure 3.15.</b> TFA absorption and fluorescence spectra titration of MSN-(NaphPIP).....	58
<b>Figure 3.16.</b> PET mechanism in MSN-(NaphPIP) upon acid addition. ....	58
<b>Figure 3.17.</b> Fluorescence intensity behavior in a pH=4.5-5.5 range.....	59
<b>Figure 3.18.</b> Representation of the ICT excited state in 4-amine-1,8-naphthalimide.....	59
<b>Figure 3.19.</b> TFA absorption and fluorescence spectra titration of MSN-(NaphBut).....	60
<b>Figure 3.20.</b> TFA absorption and fluorescence spectra titration of MSN-(NaphMetProp).....	60
<b>Figure 3.21.</b> Fluorescence and Stern Volmer plots MSN(NaphBut);MSN(NaphMetProp).....	61
<b>Figure 3.22.</b> F <sup>-</sup> absorption spectra titration of MSN-(NaphBut).....	62
<b>Figure 3.23.</b> Proposed binding mode of F <sup>-</sup> with MSN-(NaphBut).....	62
<b>Figure 3.24.</b> PET behavior upon addition of F <sup>-</sup> .....	63
<b>Figure 3.25.</b> Stern Volmer plot of MSN-(NaphBut) .....	63
<b>Figure 3.26.</b> Color changes upon TFA and F <sup>-</sup> titrations. ....	64
<b>Figure 3.27.</b> Absorption spectra titration of MSN-(NaphBut).....	65
<b>Figure 4.1.</b> Cytoplasmic membrane. ....	71
<b>Figure 4.2.</b> HIV-1 encoded peptide TAT structure and endocytosis.....	72
<b>Figure 4.3.</b> Applications of aromatic quinoline foldamers.....	73
<b>Figure 4.4.</b> General quinoline foldamer structure .....	74
<b>Figure 4.5.</b> Foldamer functionalization strategy.....	75
<b>Figure 4.6.</b> Alkyne introduction in foldamer structure.....	75
<b>Figure 4.7.</b> Non regioselective Amino-Azido-MSNs .....	76
<b>Figure 4.8.</b> Complete regioselective bifunctionalization of amino-azido-MSNs.....	76
<b>Figure 4.9.</b> Reactive linker for azido introduction in MSNs.....	76
<b>Figure 4.10.</b> 3-azidopropionic acid succinimidyl ester linker ( <b>22</b> ).....	77
<b>Figure 4.11.</b> Synthetic approach of 3-azidopropionic acid succinimidyl ester.....	77
<b>Figure 4.12.</b> FT-IR MSN-(NH <sub>2</sub> )CTAB, MSN-(NH <sub>2</sub> -N <sub>3</sub> )CTAB(EtOH);MSN-(NH <sub>2</sub> -N <sub>3</sub> )HCl....	78
<b>Figure 4.13.</b> FT-IR of bifunctionalized amino-azido MSNs with CTAB. ....	78
<b>Figure 4.14.</b> Isothermal linear plots of CTAB removal study.....	80
<b>Figure 4.15.</b> TEM micrographs of MSN-(NH <sub>2</sub> ) <sub>i</sub> (N <sub>3</sub> ) <sub>o</sub> .....	80
<b>Figure 4.16.</b> FT-IR of regioselective bifunctionalization MSN-(NH <sub>2</sub> ) <sub>i</sub> (N <sub>3</sub> ) <sub>o</sub> .....	81
<b>Figure 4.17.</b> Isothermal linear plot pore volume of regioselective MSN-(NH <sub>2</sub> ) <sub>i</sub> (N <sub>3</sub> ) <sub>o</sub> .....	82
<b>Figure 4.18.</b> Powder XDR of MSN-(NH <sub>2</sub> ) <sub>i</sub> (N <sub>3</sub> ) <sub>o</sub> .....	82
<b>Figure 4.19.</b> FITC and alkyne quinoline foldamer MSN-(NH <sub>2</sub> ) <sub>i</sub> (N <sub>3</sub> ) <sub>o</sub> .....	83
<b>Figure 4.20.</b> MSN-(FITC) and MSN-(FITC) <sub>i</sub> (Fold) <sub>o</sub> .....	84
<b>Figure 4.21.</b> Size distribution of a solution of MSN-(FITC) <sub>i</sub> (Fold) <sub>o</sub> .....	84
<b>Figure 4.22.</b> Zeta potential MSN-NH <sub>2</sub> , MSN-(FITC) <sub>i</sub> (N <sub>3</sub> ) <sub>o</sub> , MSN-(FITC) <sub>i</sub> (Fold) <sub>o</sub> .....	85
<b>Figure 4.23.</b> Absorption spectrum of MSN-(FITC) <sub>i</sub> (Fold) <sub>o</sub> .....	85
<b>Figure 4.24.</b> FT-IR of MSN-(FITC) <sub>i</sub> (N <sub>3</sub> ) <sub>o</sub> and MSN-(FITC) <sub>i</sub> (Fold) <sub>o</sub> .....	85
<b>Figure 4.25.</b> AlkynePEGFITC <b>30</b> synthetic scheme. ....	86
<b>Figure 4.26.</b> Functionalization of MSN-(FITC) <sub>i</sub> (Fold-N <sub>3</sub> ) <sub>o</sub> with fluorescent PEG <b>30</b> .....	87
<b>Figure 4.27.</b> Relative cell viability for MSN-(FITC) <sub>i</sub> (Fold) <sub>o</sub> and MSN-(FITC).....	88
<b>Figure 4.28.</b> Relative cell viability of MSN-(FITC) <sub>i</sub> (PEGFITC) <sub>o</sub> ; MSN-(Fold-PEGFITC).....	89
<b>Figure 4.29.</b> Control-MSN and foldamer-MSN uptake in Hela cells.....	90
<b>Figure 4.30.</b> MSN-(FITC) <sub>i</sub> (Fold) <sub>o</sub> uptake stained with DAPI and phalloidine. ....	91

<b>Figure 4.31.</b> MSN-(FITC) and MSN-(FITC) <sub>i</sub> (Fold) <sub>o</sub> at visible light and at 254 nm.....	91
<b>Figure 4.32.</b> Citometry Bars of MSN-(FITC) and MSN-(Fold).....	92
<b>Figure 4.33.</b> MSN-(FITC) <sub>i</sub> (PEG-FITC) <sub>o</sub> and MSN-(FITC) <sub>i</sub> (Fold-PEG-FITC) <sub>o</sub> uptake. ....	93
<b>Figure 4.34.</b> 3D ApoTome reconstruction of internalized MSN-(FITC) <sub>i</sub> (PEG-FITC) <sub>o</sub> . ....	93
<b>Figure 4.35.</b> Absorbed MSN-(DOX)release.....	95
<b>Figure 4.36.</b> DOX loading in MSNs with low and high density. ....	96
<b>Figure 4.37.</b> MSN-(DOX)(l-Fold) <sub>o</sub> release.....	96
<b>Figure 4.38.</b> MSN-(DOX)(h-Fold) <sub>o</sub> release.....	97
<b>Figure 4.39.</b> MSN-(NH <sub>2</sub> ) <sub>i</sub> (N <sub>3</sub> ) <sub>o</sub> DOX, MSN-(DOX)(l-Fold) <sub>o</sub> ,MSN-(DOX)(h-Fold) <sub>o</sub> viability..	98
<b>Figure 4.40.</b> Uptake of MSN(NH <sub>2</sub> ) <sub>i</sub> (N <sub>3</sub> ) <sub>o</sub> DOX, MSN-(DOX)(l-Fold) <sub>o</sub> ,MSN-(DOX)(h-Fold) <sub>o</sub> .	99
<b>Figure 4.41.</b> New strategy functionalization. ....	101
<b>Figure 5.1.</b> Synthetic approach of MSN-(NCS). ....	110
<b>Figure 5.2.</b> FTIR spectra of MSN(NH <sub>2</sub> ) and MSN(NCS). ....	110
<b>Figure 5.3.</b> TEM micrographs of MSN-(NCS) ....	111
<b>Figure 5.4.</b> N <sub>2</sub> adsorption-desorption and BJH pore size of MSN-(NH <sub>2</sub> ) and MSN-(NCS) ....	112
<b>Figure 5.5.</b> SXDR of MSN-(NCS) of 100 nm.....	112
<b>Figure 5.6.</b> MSN-(NCS) functionalization with amine naphthalimide <b>11</b> (MSN-(UNaph). ....	113
<b>Figure 5.7.</b> FTIR spectra of MSN-(UNaph). ....	114
<b>Figure 5.8.</b> MSN-(N <sub>3</sub> ) functionalization with alkyne naphthalimide <b>32</b> (MSN-(TNaph))......	114
<b>Figure 5.9.</b> FTIR spectra of MSN-(TNaph).....	114
<b>Figure 5.10.</b> Absorption spectra of MSN-(UNaph) and MSN-(TNaph). ....	115
<b>Figure 5.11.</b> MSNs orthogonal bifunctionalization of MSN-(NH <sub>2</sub> ) <sub>i</sub> (NCS) <sub>o</sub> .....	116
<b>Figure 5.12.</b> FTIR spectra of bifunctionalized MSN-(NH <sub>2</sub> ) <sub>i</sub> (NCS) <sub>o</sub> .....	117
<b>Figure 5.13.</b> TEM micrographs of MSN(NH <sub>2</sub> ) <sub>i</sub> (NCS) <sub>o</sub> ....	118
<b>Figure 5.14.</b> N <sub>2</sub> adsorption-desorption MSN-NH <sub>2</sub> (CTAB), MSN-(NH <sub>2</sub> ) <sub>i</sub> ,MSN-(NH <sub>2</sub> ) <sub>i</sub> (NCS) <sub>o</sub>	118
<b>Figure 5.15.</b> SXDR of MSN-(NH <sub>2</sub> ) <sub>i</sub> (NCS) <sub>o</sub> . ....	119
<b>Figure 5.16.</b> Accumulation of Alexa-680-MSNs in mice affected by DMD. ....	120
<b>Figure 5.17.</b> Key components for drug release capping system. ....	122
<b>Figure 5.18.</b> Key functional groups for capping agent synthesis. ....	123
<b>Figure 5.19.</b> Synthesis of <i>tert</i> -butyl(2-((2-isothiocyanatoethyl)disulfanyl)ethyl)carbamate ....	123
<b>Figure 5.20.</b> Synthesis of triethylene glycol 2-methyl amino methyl ether ( <b>32</b> ).....	123
<b>Figure 5.21.</b> Synthetic approach of capping agent <b>41</b> . ....	124
<b>Figure 5.22.</b> Synthesis of MSN(NH <sub>2</sub> ) <sub>i</sub> (S-PEG) <sub>o</sub> Ru and MSN(NH <sub>2</sub> ) <sub>i</sub> (L-PEG) <sub>o</sub> Ru ....	125
<b>Figure 5.23.</b> Release of MSN(NH <sub>2</sub> ) <sub>i</sub> (S-PEG) <sub>o</sub> Ru in the absence and presence of GSH ....	125
<b>Figure 5.24.</b> Ru(bipy) <sub>3</sub> <sup>2+</sup> release of MSN(NH <sub>2</sub> ) <sub>i</sub> (L-PEG) <sub>o</sub> Ru ....	126
<b>Figure 5.25.</b> Release of MSN(NCS)(L-PEG) <sub>o</sub> Ru in the absence and presence of GSH. ....	126
<b>Figure 5.26.</b> Chemical structure of Ataluren. ....	127
<b>Figure 5.27.</b> MSN-Ataluren release. ....	128
<b>Figure 5.28.</b> MSN(NH <sub>2</sub> ) <sub>i</sub> (S-PEG) <sub>o</sub> Ata and MSN(NH <sub>2</sub> ) <sub>i</sub> (L-PEG) <sub>o</sub> Ata functionalization.....	129
<b>Figure 5.29.</b> MSN(NH <sub>2</sub> ) <sub>i</sub> (S-PEG) <sub>o</sub> Ata release.....	129
<b>Figure 5.30.</b> MSN(NH <sub>2</sub> ) <sub>i</sub> (L-PEG) <sub>o</sub> Ata release. ....	129
<b>Figure 6.1.</b> DOX and CPT chemical structure. ....	138
<b>Figure 6.2.</b> Dual drug release system scheme. ....	140
<b>Figure 6.3.</b> Proposed components for dual system application. ....	141
<b>Figure 6.4.</b> Components for dual system application. ....	142
<b>Figure 6.5.</b> Synthesis of aldehyde MSNs. ....	143
<b>Figure 6.6.</b> FTIR of MSN-(CHO). ....	143
<b>Figure 6.7.</b> 2,4-dinitrophenylhydrazine ( <b>38</b> ) reaction with MSN-(CHO). ....	144

<b>Figure 6.8.</b> Bifunctionalized MSN-(NH <sub>2</sub> ) <sub>i</sub> (CHO) <sub>o</sub> scheme.....	145
<b>Figure 6.9.</b> FTIR of bifunctionalized MSN-(NH <sub>2</sub> ) <sub>i</sub> (CHO) <sub>o</sub> .....	145
<b>Figure 6.10.</b> TEM micrographs of monodispersed MSN-(NH <sub>2</sub> ) <sub>i</sub> (CHO) <sub>o</sub> .....	146
<b>Figure 6.11.</b> SXDR of MSN-(NH <sub>2</sub> ) <sub>i</sub> (CHO) <sub>o</sub> .....	146
<b>Figure 6.12.</b> N <sub>2</sub> adsorption-desorption and BJH pore size of MSN-(NH <sub>2</sub> ) <sub>i</sub> (CHO) <sub>o</sub> .....	147
<b>Figure 6.13.</b> Schematic synthesis of the capping gate linker. ....	147
<b>Figure 6.14.</b> MSN-(MB).....	148
<b>Figure 6.15.</b> MSN-(MB) release .....	148
<b>Figure 6.16.</b> Schematic reaction of dual MB/DOX loading. ....	149
<b>Figure 6.17.</b> Absorption supernatants of MB and DOX.....	150
<b>Figure 6.18.</b> Visual release of MSN-(NH <sub>2</sub> ) <sub>i</sub> (PEGDOX) <sub>o</sub> MB .....	150
<b>Figure 6.19.</b> DOX Release at pH=4 and pH=7.....	151
<b>Figure 6.20.</b> CPT release at pH=4 and pH=7. ....	151
<b>Figure 6.21.</b> Supernatants release at pH=4 at different times.....	152
<b>Figure 6.22.</b> Supernatants release at pH=7 at different times before and after acid addition...	152
<b>Figure 6.23.</b> MSN(CPT) fluorescence.....	153
<b>Figure 6. 24.</b> Schematic synthesis of dual CPT/DOX system release.....	154
<b>Figure 6.25.</b> Absorption supernatants of CPT and DOX at pH=7 and pH=4.....	155
<b>Figure 6.26.</b> Supernatants of MSN-(NH <sub>2</sub> ) <sub>i</sub> CPT(PEGDOX) <sub>o</sub> at visible light. ....	155
<b>Figure 6.27.</b> Supernatants of MSN-(NH <sub>2</sub> ) <sub>i</sub> CPT(PEGDOX) <sub>o</sub> at 366 nm. ....	156
<b>Figure 6.28.</b> DOX release at pH=4 and pH=7.....	156
<b>Figure 6.29.</b> CPT release at pH=4 and pH=7. ....	157
<b>Figure 6.30.</b> Control MSN-(NH <sub>2</sub> ) <sub>i</sub> (DOX) <sub>o</sub> and MSN-(NH <sub>2</sub> ) <sub>i</sub> (DOX) <sub>o</sub> CPT viability .....	158
<b>Figure 6.31.</b> Uptake MSN(NH <sub>2</sub> ) <sub>i</sub> (DOX) <sub>o</sub> and MSN(NH <sub>2</sub> ) <sub>i</sub> (DOX) <sub>o</sub> CPT .....	159
<b>Figure 7.1.</b> Twelve well plate of MSNs incubated in Hela cells and cells fixed in covers. ....	170
<b>Figure 7.2.</b> Ninety six well plate of MSNs incubated in Hela cells. ....	171

## List of tables

<b>Table 1.1.</b> Description of main nanoparticles.....	4
<b>Table 1.2.</b> Active agents used in MSNs.....	7
<b>Table 1.3.</b> Types of gates and stimuli.....	10
<b>Table 2.1.</b> Temperature and stirring rate low and high levels .	36
<b>Table 2.2.</b> Temperature and stirring rate effects.....	36
<b>Table 2.3.</b> Temperature and [NH <sub>4</sub> OH] low and high levels .	37
<b>Table 2.4.</b> Temperature and [NH <sub>4</sub> OH] effects.....	37
<b>Table 2.5.</b> Simplex factors conditions.....	38
<b>Table 2.6.</b> DLS and TEM MSNs size.....	40
<b>Table 2.7.</b> N <sub>2</sub> adsorption-desorption and BJH pore size MSN-(NH <sub>2</sub> )	42
<b>Table 3.1.</b> TGA quantification of naphthalimide.....	56
<b>Table 3.2.</b> Truth table of NOR logic gate	65
<b>Table 4.1.</b> OEA study of CTAB removal.....	79
<b>Table 4.2.</b> BET results of CTAB removal.....	79
<b>Table 4.3.</b> MSN(NH <sub>2</sub> ) <sub>i</sub> (N <sub>3</sub> ) <sub>o</sub> size and ζ-potential values.....	80
<b>Table 4.4.</b> BET results of regioselective MSN-(NH <sub>2</sub> ) <sub>i</sub> (N <sub>3</sub> ) <sub>o</sub>	81
<b>Table 4.5.</b> DOX loading and release values.....	97
<b>Table 5.1.</b> Size and ζ-potential values of MSN-(NH <sub>2</sub> ) and MSN-(NCS)	111
<b>Table 5.2.</b> N <sub>2</sub> adsorption-desorption and BJH pore size of MSN-(NH <sub>2</sub> ) and MSN-(NCS).....	112
<b>Table 5.3.</b> OEA analysis of MSN-(NCS), MSN-(UNapht), MSN-(N <sub>3</sub> ) and MSN-(TNaph).....	115
<b>Table 5.4.</b> Size and ζ-potential values of MSN-(NH <sub>2</sub> ) and MSN-(NH <sub>2</sub> ) <sub>i</sub> (NCS) <sub>o</sub>	117
<b>Table 5.5.</b> N <sub>2</sub> adsorption-desorption MSN-NH <sub>2</sub> (CTAB), MSN-(NH <sub>2</sub> ),MSN-(NH <sub>2</sub> ) <sub>i</sub> (NCS) <sub>o</sub> ...	119
<b>Table 5.6.</b> Loading and release of Ru(bipy) <sub>3</sub> <sup>2+</sup>	127
<b>Table 5.7.</b> Loading and release of Ataluren.....	130
<b>Table 6.1.</b> MSN-(CHO) size.....	143
<b>Table 6.2.</b> MSN-(NH <sub>2</sub> ) <sub>i</sub> (CHO) <sub>o</sub> size.....	146
<b>Table 6.3.</b> N <sub>2</sub> adsorption-desorption and BJH pore size of MSN-(NH <sub>2</sub> ) <sub>i</sub> (CHO) <sub>o</sub>	147
<b>Table 6.4.</b> Loading and release values of MB and DOX.....	153
<b>Table 6.5.</b> OEA Loadings of CPT depending on the solvent.....	153
<b>Table 6.6.</b> Maximum release of CPT and DOX in MSN-(NH <sub>2</sub> ) <sub>i</sub> (PEGDOX) <sub>o</sub> CPT.....	157





## List of abbreviations

$\lambda_{\text{abs}}$ : Maximum absorption wavelength

$\lambda_{\text{em}}$ : Maximum emission wavelength

$\epsilon$ : Molar absorptivity coefficient

$\Phi_f$ : Fluorescence quantum yield

$\tau_f$ : Fluorescence lifetime

$^1\text{H-NMR}$ : Proton nuclear magnetic resonance

$^{13}\text{C-NMR}$ : Carbon nuclear magnetic resonance

**Abs**: Absorption

**AML**: Myeloid leukemia

**ACN**: Acetonitrile

**AcOEt**: Ethyl acetate

**AlkyneFITCPEG**: Product **30**, 1-(3',6'-dihydroxy-3-oxo-3H-spiro[isobenzofuran-1,9'-xanthen]-5-yl)-3-(3,6,9,12-tetraoxapentadec-14-yn-1-yl)thiourea

**Anh**: Anhydrous

**APTES**: (3-aminopropyl)triethoxysilane

**APTMS**: (3-aminopropyl)trimethoxysilane

**BET**: Brunauer-Emmet-Teller theory,  $\text{N}_2$  adsorption and desorption isotherms

**BJH**: Barret-Joyner-Hallenda analysis, adsorption cumulative volume pore

**BOC**: *Tert*-butyloxycarbonyl

**Cy**: Cyclohexane

**CPPs**: Cell penetrating peptides

**CPT**: Camptothecin

**CuAAC**: Copper catalized Azide Alkyne Cycloaddition

**CuDTTC**: Copper and *N,N*-diethyldithiocarbamate complex

**CuEDTA**: Copper and EDTA complex

**CTAB**: Hexadecyltrimethylammonium bromide

**DAPI**: 4',6-diamidino-2-phenylindole

**DCM**: Dichloromethane

**DDS**: Drug delivery systems

**DDTC**: *N,N*-diethyldithiocarbamate sodium

**DiesterPEG**: Product **49**, diethyl 3,6,9,12,15-pentaoxaheptadecanedioate

**DihydrazidePEG**: Product **45**, dimethyl 3,6,9,12,15-pentaoxaheptadecanedihydrazide

**DLS**: Dynamic Light Scattering

**DMD**: Duchenne Muscular Dystrophy

**DMEM:** Dubecco's Modified Eagle's Medium (complete medium)

**DMF:** Dimethylamine formamide

**DOX:** Doxorubicin

**EdaBOC:** Mono *tert*-butyloxycarbonyl ethylenediamine (**2**)

**EdaBOCNaphBr:** Structure **3**, *tert*-butyl(2-(6-bromo-1,3-dioxo-1*H*-benzoisoquinolin-2(3*H*)-yl)ethyl)carbamate

**EDC:** 1-ethyl-3-(dimethylaminopropyl)carbodiimide

**EDTA:** Ethylenediaminetetraacetic acid

**Em:** emission

**EPR:** Enhanced permeability retention effect

**EtOH:** Ethanol

**FITC:** Isothiocyanate fluorescein

**FTIR:** Fourier transformed infrared spectroscopy

**GSH:** Glutathione

**HRMS:** High Resolution Mass Spectrometry

**LFBS:** Bovine serum protein

**L-PEG:** Long PEG **41**, **n=15**

**MB:** Methylene blue (**50**)

**MCM:** Mobil Composition of Matter

**MeOH:** Methanol

**MM:** Model Molecule, reference naphthalimides

**MM-Br:** Bromo-naphthalimide **16**, 1-(2-(6-bromo-1,3-dioxo-1*H*-benzoisoquinolin-2(3*H*)-yl)ethyl)-3-butylthiourea

**MM-But:** Butyl-naphthalimide **18**, 1-butyl-3(2-(6-(butylamino)-1,3-dioxo-1*H*-benzoisoquinolin-2(3*H*)-yl)ethyl)thiourea

**MM-MetProp:** Methylpropyl-naphthalimide **19**, 1-butyl-3(2-(6-(methylpropylamino)-1,3-dioxo-1*H*-benzoisoquinolin-2(3*H*)-yl)ethyl)thiourea

**MM-PIP:** Piperazine-naphthalimide **17**, 1-butyl-3(2-(6-(4-methylpiperazin-1-yl)-1,3-dioxo-1*H*-benzoisoquinolin-2(3*H*)-yl)ethyl)thiourea

**MRI:** Magnetic resonance imaging

**MSNs:** Mesoporous silica nanoparticles

**MSN-(Acet):** MSNs with acetal moiety **46** both in inner and outer surface.

**MSN-(CHO):** MSNs with aldehyde moiety both in inner and outer surface.

**MSN-(NH<sub>2</sub>)<sub>i</sub>(N<sub>3</sub>)<sub>o</sub>DOX:** MSNs with DOX loaded at the inner pores and external azido moiety

**MSN-(DOX)(l-Fold)<sub>o</sub>:** MSNs with DOX loaded and low density of quinoline-foldamer at the external surface.

**MSN-(DOX)(h-Fold)<sub>o</sub>:** MSNs with DOX loaded and high density of quinoline-foldamer at the external surface.

**MSN-(FITC):** MSNs covalently functionalized at both in inner and outer surface

**MSN-(FITC)<sub>i</sub>(Fold)<sub>o</sub>**: MSNs with FITC covalently linked at the pores and quinoline foldamer at the external surface

**MSN-(FITC)<sub>i</sub>(Fold-N<sub>3</sub>)<sub>o</sub>**: MSNs with FITC covalently linked at the pores, quinoline foldamer at the external surface and remaining azides moieties

**MSN-(FITC)<sub>i</sub>(Fold-FITC-PEG)<sub>o</sub>**: MSNs with FITC covalently linked at the pores, quinoline foldamer at the external surface and PEGFITC at the external surface

**MSN-(FITC)<sub>i</sub>(N<sub>3</sub>)<sub>o</sub>**: MSNs with FITC covalently linked at the pores and azido moieties at the external surface

**MSN-(FITC)<sub>i</sub>(PEG-FITC)<sub>o</sub>**: MSNs with FITC covalently linked at the pores and PEGFITC **20** at the external surface

**MSN-(N<sub>3</sub>)**: MSNs with azido moieties both in inner and outer surface

**MSN-(NH<sub>2</sub>)**: Reference amino-MSNs

**MSN-(NH<sub>2</sub>)<sub>i</sub>(Acet)<sub>o</sub>**: Inner amino MSNs with acetal moieties at the external surface. Regioselective bifunctionalized amino-acetal MSNs

**MSN-(NH<sub>2</sub>)<sub>i</sub>(Acet)<sub>o</sub>CTAB**: Inner amino MSNs with acetal moieties at the external surface in the presence of CTAB

**MSN-(NH<sub>2</sub>)<sub>i</sub>(CHO)<sub>o</sub>**: Inner amino MSNs with outer aldehyde moieties. Regioselective bifunctionalized amino-aldehyde MSNs

**MSN-(NH<sub>2</sub>)CTAB**: Amino MSNs with CTAB in the inner surface

**MSN-(NH<sub>2</sub>)<sub>i</sub>(L-PEG)<sub>o</sub>Ata**: Loaded Ataluren MSNs with long disulfidePEG chain **41**, **n=15** functionalized at the external surface

**MSN-(NH<sub>2</sub>)<sub>i</sub>(L-PEG)<sub>o</sub>Ata-GSH**: Loaded Ataluren MSNs with long disulfidePEG chain **41**, **n=15** functionalized at the external surface in the presence of GSH

**MSN-(NH<sub>2</sub>)<sub>i</sub>(L-PEG)<sub>o</sub>Ru**: Loaded Ru(bipy)<sub>3</sub><sup>2+</sup> MSNs with long disulfidePEG chain **41**, **n=15** functionalized at the external surface

**MSN-(NH<sub>2</sub>)<sub>i</sub>(L-PEG)<sub>o</sub>Ru-GSH**: Loaded Ru(bipy)<sub>3</sub><sup>2+</sup> MSNs with long disulfidePEG chain **41**, **n=15** functionalized at the external surface in the presence of GSH.

**MSN-(NH<sub>2</sub>)<sub>i</sub>(N<sub>3</sub>)<sub>o</sub>**: Inner amino MSNs with outer azido moieties. Regioselective bifunctionalized amino-azide MSNs

**MSN-(NH<sub>2</sub>)<sub>i</sub>(N<sub>3</sub>)<sub>o</sub>CTAB**: Inner amino MSNs with outer azido moieties in the presence of CTAB.

**MSNs-(NH<sub>2</sub>-N<sub>3</sub>)EtOH**: Amino-azido MSNs where CTAB has been removed in EtOH

**MSN-(NH<sub>2</sub>)<sub>i</sub>(NCS)<sub>o</sub>**: Inner amino MSNs with outer isothiocyanate moieties. Regioselective bifunctionalized amino-isothiocyanate MSNs

**MSN-(NH<sub>2</sub>)<sub>i</sub>(NCS)<sub>o</sub>(CTAB)**: Inner amino MSNs with outer isothiocyanate moieties in the presence of CTAB.

**MSN-(NH<sub>2</sub>)<sub>i</sub>(PEG-DOX)<sub>o</sub>CPT**: Loaded CPT MSNs with DOX-hydrazinePEG chain **45** functionalized at the external surface

**MSN-(NH<sub>2</sub>)<sub>i</sub>(PEG-DOX)<sub>o</sub>MB**: Loaded MB MSNs with DOX-hydrazinePEG chain **45** functionalized at the external surface

**MSN-(NH<sub>2</sub>)<sub>i</sub>(S-PEG)<sub>o</sub>Ata**: Loaded Ataluren MSNs with small disulfidePEG chain **41**, **n=3** functionalized at the external surface

**MSN-(NH<sub>2</sub>)<sub>i</sub>(S-PEG)<sub>o</sub>Ata-GSH**: Loaded Ataluren MSNs with small disulfidePEG chain **41**, **n=3** functionalized at the external surface in the presence of GSH

**MSN-(NH<sub>2</sub>)<sub>i</sub>(S-PEG)<sub>o</sub>Ru**: Loaded Ru(bipy)<sub>3</sub><sup>2+</sup> MSNs with small disulfidePEG chain **41**, **n=3** functionalized at the external surface

**MSN-(NH<sub>2</sub>)<sub>i</sub>(S-PEG)<sub>o</sub>Ru-GSH**: Loaded Ru(bipy)<sub>3</sub><sup>2+</sup> MSNs with small disulfidePEG chain **41**, **n=3** functionalized at the external surface in the presence of GSH

**MSN-(NaphBr)**: Functionalized MSNs with bromo naphthalimide **6** both in inner and outer surface

**MSN-(NaphBut)**: Functionalized MSNs with buthyl naphthalimide **14** both in inner and outer surface

**MSN-(NaphMetProp)**: Functionalized MSNs with methyl propyl naphthalimide **15** both in inner and outer surface

**MSN-(NaphPIP)**: Functionalized MSNs with piperazine naphthalimide **13** both in inner and outer surface

**MSN-(UNaph)**: amine MSNs functionalized with buthyl naphthalimide **11** both in inner and outer surface, Urea bond formation

**MSN-(TNaph)**: azido MSNs functionalized with propargyl naphthalimide **32** both in inner and outer surface, Triazol bond formation

**MRI**: Magnetic Resonance Imaging

**MTT**: 3-(4,5-dimethylthiazol-2-yl)-2,5-diphenyltetrazolium bromide

**NPs**: Nanoparticles in general

**Naph**: Naphthalimide

**OEA**: Organic Elemental Analysis

**OMePEG**: Product **33**, tetraethyleneglycol monomethyl ether

**PDT**: Photodynamic Therapy

**PET**: Photoinduced Electron Transfer

**PEG**: Polyethylene glycol polymer

**PEG-FITC**: Polyethylene glycol polymer functionalized with FITC (**30**)

**QDs**: Quantum dots

**RES**: Reticuloendothelial system

**Ru(bipy)<sub>3</sub><sup>2+</sup>**: Tris(bipyridine)ruthenium(II) chloride

**SBA**: Santa Barbara MSNs

**S-PEG**: Small PEG **41**, **n=3**

**SiRNA**: Small interfering ribonucleic acid

**SXDR**: Small angle powder X-ray diffraction

**T**: Temperature

**TAT**: Human immunodeficiency virus type 1 (HIV-1) encoded peptide

**TEM**: Transmission electron microscopy

**TEOS**: Tetraethyl orthosilicate

**TFA**: Trifluoro acetic acid

**TGA**: Termogravimetric analysis

**UV-Vis**: Ultraviolet-visible

# Index: Table of contents

<b>Chapter 1. Introduction</b> .....	3
1.1. Nanoparticles.....	3
1.2. Mesoporous silica nanoparticles (MSNs).....	5
1.3. MSNs applications in biomedicine as nanoplatforms .....	6
1.3.1. MSNs applications as sensors .....	8
1.3.2. MSNs applications as drug delivery systems .....	9
1.4. Clinical applications of MSNs and outlook .....	11
1.5. Introduction of organic moieties to MSNs surface .....	13
1.5.1. Anchorage .....	13
1.5.2. Grafting .....	14
1.5.3. Co-condensation.....	14
1.6. Regioselective bifunctionalization .....	15
1.7. MSNs covalent strategies for functionalization .....	16
1.7.1. Steglich reaction: carbodiimide coupling .....	17
1.7.2. CuACC cycloaddition: the “click” chemistry .....	17
1.7.3. Disulfide formation .....	18
1.7.4. Isocyanates .....	19
1.7.5. Isothiocyanates .....	19
1.7.6. Carbonyl nucleophilic substitution.....	20
1.8. Aims .....	21
1.9. Bibliography.....	23
<b>Chapter 2. Synthesis of aminated MSNs as precursor nanoparticles</b> .....	31
2.1. Introduction .....	31
2.2. Synthesis of small aminated-MSNs .....	34
2.2.1. Experimental planning .....	35
2.2.2. Simplex optimization methodology .....	38
2.2.3. MSNs scale up.....	39
2.3. MSNs characterization .....	39
2.3.1. CTAB removal .....	39
2.3.2. Size determination.....	40
2.3.3. Surface Area and porous order characterization .....	41
2.3.4. X-Ray diffraction (SXR).....	43

2.4.	Quantitative determination of amino groups in MSNs.....	43
2.5.	Conclusions .....	44
2.6.	Bibliography.....	45
<b>Chapter 3. Amine-naphthalimide functionalized MSNs for chemical sensing .....</b>		<b>49</b>
3.1.	Introduction .....	49
3.2.	Design of pH and fluoride sensor naphthalimide-MSN .....	51
3.3.	Synthesis of pH and fluoride sensor naphthalimide-MSN .....	52
3.3.1.	Functionalization quantification.....	56
3.3.2.	Reproducibility of MSNs functionalization .....	57
3.4.	Synthesis of reference naphthalimides .....	57
3.5.	Titration with acid .....	58
3.6.	Fluoride titration of MSN-(NaphBut) .....	62
3.7.	Conclusions and Outlook .....	66
3.8.	Bibliography.....	67
<b>Chapter 4. Amine-azido-MSNs for their use as penetrating cell carriers.....</b>		<b>71</b>
4.1.	Introduction .....	71
4.1.1.	The importance of crossing the cellular barrier.....	71
4.1.2.	Strategies to cross cytoplasm membranes .....	71
4.1.2.1.	CPPs (Cell penetrating peptides).....	72
4.1.2.2.	Cationic charged molecules.....	72
4.1.2.3.	Cationic quinoline foldamers .....	73
4.2.	Foldamer-MSNs design.....	74
4.3.	Amino-azido MSNs synthesis and characterization.....	75
4.3.1.	Synthesis of 3-azidopropionic acid succinimidyl ester .....	77
4.3.2.	Amino-azido MSNs functionalization.....	77
4.3.3.	Amino-azido MSN characterization.....	80
4.4.	MSNs functionalization with alkyne-foldamer <b>24</b> .....	82
4.4.1.	Synthesis of alkyne-foldamer-MSNs .....	82
4.4.2.	Biological experiments.....	87
4.4.2.1.	Experimental conditions.....	87
4.4.2.2.	Viability experiments .....	88
4.4.2.3.	Uptake experiments.....	89
4.4.2.4.	Uptake quantification assays .....	94
4.5.	Intracellular delivery of DOX with foldamer-MSN.....	94

4.5.1.	DOX loading in MSN-(NH <sub>2</sub> ) <sub>i</sub> (N <sub>3</sub> ) <sub>o</sub> .....	95
4.5.2.	DOX loading in foldamer-MSN .....	95
4.5.3.	Viability and uptake experiments of MSN-(Fold) <sub>o</sub> DOX.....	98
4.6.	Conclusions and Outlook .....	99
4.7.	Bibliography.....	102
<b>Chapter 5. Amino-isothiocyanate MSNs for the controlled release of Ataluren .....</b>		<b>107</b>
5.1.	Introduction .....	107
5.2.	Synthesis and characterization of isothiocyanate-MSNs .....	109
5.3.	Assessment of MSN-(NCS) functionalization .....	113
5.4.	Orthogonal regioselective difunctionalization of MSN-(NH <sub>2</sub> ) <sub>i</sub> (NCS) <sub>o</sub> .....	116
5.5.	Controlled release of Ataluren .....	120
5.5.1.	Design of the nanocarrier .....	121
5.5.2.	Controlled Ru(bipy) <sub>3</sub> <sup>2+</sup> release .....	124
5.5.3.	Ataluren Release .....	127
5.6.	Conclusions and Outlook .....	131
5.7.	Bibliography.....	132
<b>Chapter 6. Amino-Aldehyde MSNs for their application as dual drug delivery system ..</b>		<b>137</b>
6.1.	Introduction .....	137
6.2.	Strategy for dual drug release.....	140
6.3.	Synthesis of aldehyde-MSNs .....	142
6.4.	Functionalization test of MSN-(CHO).....	144
6.5.	Synthesis of bifunctionalized amino-aldehyde MSNs .....	144
6.6.	Synthesis of capping dihydrazine PEG linker .....	147
6.7.	Dual MB and DOX drug release nanocarrier .....	148
6.7.1.	MB Loading .....	148
6.7.2.	DOX/MB release.....	149
6.8.	Dual CPT and DOX drug release nanocarrier .....	153
6.8.1.	CPT loading.....	153
6.8.2.	CPT-DOX release .....	154
6.9.	Preliminary biological experiments.....	158
6.10.	Conclusions and Outlook .....	160
6.11.	Bibliography.....	161

<b>Chapter 7. Experimental Part</b> .....	167
7.1. Instrumentation.....	167
7.2. Protocols.....	169
7.3. Synthesis Chapter 2.....	173
7.3.1. General procedure for the synthesis of MSNs.....	173
7.3.2. FITC functionalization for NH <sub>2</sub> determination.....	174
7.4. Synthesis Chapter 3.....	175
7.4.1. Synthesis of <i>tert</i> -butyl(2-(6-bromo-1,3-dioxo-1H-benzoisoquinolin-2(3H)-yl)ethyl)carbamate), EdaBOCNapht ( <b>3</b> ).....	175
7.4.2. General procedure for synthesis of EdaBOC-naphthalimides ( <b>7-9</b> ).....	175
7.4.3. General procedure for synthesis of isothiocyanate-naphthalimides ( <b>6;13-15</b> ).....	176
7.4.4. General procedure for model naphthalimides ( <b>16-19</b> ).....	178
7.4.5. Absorption and fluorescent properties of MSN and MM naphthalimides.....	179
7.4.6. MSNs functionalization with naphthalimides.....	180
7.5. Synthesis Chapter 4.....	181
7.5.1. Synthesis of 3-azidopropanoic acid ( <b>21</b> ).....	181
7.5.2. Synthesis of 3-azidopropionic acid succinimidyl ester ( <b>22</b> ).....	181
7.5.3. Synthesis of bifunctionalized amino-azide nanoparticles (MSN-(NH <sub>2</sub> ) <sub>i</sub> (N <sub>3</sub> ) <sub>o</sub> ).....	182
7.5.4. Synthesis of alkyne-FITC-PEG <b>30</b> .....	182
7.5.4.1. Synthesis of 3,6,9,12-tetraoxapentadec-14-yn-1-ol ( <b>26</b> ).....	182
7.5.4.2. Synthesis of 3,6,9,12-Tetraoxapentadec-14-yn-1-yl-4-methylbenzene-sulfonate ( <b>27</b> ).....	183
7.5.4.3. Synthesis of 1-azido-3,6,9,12-tetraoxapentadec-14-yne ( <b>28</b> ).....	183
7.5.4.4. Synthesis of 3,6,9,12-tetraoxapentadec-14-yn-1-amine ( <b>29</b> ).....	184
7.5.4.5. Synthesis of 1-(3',6'-dihydroxy-3-oxo-3H-spiro[isobenzofuran-1,9'-xanthen]-5-yl)-3-(3,6,9,12-tetraoxapentadec-14-yn-1-yl)thiourea ( <b>30</b> ).....	184
7.5.5. Synthesis of MSN-(FITC) <sub>i</sub> (Fold) <sub>o</sub> .....	185
7.5.6. Synthesis of MSN-(FITC) <sub>i</sub> (Fold-FITC-PEG) <sub>o</sub> .....	186
7.5.7. Synthesis of reference MSN-(FITC) <sub>i</sub> (FITC-PEG) <sub>o</sub> .....	187
7.5.8. DOX loading in MSN-(NH <sub>2</sub> ) <sub>i</sub> (N <sub>3</sub> ) <sub>o</sub> (MSN-(DOX)).....	188
7.5.9. DOX loading with different densities of foldamer (MSN-(DOX)(1-Fold) <sub>o</sub> and MSN-(DOX)(h-Fold) <sub>o</sub> ).....	188
7.6. Synthesis Chapter 5.....	190
7.6.1. Synthesis of isothiocyanate MSNs ((MSN-(NCS)).....	190
7.6.2. Functionalization of MSN-(NCS) with 4-( <i>n</i> -butylamino)- <i>N</i> -(2-aminoethyl)-1,8-naphthalimide (MSN-(UNaph)).....	190
7.6.3. Synthesis of azido MSNs (MSN-(N <sub>3</sub> )).....	191



7.6.4.	Propargyl 8-butylamine naphthalimide ( <b>32</b> ) .....	191
7.6.5.	Functionalization of (MSN-(N <sub>3</sub> )) with 4-( <i>n</i> -butylamino)- <i>N</i> -(2-propargyl)-1,8-naphthalimide (MSN-(TNaph)).....	192
7.6.6.	Synthesis of bifunctionalized amino-isothiocyanate MSNs (MSN-(NH <sub>2</sub> ) <sub><i>i</i></sub> (NCS) <sub><i>o</i></sub> )	192
7.6.7.	Synthesis of disulfide small and long PEG ( <b>41</b> , <b>n=3</b> and <b>n=15</b> ).....	193
7.6.7.1.	Synthesis of <i>tert</i> -butyl(2-((2-aminoethyl)disulfanyl)ethyl)carbamate ( <b>35</b> )...	193
7.6.7.2.	<i>tert</i> -butyl(2-((2-isothiocyanateethyl)disulfanyl)ethyl) carbamate ( <b>36</b> ) .....	193
7.6.7.3.	Synthesis of triethylene glycol 2-methyl tosylate methyl ether ( <b>37</b> ).....	194
7.6.7.4.	Synthesis of triethylene glycol 2-methyl azide methyl ether ( <b>38</b> ).....	194
7.6.7.5.	Synthesis of triethylene glycol 2-methyl amino methyl ether ( <b>39</b> ) .....	195
7.6.7.6.	Synthesis of <i>tert</i> -butyl(15-thioxo-2,5,8,11-tetraoxa-19,20-dithia-14,16-diazadocosa-22-yl)carbamate ( <b>40</b> ; <b>n=3</b> and <b>n=15</b> ) .....	195
7.6.7.7.	Synthesis of 1-(2-((2-aminoethyl)disulfanyl)ethyl)-3-(2,5,8,11-tetraoxatrideca-13-yl)thiourea ( <b>41</b> ; <b>n=3</b> and <b>n=15</b> ).....	196
7.6.8.	Ru(bipy) <sub>3</sub> <sup>2+</sup> loading in amino-isothiocyanate MSNs (MSN-(NH <sub>2</sub> ) <sub><i>i</i></sub> (NCS) <sub><i>o</i></sub> Ru).....	196
7.6.9.	Ru(bipy) <sub>3</sub> <sup>2+</sup> loading in amino-isothiocyanate MSNs with small and long PEG <b>41</b> ( <b>n=3</b> and <b>n=15</b> ) (MSN-(NH <sub>2</sub> ) <sub><i>i</i></sub> (S-PEG) <sub><i>o</i></sub> Ru and MSN-(NH <sub>2</sub> ) <sub><i>i</i></sub> (L-PEG) <sub><i>o</i></sub> Ru).....	197
7.6.10.	Ataluren loading in amino-isothiocyanate MSNs (MSN-(NH <sub>2</sub> ) <sub><i>i</i></sub> (NCS) <sub><i>o</i></sub> Ru) .....	197
7.6.11.	Ataluren loading in amino-isothiocyanate MSNs with small and long PEG <b>41</b> ( <b>n=3</b> and <b>n=15</b> ) MSN-(NH <sub>2</sub> ) <sub><i>i</i></sub> (S-PEG) <sub><i>o</i></sub> Ata and MSN-(NH <sub>2</sub> ) <sub><i>i</i></sub> (L-PEG) <sub><i>o</i></sub> Ata .....	198
7.7.	Synthesis Chapter 6.....	199
7.7.1.	Synthesis of 2-isothiocyanate-1,1-dimethoxyethane ( <b>46</b> ) .....	199
7.7.2.	Synthesis of MSN-(CHO) .....	199
7.7.3.	Functionalization of MSN-(CHO) with 2,4-dinitrophenylhydrazine .....	200
7.7.4.	Synthesis of bifunctionalized amino-aldehyde MSNs (MSN-(NH <sub>2</sub> ) <sub><i>i</i></sub> (CHO) <sub><i>o</i></sub> ) .....	200
7.7.5.	Synthesis of the linker .....	201
7.7.5.1.	Synthesis of diethyl 3,6,9,12,15-pentaoxaheptadecanedioate ( <b>49</b> ) .....	201
7.7.5.2.	Synthesis of dimethyl 3,6,9,12,15-pentaoxaheptadecanedihydrazide ( <b>45</b> ) ...	201
7.7.6.	MB loading in amino-aldehyde nanoparticles (MSN-(NH <sub>2</sub> ) <sub><i>i</i></sub> (CHO) <sub><i>o</i></sub> MB) .....	202
7.7.7.	Dual MB-DOX nanocarrier.....	202
7.7.8.	CPT loading in amino-aldehyde nanoparticles (MSN-(NH <sub>2</sub> ) <sub><i>i</i></sub> (CHO) <sub><i>o</i></sub> CPT).....	203
7.7.9.	Dual CPT-DOX nanocarrier.....	203
7.8.	Bibliography.....	204
<b>Chapter 8. Conclusions</b> .....		<b>207</b>



# Chapter 1. Introduction

---

Currently, a large number of scientific advances are based on the use of nanoparticles as functional transport vehicles, in processes related to applications in catalysis, information technology, new materials and biomedicine. This general introduction focuses on the functionalization of mesoporous silica nanoparticles surface for its use as nanoplatforms for biomedicine applications.



## Chapter 1. Introduction

### 1.1. Nanoparticles

Nanoparticles (NPs) are defined as microscopic particles with a size ranging from 1 to 100 nm.<sup>1</sup> NPs size lies between little proteins and viruses (Figure 1.1). This similar size compatibility, allows the applications of NPs in many different fields such as biotechnology, medicine, catalysis, energy, environment, information technology, textile industry and cosmetics.<sup>2</sup>

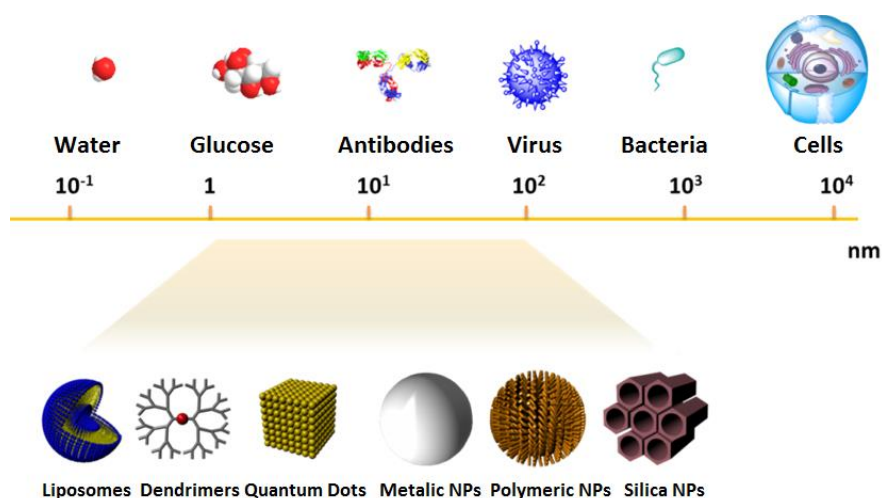


Figure 1.1. Size scale.

By and large, nanoparticles are classified according to their organic or inorganic nature. Organic nanoparticles consist of polymeric systems, repetitive structures, such as dendrimers, and lipid bilayers like liposomes, while inorganic nanoparticles contain metals and inert materials such as titanium dioxide, hydroxyapatite and silica.<sup>3</sup> In table 1.1, a brief list of the most relevant nanoparticles is presented.

Although NPs have been used in many different applications, it is in the field of biomedicine that NPs have been widely studied. More specifically, NPs have been used as multinanoplatfroms or drug delivery systems (DDS) for the detection and delivery of therapeutic agents into targeted sites (Figure 1.2).<sup>4-7</sup>

Table 1.1. Description of main nanoparticles.

<b>Organic Nanoparticles</b>	<b>Polymeric nanoparticles</b>	Nanoparticles formed by a polymer matrix. Used in medical applications. Nevertheless, depending on the polymer they have a non-specific biodistribution and low loadings cargos. They are prone to hydrolysis and enzymatic degradation. <sup>8</sup>
	<b>Dendrimers</b>	Definite macromolecules. They present a highly branched structure formed by a nucleus and multiple layers. Its molecular structure allows dendrimers to load different cargos. <sup>9</sup>
	<b>Liposomes</b>	Spherical nanosystems formed by a lipid bilayer that allows the encapsulation of hydrophobic and hydrophilic drugs. Although liposomes are widely studied, their fast elimination from the body is one of their major drawbacks. <sup>10</sup>
	<b>Micelles</b>	Colloidal aggregates of amphiphilic molecules. Micelles consist of two different domains. An internal hydrophobic part and a hydrophilic domain that allow the encapsulation of non-polar drugs for its transport. <sup>11</sup>
<b>Inorganic Nanoparticles</b>	<b>Silica nanoparticles</b>	Silica nanoparticles are inert, biodegradable and present good biodistribution properties. They can be easily synthesized with any desirable shape and size. <sup>12</sup>
	<b>Gold nanoparticles</b>	Metal nanoparticles exhibit optical and electronic properties that depend entirely on their shape and size. They have no intrinsic toxicity. <sup>13</sup>
	<b>Quantum dots (QDs)</b>	Active nanoparticles that are generally used as sensing probes due to their high quantum fluorescence yields and high photostability. Moreover, their fluorescence emission can be tuned by changing QDs size. Nevertheless, QDs are neither biodegradable nor biocompatible with human organism which is a very restrictive condition for medical applications. <sup>14</sup>
	<b>Carbon nanotubes</b>	Graphene monolayers wrapped in cylinder shape. They present a high surface area that enhances the anchor of different molecules. Nevertheless they are toxic if not properly functionalized. <sup>15</sup>

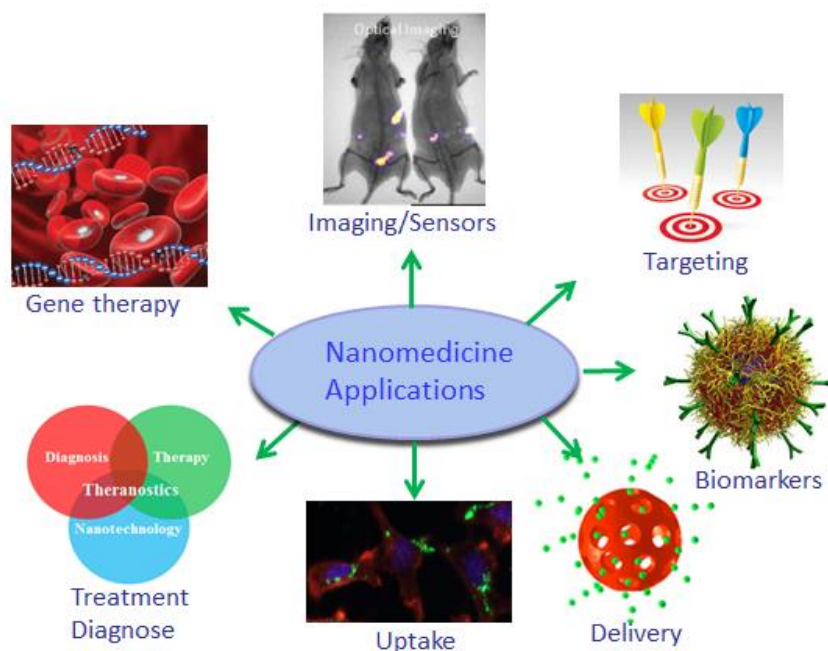


Figure 1.2. Nanotechnology applications in biomedicine.

Among the different types of nanoparticles that have been described, inorganic mesoporous silica nanoparticles have emerged as promising biomaterials due to their exceptional properties such as good biocompatibility and excellent chemical and morphological singularity.<sup>4,16–18</sup>

## 1.2. Mesoporous silica nanoparticles (MSNs)

Since its discovery in 1991, mesoporous silica nanoparticles (MSNs) have been widely used in catalysis and biomedicine applications due to their unique physicochemical properties, mechanical resistance, chemical stability, biocompatibility and high synthetic versatility.<sup>19,20</sup> MSNs consist of a silica matrix filled with porous cavities with a size between 2 and 50 nm.<sup>21</sup> This exceptional peculiarity gives MSNs two different surfaces: the external outer surface and the inner porous surface (Figure 1.3).

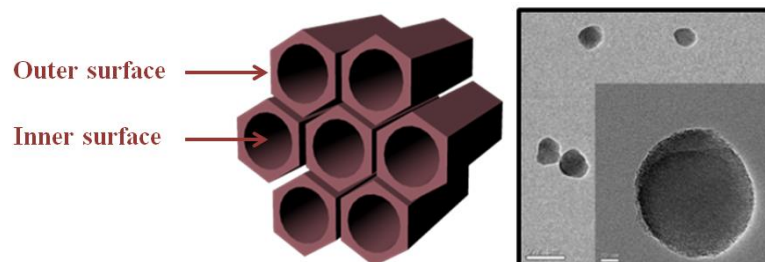


Figure 1.3. Schematic representation of MSNs channels and TEM micrograph.

Some of the most important MSNs features are:

- Two different surface areas (inner and outer).
- High surface area ( $>1000 \text{ m}^2 \cdot \text{g}^{-1}$ ) which allows high cargo loadings ( $<35 \%$ ).
- High porous volume ( $>1 \text{ cm}^3 \cdot \text{g}^{-1}$ ), high porosity and porous order.
- Fine-tuning of the porous size (2-10 nm).
- Good chemical and thermal stability.
- Non-toxic and biocompatible with human organism.
- Size and shape control.
- Easy to synthesize and functionalize.
- Stable mesostructure.

The first obtaining of mesoporous materials is contemporary to the 90s. At that time, the solid porous industry was looking for porous materials with a higher porous size than zeolites. It was Mobil Oil Corporation in 1992 that synthesized MCM (Mobil Composition of Matter) by mixing a silica precursor with an amphiphilic tensioactive. The great advantage of these new materials over zeolites was that their porous size could easily be tuned in 2-10 nm range.<sup>22,23</sup> These MCMs materials, also known as MSNs, present a very versatile synthetic route, which enables the fine-tuning of their size and porosity by controlling different conditions, such as the type of surfactant, pH and temperature.<sup>24</sup>

Although MSNs were initially developed for catalytic applications,<sup>25</sup> it is in the field of medical research, as multinanoplatfoms for drug delivery and sensing applications, where MSNs have lately been used.<sup>7,17,18,26-31</sup> MSNs high surface area and porous volume allow them to carry different payloads such as drugs, sensors or proteins,<sup>18,32</sup> while being protected from aggressive environments, and enzyme degradations in the stomach, liver or intestines.<sup>26</sup>

### **1.3. MSNs applications in biomedicine as nanoplatfoms**

Multinanoplatfoms are a new generation of drug delivery systems that consist of a nanocarrier vehicle loaded with an effective drug, envisaged to control drug delivery, monitor its dosage and target the drug specifically to the site of action. High specific surface, chemical and morphological versatility and non-toxicity make of mesoporous silica nanoparticles a promising material for drug delivery applications<sup>16,17,27,33-35</sup> and therefore, MSNs are foreseen to become “theranostic agents”.<sup>6,7</sup> “Theranostics” is derived from the combination of the words therapy and diagnosis (Figure 1.4). Thus, the “theranostic” concept relates to the ability of detecting and treating a specific disease in the organism at the same time.<sup>32</sup>



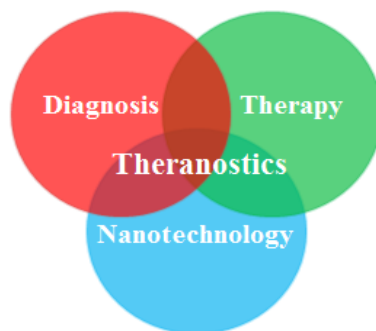


**Figure 1.4. Theranostic concept.**

The next generation of MSNs are designed to be capable of diagnosing, treating, detecting, monitoring, screening and releasing a payload specifically.<sup>30</sup> Therefore, a complete multinanoplatform (Figure 1.5) would incorporate a drug inside the MSNs channels, while the external surface will be decorated with different elements to improve its biodistribution such as polyethylene glycol (PEG),<sup>36</sup> cationic polymers,<sup>37</sup> SiRNA chains<sup>38</sup> and peptides<sup>39</sup> to cross cytoplasmic membranes,<sup>40</sup> antibodies to increase selectivity to the affected tissues<sup>41</sup> and sensors to monitor MSNs pathway at any moment with contrast agents,<sup>42</sup> or fluorescent probes<sup>43</sup> for intracellular biosensing applications<sup>32,44,45</sup> (Table 1.2).<sup>18,28</sup> Additionally, the incorporation of anions and cations sensors would provide information on the composition of the chemical environment.<sup>46,47</sup> Therefore, multinanoplatforms would ideally be decorated with different gates, tags, drugs, sensors, receptors and active agents

**Table 1.2. Active agents used in MSNs.**

<b>Active agents</b>	<b>Properties</b>
Drug	Disease treatment
Antibodies	Selective transport
DNA/SiRNA	Genetic transduction
Photosensitizers	Photodynamic therapy (PDT)
Proteins	Active site, selectivity
Cationic polymers	Cellular uptake
Biodegradable polymers	Biodistribution and stability
Contrast agents	Magnetic Resonance Imaging (MRI)
Fluorophore	Location and recognition
Ion sensing and pH	Sensor, diagnosis
Phospholipids	Molecular encapsulation

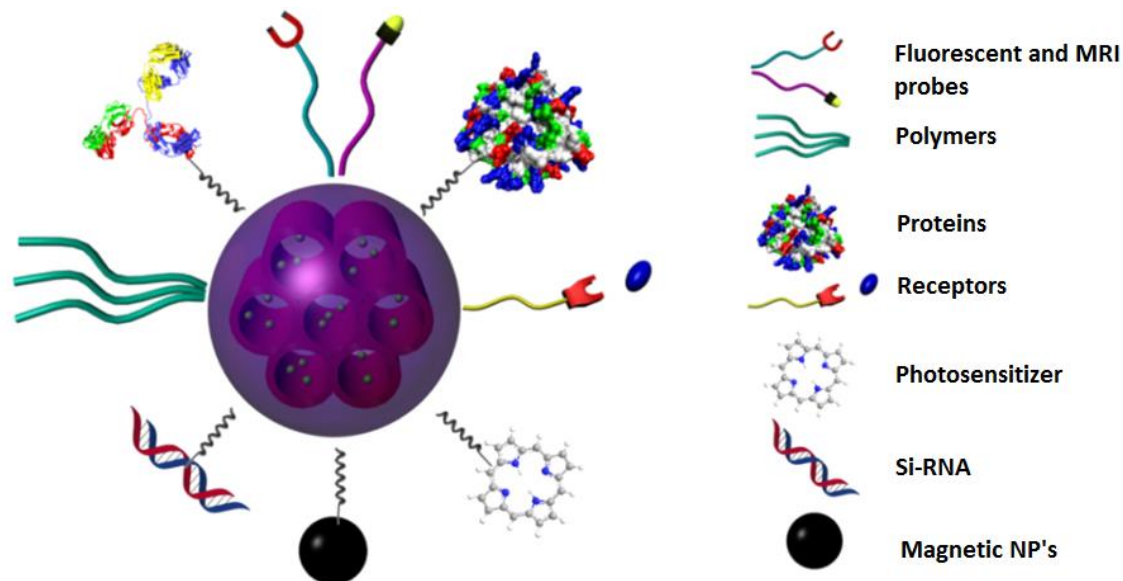


Figure 1.5. Example of nanoplatform.

Given this multifunctional capability, such combinatorial nanostructures may eventually provide the means to achieve the so-called “personalized medicine” by tailoring drug delivery to individual response. Although this may appear futuristic, great encouraging improvements have been done in order to apply these systems in the near future as smart sensors and drug delivery systems.<sup>5,48,49</sup>

### 1.3.1. MSNs applications as sensors

Exploring biochemical intracellular processes, labelling or imaging cell components are major tasks in biological and medical research. To this end, fluorophores can be used for applications such as staining cell membranes, nuclei and lysosomes, but also to visualize intracellular pH and quantify intracellular analyte concentrations in real time, which can give new insights into the chemical microenvironment on the subcellular level.<sup>50</sup>

Significant advances in fluorescence based sensing technology have given rise to the development of new fluorescence sensing mechanisms and measurement instrumentation. Fluorescence sensing technology has been achieved as a powerful and versatile toolbox in the field of physiology and molecular biology, environmental monitoring and clinical diagnosis with the advantage of high selectivity and sensitivity, spatiotemporal resolution, and visibility.<sup>50–52</sup>

In addition, the development of new molecular systems for the detection of anions, cations or neutral molecules has gained prime importance in recent years due to the fundamental need to detect target species in biological and environmental samples. In this area, specific receptors are

able to transform, upon coordination, host–guest interactions into a measurable signal which allows analyte recognition and sensing through optical or electrochemical responses.<sup>53</sup> In fact, some of the most promising sensors are based on fluoroionophores functionalized in nanoparticles.<sup>54</sup> NPs are brighter than individual fluorophores, since one particle contains a high number of dye molecules. Furthermore, the entrapment of the dye in NPs surface enhances stability and biocompatibility of the fluorophore.<sup>50</sup> Among different types of nanoparticles, the main advantages of silica MSNs for sensing applications is that silica is photophysically inert, transparent and can protect and stabilize incorporated dyes in its inner surface. In part, this is the reason why the encapsulation of fluorophores into MSNs and their application as optical sensors for various analytes in suspension has become an interesting and widespread research field in the last decades.<sup>31</sup>

### 1.3.2. MSNs applications as drug delivery systems

The need for more efficient therapies and the advances in nanotechnology has led to the development of drug delivery systems (DDS) focused on improving their effectiveness and tolerability, and simplifying drug administration. In this field, mesoporous silica materials present promising properties for drug delivery applications due to their ability to encapsulate different types of molecules within their pore channels. Drugs are generally loaded in MSNs by adsorbing them onto the particles and then releasing them to the desired medium. In such a case, there is no control over the pore openings and the resulting system performs a burst-like unsustained release. Nevertheless, it is possible to achieve MSN-based controlled release systems by applying mechanical controls over the pore openings. Through capping and opening the porous entrance, nanogates that would allow selective transport and efficient release can be built (Figure 1.6).<sup>7</sup>

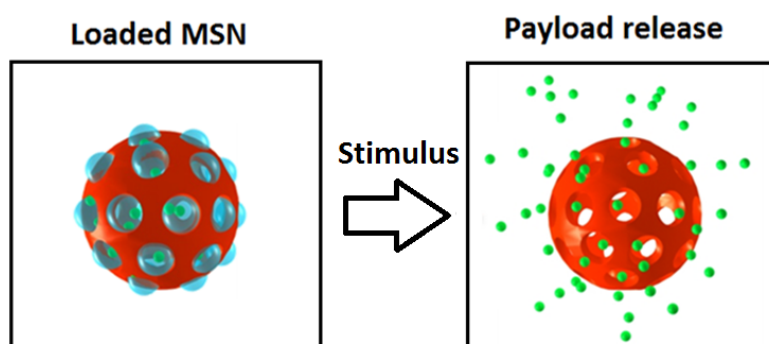


Figure 1.6. Nanogate triggered release by external or internal stimulus.

In fact, a great deal of research attention has been focused on developing nanovalves on the surface of MSNs for on-command release of their guest molecules in response to different

stimuli.<sup>4,17,18,30</sup> Mainly, there are two types of stimuli: internal stimuli such as pH,<sup>55,56</sup> enzymatic activity<sup>57</sup> or reductive environment,<sup>58</sup> which depend on cell homeostasis; and external stimuli such as light,<sup>59</sup> ultrasound<sup>60</sup> or magnetic fields<sup>61</sup> that can be applied as desired.<sup>7,62</sup> External stimuli present the advantage that they can be controlled in time and location. In table 1.3, the more used stimuli for control drug delivery are described.

**Table 1.3. Types of gates and stimuli.**

<b>Stimuli</b>	<b>Type of gates</b>
pH	Labile bonds (hydrazones, esters and imines)
Temperature	Thermosensible polymers
Redox reactions	Disulfide bridges
Light	<i>Cis-trans</i> isomers
Magnetic fields	Magnetic Nanoparticles
Enzymes	Glucose, biotine-avidine, glycosidic bond, aptamers interaction

Taking into account that pH values in the vicinity of cancerous tissues (pH=6.5) and in endo/lysosomes (pH 4-6) are lower than in blood and normal tissues (pH= 7.4), pH sensitive gates are been widely used for cancer applications.<sup>55,56,63,64</sup>

MSNs-based controlled release systems have been developed by applying mechanical controls over the pore openings (Figure 1.7)<sup>4,35,45,65-67</sup> The first way to achieve a controllable release is to attach bulky groups such as Au or CdS nanocrystals over the pore openings.<sup>68,69</sup> These bulky groups serve as gatekeepers for the encapsulated cargo. Removal of the bulky blocking groups via chemical methodologies initiates cargo release. In figure 1.7.a, the attachment and removal of bulky groups such as Au and Cds nanocrystals is represented.<sup>68,69</sup>

When bulky groups are assembled by non-covalent interactions, they become nanomachines, such as “nanovalves”<sup>70</sup> and “snap-top”<sup>71</sup> machines. These nanomachines usually contain a static stalk covalently attached to the particles surface and a bulky cyclic moving component, which encircles the stalk via non-covalent interactions. The blocking and un-blocking of the pore openings is achieved by such motions. Figure 1.7.b corresponds to the threading and dethreading of a cyclic torus molecule in a “snap-top” nanomachine design<sup>71</sup> or the shuttling of a cyclic molecule between two recognizing sites along a molecular stalk towards and away from the pore opening in a supramolecular “nanovalve” design.<sup>70</sup>

Polymers that are either adsorbed or covalently bonded to the surface of the MSNs have also served as a mechanized controlled release system.<sup>72</sup> Under their “close” condition, the polymer chains tightly wrap around the particle surface, blocking pore openings. Then the polymers are induced by certain stimuli to undergo swelling or coiling, so that the pore openings are re-exposed and cargo is released through the unblocked pores. In Figure 1.7.c, the shrinking and swelling of polymer chain coated on particle surface is shown.<sup>72</sup>

Finally, another way to mechanically block the pores is to form chemical bonds directly over the pore openings that can later be cleaved upon the presence of some stimuli, such as disulfides bonds with glutathione,<sup>58</sup> proteases,<sup>73</sup> amidases,<sup>57</sup> esterases,<sup>74</sup> or hydrazones.<sup>75–77</sup> In Figure 1.7.d the formation and breaking of covalent bonds is represented.

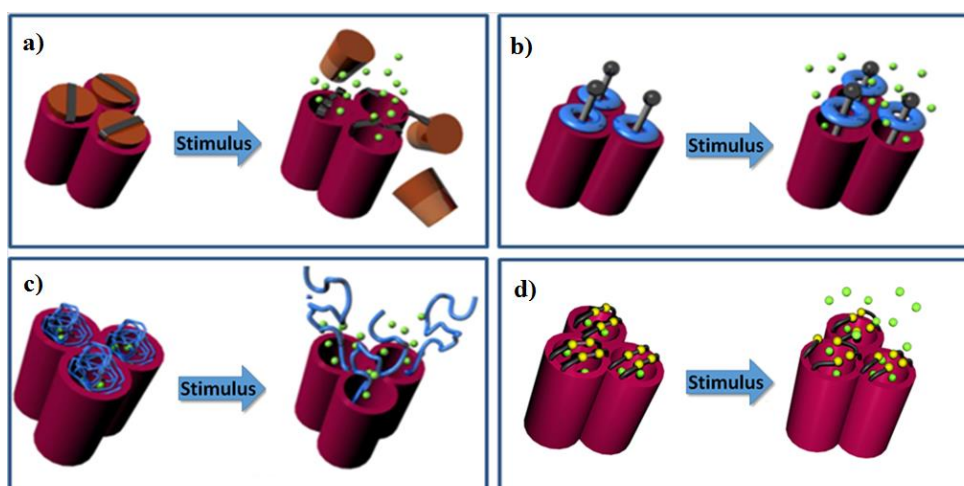


Figure 1.7. Relevant strategies for controlled release systems.

#### 1.4. Clinical applications of MSNs and outlook

In order to use MSNs in biomedical applications, a wide range of physical, chemical, biological and physiological properties must be fulfilled.<sup>19,78,79</sup>

- MSNs must be biocompatible and biodegradable.
- They must ensure a high loading capacity and deliver active agents selectively.
- Should not release the drug prematurely. Release must be controlled.
- MSNs must present a homogeneous size distribution and low polydispersity.
- MSNs must be stable and should not aggregate.

Although MSNs meet many of these requirements, there is still no MSNs approved in clinical trials, maybe because of the complex interactions between nanoparticles and human organism.<sup>80</sup> Still, great progress has been achieved over a decade, from morphological characterization to *in vivo* treatments (Figure 1.8).

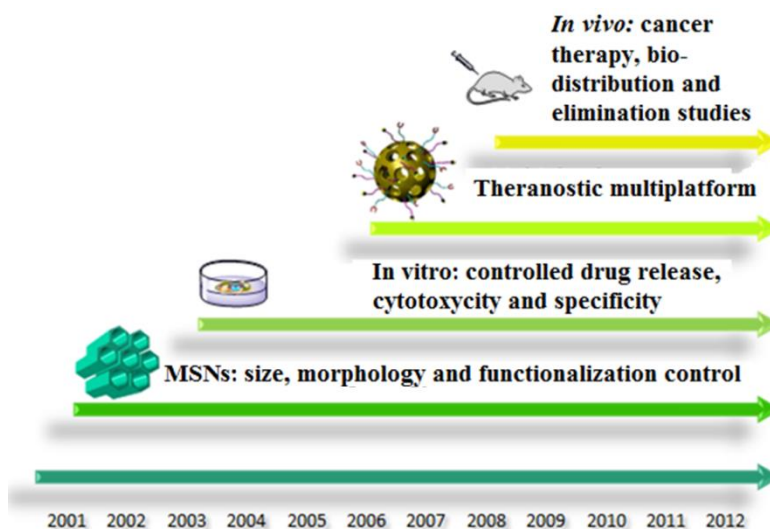


Figure 1.8. Advances in MSNs clinical applications.

A key issue for the application of nanoparticles in biomedicine is their toxicity.<sup>81</sup> Although, MSNs are intrinsically non-toxic; its final toxicity depends on the final anchored active agents. So, in each case, toxicity of final MSNs must be studied. Concerning MSNs elimination and accumulation, in general, liver and spleen are the major organs where MSNs accumulate.<sup>81</sup> The silica elimination occurs mostly through its orthosilicic acid decomposition and subsequent excretion via renal system.<sup>19</sup> Nevertheless, the exact process is still unknown.

One of the main challenges in developing nanoparticle systems for drug delivery is to predict and control the physicochemical properties that will act *in vivo*, as well as setting up analytical techniques capable of characterizing the properties of these systems.<sup>82</sup> The main drawback of nanoparticles in general as delivery systems is that these materials are very complex and require a very detailed characterization. Each batch is different and prone to vary in size or organization. The constant improvement of characterization techniques would allow, in the near future, a way to establish correlations between *in vitro* and *in vivo* behaviors, reducing the number of studies to perform an accurate characterization and enhancing reproducibility between batches. *In vitro* and *in vivo* characterizations are crucial to avoid toxicological effects, immunological reactions or undesired accumulation in macrophages, liver, kidneys, spleen and lungs.<sup>83</sup>

Unfortunately, another challenge is the stability of most nanomaterials in biological fluids. The incorporation of nanoparticles into the bloodstream causes a strong reaction with serum proteins, lipids, membranes, cells, DNA, different organelles and small molecules, forming a shell of aggregated compounds known as the “protein corona”.<sup>84</sup> This protein corona alters the size and interfacial composition of a nanomaterial, giving it a biological identity that is distinct from its initial synthetic identity.<sup>80,85</sup> This is the reason why many of the questions regarding the biocompatibility and biodistribution of MSNs *in vivo* still remain unanswered.<sup>86</sup>

Despite these drawbacks, nanoparticles in general and MSNs in particular possess excellent properties to be approved one day as multifunctional nanoplatfoms. It is about time that the effort made in nanotechnology paid off. Definitely, there is plenty of room at the bottom for improvement!<sup>87</sup>

## **1.5. Introduction of organic moieties to MSNs surface**

In order to synthesize new generation multinanocarriers with different active agents such as PEG, Ab, proteins, siRNA, drugs, gatekeepers or probes, an easy, fast and robust chemistry must be applied. Thus, organic moieties must be introduced into the inorganic silica nanoparticle structure. Luckily enough, MSNs can be produced and functionalized easily.<sup>30,35,88</sup> In fact, one of the main advantages of using MSNs is that organic moieties can easily be introduced through co-condensation or silanization processes and therefore, MSNs can be functionalized with any desirable moiety. This quality is crucial for the use of these nanoparticles as bioactive multinanoplatfoms. In fact, MSNs are considered to be organic nanoparticles in an inorganic matrix, which introduces the concept of hybrid organic-inorganic nanoparticles.<sup>23,34</sup>

As previously outlined before, MSNs present two possible functionalization domains: the inner surface inside the porous channels and the outer external surface. Thus, there are three possible strategies to incorporate different organic moieties in MSNs surfaces: by anchorage, grafting and co-condensation.<sup>22,23</sup>

### **1.5.1. Anchorage**

Anchorage is generally used for fluorescent molecules, imaging probes or contrast agents in order to either determine the location or monitor the nanocarriers in the organism.<sup>89,44</sup> These sensing probes are generally anchored inside MSNs matrix through co-condensation processes

during MSN formation (Figure 1.9). Therefore, any possible interference with later reactions is avoided.<sup>89</sup>



Figure 1.9. Image probe anchored in MSNs matrix.

### 1.5.2. Grafting

Grafting or post-synthetic approach is a methodology that modifies MSN-walls through silanization, once nanoparticles have already been formed.<sup>22,23</sup> In this process, superficial silanols (Si-OH) act as anchorages when a functional silane is introduced (Figure 1.10). Grafting approach adds functional moieties in both inner and outer surface but it is widely believed that external surface is generally more accessible than the inner domain.<sup>90,91</sup>

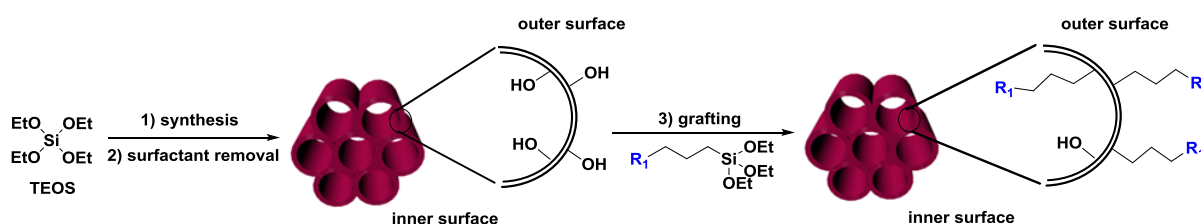


Figure 1.10. Post-synthetic grafting functionalization.

Grafting silanization takes place either through free ( $\equiv$  Si-OH) or geminal silanol groups ( $=$  Si(OH)<sub>2</sub>). The original structure of MSNs is generally maintained although some examples in the literature describe that grafting can easily erode MSNs surface.<sup>92</sup> Moreover, grafting is described as a non-homogenous process where functional groups are added heterogeneously. However, the main advantage of the grafting process is that it allows an easy functionalization in the outer surface of MSNs.

### 1.5.3. Co-condensation

The co-condensation approach is based on the sol-gel process.<sup>22,23</sup> In this case, a functionalized silane is added simultaneously with a silica precursor (TEOS) in MSNs formation. Therefore, it is a one-step process (Figure 1.11). Co-condensation, normally allows an homogeneous addition of functional groups in both inner and outer surface.<sup>91,92</sup> Depending on the nature of the silane precursor it is possible to reach preferably one surface over the other.<sup>22,23</sup> For example, in the



case of amino silane groups, such as aminopropyltriethoxy silane (APTES), amine moieties seem to be preferably added into the inner surface than on the external domain.<sup>93</sup>

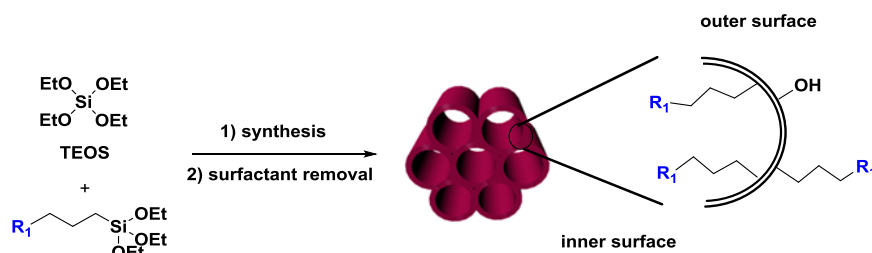


Figure 1.11. One-pot co-condensation process.

In fact, Lim *et al.*,<sup>92</sup> compared the differences between post grafting and co-condensation processes when a same functional silane, in this case vinyl silane, was added to MSNs. The authors finally concluded that co-condensed MSNs had a homogenous vinyl group distribution while post grafting methodology gave a disordered material. Nevertheless, both grafting and co-condensation approaches functionalize MSNs on the inner and the outer surface and therefore do not guarantee a regioselective functionalization.<sup>90,91</sup>

## 1.6. Regioselective bifunctionalization

In order to attain the level of complexity needed for the design of “smart” nanocarriers, it is necessary to develop, not only new methods for the introduction of organic moieties, but also efficient methodologies for the regioselective functionalization of the two surfaces of the MSNs with orthogonal groups.<sup>20,94</sup> A regioselective and orthogonal coating of the external and inner porous surface with the proper functional group is crucial for the fine tuning of the payload release. For instance, the presence of inner amines moieties<sup>95–97</sup> facilitates both the loading and release of drugs while, the external surface is suitable for installing stimulus-responsive systems for drug release<sup>4</sup> or for the attachment of functional moieties for cell targeting.<sup>98</sup>

A search in literature revealed that a way to introduce some regioselectivity in the bifunctionalization of MSNs consist of using monofunctionalized nanoparticles with the porous blocked by the surfactant.<sup>99</sup> From monofunctionalized MSNs, introduced by a co-condensation methodology,<sup>100–102</sup> a later grafting process, while the surfactant is still present in MSN matrix, results in the functionalization of **R**<sub>2</sub> only on the outer surface (Figure 1.12). Due to the protecting effect of the surfactant, the inner surface is not affected by the grafting procedure and only the external domain is accessible.

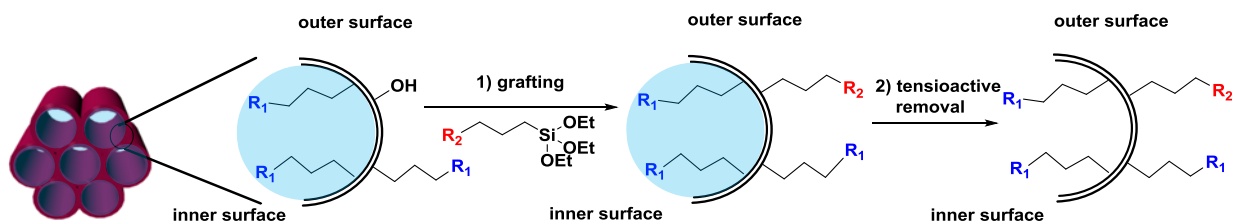


Figure 1.12. Non-regioselective bifunctionalization.

Nevertheless, since the starting material is already monofunctionalized, both at the inner and at the outer surface, the outer surface will be functionalized with a mix of functional groups ( $R_1$  and  $R_2$ ), providing that these functional groups are chemically compatible. Otherwise, this methodology is not possible.

In conclusion, strictly speaking there is no regioselective procedure for the regioselective functionalization of nanoparticles.

### 1.7. MSNs covalent strategies for functionalization

Once MSNs have been functionalized with organic moieties, multifunctional materials can be prepared. In order to incorporate different sensors, drugs or gates to MSN, bioconjugate techniques can be used.<sup>103</sup>

As a matter of fact, much of the inspiration for building reactive nanoparticles is based on "click" chemistry reactions.<sup>104</sup> The "click" chemistry concept was first introduced by KB Sharpless in 2001 and describes any chemical reaction with quantitative yields, high efficiency, selective, with no purifications and that can be used in mild reaction conditions.

Among all possible functional groups that could be used for "click" reactions, only a few are used in the vast majority of peptides and proteins, which consist mostly of primary amines, carboxylic acids and thiols. Therefore, all nanoparticle functionalization strategy should focus on the use of easy, quick and effective reagents for the reaction with these functional groups. Here we summarize some of the most interesting coupling strategies for nanoparticles conjugation: amide formation, CuAAC cycloaddition, thiol, urea, thiourea, imine and hydrazone formation.<sup>103,105,106</sup>

### 1.7.1. Steglich reaction: carbodiimide coupling

Amide formation requires the participation of an activating acid reagent. A widely used protocol is the Steglich reaction or carbodiimide method, which consist of the activation of carboxylic acid, for instance with the formation of the corresponding *N*-hydroxysuccinimide ester. This activation is carried out in the presence of a coupling agent such as 1-ethyl-3-(dimethylaminopropyl) carbodiimide (EDC). Finally the desired amine reacts with the activated ester to provide amide bond with excellent yields (> 90%) (Figure 1.13).

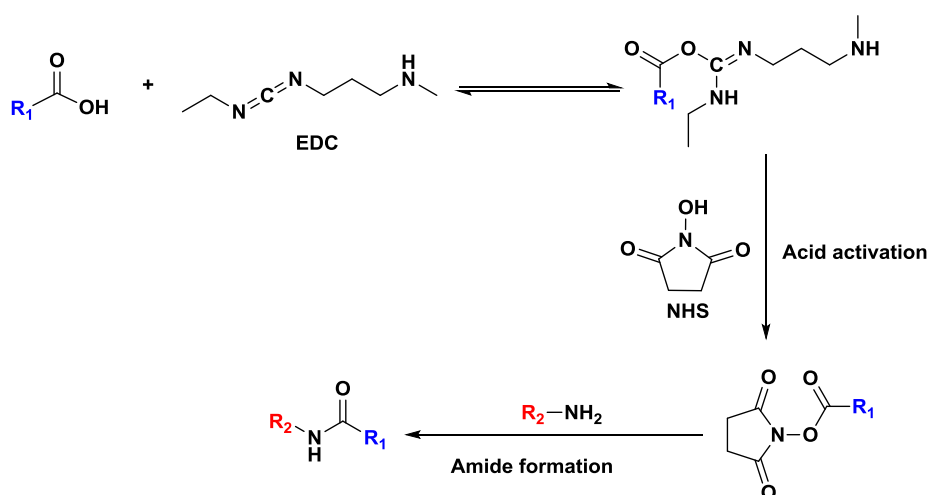


Figure 1.13. Amide bond formation.

Since a great number of molecules bear an ester or carboxylic acid functionality, this is probably one of the most popular ways to functionalize amine nanoparticles.<sup>40,93</sup>

### 1.7.2. CuACC cycloaddition: the “click” chemistry

Another noteworthy bioconjugation reaction is the well-known azide-alkyne cycloaddition catalyzed by Cu (I), (CuAAC)<sup>104,107–109</sup> This type of chemistry involves the formal cycloaddition of an alkyne and an azide to form a 1,2,3-triazole ring, which serves as a strong linkage between the nanoparticle and the molecule that is going to be attached (Figure 1.14).

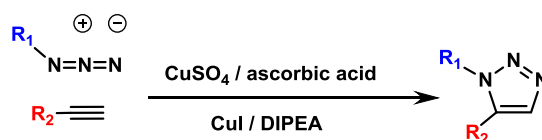


Figure 1.14. 1,2,3-triazol formation.

This process has been proved to be highly versatile in the conjugation of small and bulky molecules, such as peptides, enzymes or proteins, at the external surface of mesoporous silica nanoparticles.<sup>90,100,110,111</sup> However this reaction has a great disadvantage which is that it uses copper as a catalyst and therefore, it is vital to assure the total removal of any Cu trace.<sup>112</sup> Current strategies for Cu elimination are the use of EDTA and *N,N*-diethyldithiocarbamate complexants. Nevertheless, these strategies present several problems such as a loss of nanoparticles by washing with EDTA<sup>90</sup> or an increased toxicity when using *N,N*-diethyldithiocarbamate.<sup>113</sup>

### 1.7.3. Disulfide formation

Maleimides are electrophilic molecules which are highly reactive and selective towards thiols. These moieties can easily be formed through the reaction of an amine with maleic anhydride. Moreover, thiols are present in a large number of proteins and peptides as cysteine residues, which makes this strategy one of the most used approaches for coupling proteins and peptides (Figure 1.15).<sup>114</sup> In addition, this reaction can take place in water, DMSO and DMF.

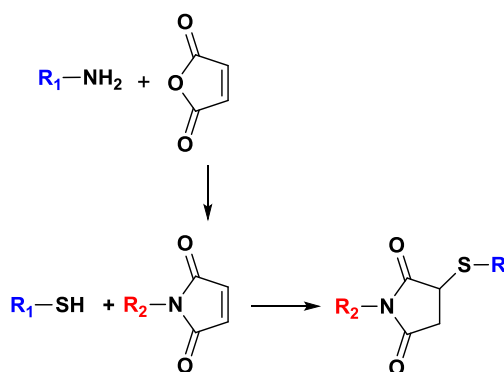


Figure 1.15. Selective reaction between a thiol and a maleimide.

Another possibility to selectively functionalize thiol groups is by using their ability to form disulfide bonds by oxidation (Figure 1.16). However, this strategy needs both the linker and the desirable specie to present a thiol functionality.

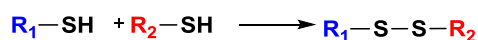


Figure 1.16. Disulfide formation from two dithiols.

The last strategy used for the formation of disulfide bonds is the utilization of pyridyl disulfide (Figure 1.17).<sup>115,116</sup> One great advantage of this methodology is that pyridine-2-thione is released during the reaction and can easily be monitored by spectrophotometry.

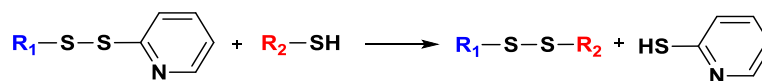


Figure 1.17. Disulfide formation with pyridine-2-thione.

#### 1.7.4. Isocyanates

Isocyanates can easily react with a wide range of nucleophiles such as amines, alcohols, and even water (Figure 1.18).<sup>117</sup> Therefore, isocyanates are unspecific, non-selective and prone to hydrolysis, not allowing their use with non-anhydrous solvents and precluding their storage.<sup>118</sup>

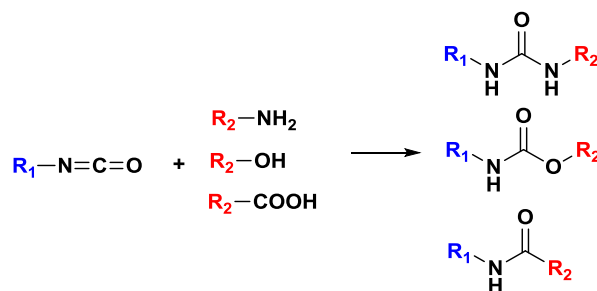


Figure 1.18. Urea, urethane and amide formation.

#### 1.7.5. Isothiocyanates

Unlike isocyanates, isothiocyanates are highly selective to amine moieties and do not react in water or alcohol solvents. Moreover, isothiocyanates are stable and can be stored. The reaction is quantitative and can be used with different solvents such as DMSO,  $\text{CHCl}_2$ ,  $\text{H}_2\text{O}$  or EtOH (Figure 1.19). Moreover, isothioureia formation is a widely used protocol in bioconjugation, for example in the case of isothiocyanate fluorescein (FITC) conjugation. Nevertheless, in the case of MSNs, by and large, FITC is introduced through grafting, by a silane linker.<sup>89,119</sup> Very few examples of isothioureia functionalization in MSNs have been described.<sup>120</sup>

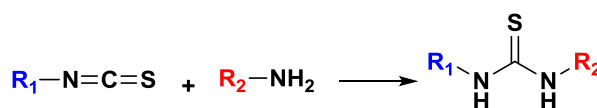


Figure 1.19. Thiourea formation.

### 1.7.6. Carbonyl nucleophilic substitution

The electrophilic carbon atoms of aldehydes and ketones are suitable for nucleophilic attack by amines. In this reaction, the initial C=O double bond is replaced by the formation of C=N bond (Figure 1.20).<sup>105,106</sup> The final compound is an imine moiety, also known as Schiff base. Imines are formed when any primary amine reacts with an aldehyde or ketone under acid catalysis; otherwise the reaction is very slow or incomplete.

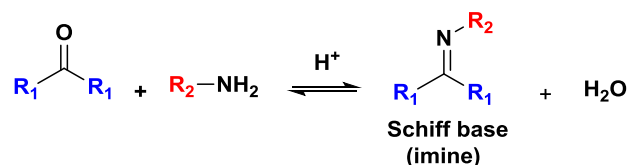


Figure 1.20. Imine formation.

Hydrazone formation is a reaction between aldehydes /ketones and hydrazines (Figure 1.21). The hydrazone bond is pH sensitive, and hydrolyzation occurs at low pH. Hydrazones are widely used as pH scissile linkers to control drug release in acidic environments.<sup>75,76</sup>

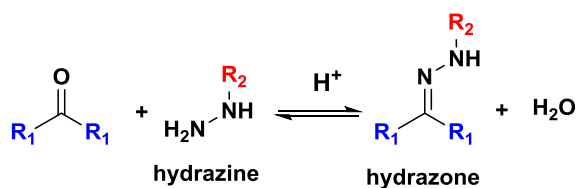
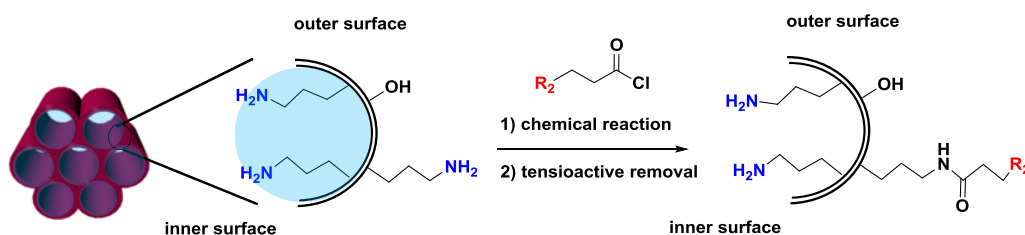


Figure 1.21. Hydrazone formation.

## 1.8. Aims

With high loading surface areas and low toxicity, MSNs exhibit outstanding properties for their application as carriers in drug delivery. However, diverse anchoring synthetic strategies are needed in order to functionalize MSNs domains with multiple substituents. A quick, clean, high yield and selective chemistry is necessary to functionalize different agents with the simplest and most direct procedure, which today is known under the concept of "click chemistry". In this PhD dissertation, it is proposed to explore efficient "click" reactions for the obtaining of Regioselective Orthogonal Bifunctionalized MSNs, in order to apply them for sensing and biomedical applications. To do so, a general methodology for the obtaining of complete regioselective materials must be carried out. Therefore, by synthesizing monofunctionalized MSNs by co-condensation approach, without removing the tensioactive, and by a direct reaction instead of a grafting process, it is possible to regioselectively bifunctionalize the outer surface with any desirable moiety. For example, if amino groups were added by co-condensation, while surfactant is protecting the inner surface, amines can easily react with activated acids or isothiocyanates that would give a new functionality, only on the external surface (Figure 1.22). This approach will yield complete regioselective bifunctionalized MSNs.



**Figure 1.22. Complete regioselective bifunctionalization of MSNs.**

Therefore, these regioselective bifunctionalized MSNs will be used for the design of new nanocarriers for biomedical applications.

To this purpose, aminated-MSNs are used. Amino-MSNs have been widely studied,<sup>121–123</sup> since they are easy to obtain and functionalize,<sup>103,124</sup> in addition to having excellent properties for drug loading and release applications.<sup>27,96,97,125</sup> Thus, from amino-MSNs, the preparation of three efficient regioselective bifunctionalized MSNs is proposed: amino-azide MSNs, amino-isothiocyanate MSNs and amino-aldehyde MSNs (Figure 1.23).

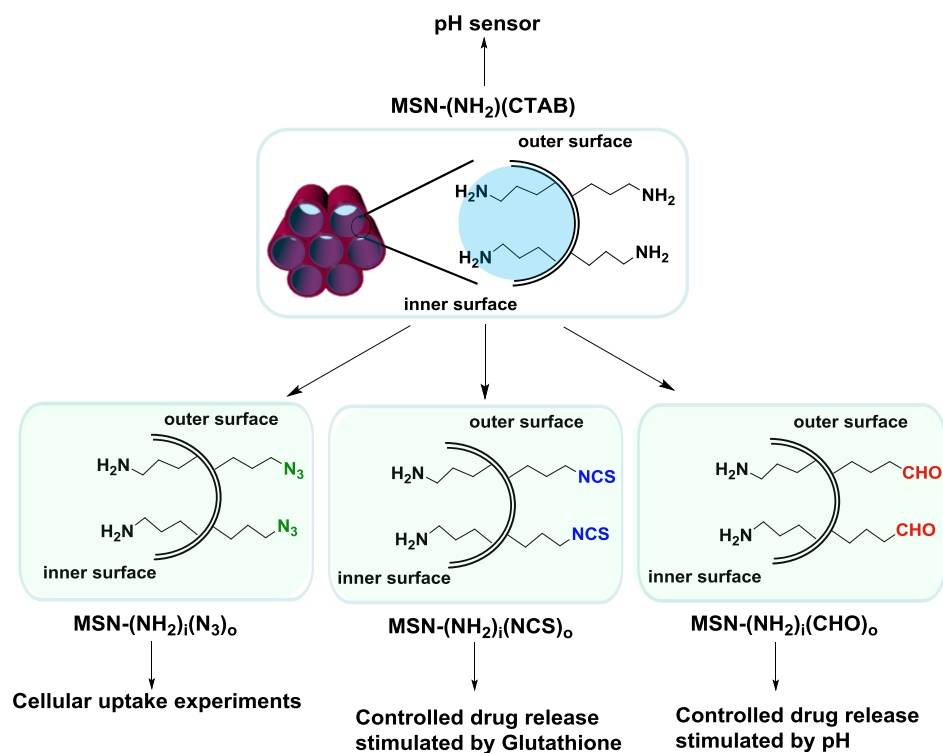


Figure 1.23. Schematic representation of the thesis aims.

Therefore, the aims of this PhD thesis are summarized as follows:

1. Development of a methodology for the preparation of monodispersed and small (50-100 nm) aminated-MSN (Chapter 2).
2. Development of a general methodology for the functionalization of amino-MSNs with 4-amino-1,8-naphthalimides to use them in sensor applications as logic gates (Chapter 3).
3. Development of a regioselective methodology for the synthesis of amine-azide, amine-isothiocyanate and amine-aldehyde MSNs.
  - 3.1. Synthesis, characterization and regioselective orthogonal bifunctionalization of amino-azido MSNs (MSN-(NH<sub>2</sub>)<sub>i</sub>(N<sub>3</sub>)<sub>o</sub>) for their application as cell penetrating systems with quinolin foldamers (Chapter 4).
  - 3.2. Synthesis, characterization and regioselective orthogonal bifunctionalization of amino-isothiocyanate MSNs. Application of these MSN-(NH<sub>2</sub>)<sub>i</sub>(NCS)<sub>o</sub> for controlled release of Ataluren for the treatment of Duchenne Muscular Dystrophy (DMD), stimulated by a high glutathione redox potential (GSH) media (Chapter 5).
  - 3.3. Synthesis, characterization and regioselective orthogonal bifunctionalization of amino-aldehyde MSNs (MSN-(NH<sub>2</sub>)<sub>i</sub>(CHO)<sub>o</sub>) for their application as a dual doxorubicin-camptothecin pH controlled drug release system, for cancer treatment (Chapter 6).



## 1.9. Bibliography

- (1) Thassu, D.; Pathak, Y.; Deleers, M. *Nanoparticulate drug delivery systems : An overview*; Informa Healthcare, Ed.; New York, NY, 2007.
- (2) Llorente, C. B.; Junquera, E. C.; Gago, J. Á. M.; Domingo, P. A. S. *Nanociencia y nanotecnología. Entre la ciencia ficción del presente y la tecnología del futuro. FECYT (Fundación española para la ciencia y la tecnología)*; Madrid, 2008.
- (3) Zhang L, Gu FX, Chan JM, Wang AZ, Langer RS, F. O. *Clin Pharmacol Ther* **2008**, *83* (5), 761–769.
- (4) Li, Z.; Barnes, J. C.; Bosoy, A.; Stoddart, J. F.; Zink, J. I. *Chem. Soc. Rev.* **2012**, *41* (7), 2590–2605.
- (5) Choi, K. Y.; Liu, G.; Lee, S.; Chen, X. *Nanoscale* **2012**, *4* (2), 330–342.
- (6) Chen, N.-T.; Cheng, S.-H.; Souris, J. S.; Chen, C.-T.; Mou, C.-Y.; Lo, L.-W. *J. Mater. Chem. B* **2013**, *1* (25), 3128–3135.
- (7) Ambrogio, M. W.; Thomas, C. R.; Zhao, Y. L.; Zink, J. I.; Stoddart, J. F. *Acc. Chem. Res.* **2011**, *44* (10), 903–913.
- (8) Rao, J. P.; Geckeler, K. E. *Prog. Polym. Sci.* **2011**, *36* (7), 887–913.
- (9) Scott, R.; Wilson, O.; Crooks, R. *J. Phys. Chem. B* **2005**, *109* (2), 692–704.
- (10) Yogeshkumar Malam, Marilena Loizidou, A. M. S. *Trends Pharmacol. Sci.* **2009**, *30* (11), 592–599.
- (11) Dhembre, G. N.; Moon, R. S.; Kshirsagar, R. V. *Int. J. Pharma Bio Sci.* **2011**, *2* (2), 109–116.
- (12) Tang, L.; Cheng, J. *Nano Today* **2013**, *8* (3), 290–312.
- (13) Saha, K.; Agasti, S. S.; Kim, C.; Li, X.; Rotello, V. M. *Chem. Rev.* **2012**, *112* (5), 2739–2779.
- (14) Algar, W. R.; Tavares, A. J.; Krull, U. J. *Anal. Chim. Acta* **2010**, *673* (1), 1–25.
- (15) De Volder, M. F. L.; Tawfick, S. H.; Baughman, R. H.; Hart, a J. *Science* **2013**, *339* (6119), 535–539.
- (16) Tarn, D.; Ashley, C. E.; Xue, M. I. N.; Carnes, E. C.; Zink, J. I.; Brinker, C. J. *Acc. Chem. Res.* **2013**, *46* (3), 792–801.
- (17) Colilla, M.; González, B.; Vallet-Regí, M. *Biomater. Sci.* **2013**, 114–134.
- (18) Argyo, C.; Weiss, V.; Bräuchle, C.; Bein, T. *Chem. Mater.* **2014**, *26* (1), 435–451.
- (19) Mamaeva, V.; Sahlgren, C.; Lindén, M. *Adv. Drug Deliv. Rev.* **2013**, *65* (5), 689–702.
- (20) Slowing, I. I.; Vivero-Escoto, J. L.; Trewyn, B. G.; Lin, V. S.-Y. *J. Mater. Chem.* **2010**, *20* (37), 7924–7937.
- (21) Beck, J. S.; Vartuli, J. C.; Roth, W. J.; Leonowicz, M. E.; Kresge, C. T.; Schmitt, K. D.; Chu, C. T. W.; Olson, D. H.; Sheppard, E. W.; McCullen, S. B.; Higgins, J. B.; Schlenkert, J. L. *J. Am. Chem. Soc.* **1992**, *114*, 10834–10843.
- (22) Hoffmann, F.; Cornelius, M.; Morell, J.; Fröba, M. *Angew. Chemie Int. Ed.* **2006**, *45* (20), 3216–3251.
- (23) Andreas Stein, Brian J Melde, R. C. S. *Adv. Mater.* **2000**, *12* (19), 1403–1418.
- (24) Harrison Wanyika. *African J. Pharm. Pharmacol.* **2011**, *5* (21), 2402–2410.
- (25) Lai, C. J. *Thermodyn. Catal* **2013**, *5* (1), 1–3.

- (26) Rosenholm, J. M.; Sahlgren, C.; Lindén, M. *Nanoscale* **2010**, 2 (10), 1870–1883.
- (27) Vallet-Regí, M.; Balas, F.; Arcos, D. *Angew. Chemie Int. Ed.* **2007**, 46 (40), 7548–7558.
- (28) Vallet-Regí, M. *ISRN Mater. Sci.* **2012**, 2012, 1–20.
- (29) Vallet-Regí, M. *J. Intern. Med.* **2010**, 267 (1), 22–43.
- (30) Mai, W. X.; Meng, H. *Integr. Biol.* **2012**, 19–28.
- (31) Sancenón, F.; Pascual, L.; Oroval, M.; Aznar, E.; Martínez-Máñez, R. *Chem. Open* **2015**, 4 (4), 418–437.
- (32) McNeil, S. E. *J. Leukoc. Biol.* **2005**, 78 (3), 585–594.
- (33) Slowing, I. I.; Vivero-Escoto, J. L.; Wu, C.-W.; Lin, V. S. Y. *Adv. Drug Deliv. Rev.* **2008**, 60 (11), 1278–1288.
- (34) Vallet-Regí, M.; Colilla, M.; González, B. *Chem. Soc. Rev.* **2011**, 40 (2), 596–607.
- (35) Cotí, K. K.; Belowich, M. E.; Liong, M.; Ambrogio, M. W.; Lau, Y.; Khatib, H.; Zink, J. I.; Khashab, N. M.; Stoddart, J. F. *Nanoscale* **2009**, 1 (1), 16–39.
- (36) Haag, R. *Angew. Chemie - Int. Ed.* **2004**, 43 (3), 278–282.
- (37) Jeffrey I. Zink, Andre E. Nel, Tian Xia, Zhaoxia Ji, Huan Meng, Zongxi Li, Monty Liong, Min Xue, D. Y. T. US 2012/0207795 A1-Cationic polymer coated mesoporous silica nanoparticles and uses thereof, 2012.
- (38) Meng, H.; Mai, W. X.; Zhang, H.; Xue, M.; Xia, T.; Lin, S.; Wang, X.; Zhao, Y. *ACS Nano* **2013**, 7 (2), 994–1005.
- (39) James B Delehanty, Kelly Boeneman, Christopher E Bradburne, Kelly Robertson, Jason E Bongard, I. L. M. *Ther. Deliv.* **2010**, 1 (3), 411–433.
- (40) Pan, L.; He, Q.; Liu, J.; Chen, Y.; Ma, M.; Zhang, L.; Shi, J. *J. Am. Chem. Soc.* **2012**, 134 (13), 5722–5725.
- (41) Tsai, C. P.; Chen, C. Y.; Hung, Y.; Chang, F. H.; Mou, C. Y. *J. Mater. Chem.* **2009**, 19 (32), 5737–5743.
- (42) Joshi, H. M.; De, M.; Richter, F.; He, J.; Prasad, P. V.; Dravid, V. P. *Contrast Media Mol Imaging* **2012**, 7 (5), 460–468.
- (43) Rossi, L. M.; Shi, L.; Quina, F. H.; Rosenzweig, Z. *Langmuir* **2005**, 21 (10), 4277–4280.
- (44) Slowing, I. I.; Trewyn, B. G.; Giri, S.; Lin, V. S. Y. *Adv. Funct. Mater.* **2007**, 17 (8), 1225–1236.
- (45) Trewyn, B. G.; Giri, S.; Slowing, I. I.; Lin, V. S.-Y. *Chem. Commun.* **2007**, No. 31, 3236–3245.
- (46) Moro, A. J.; Schmidt, J.; Doussineau, T.; Lapresta-Fernandéz, A.; Wegener, J.; Mohr, G. *J. Chem. Commun.* **2011**, 47 (21), 6066–6068.
- (47) Veale, E. B.; Gunnlaugsson, T. *Annu. reports B* **2010**, 106, 376–406.
- (48) Wang, A. Z.; Langer, R.; Farokhzad, O. C. *Annu. Rev. Med.* **2012**, 63 (1), 185–198.
- (49) Cheng, S. H.; Lee, C. H.; Chen, M. C.; Souris, J. S.; Tseng, F. G.; Yang, C. S.; Mou, C. Y.; Chen, C. T.; Lo, L. W. *J. Mater. Chem.* **2010**, 20 (29), 6149–6157.
- (50) Schulz, A.; McDonagh, C. *Soft Matter* **2012**, 8 (9), 2579–2585.
- (51) Ai, H. W. *Sensors* **2014**, 14 (9), 17829–17831.
- (52) Isherwood, B.; Timpson, P.; McGhee, E. J.; Anderson, K. I.; Canel, M.; Serrels, A.; Brunton, V. G.; Carragher, N. O. *Pharmaceutics* **2011**, 3 (2), 141–170.

- 
- (53) Agasti, S. S.; Rana, S.; Park, M. H.; Kim, C. K.; You, C. C.; Rotello, V. M. *Adv. Drug Deliv. Rev.* **2010**, *62* (3), 316–328.
- (54) Ruedas-Rama, M. J.; Walters, J. D.; Orte, A.; Hall, E. A. H. *Anal. Chim. Acta* **2012**, *751*, 1–23.
- (55) Gao, W.; Chan, J.; Farokhzad, O. C. *Mol. Pharm.* **2010**, *7* (6), 1913–1920.
- (56) Yang, K. N.; Zhang, C. Q.; Wang, W.; Wang, P. C.; Zhou, J. P.; Liang, X. J. *Cancer Biol. Med.* **2014**, *11* (1), 34–43.
- (57) Agostini, A.; Mondragón, L.; Coll, C.; Aznar, E.; Marcos, M. D.; Martínez-Máñez, R.; Sancenón, F.; Soto, J.; Pérez-Payá, E.; Amorós, P. *Chem. Open* **2012**, *1* (1), 17–20.
- (58) El Sayed, S.; Giménez, C.; Aznar, E.; Martínez-Máñez, R.; Sancenón, F.; Licchelli, M. *Org. Biomol. Chem.* **2015**, *13* (4), 1017–1021.
- (59) Mei, X.; Yang, S.; Chen, D.; Li, N.; Li, H.; Xu, Q.; Ge, J.; Lu, J. *Chem. Commun.* **2012**, *48* (80), 10010–10012.
- (60) Hyun-Jong Kim, Hirofumi Matsuda, Haoshen Zhou, and I. H. *Adv. Mater.* **2006**, *18*, 3083–3088.
- (61) Bringas, E.; Köysüren, Ö.; Quach, D. V.; Mahmoudi, M.; Aznar, E.; Roehling, J. D.; Marcos, M. D.; Martínez-Máñez, R.; Stroeve, P. *Chem. Commun.* **2012**, *48* (45), 5647–5649.
- (62) Tamanoi, F.; Yanes, R. *Ther. Deliv.* **2013**, *3* (3), 389–404.
- (63) Lindén, J. M. R. V. M. C. S. M. *Nanomedicine* **2012**, *7* (1), 111–120.
- (64) Rosenholm, J. M.; Mamaeva, V.; Sahlgren, C.; Lindén, M. *Nanomedicine* **2012**, *7* (1), 111–120.
- (65) Vivero-Escoto, J. L.; Slowing, I. I.; Trewyn, B. G.; Lin, V. S. Y. *Small* **2010**, *6* (18), 1952–1967.
- (66) Wang, C.; Li, Z.; Cao, D.; Zhao, Y. L.; Gaines, J. W.; Bozdemir, O. A.; Ambrogio, M. W.; Frasconi, M.; Botros, Y. Y.; Zink, J. I.; Stoddart, J. F. *Angew. Chemie* **2012**, *51* (22), 5460–5465.
- (67) Angelos, S.; Liong, M.; Choi, E.; Zink, J. I. *Chem. Eng. J.* **2008**, *137* (1), 4–13.
- (68) Lai, C. Y.; Trewyn, B. G.; Jeftinija, D. M.; Jeftinija, K.; Xu, S.; Jeftinija, S.; Lin, V. S. Y. *J. Am. Chem. Soc.* **2003**, *125* (15), 4451–4459.
- (69) Chen, X.; Cheng, X.; Soeriyadi, A. H.; Sagnella, S. M.; Lu, X.; Scott, J. a.; Lowe, S. B.; Kavallaris, M.; Gooding, J. J. *Biomater. Sci.* **2014**, *2* (1), 121–130.
- (70) Dong, J.; Xue, M.; Zink, J. J. I. *Nanoscale* **2013**, *5* (21), 10300–10306.
- (71) Gayam, S. R.; Wu, S.-P. *J. Mater. Chem. B* **2014**, *2* (40), 7009–7016.
- (72) Chang, B.; Chen, D.; Wang, Y.; Chen, Y.; Jiao, Y.; Sha, X.; Yang, W. *Chem. Mater.* **2013**, *25* (4), 574–585.
- (73) Mondragón, L.; Mas, N.; Ferragud, V.; de la Torre, C.; Agostini, A.; Martínez-Máñez, R.; Sancenón, F.; Amorós, P.; Pérez-Payá, E.; Orzáez, M. *Chem. Eur. J.* **2014**, *20* (18), 5271–5281.
- (74) Agostini, A.; Mondragón, L.; Pascual, L.; Aznar, E.; Coll, C.; Martínez-Máñez, R.; Sancenón, F.; Soto, J.; Marcos, M. D.; Amorós, P.; Costero, A. M.; Parra, M.; Gil, S. *Langmuir* **2012**, *28* (41), 14766–14776.
- (75) Fan, J.; Fang, G.; Wang, X.; Zeng, F.; Xiang, Y.; Wu, S. *Nanotechnology* **2011**, *22* (455102), 1–11.

- (76) Lee, C. H.; Cheng, S. H.; Huang, I. P.; Souris, J. S.; Yang, C. S.; Mou, C. Y.; Lo, L. W. *Angew. Chemie Int. Ed.* **2010**, *49* (44), 8214–8219.
- (77) Cheng, Y.; Morshed, R.; Cheng, S.H; Tobias, A; Auffinger, B; Wainwright, D.A.;Zhang, L.; Yunis, C; Han, Y.; Chen, C.T; Lo, L. W.; Aboody, K. S.; Ahmed, A. U.; Lesniak, M. *Small* **2013**, *9* (14), 4123–4129.
- (78) Asefa, T.; Tao, Z. *Chem. Res. Toxicol.* **2012**, *25* (11), 2265–2284.
- (79) Lin, Y. S.; Hurley, K. R.; Haynes, C. L. *J. Phys. Chem. Lett.* **2012**, *3* (3), 364–374.
- (80) Clemments, A. M.; Muniesa, C.; Landry, C. C.; Botella, P. *RSC Adv.* **2014**, *4* (55), 29134–29138.
- (81) Yu, T.; Greish, K.; McGill, L. D.; Ray, A.; Ghandehari, H. *ACS Nano* **2012**, *6* (3), 2289–2301.
- (82) W. Jiang, R. Lionberger, L. Y. *Bioanalysis* **2011**, *3* (3), 333–344.
- (83) Wang, A. Z. *Nanomedicine* **2012**, *7* (10), 1463–1465.
- (84) Nel, A. E.; Mädler, L.; Velegol, D.; Xia, T.; Hoek, E. M. V; Somasundaran, P.; Klaessig, F.; Castranova, V.; Thompson, M. *Nat. Mater.* **2009**, *8* (7), 543–557.
- (85) Paula, A. J.; Araujo Júnior, R. T.; Martinez, D. S. T.; Paredes-Gamero, E. J.; Nader, H. B.; Durán, N.; Justo, G. Z.; Alves, O. L. *ACS Appl. Mater. Interfaces* **2013**, *5* (17), 8387–8393.
- (86) Walkey, C. D.; Chan, W. C. W. *Chem. Soc. Rev.* **2012**, *41* (7), 2780–2799.
- (87) Richard P. Feynman. Plenty of Room at the Bottom; Richard P. Feynman talk to the American Physical Society in Pasadena on December 1959.
- (88) Trewyn, B. G.; Slowing, I. I.; Giri, S.; Chen, H. T.; Lin, V. S. Y. *Acc. Chem. Res.* **2007**, *40* (9), 846–853.
- (89) Lu, F.; Wu, S. H.; Hung, Y.; Mou, C. Y. *Small* **2009**, *5* (12), 1408–1413.
- (90) Malvi, B.; Sarkar, B. R.; Pati, D.; Mathew, R.; Ajithkumar, T. G.; Sen Gupta, S. *J. Mater. Chem.* **2009**, *19* (10), 1409–1416.
- (91) Hara, K.; Akahane, S.; Wiench, J. W.; Burgin, B. R.; Ishito, N.; Lin, V. S.-Y.; Fukuoka, A.; Pruski, M. *J. Phys. Chem. C* **2012**, *116* (12), 7083–7090.
- (92) Lim, M. H.; Stein, A. *Chem. Mater.* **1999**, *11* (11), 3285–3295.
- (93) Cheng, S. H.; Lee, C. H.; Yang, C. S.; Tseng, F. G.; Mou, C. Y.; Lo, L. W. *J. Mater. Chem.* **2009**, *19* (9), 1252–1257.
- (94) Huang, Y.; Xu, S.; Lin, V. S. Y. *Angew. Chemie Int. Ed.* **2011**, *50* (3), 661–664.
- (95) Wang, G.; Otuonye, A. N.; Blair, E. a.; Denton, K.; Tao, Z.; Asefa, T. *J. Solid State Chem.* **2009**, *182* (7), 1649–1660.
- (96) Natarajan, S. K.; Selvaraj, S. *RSC Adv.* **2014**, *4* (28), 14328–14334.
- (97) Kamarudin, N. H. N.; Jalil, A.; Triwahyono, S.; Salleh, N. F. M.; Karim, A. H.; Mukti, R. R.; Hameed, B. H.; Ahmad, A. *Microporous Mesoporous Mater.* **2013**, *180*, 235–241.
- (98) Rosenholm, J.; Sahlgren, C.; Lindén, M. *J. Mater. Chem.* **2010**, *20* (14), 2707–2713.
- (99) F. de Juan and E. Ruiz-Hitzky. *Adv. Mater.* **2000**, *12* (6), 430–432.
- (100) Dickschat, A. T.; Behrends, F.; Bühner, M.; Ren, J.; Weiß, M.; Eckert, H.; Studer, A. *Chem. Eur. J.* **2012**, *18* (52), 16689–16697.
- (101) Wan, X.; Yao, S.; Liu, H.; Yao, Y. *J. Mater. Chem. A* **2013**, *1* (35), 10505–10512.

- 
- (102) Huang, Y.; Xu, S.; Lin, V. S. Y. *Angew. Chemie Int. Ed.* **2011**, *50* (3), 661–664.
- (103) Thanh, N. T. K.; Green, L. a W. *Nano Today* **2010**, *5* (3), 213–230.
- (104) Wong, C. H.; Zimmerman, S. C. *Chem. Commun.* **2013**, *49* (17), 1679–1695.
- (105) Khung, Y. L.; Narducci, D. *Adv. Colloid Interface Sci.* **2015**, *226*, 166–186.
- (106) Tabujew, I.; Peneva, K. *RSC Polymer Chemistry series, Chapter 1, Functionalization of Cationic Polymers for Drug Delivery Applications*; Germany, 2014.
- (107) Rostovtsev, V. V.; Green, L. G.; Fokin, V. V.; Sharpless, K. B. *Angew. Chemie Int. Ed.* **2002**, *41* (14), 2596–2599.
- (108) Himo, F.; Lovell, T.; Hilgraf, R.; Rostovtsev, V. V.; Noodleman, L.; Sharpless, K. B.; Fokin, V. V. *J. Am. Chem. Soc.* **2005**, *127* (1), 210–216.
- (109) Thirumurugan, P.; Matosiuk, D.; Jozwiak, K. *Chem. Rev.* **2013**, *113* (7), 4905–4979.
- (110) Moitra, N.; Trens, P.; Raehm, L.; Durand, J. O.; Cattoën, X.; Chi Man, M. W. *J. Mater. Chem.* **2011**, *21* (35), 13476–13482.
- (111) Kar, M.; Malvi, B.; Das, A.; Panneri, S.; Gupta, S. Sen. *J. Mater. Chem.* **2011**, *21* (18), 6690–6697.
- (112) Gao, J.; Zhang, X.; Xu, S.; Tan, F.; Li, X.; Zhang, Y.; Qu, Z.; Quan, X.; Liu, J. *Chem. Eur. J.* **2014**, *20* (7), 1957–1963.
- (113) Tonkin, E. G.; Valentine, H. L.; Milatovic, D. M.; Valentine, W. M. *Toxicol. Sci.* **2004**, *81* (1), 160–171.
- (114) Li, L. Le; Yin, Q.; Cheng, J.; Lu, Y. *Adv. Healthc. Mater.* **2012**, *1* (5), 567–572.
- (115) Gong, H.; Xie, Z.; Liu, M.; Zhu, H.; Sun, H. *RSC Adv.* **2015**, *5* (73), 59576–59582.
- (116) Nadrah, P.; Maver, U.; Jemec, A.; Tišler, T.; Bele, M.; Dražić, G.; Benčina, M.; Pintar, A.; Planinšek, O.; Gaberšček, M. *ACS Appl. Mater. Interfaces* **2013**, *5* (9), 3908–3915.
- (117) Zhang, Q.; Neoh, K. G.; Xu, L.; Lu, S.; Kang, E. T.; Mahendran, R. *Langmuir* **2014**, *30*, 6151–6161.
- (118) Malti, W. El; Mongin, O.; Blanchard-Desce, M.; Raehm, L.; Durand, J. O. *Comptes Rendus Chim.* **2011**, *14* (12), 1055–1058.
- (119) Slowing, I.; Trewyn, B. G.; Lin, V. S. Y. *J. Am. Chem. Soc.* **2006**, *128* (46), 14792–14793.
- (120) Xu, W.; Riikonen, J.; Nissinen, T.; Suvanto, M.; Rilla, K.; Li, B.; Wang, Q.; Deng, F.; Lehto, V. P. *J. Phys. Chem. C* **2012**, *116* (42), 22307–22314.
- (121) Huh, S.; Wiench, J. W.; Yoo, J. C.; Pruski, M.; Lin, V. S. Y. *Chem. Mater.* **2003**, *15* (22), 4247–4256.
- (122) Suteewong, T.; Sai, H.; Cohen, R.; Wang, S.; Bradbury, M.; Baird, B.; Gruner, S. M.; Wiesner, U. *J. Am. Chem. Soc.* **2010**, *133* (110), 172–175.
- (123) Suteewong, T.; Sai, H.; Bradbury, M.; Estroff, L.; Gruner, S. M.; Wiesner, U. *Chem. Mater.* **2012**, *24* (20), 3895–3905.
- (124) Khung, Y. L.; Narducci, D. *Adv. Colloid Interface Sci.* **2015**, *226*, 166–186.
- (125) Gu, H.; Guo, Y.; Wong, S. Y.; Zhang, Z.; Ni, X.; Zhang, Z.; Hou, W.; He, C.; Shim, V. P. W.; Li, X. *Microporous Mesoporous Mater.* **2013**, *170*, 226–234.



## Chapter 2. Synthesis of aminated-MSNs as precursor nanoparticles

---

A reproducible experimental protocol for the synthesis and characterization of aminated MSNs to use them in later functionalizations is presented. The best conditions for the preparation of homogenous and reproducible MSN-(NH<sub>2</sub>) with a size between 50-100 nm are studied.





## Chapter 2. Synthesis of aminated MSNs as precursor nanoparticles

### 2.1. Introduction

The preparation of mesoporous silica nanoparticles was first reported by Mobil Company in 1992 as part of a project to find mesoporous materials with larger pores than zeolites.<sup>1</sup> The synthetic methodology is based on the condensation of silica precursors, such as sodium silicate, tetraethylorthosilicate or tetramethylammonium silicate, in the presence of cationic surfactants in acidic or basic conditions. In fact, the procedure is an adaptation of Stöber's methodology to prepare silica nanoparticles with a cationic surfactant incorporation.<sup>2</sup> Thus, it is a combination of the so-called sol-gel process, widely used to prepare inorganic glasses, with cationic surfactants allowing the formation of monodisperse and ordered structures by micelle formation technique. Therefore, micelles act as a mold or template and give rise to the porous structure.<sup>3,4</sup> MSNs formation is achieved by two key reactions, hydrolysis and condensation (Figure 2.1).<sup>5</sup>

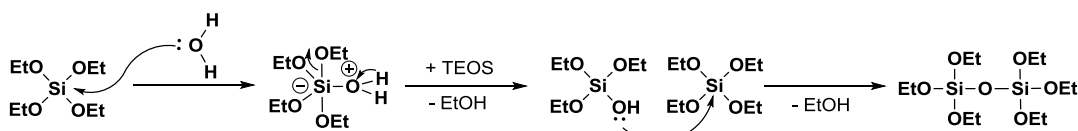


Figure 2.1. Mechanism of silica condensation.

The first stage of MSNs formation involves alkoxide hydrolysis around micelles, which are crucial to form the template porous structure. Then, (Si-OH) silanol groups are formed and a colloidal suspension is obtained. Finally, in the following step, silanol moieties polymerize by condensation to form three dimensional structures held together by siloxane bonds (Si-O-Si).<sup>6</sup> At this point, a compact and dense gel is formed (Figure 2.2).

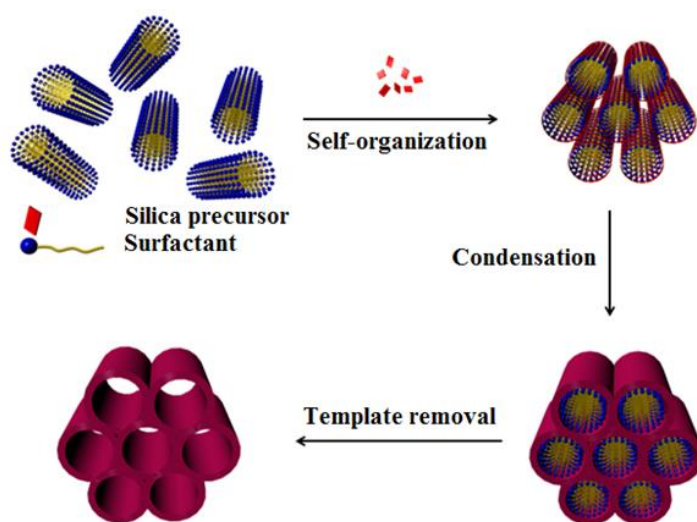


Figure 2.2. Preparation of MSNs scheme.

Cationic surfactant attracts the negatively charged silica species that are gathered around the micelles forming spherical silica structures (Figure 2.3). The hollow spaces that will provide the exotemplate framework of MSNs are filled with the inorganic precursor, which is then cured by hydrolysis and condensation. This way, the pore system of the template is copied as a “negative image”. After removal of the now-filled exotemplate framework, the incorporated material is obtained with a large specific surface area.<sup>7</sup>

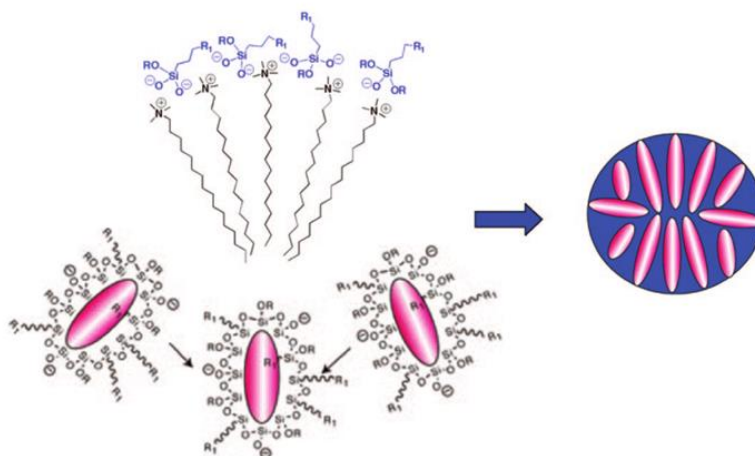


Figure 2.3. Formation of spherical MSNs.<sup>7</sup>

The pH of MSNs solution decreases as the reaction proceeds, due to the loss of silica protons that have been protonated during the hydrolysis step. Once nucleation occurs, nanoparticles become opaque. Depending on the size of the nanoparticle, a higher or lower opacity is obtained and MSNs formation can be followed by naked eye. This process is also known as Tyndall effect (Figure 2.4).<sup>8</sup>

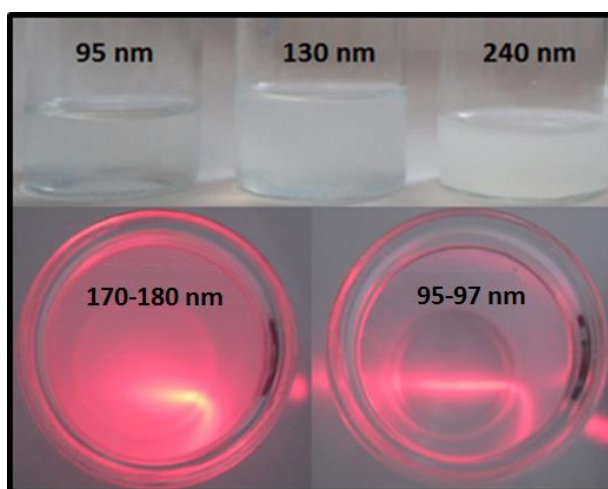


Figure 2.4. Tyndall effect.

Finally, after the mesoporous nanoparticles have been formed, surfactant must be removed. To do so, three methods have been reported: calcination,<sup>5</sup> reflux with ethanolic hydrochloric acid solution<sup>9</sup> and ion exchange process with  $\text{NH}_4\text{NO}_3$ .<sup>10</sup> These treatments allow the dissociation of electrostatic interactions between cationic surfactant head groups and anionic silicates, facilitating surfactant removal, giving the final MSNs.

In order to obtain homogeneous nanoparticles, with the same size and shape, a great number of parameters, such as temperature, rate of addition, stirring, the amount of catalyst or pH must be controlled.<sup>11–15</sup>

On the other hand, in order to confer complexity to MSNs, organic moieties must be functionalized into the inorganic surface of MSNs. A useful functional group that has been widely studied in co-condensation processes is amino moiety.<sup>7,16,17</sup> Amines in general are used in bioconjugation since they can easily and selectively react with activated acids, isothiocyanates and aldehydes.<sup>18,19</sup> Moreover, it has been reported that amine functionalized MSNs improve drug loading and enhance sustained drug release.<sup>20–23</sup>

Furthermore, if amino moieties are introduced by co-condensation with the surfactant still present in MSNs matrix, it is possible to selectively and covalently functionalize the outer surface without eroding the inner domain. Therefore, amino regioselective and bifunctional MSNs with orthogonal groups can be obtained.

Amino moieties are introduced by co-condensation processes usually by using aminopropyltriethoxysilane (APTES) or aminopropyltrimethoxysilane (APTMS) during the MSNs condensation step.<sup>9,20,21,23</sup>

A search in the literature revealed that, one of the most extended strategies for amino co-condensation formation is the use of tetraethyl orthosilicate (TEOS) as silica precursor, cetrimonium bromide (CTAB) as surfactant and APTES as amine functional group, in a basic medium of NaOH or  $\text{NH}_4\text{OH}$ .<sup>9,17,20,21,24</sup> This synthetic process is known as  $\text{S}^+\text{I}$ , where ( $\text{S}^+$ ) is the quaternary amine surfactant in a basic medium and (I) corresponds to the anionic silica precursor.<sup>25</sup>

In addition, it has been proved that APTES is capable of orienting around water micelle interface and intercalate to the hydrophobic regions of the CTAB micelles during the co-condensation reaction (Figure 2.5).<sup>7,17,26</sup> This is the reason why amino moieties are preferably present inside the porous than at the external surface.<sup>25,27</sup> Notwithstanding, in order to obtain stable structures, the upper limit of APTES incorporation into MSNs has been estimated to be less than 40%.<sup>17,25</sup>

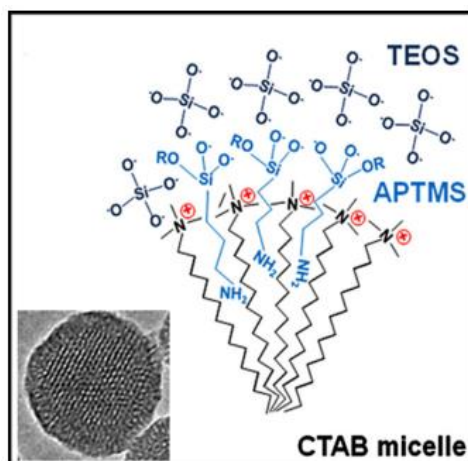


Figure 2.5. APTES intercalation in tensioactive micelles.<sup>21</sup>

As far as MSNs synthesis is concerned, many different experimental procedures are described in the literature.<sup>5,27</sup> MSNs preparation generally differ in the type of surfactant,<sup>28</sup> the reaction medium (acidic or basic),<sup>5</sup> the type of catalyst (NaOH or NH<sub>3</sub>),<sup>12</sup> pH,<sup>24</sup> temperature,<sup>13</sup> the solvent (MeOH or EtOH)<sup>2</sup> and the quantity<sup>17</sup> and type<sup>7</sup> of the functionalizing silane agent. Above all MSNs procedures that have been published,<sup>21</sup> a methodology that is described as a two-step procedure for the obtaining of uniform aminated MSNs must be highlighted.<sup>9</sup> In this process Leu Wei Lo *et al.*<sup>9</sup> claim to obtain regular and monodispersed shape nanoparticles by adding directly amino groups into MSNs surface through co-condensation process. Nevertheless, this procedure has only been described for the preparation of 150 nm MSNs, and therefore it would be crucial to control the size of MSNs. Therefore, a study of the parameters that must be adjusted in order to obtain different MSNs size must be carried out.

## 2.2. Synthesis of small aminated-MSNs

As mentioned before, Leu Wei Lo *et al.* procedure for the obtaining of regular and uniform aminated-MSNs was only described for nanoparticles of 150 nm. Nevertheless, MSNs of 150 nm size are too big for cellular applications. In fact, the optimal range for biological applications is within the 50-100 nm range, since smaller MSNs are cytotoxic and large MSNs are rapidly eliminated by RES (Reticuloendothelial System).<sup>29-31</sup> Therefore, smaller MSNs need to be synthesized. Unfortunately, no studies of controlling the size of aminated-MSNs obtained by a two-step process have been reported. Therefore it is proposed to study what parameters can change the size of MSNs, in order to obtain MSNs in the range of 50-100 nm.

### 2.2.1. Experimental planning

Therefore, to prepare smaller MSNs, first, the parameters that directly affect in MSNs size need to be determined.

Variables that can affect MSNs size:

- Concentration or quantity of surfactant, silica precursor and functional silane agent.
- pH.
- Temperature.
- Speed of stirring.
- Addition rate.
- Reaction volume.
- Lab material: flasks, magnets, syringes, heating and stirring plates.
- Number of washing cycles.

Above all these variables, a search in the literature revealed that parameters that affect the most in regular non functionalized MSNs size are pH, temperature and stirring rate.<sup>11-13</sup> Thus pH, temperature and stirring rate variables were studied, while the other variables were fixed as the original methodology.<sup>9</sup>

Variables that are kept invariable:

- CTAB, TEOS and APTES concentration.
- Lab materials: 250 mL round flask, magnet, heating and stirring plate and automatic injector.
- Addition rate: 4.8 mL / h.
- 24 h harvesting process.
- Washing cycles: 3 x H<sub>2</sub>O and 3 x EtOH.
- CTAB removal with ethanolic [HCl].

Consequently, different nanoparticles, varying temperature, pH and stirring speed, are synthesized and a statistical study, following Yates factorial designs  $2^{(f-1)}$ , where  $f=2$ , is performed. With this technique, it is very easy to determine which of the three studied parameters is critical in MSNs synthesis for the obtaining of small nanoparticles. First, the effect of temperature and stirring rate is studied in a constant basic medium concentration,  $[\text{NH}_4\text{OH}] = 0.5 \text{ M}$ . Two levels of study, high and low, are chosen (Table 2.1).

**Table 2.1.** Temperature and stirring rate low and high levels of factorial design  $2^{(f-1)}$  where  $f=2$ .

Parameters level	Low	High
Temperature / °C	50	70
Stirring rate / rpm	600	1100

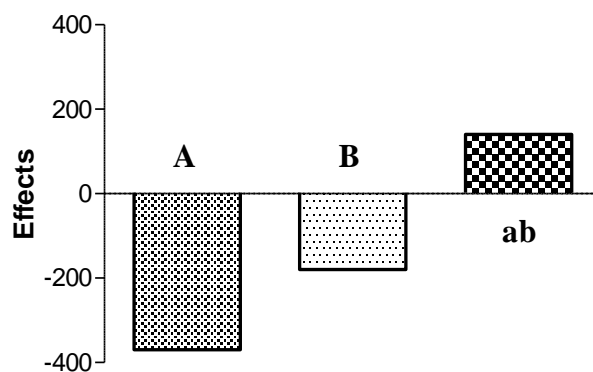
A  $2^1$  factors statistical experiment is performed, where A represents temperature and B corresponds to the stirring rate. In this case it is studied which factor is responsible for increasing MSNs size. MSNs size was measured by dynamic light scattering (DLS) by means of Z-average value or cumulants mean, which is the mean value of NPs size. Z-average is the variable to use in DLS if a number is required for quality monitoring purposes. Although MSNs size is preferably assessed by microscopy,<sup>11,13</sup> for practical reasons DLS was used. The half-width of the particle size distribution is about 10 % of the particle size.

A positive effect increases MSNs size when the factor is increased, while a negative effect decreases the size when the factor is increased. The effects of temperature and stirring speed are summarized in Table 2.2.

**Table 2.2.** Temperature and stirring rate effects.

Samples	Notation	A	B	Z-average / nm	E1	E2	Effects
MSN <sub>2</sub>	1	-	-	410	565	950	475
MSN <sub>6</sub>	a	+	-	155	385	-370	-370
MSN <sub>1</sub>	b	-	+	250	-255	-180	-180
MSN <sub>4</sub>	ab	+	+	135	-115	140	140

To visualize the effect of each condition a Length diagram is performed (Figure 2.6).

**Figure 2.6.** Length diagram effects of temperature and stirring rate.

Clearly, the highest effect is temperature (A). As it is a negative effect, a decrease in temperature results in the formation of larger nanoparticles. Thus, for the formation of small MSNs, temperature must be increased. Since temperature affects more than stirring rate in MSNs size, the effect of temperature and catalyst concentration (pH) on MSNs size is studied, with a constant stirring rate of 1100 rpm. Again, two levels of study, high and low, are chosen (Table 2.3).

**Table 2.3. Temperature and [NH<sub>4</sub>OH] low and high levels of factorial design 2<sup>(f-1)</sup> where f=2.**

Parameters level	Low	High
Temperature / °C	50	60
[NH <sub>4</sub> OH] / M	0.2	0.5

In this case, A represents temperature and B' corresponds to [NH<sub>4</sub>OH]. The effects of temperature and [NH<sub>4</sub>OH] are summarized in Table 2.4.

**Table 2.4. Temperature and [NH<sub>4</sub>OH] effects.**

Samples	Notation	A	B'	Z- average / nm	E1	E2	Effects
MSN <sub>11</sub>	1	-	-	130	246	896	448
MSN <sub>13</sub>	a	+	-	116	650	-184	-184
MSN <sub>2</sub>	c	-	+	410	-14	404	404
MSN <sub>7</sub>	ac	+	+	240	-170	-156	-156

To visualize the effect of each condition a Lengh diagram is performed (Figure 2.7).

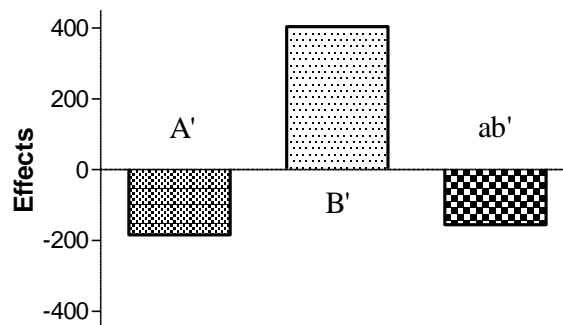


**Figure 2.7. Length diagrame effects of temperature and [NH<sub>4</sub>OH].**

In this case, the factor that affects the most in MSNs size is [NH<sub>4</sub>OH]. The higher the amount of catalyst the larger the particle size is achieved. Therefore, in order to minimize MSNs size,

[NH<sub>4</sub>OH] concentration must be decreased. The temperature effect compared with the amount of catalyst has practically no influence. Thus, [NH<sub>4</sub>OH] concentration is essential for the control of MSNs size.

To sum up, the conditions that allow the preparation of small MSNs are 1100 rpm, 60 °C and [NH<sub>4</sub>OH] = 0.2 - 0.5 M, where 0.2 M was used for 50 nm, and 0.5 M for 100 nm. Moreover, the factors that affect the most in MSNs size are the amount of catalyst, followed by temperature and stirring. These results are consistent with those described in the literature for non aminated mesoporous silica nanoparticles.<sup>11-13</sup>

### 2.2.2. Simplex optimization methodology

For the preparation of 50-100 nm MSNs, [NH<sub>4</sub>OH] concentration must range between 0.2 M - 0.5 M, for a fixed 60 °C temperature and 1100 rpm stirring rate. Nevertheless, even though these conditions led to the formation of small MSNs, it is not known if these values are optimized or not. An excellent optimization method to use when good experimental results are obtained is the iterative sequential method, also known as Simplex algorithm. This methodology examines the feasible set adjacent vertices in sequence to ensure that, at every new vertex, the objective function increases or is unaffected. For each iteration, it chooses the variable that can make the biggest modification toward the minimum solution. That variable then replaces one of its covariables, which is most drastically limiting it, thereby shifting the simplex method to another part of the solution set and toward the final solution.<sup>32</sup>

Based on the obtained best results (0.2 M, T = 60 °C and 1100 rpm) it is decided to vary the step of the three factors (pH, temperature and stirring rate) with an amplitude of 10 %. Temperature varies  $\pm 5$  °C, stirring rate  $\pm 100$  rpm and catalyst concentrations  $\pm 0.05$  M. The rest of the remaining variables are fixed as before. Initial conditions are presented in Table 2.5.

Table 2.5. Simplex factors conditions.

Samples	Temperature / °C	Stirring rate /rpm	[NH <sub>4</sub> OH] / M	Size / nm
Reference	60	1100	0.2	95
A	60	1100	<b>0.25</b>	113
B	60	<b>1000</b>	0.2	109
C	<b>65</b>	1100	0.2	104

By changing [NH<sub>4</sub>OH] concentration, temperature and rate stirring values 10 % from initial reference, very similar MSNs size are obtained. Small size differences fall within DLS variability, which is more or less 10 %. Based on these results, a 10 % amplitude is no



significant enough to observe any difference in MSNs size. Nonetheless, a higher increase would give the same results that were obtained for factorial designs  $2^{(f-1)}$ . Therefore, in this case, the best conditions for the obtaining of 50 nm MSNs, are  $T = 60\text{ }^{\circ}\text{C}$ , 1100 rpm and  $[\text{NH}_4\text{OH}] = 0.2\text{ M}$  and  $T = 60\text{ }^{\circ}\text{C}$ , 1100 rpm and  $[\text{NH}_4\text{OH}] = 0.5\text{ M}$  for 100 nm MSNs.

### 2.2.3. MSNs scale up

Regarding the original procedure,<sup>9</sup> the volume was doubled satisfactorily from 50 mL to 100 mL, obtaining regular MSNs. A scale-up procedure was also intended, ten times the initial volume, but it was difficult to maintain a continuous and homogeneous stirring rate and temperature, which resulted in non-regular MSNs. When the volume was quadrupled many nanoparticles were lost due to washing problems. Therefore the only way of getting large quantities of MSNs is by synthesizing several batches simultaneously, at a 100 mL volume scale, and characterize them together. By these means, regular and reproducible MSNs are synthesized.

Nevertheless, it is worth nothing to mention that small MSNs synthesis presents a major drawback in comparison with large MSNs, which is the obtaining of a very low yield. The smaller the size, the difficult it is to recover MSNs. In this case, for small MSNs, 20-40 mg of MSNs are obtained in each 100 mL batch, while for large MSNs, 150 mg are prepared. Therefore, 50 nm MSNs would be only used for cellular experiments, while larger nanoparticles will be used to explore MSNs chemical reactive possibilities.

## 2.3. MSNs characterization

As mentioned before, two types of MSNs are synthesized, 100 nm MSNs for chemical approaches and smaller 50 nm for cellular applications. Both MSNs are characterized by means of dynamic light scattering (DLS),  $\text{N}_2$  adsorption and desorption isotherms (BET, BJH), small angle powder X-ray diffraction (SXRD) and transmission electron microscopy (TEM) techniques.

### 2.3.1. CTAB removal

Before any MSNs characterization, it is vital to ensure that the surfactant can be completely removed. CTAB removal can be achieved by ethanolic hydrochloric acid solution<sup>9</sup> or by ion exchange process with  $\text{NH}_4\text{NO}_3$ .<sup>10</sup> This procedure can be monitored by the tensioactive band disappearance at  $2900\text{ cm}^{-1}$  (C-H tension) in FTIR spectrum (Figure 2.8).

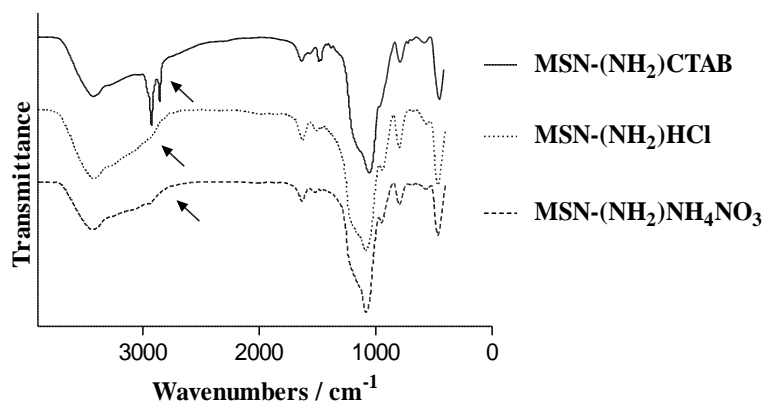


Figure 2.8. FTIR spectra of CTAB removal in MSNs.

### 2.3.2. Size determination

DLS measurements relate particles movement with their hydrodynamic radius. Therefore, depending on external functional groups and medium, DLS results can vary. It is not an absolute technique but a very fast tool to measure the polydispersity of different samples. Nevertheless, in order to obtain robust and homogeneous results it is essential to determine the suitable work concentration for each sample. For MSNs, and after several testing and adjustment experiments, a concentration of  $0.1 \text{ mg}\cdot\text{mL}^{-1}$  (EtOH) and  $0.05 \text{ mg}\cdot\text{mL}^{-1}$  ( $\text{H}_2\text{O}$ ) were found for size and zeta measurements, respectively. Better results are obtained if MSNs have just been synthesized and have not been dried.

Due to the hydrodynamic radius effect, there is a pronounced difference between the size obtained by either DLS or TEM. In fact, in the case of aminated-MSNs, DLS size is always higher than TEM.<sup>11</sup> For these experimental conditions, more or less a TEM size of 50 nm corresponds to a 100 nm DLS size, and a TEM size of 100 nm is comparable to DLS 150 nm.

Table 2.6. DLS and TEM MSNs size.

Size / nm	TEM	DLS	pDI	$\zeta$ -pot / mV
MSN-(NH <sub>2</sub> )	50	129	0.19	-1.7
	100	142	0.07	-12

As for zeta potential ( $\zeta$ -pot), considering that APTES  $\text{pK}_a$  is around 10, MSNs surface is predominantly positively charged at  $\text{pH}=7$  and therefore an increase in total zeta potential is

obtained. Typically, non-functionalized MSNs present a zeta potential around -30 mV that increase to -10-0 mV when amino groups are added.<sup>33-35</sup>

For TEM micrographs, samples were ultrasonically dispersed in EtOH at a concentration of 0.1 mg·mL<sup>-1</sup> and deposited on an amorphous, porous carbon grid. The mesoporous structure of MSNs can be clearly observed (Figure 2.9) demonstrating that MSNs have regular mesochannels of 2.2 nm.

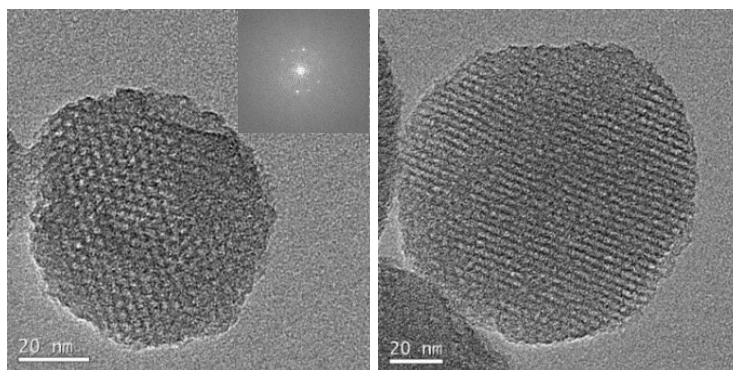


Figure 2.9. TEM micrographs of MSN-(NH<sub>2</sub>) of 50 nm (a) and 100 nm (b).

MSNs are obtained with a good polydispersity either for small or large MSNs. Both MSNs are homogeneous and monodisperse (Figure 2.10).

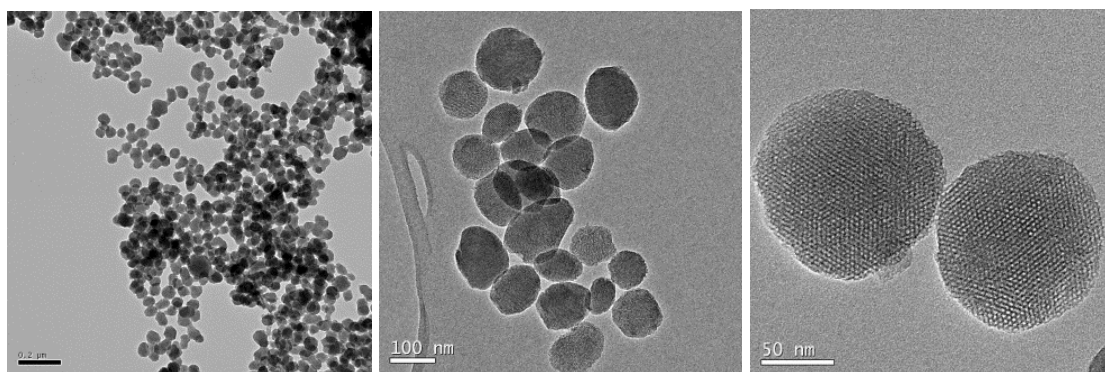
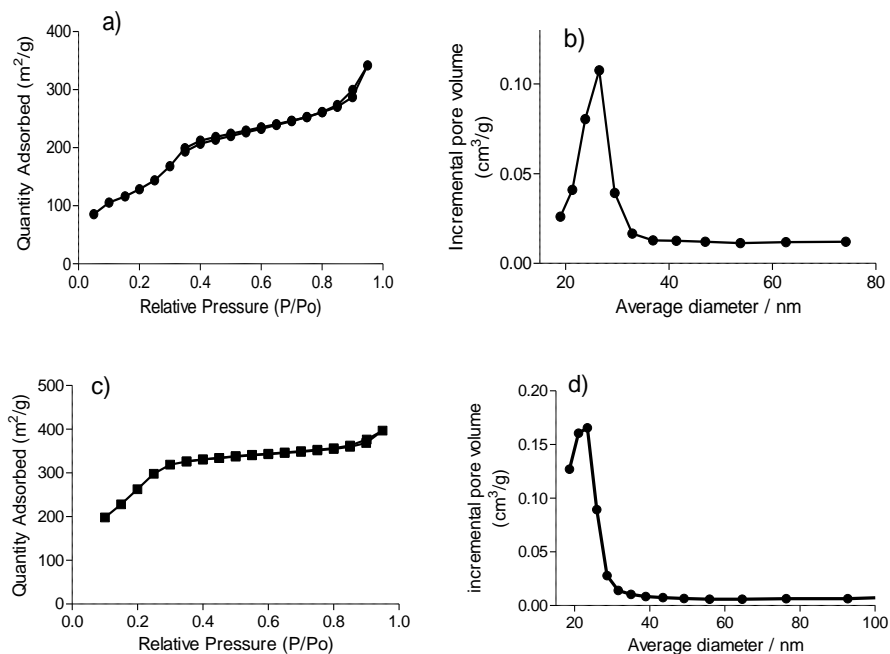


Figure 2.10. TEM micrographs showing monodispersed MSN-(NH<sub>2</sub>) of 100 nm.

### 2.3.3. Surface Area and porous order characterization

N<sub>2</sub> adsorption and desorption isotherms (BET) allow to estimate MSNs surface area. After numerous tests processes, the following conditions were determined: CTAB removal must be completely achieved, MSNs must be washed several times with water and ethanol, final ethanol solution must be removed under reduced pressure, samples must be sonicated until the

formation of a powder solid and finally MSNs must be treated in a lyophilizer at 0.05 mBar, -0.76 °C, 24 h, prior to conduct adsorption experiments. Surface areas for 50 nm and 100 nm MSNs are shown in Figure 2.11.



**Figure 2.11.** N<sub>2</sub> adsorption-desorption and BJH pore size distribution plots of MSN-(NH<sub>2</sub>) of 50 nm (a/b) and 100 nm (c/d).

N<sub>2</sub> adsorption/desorption measurements for MSN-(NH<sub>2</sub>) showed type IV isotherms, which display clear H1 hysteresis loop characteristic of mesoporous materials. BET surface areas were over 600 m<sup>2</sup>·g<sup>-1</sup> and 1100 m<sup>2</sup>·g<sup>-1</sup> for MSN-(NH<sub>2</sub>) (50 nm) and MSN-(NH<sub>2</sub>) (100 nm) respectively. BJH adsorption cumulative volume pore values recorded for MSN-(NH<sub>2</sub>) were 0.55 cm<sup>3</sup>·g<sup>-1</sup> and 0.72 cm<sup>3</sup>·g<sup>-1</sup> respectively. MSN present a very narrow pore size distribution centered at 2.5 nm (Table 2.7). These values correspond to similar reported aminated MSNs.<sup>17</sup>

**Table 2.7.** N<sub>2</sub> adsorption-desorption and BJH pore size distribution plots of MSN-(NH<sub>2</sub>) of 50 and 100 nm.

MSN-(NH <sub>2</sub> )	(50 nm)	(100 nm)
<b>BET surface area (m<sup>2</sup>/g)</b>	599.80	1120.90
<b>BJH pore volume (cm<sup>3</sup>/g)</b>	0.55	0.72
<b>Pore size (nm)</b>	2.50	2.20

### 2.3.4. X-Ray diffraction (SXR)

Small angle powered X-ray diffraction (SXR) is a non-destructive technique that allows to study the internal structure of mesoporous MSNs. The diffractograms provide information on the frequency and the internal order of the porous nanoparticles. This technique is particularly useful to verify the integrity of the mesoporous MSNs structure after chemical manipulations that can weaken its structure. Powder XRD analysis indicates highly ordered structures with d100 at 2.3 and with lighter faceted hexagon-shape at 4.1 (d110) and 4.2 nm (d200) (Figure 2.12). In this case, MSNs are prepared similarly to BET experiments.

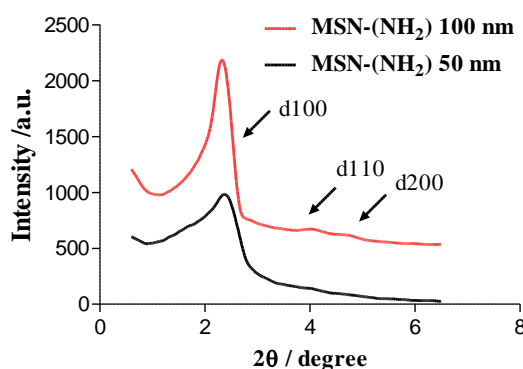


Figure 2.12. SXR of MSN-(NH<sub>2</sub>) of 50 and 100 nm.

Once MSN-(NH<sub>2</sub>) have been synthesized and characterized the reactivity of amino moieties will be tested.

## 2.4. Quantitative determination of amino groups in MSNs

In order to estimate the quantity of amino groups present in MSNs, a comparison of the organic content of non-functionalized and functionalized MSNs can be achieved. By means of TGA (Thermogravimetric analysis) and OEA (Organic elemental analysis) the estimated percentage of APTES is estimated to be 17 % and 18 % respectively. TGA and OEA techniques are very useful if the total amount of organic content wants to be determined, but cannot differentiate between internal and external functionalization.

Nevertheless, it is possible to estimate the internal and outer degree of APTES functionalization by using chemical reactions. For example, total amino surface can be reacted with FITC (Isothiocyanate fluorescein) and the degree of FITC functionalization will give total amino coverage. On the other hand, if the same process is repeated but without the tensioactive removal process, FITC will only react with external amino moieties and therefore an estimated

percentage of external amino functionalization can be obtained. The difference between total and external FITC conjugation will give the amount of inner amines.

For total APTES determination,  $4.41 \cdot 10^{-7}$  mol $\cdot$ MSNmg $^{-1}$  were obtained, whereas  $1.32 \cdot 10^{-7}$  mol $\cdot$ MSNmg $^{-1}$  corresponded to the external surface and consequently  $3.09 \cdot 10^{-7}$  mol $\cdot$ MSNmg $^{-1}$  are present in the inner surface. Thus, 70 % of amino moieties are located at the inner surface while 30 % remain at the external domain. There are twice more amino groups inside the pores than outside. These results are consistent with literature values for amino co-condensation processes, where generally amine moieties are present preferentially at the inner surface.<sup>25,27</sup>

## 2.5. Conclusions

- A methodology for the synthesis of monodispersed and uniform small (50 nm) and large (100 nm) aminated MSNs has been carried out.
- For small MSNs (50 nm) 20-40 mg per 100 mL of MSNs are obtained, while large MSNs (100 nm) give 150 mg per 100 mL.
- Monodispersed MSN-(NH<sub>2</sub>) of 50 nm and 100 nm have been entirely characterized by usual techniques (IR, DLS, BET, TEM and XRD).
- An experimental protocol for each characterization technique has been achieved in order to obtain information about MSNs, porous size, MSNs morphology, surface area and the quantity of amines that have been functionalized.

## 2.6. Bibliography

- (1) Beck, J. S.; Vartuli, J. C.; Roth, W. J.; Leonowicz, M. E.; Kresge, C. T.; Schmitt, K. D.; Chu, C. T. W.; Olson, D. H.; Sheppard, E. W.; McCullen, S. B.; Higgins, J. B.; Schlenkert, J. L. *J. Am. Chem. Soc.* **1992**, *114*, 10834–10843.
- (2) Stöber, W.; Fink, A.; Bohn, E. *J. Colloid Interface Sci.* **1968**, *26* (1), 62–69.
- (3) Teresa, M.; Palma, R.; Acuña, R. H.; Espinosa, G. *Cienc. ergo sum* **2010**, *17*, 183–188.
- (4) Zanella, R. *Mundo NANO* **2012**, *5* (1), 69–81.
- (5) Wu, S. H.; Mou, C. Y.; Lin, H. P. *Chem. Soc. Rev.* **2013**, *42* (9), 3862–3875.
- (6) Asefa, T.; Tao, Z. *Chem. Res. Toxicol.* **2012**, *25* (11), 2265–2284.
- (7) Huh, S.; Wiench, J. W.; Yoo, J. C.; Pruski, M.; Lin, V. S. Y. *Chem. Mater.* **2003**, *15* (22), 4247–4256.
- (8) Kim, K.M.; Kim, H.M.; Choi, M.H.; Lee, J.K.; Jeong, J.L. Kim, Y.S.; Paek, S.M.; Oh, J. M. *Sci. Adv. Mater.* **2014**, *6* (7), 1573–1581.
- (9) Cheng, S. H.; Lee, C. H.; Yang, C. S.; Tseng, F. G.; Mou, C. Y.; Lo, L. W. *J. Mater. Chem.* **2009**, *19* (9), 1252–1257.
- (10) Lang, N.; Tuel, A. *Chem. Mater.* **2004**, *16* (10), 1961–1966.
- (11) Chiang, Y. D.; Lian, H. Y.; Leo, S. Y.; Wang, S. G.; Yamauchi, Y.; Wu, K. C. W. *J. Phys. Chem. C* **2013**, *115* (27), 13158–13165.
- (12) Qiao, Z. A.; Zhang, L.; Guo, M.; Liu, Y.; Huo, Q. *Chem. Mater.* **2009**, *21* (16), 3823–3829.
- (13) Lin, Y. S.; Haynes, C. L. *J. Am. Chem. Soc.* **2010**, *132* (13), 4834–4842.
- (14) Beganskiene, A.; Sirutkaitis, V.; Kurtinaitiene, M.; Juskenas, R.; Kareiva, A. *Mater. Sci.* **2004**, *10* (9), 287–290.
- (15) Harrison Wanyika. *African J. Pharm. Pharmacol.* **2011**, *5* (21), 2402–2410.
- (16) Suteewong, T.; Sai, H.; Cohen, R.; Wang, S.; Bradbury, M.; Baird, B.; Gruner, S. M.; Wiesner, U. *J. Am. Chem. Soc.* **2010**, *133* (110), 172–175.
- (17) Suteewong, T.; Sai, H.; Bradbury, M.; Estroff, L.; Gruner, S. M.; Wiesner, U. *Chem. Mater.* **2012**, *24* (20), 3895–3905.
- (18) Thanh, N. T. K.; Green, L. a W. *Nano Today* **2010**, *5* (3), 213–230.
- (19) Khung, Y. L.; Narducci, D. *Adv. Colloid Interface Sci.* **2015**, *226*, 166–186.
- (20) Kamarudin, N. H. N.; Jalil, A.; Triwahyono, S.; Salleh, N. F. M.; Karim, A. H.; Mukti, R. R.; Hameed, B. H.; Ahmad, A. *Microporous Mesoporous Mater.* **2013**, *180*, 235–241.
- (21) Gu, H.; Guo, Y.; Wong, S. Y.; Zhang, Z.; Ni, X.; Zhang, Z.; Hou, W.; He, C.; Shim, V. P. W.; Li, X. *Microporous Mesoporous Mater.* **2013**, *170*, 226–234.
- (22) Vallet-Regí, M.; Balas, F.; Arcos, D. *Angew. Chemie Int. Ed.* **2007**, *46* (40), 7548–7558.
- (23) Natarajan, S. K.; Selvaraj, S. *RSC Adv.* **2014**, *4* (28), 14328–14334.
- (24) Lu, F.; Wu, S. H.; Hung, Y.; Mou, C. Y. *Small* **2009**, *5* (12), 1408–1413.
- (25) Andreas Stein, Brian J Melde, R. C. S. *Adv. Mater.* **2000**, *12* (19), 1403–1418.
- (26) Yokoi, T.; Yoshitake, H.; Yamada, T.; Kubota, Y.; Tatsumi, T. *J. Mater. Chem.* **2006**, *16* (12), 1125–1135.
- (27) Hoffmann, F.; Cornelius, M.; Morell, J.; Fröba, M. *Angew. Chemie Int. Ed.* **2006**, *45* (20), 3216–3251.

- (28) Stanley, R.; Nesaraj, A. *J. Appl. Sci. Eng.* **2013**, *10*, 9–21.
- (29) Tarn, D.; Ashley, C. E.; Xue, M. I. N.; Carnes, E. C.; Zink, J. I.; Brinker, C. J. *Acc. Chem. Res.* **2013**, *46* (3), 792–801.
- (30) Li, Z.; Barnes, J. C.; Bosoy, A.; Stoddart, J. F.; Zink, J. I. *Chem. Soc. Rev.* **2012**, *41* (7), 2590–2605.
- (31) Vallet-Regí, M. *ISRN Mater. Sci.* **2012**, *2012*, 1–20.
- (32) Lucinio G. Sabaté, X. T. *Rev. Boliv. Química* **1997**, *14* (1), 7–21.
- (33) Suteewong, T.; Sai, H.; Cohen, R.; Wang, S.; Bradbury, M.; Baird, B.; Gruner, S. M.; Wiesner, U. *J Am Chem Soc* **2008**, *42* (2), 157–162.
- (34) Xu, Y.; Claiden, P.; Zhu, Y.; Morita, H.; Hanagata, N. *Sci. Technol. Adv. Mater.* **2015**, *16* (4), 1–11.
- (35) Kardys, A. Y.; Bharali, D. J.; Mousa, S. a. *J. Nanotechnol.* **2013**, *2013*, 1–8.



## Chapter 3. Amine-naphthalimide functionalized MSNs for chemical sensing.

---

In this chapter, an efficient, high loading and fast methodology for the attachment of a variety of naphthalimides into aminated-MSNs is described. These naphthalimides have been tested as potential logic gates for the detection of  $H^+$  and  $F^-$ .



## Chapter 3. Amine-naphthalimide functionalized MSNs for chemical sensing

### 3.1. Introduction

In recent years, the study of complex systems, such as biological samples has prompted the design of fluorescent chemosensors. Fluorescent sensors provide a sensitive and selective method to recognize and evaluate the concentration of different substrates.<sup>1</sup> An effective fluorescent sensor is a system capable of interacting with the desired specie in solution and signaling its presence by changing its fluorescence properties (Figure 3.1).

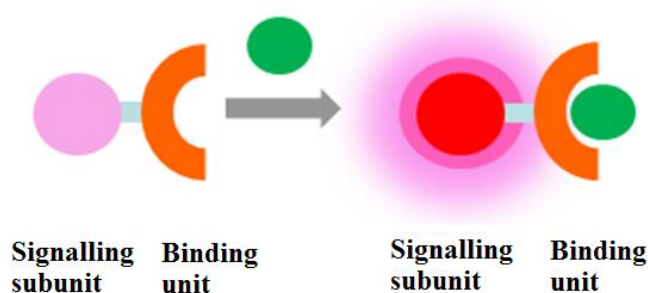


Figure 3.1. Chemosensor scheme.

By these means, fluorophores can be used for applications such as staining cell membranes, nuclei and lysosomes, but also to visualize intracellular pH, monitor pH changes, and quantify intracellular analyte concentrations in real time which can give new insights into the chemical microenvironment on the subcellular level.<sup>2</sup> For example, it has been described that pH changes might be an indicator of cancer disease development.<sup>2</sup> Therefore, the design of a chemical device sensible to pH, would be a helpful strategy for disease diagnosis.

On the other hand, anions also play a crucial role in physiologic and environmental level.<sup>3</sup> In particular, anions such as fluoride ( $F^-$ ), are harmful to the environment and consequently to humans. In addition, fluoride is of particular importance owing to its established role in dental care and treatment of osteoporosis. Fluoride is easily absorbed by the body but is slowly excreted. As a result, overexposure to fluoride can lead to acute gastric and kidney problems. In several underdeveloped countries, excessive fluoride levels in drinking water have been reported to cause bone disease fluorosis.<sup>4</sup> For these reasons, a method for the detection and sensing of  $F^-$  inside live cells, with high selectivity, is of current interest in the chemosensor research field.

Nowadays, with the development of nanotechnology applications, most of the efforts to find next generation sensors are based on fluoroionophores functionalized into nanoparticles.<sup>5</sup>

Fluorescent nanoparticles present better properties than individual molecular probes.<sup>6</sup> NPs are brighter than individual fluorophores, since one particle contains a high number of dye molecules.<sup>2</sup> Moreover, the main advantage of silica MSNs among other nanoparticles, is that silica is photophysically inert, transparent and can protect and stabilize incorporated dyes in its inner surface. Therefore, it is proposed to functionalize a pH and fluoride sensor into MSNs and test its sensibility.

Generally, ion recognition moieties are formed by polyamines, polyethers, carboxylic acids, ureas, thioureas and amide acids. As for fluorescent probes, the most studied systems are dipyrromethanes, BODIPYS, calixarenes, FITC, rhodamine and naphthalimides.<sup>7</sup> Among them, naphthalimides have been widely studied since synthetic modifications are easily accommodated on either the aromatic naphthalene (**R<sub>1</sub>**) or at the *N*-imide site moiety itself (**R<sub>2</sub>**) (Figure 3.2). This excellent property allows naphthalimides to be obtained with different and diverse functional groups and structural moieties.

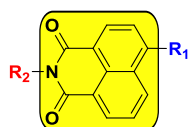


**Figure 3.2. Naphthalimide functionalization points.**

Moreover, naphthalimides present a broad emission band (460-600nm), high quantum yields and good photostability, which allow the use of these compounds as excellent sensors for fluorescent detection applications such as pH sensors.<sup>3</sup>

A search in literature revealed that, amine naphthalimides moieties are widely used as pH sensors since they are highly sensible to pH changes in the environment.<sup>3,8,9</sup> On the other hand, urea and thiourea-containing fragments have been extensively used for the formation of complexes with anions, since the hydrogen-bonding ability of these functional groups commonly results in the formation of quite stable complexes. Particularly, thioureas have been reported as excellent fluoride sensors.<sup>3,10-12</sup> Thus, a naphthalimide sensor bearing an amine and a thiourea group for fluoride and proton sensing could be used for its functionalization into MSNs.

In addition, by combining more than one receptor for different analytes, it is possible to build a system that would respond to different targets as a logic gate. A molecular logic gate is a molecule which carries out a logical operation based on one or more physical or chemical inputs with one or more response signals or outputs, normally based on spectroscopic changes. Currently, molecular logic gates are capable of applying combinatorial and sequential

operations, such as arithmetic operations and memory storage algorithms as well as operations for applications such as intelligent materials, pro-drug activation and diagnostics actuation.<sup>13,14</sup>

Since the first molecular AND gate was reported in 1993 by de Silva *et al.*<sup>15</sup>, the implementation of logic principles at the molecular level has attracted a great deal of interest. So far, various molecular logic gates have been well studied and are able to process information and perform arithmetic operations.<sup>16</sup> There are many reports on molecular logic gates that employ fluorescent changes as outputs.<sup>3,13</sup> For example, one of the most universal and versatile gates is the so-called NOR type, since it can be combined in various ways to create other gates such as NOT, AND, OR and NAND gate. These type of NOR gates have been used for example in the detection of explosive compounds and nerve agents.<sup>17</sup> In this case, a positive output is obtained when no hazardous compounds are present and a negative output is obtained if one or the two compounds are present.<sup>17</sup> In this manner, a simple assay can replace two different test protocols, commonly used for assessing each threat individually.

However, very little has been carried out with nanoparticles. In fact, to our knowledge there is only one example of naphthalimides functionalized in MSNs used as molecular logic gate and for the particular example of an INHIBIT logic gate.<sup>8</sup> Therefore, the synthesis of a naphthalimide bearing a suitable pH and fluoride moiety-sensor for its application as a logic gate is envisaged.

### 3.2. Design of pH and fluoride sensor naphthalimide-MSN

A search in literature revealed that, although there are some examples of silica nanoparticles for fluorescent sensing,<sup>18-23</sup> there are just few articles using naphthalimides in silica nanoparticles or MSNs,<sup>6,8,9,24,25</sup> where just one reference as proton and fluoride MSN-logic gate has been described.<sup>8</sup> In these examples, naphthalimides are mostly attached to the silica matrix by grafting and just few references attach naphthalimide by a covalent reaction between amino-silica nanoparticles and either activated carboxylic acid naphthalimide<sup>9,25</sup> or CuAAC click chemistry reaction.<sup>6</sup> Since, in this case, MSNs have been synthesized with amino moieties; it is proposed to functionalize naphthalimides by a covalent reaction.

By and large, amino moieties in naphthalimides systems are added by the 4-position of the aromatic naphthalene position (**R<sub>1</sub>**) either by direct bonding<sup>3,9,10</sup> or by a spacer moiety<sup>8</sup>. This position is generally chosen for proton receptors due to the nature of the internal charge transfer (ICT) state of 4-amine-1,8-naphthalimides and because it gives rise to a selective photoinduced electron transfer (PET) mechanism.

On the other hand, urea and isothiourea moieties have generally been introduced to naphthalimide sensors through a linker after amine moiety addition at the 4-position of the aromatic naphthalene ( $R_1$ ).<sup>8,11,26,27</sup> Nevertheless, instead of adding the isothiourea moiety next to the amine position, while introducing another functional group to functionalize the naphthalimide system to the MSNs, it is proposed to use directly the thiourea moiety as a linker bond, between the naphthalimide system and the MSNs.

Since MSNs present amino groups in its structure and isothiocyanates react very well with amines, giving isothioureas, it is believed that isothiourea receptor could be added directly to the MSNs, acting both as a receptor and as a linker. Therefore, it is proposed to functionalize 4-amine-1,8-naphthalimides with an isothiocyanate moiety and conjugate the system to amine-MSNs, giving the isothiourea sensor. As a result, while  $R_1$  can be used to functionalize any amine moiety, a second sensor for the detection of  $F^-$  can be easily added to the imide moiety  $R_2$  forming the thiourea receptor (Figure 3.3).

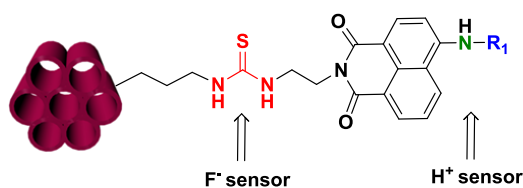


Figure 3.3. Fluoride-Proton sensor.

In order to create a little chemical library, three types of amine moieties are chosen: butyl, methylpropyl and methyl piperazine groups. Therefore, four types of naphthalimides functionalized in 4-position were proposed: 4-bromo-1,8-naphthalimide, 4-methylpiperazine-1,8-naphthalimide, 4-butyl-1,8-naphthalimide and 4-methylpropyl-1,8-naphthalimide. In this case, butyl and methylpropyl amines are directly bonded to the naphthalimide structure, while the *N*-methyl of piperazine is separated from the naphthalimide structure.

### 3.3. Synthesis of pH and fluoride sensor naphthalimide-MSN

Starting with 4-bromo-1,8-naphthalic anhydride (**1**), a mono protected diamine linker (**2**) is used to form the corresponding naphthalimide **3**. Compound **3** is then deprotected and transformed into isothiocyanate naphthalimide **6**, which further reacts with aminated-MSNs forming the thiourea bond (Figure 3.4).

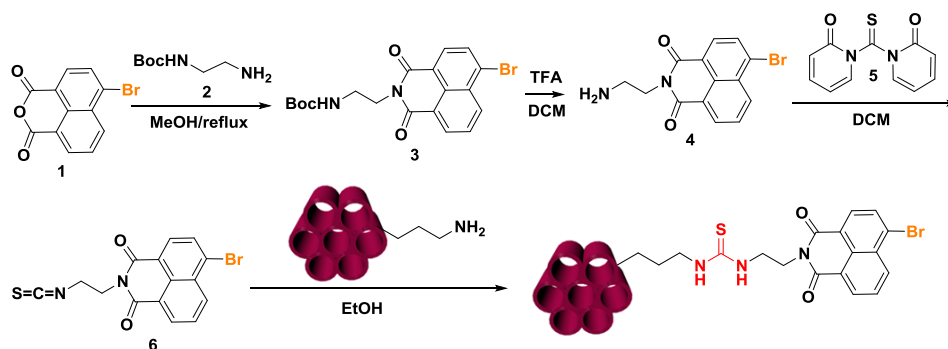


Figure 3.4. Global scheme of isothiocyanate synthetic approach.

MSNs functionalization with isothiocyanate 4-bromo-1,8-naphthalimide **6** is rapidly and successfully achieved. Yellow colored MSNs (MSN-(NaphBr)) are obtained with an absorption band at 340 nm and maximum fluorescence at 400 nm (Figure 3.5).

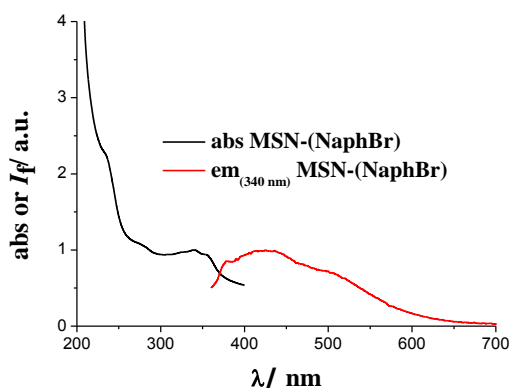


Figure 3.5. Normalized absorption and fluorescence spectra of MSN-(NaphBr).

In order to functionalize 4-amine-1,8-naphthalimides, first the direct bromo-amino nucleophilic substitution to MSN-(NaphBr) with the pertinent amino moiety (butyl, methylpropyl and methylpiperazine) is tested (Figure 3.6).

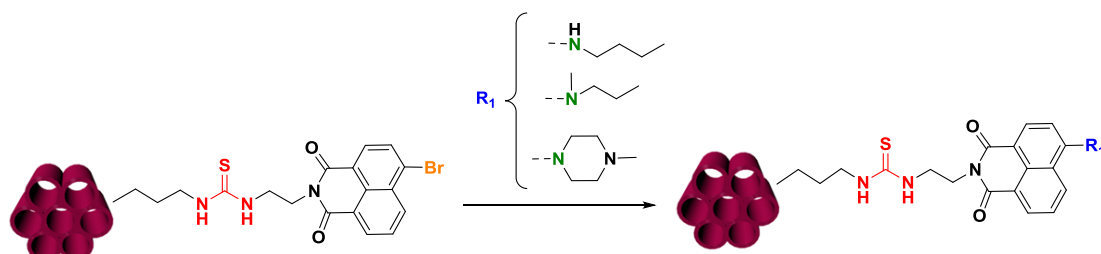


Figure 3.6. Direct bromo substitution in MSNs.

In this case, although the reaction takes place and MSNs color is more intense, a very weak absorption spectrum is obtained. This effect may be attributed to the fact that nucleophilic

substitution in solid state is not efficient. Therefore, it is better to carry out the nucleophilic substitution in solution, before MSNs functionalization. Since isothiocyanate bromo naphthalimide **3** has been easily functionalized in MSNs surface, it is proposed to repeat the same procedure for aminated naphthalimides. Therefore, an isothiocyanate moiety must be added in the naphthalimide structure. At this point, just to highlight the importance of an easy and efficient chemical reaction in solid state for the correct functionalization of MSNs.

The global scheme for the synthesis of naphthalimides bearing an amine in position 4 with an isothiocyanate linker at the *N*-imide position is presented in Figure 3.7.

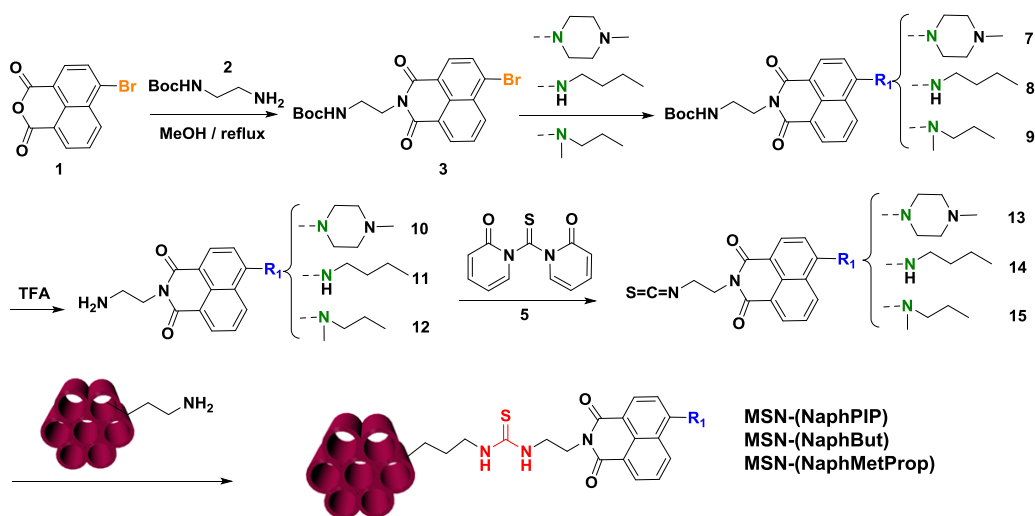


Figure 3.7. Global scheme for the conjugation of 4-amino-1,8-naphthalimides in MSNs.

First, 4-bromo-naphthalic anhydride is reacted with mono protected ethylenediamine (**2**, EdaBOC). Next, nucleophilic substitution of 4-bromo EdaBOC naphthalimide **3** with the corresponding amine, methylpiperazine, butylamine and methylpropylamine is performed. Then 4-amino EdaBOC naphthalimide **7-9** is deprotected with TFA **10-12** and isothiocyanate moiety is formed. Compounds **3;7-9** and **6;13-15** are purified and characterized by standard spectroscopic techniques ( $^1\text{H-RMN}$ ,  $^{13}\text{C-RMN}$ , IR and OEA or HRMS, Chapter 7). Finally, these new isothiocyanate naphthalimides (**13-15**) are reacted with MSNs to give MSN-(NaphPIP), MSN-(NaphBut) and MSN-(NaphMetProp). This synthetic strategy has the advantage to easily functionalize MSN-( $\text{NH}_2$ ) with any 4-naphthalimide that is not functionalized at the imide position. Moreover, MSN-naphthalimide functionalization can be carried out in EtOH and water solvents. In all cases intense yellow MSNs are formed.

As an example, by monitoring FTIR spectrum of MSN-(NaphPIP), it can be observed the formation of a new band at  $1456\text{-}1377\text{ cm}^{-1}$  corresponding to the naphthalimide rings (Figure 3.8).



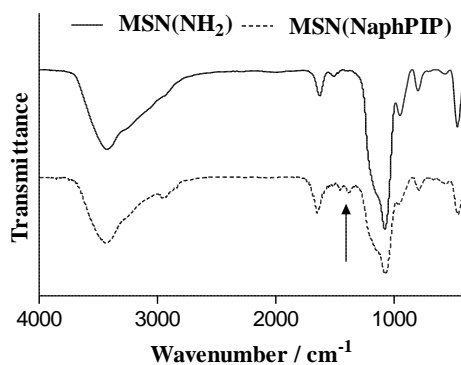


Figure 3.8. FTIR of functionalized MSN-(NaphPIP).

Absorption and fluorescence spectra of MSN-(NaphPIP), MSN-(NaphBut) and MSN-(NaphMetProp) are presented below (Figure 3.9, 3.10 and 3.11).

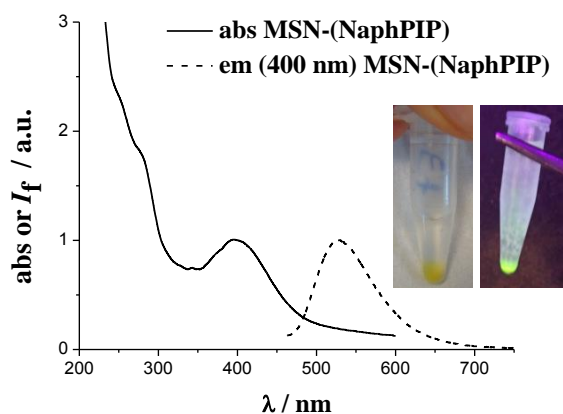


Figure 3.9. Normalized absorption and fluorescence spectra of MSN-(NaphPIP)

$$\lambda_{\max \text{abs}}=400 \text{ nm } \lambda_{\max \text{em}}=525 \text{ nm.}$$

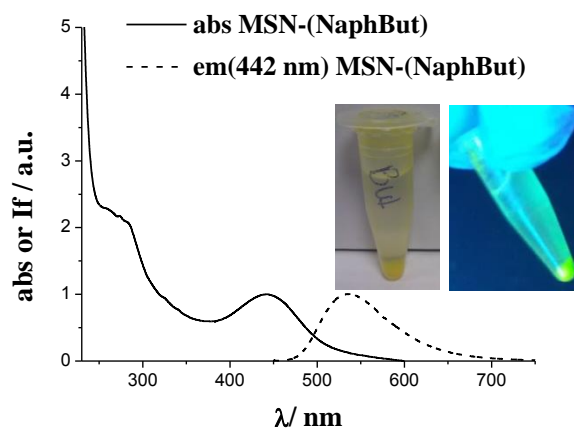


Figure 3.10. Normalized absorption and fluorescence spectra of MSN-(NaphBut)

$$\lambda_{\max \text{abs}}=442 \text{ nm } \lambda_{\max \text{em}}=529 \text{ nm}$$

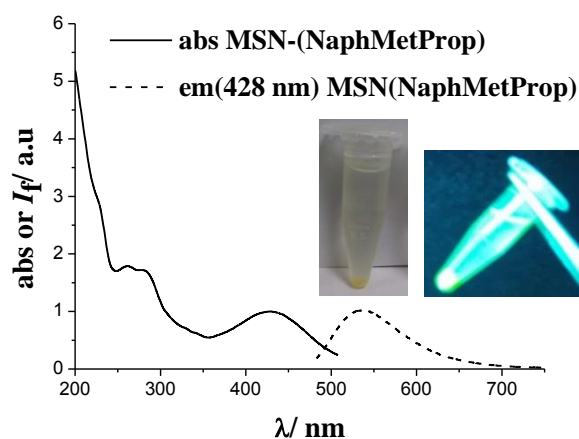


Figure 3.11. Normalized absorption and fluorescence spectra of MSN-(NaphMetProp)  
 $\lambda_{\max}\text{abs}=428\text{ nm}$   $\lambda_{\max}\text{em}=529\text{ nm}$ .

To prove that naphthalimide functionalization was not affecting MSNs morphology, TEM micrographs of Naph-MSNs were carried out. The expected spherical-hexagonal morphology was observed after the treatment. Ordered and monodispersed Naph-MSNs are obtained (Figure 3.12).

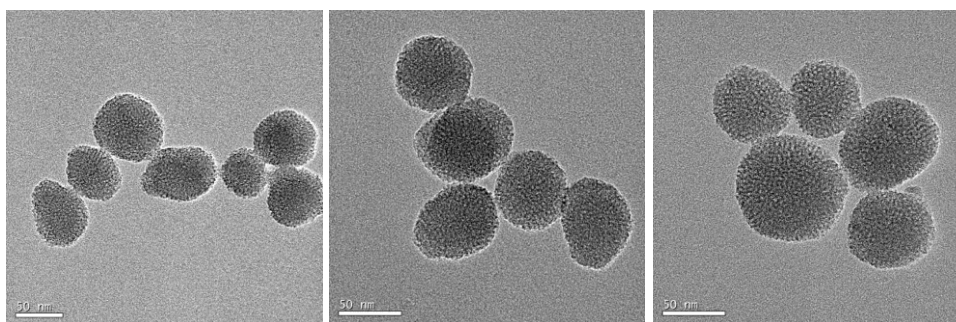


Figure 3.12. TEM micrographs of MSN-(NaphPIP), MSN-(NaphBut), MSN-(NaphMetProp).

### 3.3.1. Functionalization quantification

Thermogravimetric analysis (TGA) is used to assess the degree of naphthalimide functionalization in MSNs. To do so, initial MSNs are compared to functionalized MSNs and the difference is attributed to naphthalimide incorporation. In table 3.1 it is shown naphthalimide quantification by TGA analysis.

Table 3.1. TGA quantification of naphthalimide.

Nanoparticles	Percentage of naphthalimide / %
MSN-(NaphPIP)	21
MSN-(NaphBut)	27
MSN-(NaphMetProp)	22

The average sensor functionalization in MSNs is 23 %. This result is comparable to described values.<sup>28</sup> Furthermore, similar values were obtained by using OEA technique.

### 3.3.2. Reproducibility of MSNs functionalization

Naphthalimide functionalization is carried out by duplicate. The aim is to determine if the method is robust, repeatable and reproducible. In all the cases, naphthalimides were successfully functionalized, obtaining the same absorption and emission spectra for each duplicate. In figure 3.13 it is only presented an example for MSN-(NaphPIP).

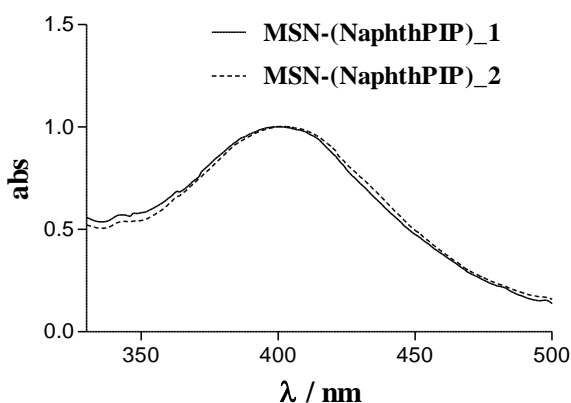


Figure 3.13. Absorption spectra of different samples of MSN-(NaphPIP).

### 3.4. Synthesis of reference naphthalimides

In order to study naphthalimide-MSNs, reference naphthalimides (MM) are synthesized (Characterization in Chapter 7). The synthesis and characterization of these reference molecules follows the same synthetic procedure that has been presented before (Figure 3.8), with the only difference that at the end, naphthalimides are reacted with butylamine instead of amine-MSNs. Therefore, reference molecules possess the same number of carbons and the same linker distance than MSNs systems and thus the only difference between the two systems is the silica matrix (Figure 3.14).

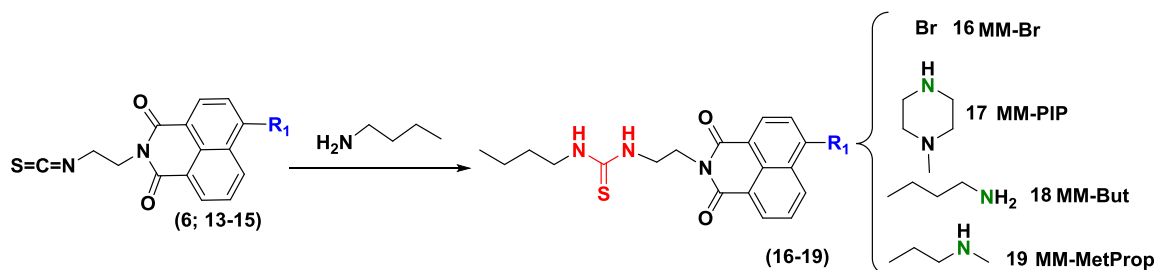


Figure 3.14. Last synthetic step of reference model molecules.

### 3.5. Titration with acid

Acid titrations of naphthalimide-MSNs systems are carried out in order to test the pH sensing performance of these systems.

Regarding MSN-(NaphPIP) system, it is observed that by increasing the amount of protons, there is virtually no change in absorption spectrum (Figure 3.16, a), while fluorescence intensity is enhanced (Figure 3.15,b).

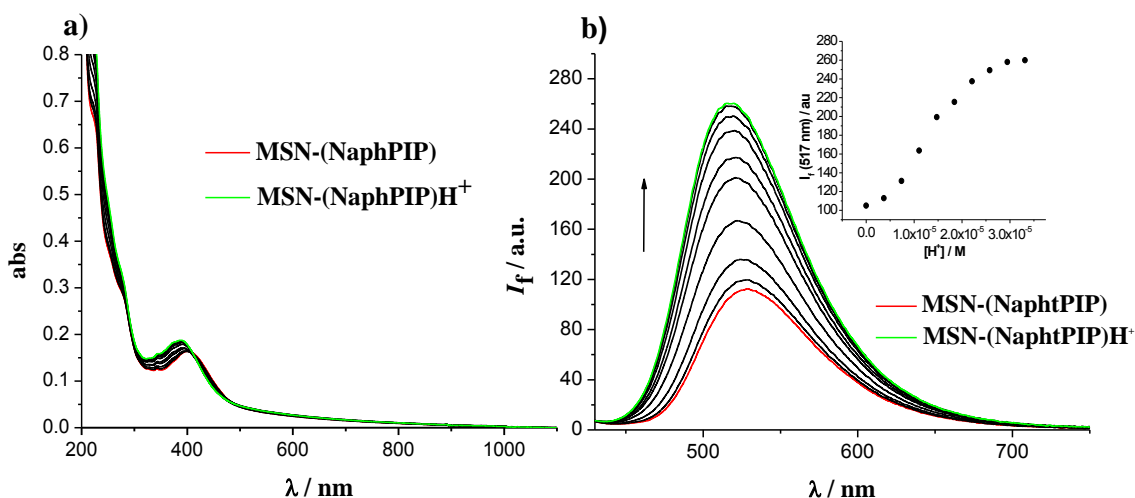


Figure 3.15. TFA a) absorption spectra and b) fluorescence spectra titration of MSN-(NaphPIP).

This fluorescence enhancement effect is reported for naphthalimides having an electron donor moiety in its structure acting as quencher of PET mechanism. When the receptor moiety and signaling subunit are covalently linked by a spacer group no ground-state  $\pi-\pi^*$  or  $n-\pi^*$  interactions are allowed to occur. When no analyte is bound, electron transfer mechanism (PET) takes place from the chelator to the fluorophore, switching off the sensor, while when the receptor is bound, redox potential is perturbed, slowing down PET process, switching on the sensor. In this regard, PET process is particularly useful, as it is an “on-off” response. Fluorescent enhancement upon addition of TFA can be attributed to the protonation of the nitrogen atom in the amino function, which can block the partial PET process (Figure 3.16).<sup>9</sup>

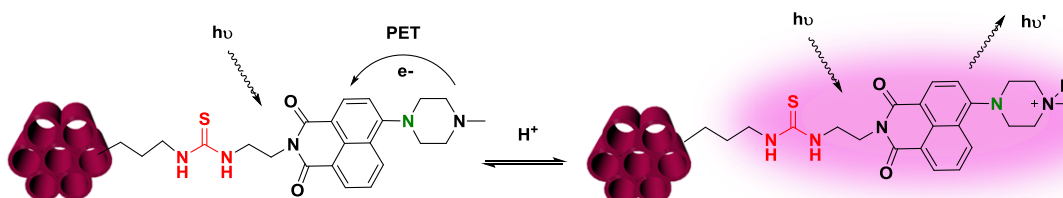


Figure 3.16. PET mechanism in MSN-(NaphPIP) upon acid addition.

The fluorescence properties of MSN-(NaphPIP) are evaluated over 4-6 range of pH. Fluorescence intensity decreases when pH increases (Figure 3.17).

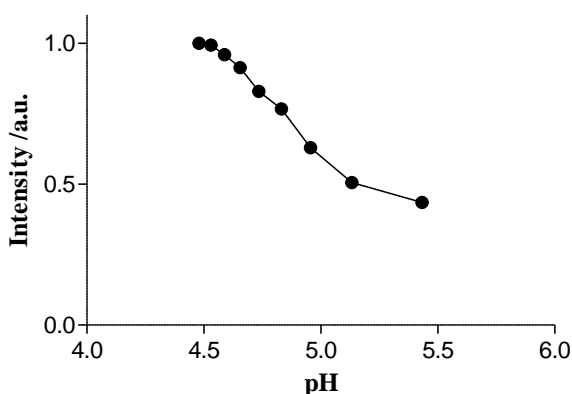


Figure 3.17. Fluorescence intensity behavior in a pH=4.5-5.5 range.

However, as for MSN-(NaphBut) and MSN-(NaphMetProp) the opposite phenomenon is observed. In this case, since butyl and methylpropyl amine are directly bound to the fluorescent sensor, the system would give a “push-pull” based internal charge transfer (ICT) excited state, caused by the electron donating amine and the electron withdrawing imide. After excitation, the charge distribution in the fluorophore is inverted (Figure 3.18). This ICT character gives rise to a large excited-state dipole and, in turn, new blue shifted band is formed at 330 nm, while 442 nm band gradually vanishes (Figure 3.19, a).

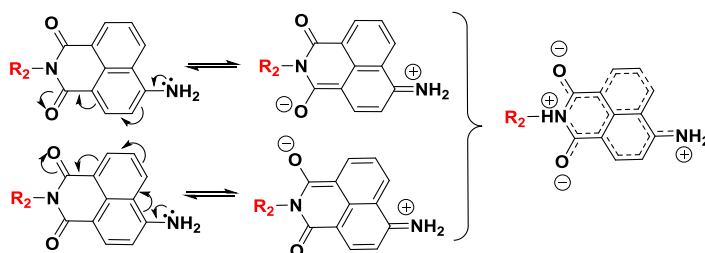


Figure 3.18. Schematic representation of the ICT excited state in 4-amine-1,8-naphthalimide.

In this case, fluorescence is not enhanced but decreases instead, fluorescence intensity is drastically minimized (Figure 3.19, b). Both absorbance and fluorescence spectra decrease exponentially with TFA additions.

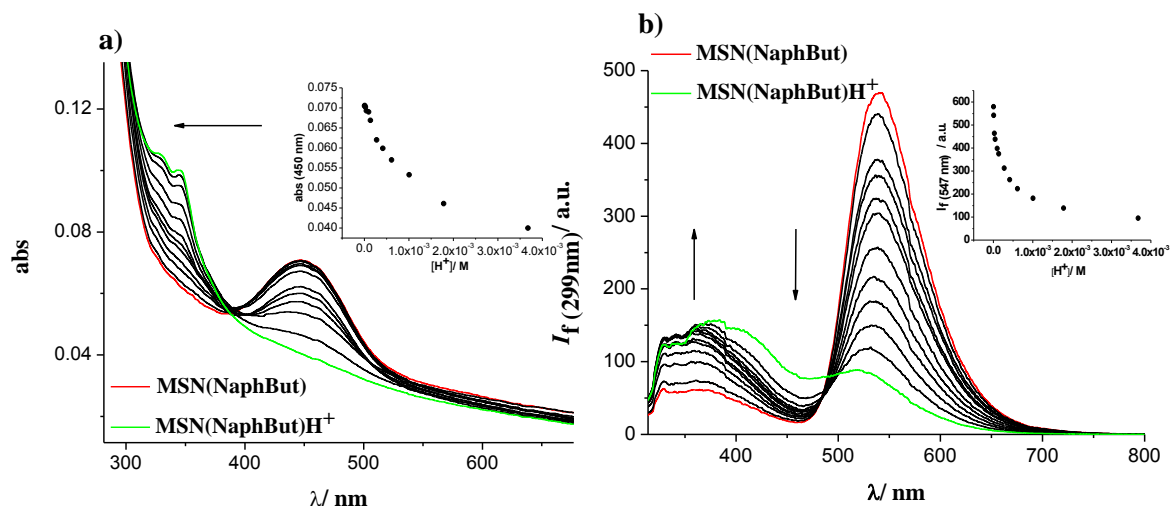


Figure 3.19. TFA a) absorption and b) fluorescence spectra titration of MSN-(NaphBut).

As for MSN-(NaphMetProp) the same behavior is observed. Absorption band at 428 nm vanishes and a new band appears at 327 nm (Figure 3.20, a). Regarding fluorescence spectrum, fluorescence intensity is exponentially diminished (Figure 3.20, b). Nonetheless, MSN-(NaphBut) fluorescence fall is higher than MSN-(NaphMetProp). MSN-(NaphBut) fluorescence intensity decreases from 500 to 150 a.u., whereas MSN-(NaphMetProp) fluorescence intensity decreases from 350 to 50 a.u. Thus, MSN-(NaphBut) seems more sensible to acid pH changes than MSN-(NaphMetProp).

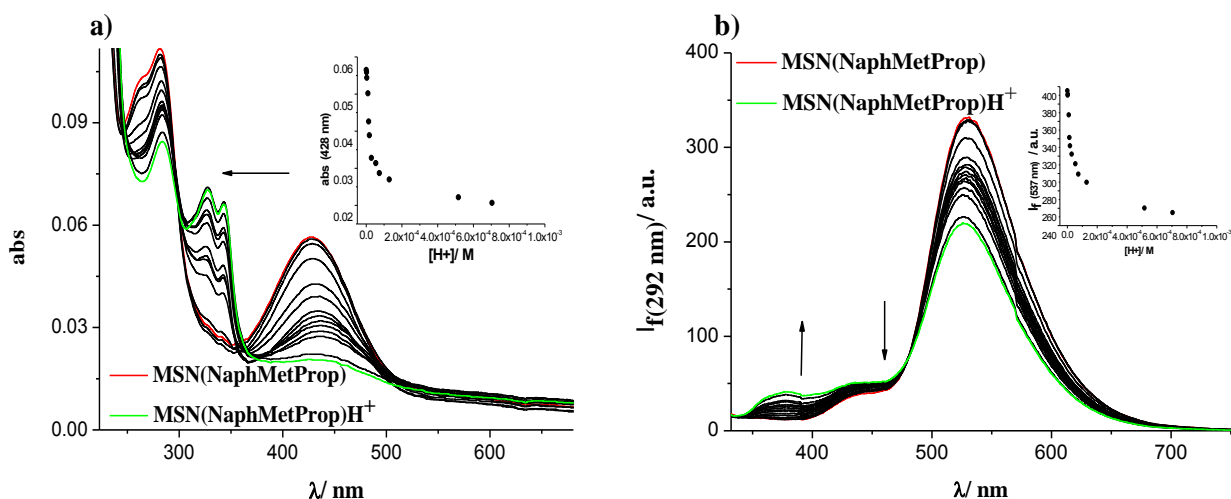
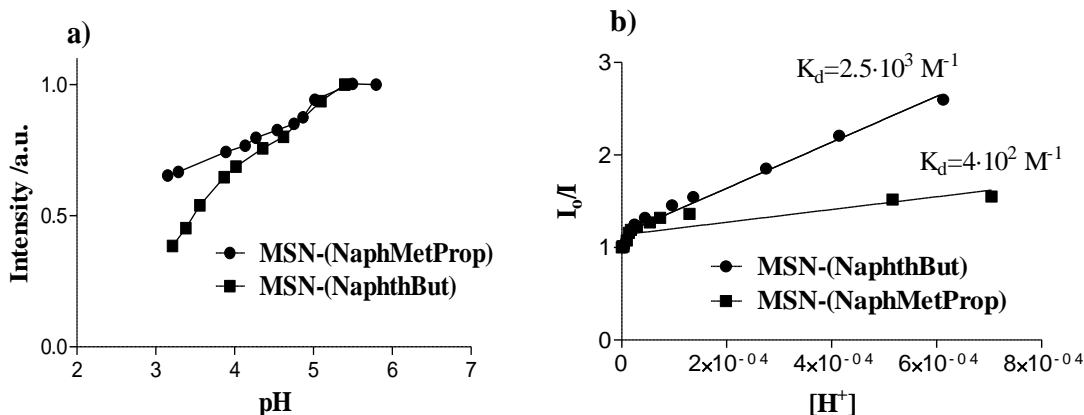


Figure 3.20. TFA a) absorption and fluorescence b) spectra titration of MSN-(NaphMetProp).

The fluorescence properties of MSN-(NaphBut) and MSN-(NaphMetProp) are evaluated over a biologically range of pH=3-6. Fluorescence intensity increases when pH increases for both MSN-(NaphBut) and MSN-(NaphMetProp) (Figure 3.21, a). To compare fluorescence deactivation between MSN-(NaphBut) and MSN-(NaphMetProp) an emission intensity vs proton concentration is plotted, which is also known as a Stern-Volmer plot (Figure 3.21, b).

MSN-(NaphBut) and MSN-(MetProp) describe a fluorescence intensity fall, more pronounced in the case of MSN-(NaphBut).



**Figure 3.21.** a) Fluorescence intensity behaviour in a pH=3-6 range, b) Stern Volmer plots of MSN-(NaphBut) and MSN-(NaphMetProp).

In this case, the constant of decay of MSN-(NaphBut) presents a one-fold decay increase ( $K_d=2.5 \cdot 10^3 M^{-1}$ ) in comparison with MSN-(NaphMetProp) ( $K_d=4 \cdot 10^2 M^{-1}$ ,  $\log K_d=3.6$ ). Therefore, MSN-(NaphBut) is one-fold more sensitive to  $H^+$  than MSN-(NaphMetProp).

It seems clear that with TFA additions, PET-based sensors such as MSN-(NaphPIP) present no absorption changes while fluorescence intensity is enhanced. Whereas ICT-based sensors such as MSN-(NaphBut) and MSN-(NaphMetProp), where amine moiety is directly bound to the naphthalimide ring, H-bonding interactions show a blue shift in the absorption maximum. MSN-(NaphBut) and MSN-(NaphMetProp) describe a fluorescence intensity fall, more pronounced in the case of MSN-(NaphBut), with a blue or hypsochromic absorption shift. So, for their use as a dual sensor system logic gate MSN-(NaphBut) seems a better candidate than MSN-(NaphPIP) and MSN-(NaphMetProp), since pH changes can be monitored easily either by absorption or fluorescence spectra.

### 3.6. Fluoride titration of MSN-(NaphBut)

In order to elucidate if MSN-(NaphBut) could be used as a valuable sensor system, its behavior with  $F^-$  addition is tested.

Concerning absorption spectra it is observed that, with little  $F^-$  addition, 450 nm absorption band is not really changed, while when large excess of  $F^-$  (50 eq.) is added a dramatic red shift takes

place at 530 nm (Figure 3.22, a). These results are in accordance with literature references for similar sensors.<sup>1,8,11</sup>

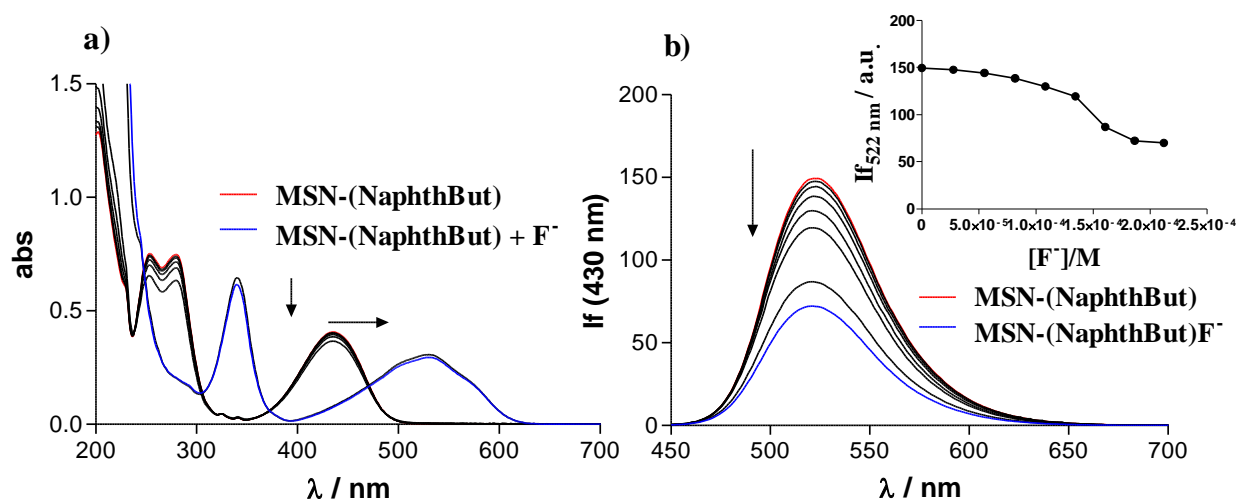


Figure 3.22.  $F^-$  absorption spectra titration of MSN-(NaphBut).

With no fluoride addition, acetonitrile solutions of MSN-(NaphBut) were yellow due to the presence of a band at 430 nm. Nevertheless, upon addition of increasing quantities of the fluoride anion, 430 nm band progressively decreased, while two new absorption bands at 550 nm and 340 nm increased in intensity, with two clear isosbestic points at 370 nm and 485 nm. The formation of these new visible bands induced a change in color from pale yellow to purple. There was a bathochromic shift of the absorption band, together with simultaneous growth of a new red-shifted band. Moreover, the isosbestic points suggests the presence of more than one species in the medium.<sup>10</sup> What it seems could be happening is a two-step process. First the formation of a hydrogen bonding complex between fluoride and thiourea takes place and secondly, the receptor is deprotonated by the anion (Figure 3.23).<sup>1,11</sup>

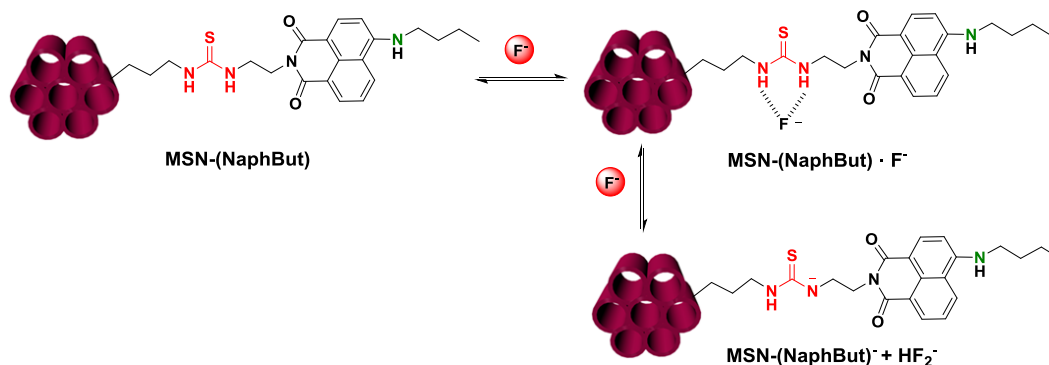


Figure 3.23. Proposed binding mode of  $F^-$  with MSN-(NaphBut).

The variation in the charge transfer reaction upon interaction with  $F^-$  may be attributed to deprotonation of acidic thiourea or through hydrogen bonding interaction.<sup>10</sup> This process is



revealed with the clear appearance of a new absorption band at longer wavelength. The absorption at 450 nm is almost “switched off” upon gradual addition of  $F^-$  while the 530 nm absorption is “switched on”.<sup>1,11</sup>

As for fluorescence behavior, fluorescence intensity is considerably minimized upon the addition of  $F^-$  (Figure 3.22,b). The influence of  $F^-$  ions on fluorescence quenching has also been reported for similar systems.<sup>1,8,11</sup>

The mechanism for this quenching process seems to follow PET process, which takes place from the thiourea receptor to the excited state of the naphthalimide fluorophore upon anion recognition. Unlike many PET sensors for cations, the fluorescence of the dye is “switched off” rather than “switched on” upon ion recognition. This quenching process may be due to the fact that, prior to the recognition process, the excited state of the fluorophore is not quenched by electron transfer from the receptor to the fluorophore. However, after adding the  $F^-$ , the formation of the anion-receptor hydrogen bonding complex occur and the reduction potential of the receptor is increased, making the electron transfer more feasible and therefore, decreasing the fluorescence intensity (Figure 3.24).<sup>1</sup>

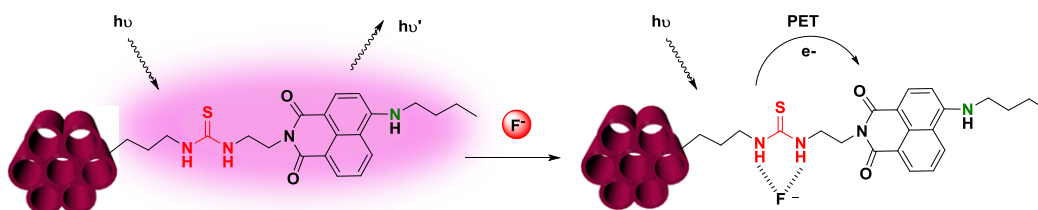


Figure 3.24. PET behavior upon addition of  $F^-$ .

In order to assess the constant of decay ( $K_d$ ) of MSN-(NaphBut), a Stern-Volmer plot of the emission intensity vs fluoride concentration is plotted (Figure 3.25).

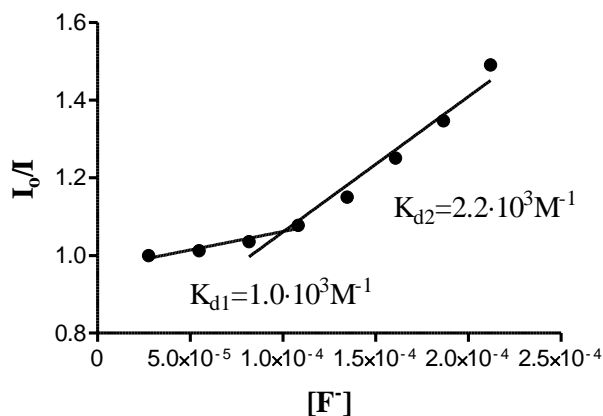


Figure 3.25. Stern Volmer plot of MSN-(NaphBut)

In this case, two constant of decay were obtained, corresponding to the two steps of the proposed fluoride binding. In the first step, fluoride and thiourea complex is achieved, with a  $K_{d1}=1.0 \cdot 10^3 \text{ M}^{-1}$  ( $\log K_{d1}=3$ ). Whereas, after deprotonation a new specie is formed, with a  $K_{d2}=2.2 \cdot 10^3 \text{ M}^{-1}$  ( $\log K_{d2}=3.3$ ). These constants of decay are comparable with the affinity of MSN-(NaphBut) with  $\text{H}^+$  ( $K_d=2.5 \cdot 10^3 \text{ M}^{-1}$ ,  $\log K_d=3.6$ ). MSN-(NaphBut) presents a similar affinity for  $\text{H}^+$  than for  $\text{F}^-$ . To the best of our knowledge, no  $K_d$  values were found for naphthalimides functionalized in MSNs.<sup>6,8,9</sup> Nevertheless, a search in literature revealed that for similar individual naphthalimides, not functionalized in MSNs, the affinity for fluoride is in the range of  $\log K=3.5$ , which is very similar to MSN-(NaphBut) constant of decay ( $K_d=2.2 \cdot 10^3 \text{ M}^{-1}$ ;  $\log K_d=3.3$ ). Moreover, for similar sensitive fluoride compounds, comparable behavior and  $K_d$  values were obtained.<sup>29</sup> Therefore it can be concluded that MSN-(NaphBut) sensibility for  $[\text{H}^+]$  and fluoride, is comparable with similar described sensors.

On the other hand, it is worth mentioning that MSN-(NaphBut) absorbance shifts and change of color, upon acid and anion addition, can be observed by naked-eye (Figure 3.26).

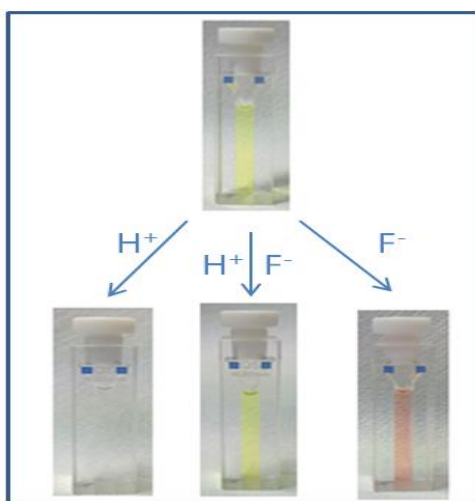


Figure 3.26. Color changes upon TFA and  $\text{F}^-$  titrations.

When TFA is added to MSN-(NaphBut), the yellow solution turns incolor with subsequent blue shift to 250 nm, while when  $\text{F}^-$  is added; the solution becomes pink with a red shift to 530 nm (Figure 3.27). When both acid and fluoride are added, solution remains yellow but its intensity is decreased. These results are in accordance with literature descriptions.<sup>30</sup>

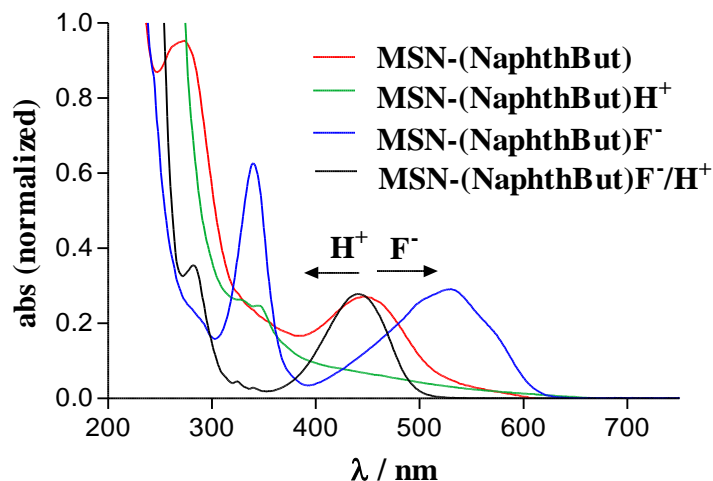



Figure 3.27. Absorption spectra titration of MSN-(NaphBut).

Thus, if fluorescence decreases when acid and fluoride are added separately but also at the same time, this system is acting as a NOR gate, where with any input the output is always 0. Only fluorescence will be detected if no protons or fluoride anions are present in the medium (Table 3.2).

Table 3.2. Truth table of NOR logic gate.

		
Input H <sup>+</sup>	Input F <sup>-</sup>	Output
0	0	1
1	0	0
0	1	0
1	1	0

Therefore, this system could be useful to detect samples with fluoride anions, in an acidic environment or that present fluoride anions in an acidic medium. With some enhancements, MSN-(NaphBut) could be used as good system for the detection of pH changes at the biologic range and anionic species in cellular media by monitoring their changes with confocal microscopy.<sup>2,31</sup>

In the case of MSN-(NaphBut), the system works as a NOR gate, which can be used as a rapid assessment of two species at the same time. With the general procedure presented before, where isothiourea is directly added to the MSNs, the synthesis of new systems from 1,8-naphthalimide scaffolds can be easily achieved.

### 3.7. Conclusions and Outlook

- A general, versatile and straightforward procedure for the introduction of 4-amino-1,8-naphthalimides onto aminated-MSNs, by using isothiocyanate “click” reaction has been developed.
- Above all systems, MSN-(NaphBut) present interesting properties as proton and fluoride sensor, since its sensitivity is comparable with similar published small molecule sensors.
- Moreover, the system respond as a NOR logic gate, which can be used as a rapid assessment of two species at the same time. Only an output is obtained when all the inputs are 0. To our knowledge, no MSN-naphthalimide have been reported as NOR gates in the literature.

Given that MSN-(NaphBut) system has been proven to respond dually to different fluoride and pH concentrations, and that there are little examples of MSNs acting as logical gate, it is firmly believed that MSN-(NaphBut) could be a potential candidate for the development of a new generation of digital devices.

### 3.8. Bibliography

- (1) Shibahara, F. *Spectrochim. Acta Part A* **2012**, *90*, 85–92.
- (2) Schulz, A.; McDonagh, C. *Soft Matter* **2012**, *8* (9), 2579–2585.
- (3) Duke, R. M.; Veale, E. B.; Pfeffer, F. M.; Kruger, P. E.; Gunnlaugsson, T. *Chem. Soc. Rev.* **2010**, *39* (10), 3936–3953.
- (4) Zhou, Y.; Zhang, J. F.; Yoon, J. *Chem. Rev.* **2014**, *114* (10), 5511–5571.
- (5) Ruedas-Rama, M. J.; Walters, J. D.; Orte, A.; Hall, E. A. H. *Anal. Chim. Acta* **2012**, *751*, 1–23.
- (6) Jin, Z.; Zhang, X. B.; Xie, D. X.; Gong, Y. J.; Zhang, J.; Chen, X.; Shen, G. L.; Yu, R. Q. *Anal. Chem.* **2010**, *82* (15), 6343–6346.
- (7) Jiao, Y.; Zhu, B.; Chen, J.; Duan, X. *Theranostics* **2015**, *5* (2), 173–187.
- (8) Tian, X.; Dong, Z.; Huang, Y.; Ma, J. *Colloids Surfaces A Physicochem. Eng. Asp.* **2011**, *387* (1-3), 29–34.
- (9) Doussineau, T.; Trupp, S.; Mohr, G. J. *J. Colloid Interface Sci.* **2009**, *339* (1), 266–270.
- (10) Misra, A.; Shahid, M.; Dwivedi, P.; Srivastava, P.; Ali, R.; Razi, S. S. *Arkivoc* **2013**, *2*, 133–145.
- (11) Duke, R. M.; Gunnlaugsson, T. *Tetrahedron Lett.* **2007**, *48* (45), 8043–8047.
- (12) Van Rossom, W.; Caers, J.; Robeyns, K.; Van Meervelt, L.; Maes, W.; Dehaen, W. *J. Org. Chem.* **2012**, *77* (6), 2791–2797.
- (13) Pischel, U.; Andréasson, J.; Gust, D.; Pais, V. F. *ChemPhysChem* **2013**, *14* (1), 28–46.
- (14) Sreejith, S.; Ajayaghosh, A. *Indian J. Chem.* **2012**, *51* (1-2), 47–56.
- (15) Prasanna A. De Silva, Nimal H. Q. Guraratne, C. P. M. *Nature* **1993**, *364*, 42–44.
- (16) Kompa, K. L.; Levine, R. D. *PNAS* **2001**, *98* (2), 410–414.
- (17) Chuang, M.-C.; Windmiller, J. R.; Santhosh, P.; Ramírez, G. V.; Katz, E.; Wang, J. *Chem. Commun.* **2011**, *47* (11), 3087–3089.
- (18) Wu, W.; Sun, Z.; Zhang, Y.; Xu, J.; Yu, H.; Liu, X.; Wang, Q.; Liu, W.; Tang, Y. *Chem. Commun.* **2012**, *48*, 11017–11019.
- (19) Teolato, P.; Rampazzo, E.; Arduini, M.; Mancin, F.; Tecilla, P.; Tonellato, U. *Chemistry* **2007**, *13* (8), 2238–2245.
- (20) Rampazzo, E.; Brasola, E.; Marcuz, S.; Mancin, F.; Tecilla, P.; Tonellato, U. *J. Mater. Chem.* **2005**, *15* (27-28), 2687–2696.
- (21) Candel, I.; Calero, P.; Martínez-Mañez, R.; Sancenón, F.; Dolores Marcos, M.; Pardo, T.; Soto, J. *Inorganica Chim. Acta* **2012**, *381* (1), 188–194.
- (22) Lodeiro, C.; Capelo, J. L. *Inorganica Chim. Acta* **2011**, *381*, 1.
- (23) Lai, J.; Shah, B. P.; Garfunkel, E.; Lee, K. B. *ACS Nano* **2013**, *7* (3), 2741–2750.
- (24) Zhang, X.; Shen, Y.; Zhang, H.; Jin, J.; Zhou, S. *Anal. Methods* **2015**, *7*, 8925–8930.
- (25) Moro, A. J.; Schmidt, J.; Doussineau, T.; Lapresta-Fernández, A.; Wegener, J.; Mohr, G. *J. Chem. Commun.* **2011**, *47* (21), 6066–6068.
- (26) Veale, E. B.; Gunnlaugsson, T. *Annu. reports B* **2010**, *106*, 376–406.
- (27) Kluciar, M.; Ferreira, R.; Castro, B. De; Pischel, U. *J. Org. Chem.* **2008**, *73*, 6079–6085.
- (28) Mamaeva, V.; Sahlgren, C.; Lindén, M. *Adv. Drug Deliv. Rev.* **2013**, *65* (5), 689–702.

- (29) Yang, Z.; Zhang, K.; Gong, F.; Li, S.; Chen, J.; Ma, J. S.; Sobenina, L. N.; Mikhaleva, A. I.; Yang, G.; Trofimov, B. a. *Beilstein J. Org. Chem.* **2011**, *7*, 46–52.
- (30) T. Gunnlaugsson, P. E. Kruger, P. Jensen, F. M. Pfeffer, G. M. H. *Tetrahedron Lett.* **2003**, *44* (49), 8909–8913.
- (31) A. Burns, P. Sengupta, T. Zedayko, B. B. and U. W. *Small* **2006**, *2*, 723–726.

## Chapter 4. Amine-azido-MSNs for their use as penetrating cell carriers.

---

A protocol to prepare regioselective bifunctionalized azido-amine MSNs has been described. These MSNs have been functionalized with a quinolin cationic foldamer for the first time. The ability of these foldamer-MSNs to cross cytoplasmic membranes has been studied. Intracellular DOX release applications have also been carried out.





## Chapter 4. Amine-azido-MSNs for their use as penetrating cell carriers

### 4.1. Introduction

#### 4.1.1. The importance of crossing the cellular barrier

One of the key points for an efficient drug delivery system is the cellular uptake of the carrier. Pharmaceutical drugs must be delivered intracellularly to perform their therapeutic action in the cytoplasm or in individual organelles, such as nuclei for gene therapy, lysosomes for the treatment of lysosomal storage diseases and mitochondria for cancer. Nevertheless, cellular membranes prevent proteins, peptides, and loaded drugs vehicles to enter the cells. Thus, these cellular membranes act as a cellular shield and protect living cells from their surroundings (Figure 4.1). Therefore cytoplasmic barriers only allow the transport of small compounds preventing hydrophilic and large drugs from being internalized.

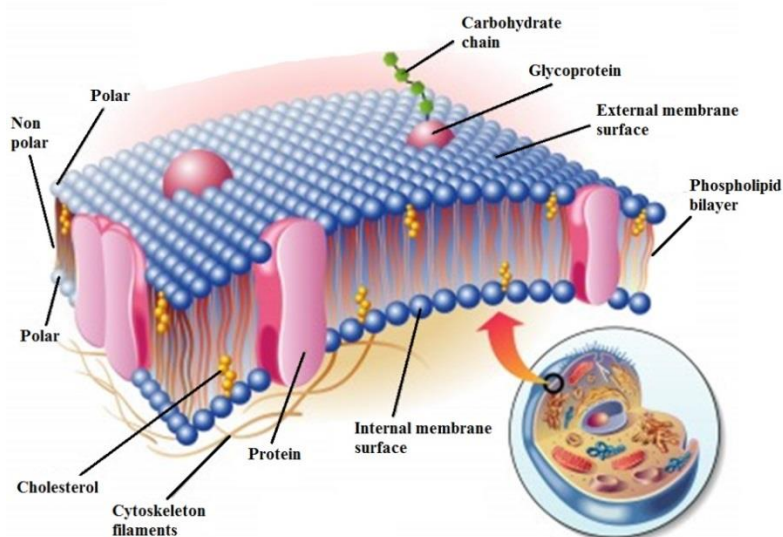


Figure 4.1. Cytoplasmic membrane.<sup>1</sup>

#### 4.1.2. Strategies to cross cytoplasmic membranes

The recent discovery of new therapeutic molecules that do not reach clinical phase due to poor delivery and low bioavailability has prompted the design of new therapeutic technologies in order to solve the drug cellular uptake problem. One possible solution to cross this cellular barrier and deliver drugs intracellularly, is the use of certain proteins or peptides, such as CPPs, capable of moving through the plasma membrane and deliver their payload intracellularly.<sup>2-4</sup>

#### 4.1.2.1. CPPs (Cell penetrating peptides)

CPPs are positively charged peptides capable of penetrating cell membranes at low concentrations without causing damage to the barrier.<sup>5-8</sup> The most common and extensively studied CPP is the human immunodeficiency virus type 1 (HIV-1) encoded peptide TAT,<sup>5,9</sup> which entrance mechanism is generally based on endocytic pathways (Figure 4.2).<sup>6,10</sup>

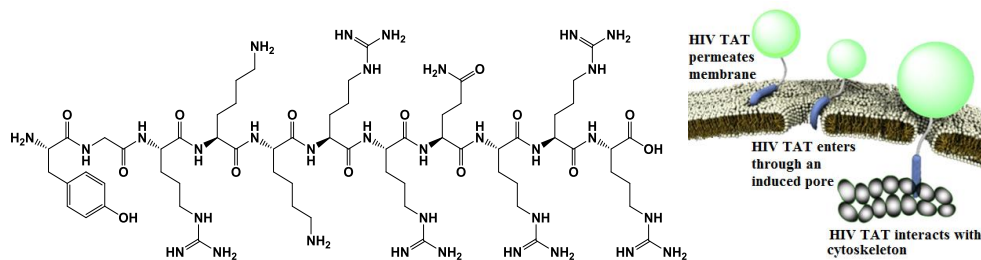


Figure 4.2. HIV-1 encoded peptide TAT structure and endocytosis.<sup>11</sup>

By and large, MSNs have been decorated with charged peptides such as TAT<sup>12,13</sup> or poly-L-arginine chains<sup>14</sup> in order to enhance MSNs uptake. Nevertheless, MSNs by their own are also capable of crossing cell membranes, but its uptake depends on their size and morphology.<sup>15</sup> Other systems have also been prepared to study MSNs uptake<sup>16</sup> but the use of CPPs seems the most appropriate strategy to enhance MSNs ability to cross cell membranes.<sup>17,2</sup> Specifically, two reports must be highlighten.<sup>12,14</sup> The first example in the literature,<sup>12</sup> is the use of a FITC-Arginine-TAT peptide for MSNs internalization, which is added to the MSNs through the reaction of an activated carboxylic acid FITC-TAT to amino-MSNs. The second example,<sup>14</sup> is a poly-arginine peptide added into fluorescent azido-MSNs through CuAAC click reaction. In both examples, the penetrating properties of MSNs are used for the intracellular delivery of a therapeutic agent, in this case doxorubicin (DOX). Therefore, penetrating MSNs act as a targeted system able to deliver DOX intracellularly, enhancing its final effectiveness.

Nevertheless, although CPPs have been widely studied and can easily penetrate cellular barriers, they present a critical drawback, which is that CPPs are susceptible to be degraded by proteases during uptake processes.

#### 4.1.2.2. Cationic charged molecules

An alternative approach is based on the use of aliphatic or aromatic chains that contain positively charged species. For example, cationic polyethylene glycol chains,<sup>18-20</sup> pyridine rings<sup>21</sup> or amide bonds have been used to internalize mesoporous silica nanoparticles<sup>22</sup> as well

as positively charged pyridines<sup>23</sup> and triethylamines.<sup>24</sup> Since the cytoplasmic membrane is negatively charged, cationic species will enhance MSNs internalization processes through the cytoplasmic barriers.

#### 4.1.2.3. Cationic quinoline foldamers

In addition to CPPs and cationic charged molecules, the penetrating capability of cationic quinoline foldamers has recently been demonstrated.<sup>25</sup> Quinoline foldamers are synthetic quinolone oligomers that are capable of adopting well-defined conformations, which are stabilized by non-covalent hydrogen bonding interactions.<sup>26</sup> The efficiency of these artificial systems is comparable to HIV Tat peptide.<sup>27</sup> In addition, quinoline foldamers present a major advantage over peptides, which is that foldamers are stable and do not degrade in biological environments. Moreover, quinoline foldamers can be easily and quickly synthesized<sup>28,29</sup> and modified.<sup>26,30</sup>

Artificial foldamers based on quinoline rings are prepared and studied by Dr. Ivan Huc group at *Institut Européen de Chimie et Biologie* (IECB) in Bordeaux. An example of a synthetic quinoline foldamer and its applications is shown in Figure 4.3. These helical aromatic derivatives, with conformational stability, are also suitable building blocks to synthetically produce larger shaped architectures that can fold to double and quadruple helix sequences and selectively interact with G-quadruplex DNA structure.<sup>31–33</sup> Furthermore, water soluble analogues present a large number of promising properties not only as spontaneous cell internalization,<sup>25</sup> but also as specific recognition of complex analytes such as monosaccharides.<sup>34</sup>

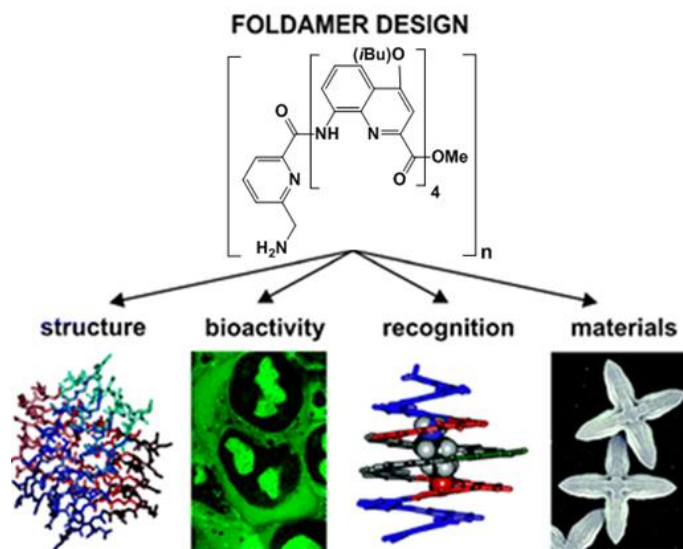


Figure 4.3. Applications of aromatic quinoline foldamers.<sup>26</sup>

All of these promising properties highlight the importance of studying foldamer applications. Moreover, cationic quinoline foldamers have not been used for nanoparticle internalization. Therefore, since there are no examples of cationic quinoline foldamers functionalized in nanoparticles, the study of these systems is envisaged. Furthermore, the penetrating ability of foldamer-MSNs will be used for the intracellular delivery of DOX in the cellular media.

## 4.2. Foldamer-MSNs design

Quinoline foldamers present two reactive groups prone to functional modifications: nitro ( $\text{NO}_2$ ) and ester ( $\text{COOMe}$ ) moieties (Figure 4.4).<sup>25</sup>

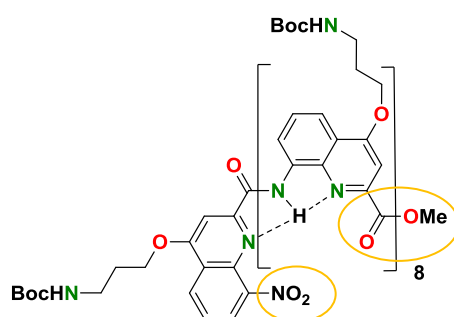


Figure 4.4. General quinoline foldamer structure.<sup>25</sup>

Between  $\text{NO}_2$  and  $\text{CO}_2\text{Me}$  position it seems easier to functionalize the quinoline foldamer through  $\text{CO}_2\text{Me}$  moiety, since it can be simply transformed into an acyl chloride moiety for nucleophilic substitutions or activated to be functionalized with amine groups. Therefore,  $\text{CO}_2\text{Me}$  derivatization is chosen to insert a suitable moiety for bioconjugation processes.

By and large, two main strategies are widely used for bioconjugation: amide and triazole formation from activated acid-amine reaction and azido-alkyne reaction, respectively. Since both foldamer and MSNs present amines, amide formation approach is not recommended. Thus, azido-alkyne reaction seems the best choice. Furthermore, triazole formation has been used in a wide variety of bioconjugation examples with MSNs.<sup>35,36</sup> To this end, an alkyne and azide functionality must be added in both foldamer and MSNs surface. In the particular case of quinoline foldamer it is easier to introduce a terminal acetylene moiety, than an azide group, which is explosive and difficult to handle. Therefore,  $\text{N}_3$  moiety will be introduced in MSNs surface. Moreover, many azido-MSNs have been described in the literature,<sup>14,37</sup> in comparison to few examples of alkyne MSNs.<sup>36,38</sup> Thus, it is considered to synthesize an azido-MSN vehicle with an alkyne-foldamer (Figure 4.5).

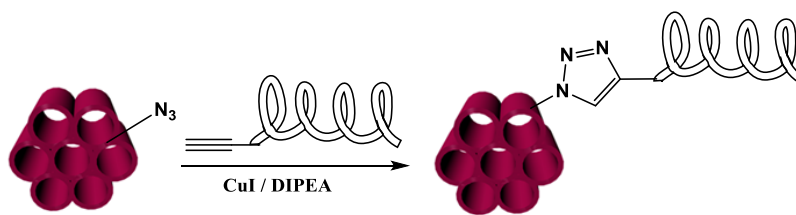


Figure 4.5. Foldamer functionalization strategy.

Moreover, a wide range of commercial amino-alkyne linkers can be used to introduce alkyne moiety in foldamer CO<sub>2</sub>Me position. For example, alkyne foldamer could be easily obtained by the reaction between foldamer acyl chloride and an alkyne-amine chain, such as hex-5-yn-1-amine (Figure 4.6).

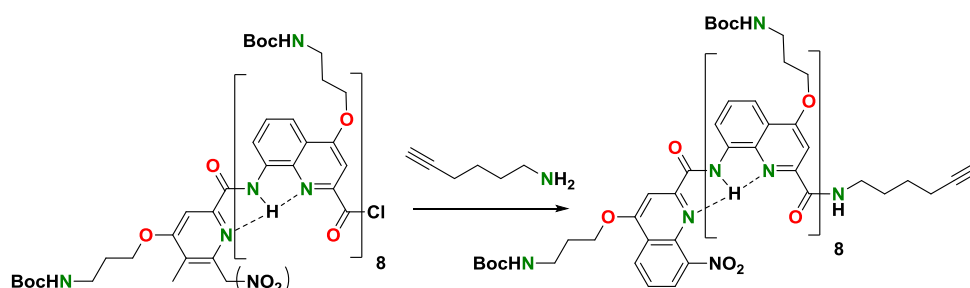
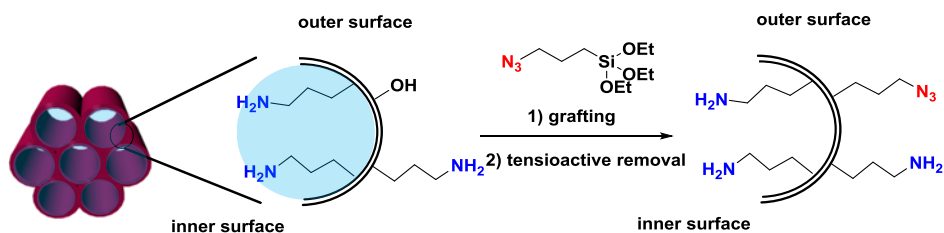


Figure 4.6. Alkyne introduction in foldamer structure.

Regarding MSNs derivatization, since it has been described that amine moieties are capable of enhancing DOX loading and release<sup>39,40</sup> it is desired to synthesize regioselective amino-azido MSNs, in order to use these systems as a intracellular DOX delivery nanoplatform. Therefore, azide and amine moieties, for the introduction of quinoline foldamer and doxorubicin, are needed in MSNs surface. Consequently, amino-azido bifunctional mesoporous silica nanoparticles must be synthesized.

### 4.3. Amino-azido MSNs synthesis and characterization

A research in literature revealed that, even if azido-MSNs have been widely used,<sup>35–37,41</sup> only one work by Wan *et al.*<sup>42</sup> describe the synthesis of amino-azido MSNs. However, the regioselectivity of these MSNs is not demonstrated. Even if Wan *et al.*<sup>42</sup> describe an amino-azido bifunctionalization it is in fact not completely regioselective: 1) external MSN surface present amino and azido groups, since azide moiety is introduced by grafting (Figure 4.7)<sup>43</sup> and 2) no tensioactive removal control is achieved with MeOH, since only toluene has been reported as a non-tensioactive removal solvent.<sup>44</sup>



**Figure 4.7.** Non-regioselective amino-azido-MSNs functionalized by amino co-condensation and azido grafting process

Furthermore, the same authors use a two-step procedure to functionalize azido moiety. First, 3-chloropropyltriethoxysilane (CPTS) is grafted on the outer MSNs surface and then it is reacted with  $\text{NaN}_3$  in a DMF solution. This synthetic approach underlines basically two drawbacks; 1)  $\text{NaN}_3$  and DMF are toxic and they are not desired in a MSNs solution and 2) a two-step reaction is carried out, which could have been done in one step avoiding extensive washing.

To solve this problem, a new, easy and completely regioselective approach that would give inner amino and outer azido MSNs is proposed. This strategy would use the external amino groups to covalently introduce azide moieties in MSNs, while tensioactive is still present. This new strategy needs the preparation of an azide containing amino reactive linker (**R**) (Figure 4.8).

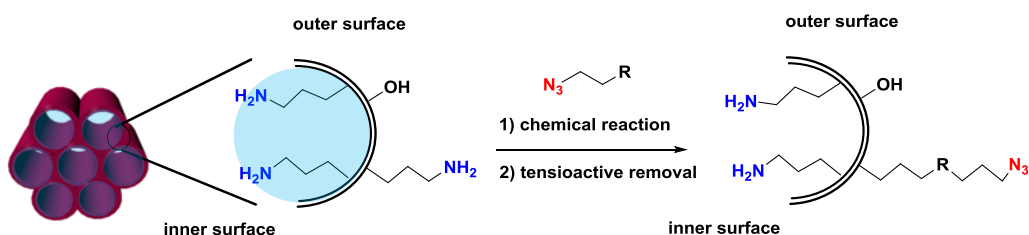


**Figure 4.8.** Complete regioselective bifunctionalization of amino-azido MSNs.

Amines in general react easily with activated acids. Thus, an azide-activated acid linker would be an excellent choice to introduce azido moiety in the external surface of MSNs (Figure 4.9). Consequently, the activated acid would react with amines introducing the new azido functionality.

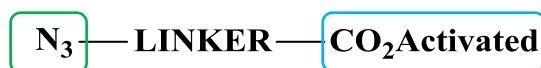


**Figure 4.9.** Reactive linker for azido introduction in MSNs.

### 4.3.1. Synthesis of 3-azidopropionic acid succinimidyl ester

First of all, the azido-activated acid linker which will provide the azido functionality to MSNs must be synthesized. Eventually, the linker must be long enough to hold both functionalities but not too much to cap the porous entrance. For example, an intermediate length about three carbon atoms could be appropriate. A suitable candidate thus, is 3-azidopropionic acid succinimidyl ester (**22**) (Figure 4.10).

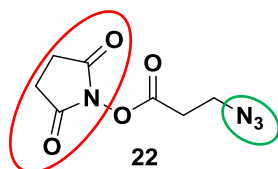


Figure 4.10. 3-azidopropionic acid succinimidyl ester linker (**22**).

From bromopropionic acid, azido moiety can be introduced to the linker by  $\text{NaN}_3$  nucleophilic substitution of the bromine atom and afterwards activate the carboxylic acid moiety by using *N*-hydroxysuccinimide with a coupling agent such as DCC, PyBOP or EDC. EDC is the best candidate, since it is easily purified with water. 3-azidopropionic acid succinimidyl ester (**22**) is synthesized first by treating bromopropionic acid (**20**) with  $\text{NaN}_3$  and then activating the carboxylic acid **21** to finally yield the azido linker **22** (Figure 4.11).<sup>45</sup>

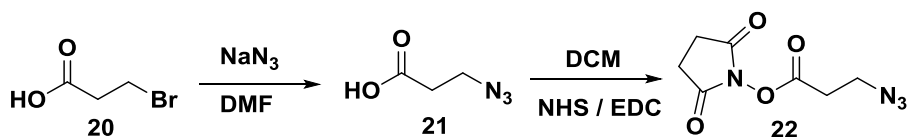


Figure 4.11. Synthetic approach of 3-azidopropionic acid succinimidyl ester.

### 4.3.2. Amino-azido MSNs functionalization

Co-condensed aminated MSNs are synthesized (Chapter 2) and prior to CTAB removal, 3-azidopropionic acid succinimidyl ester (**22**) is added. Further tensioactive removal will yield amino-azido regioselectively functionalized MSNs ( $\text{MSN}(\text{NH}_2)_i(\text{N}_3)_o$ ).

Generally, in order to preserve the tensioactive inside MSNs porous, toluene is used as a solvent in external functionalization processes.<sup>24,46</sup> Since 3-azidopropionic acid succinimidyl ester is not soluble in toluene, another solvent must be used. Most of CTAB elimination processes use harsh conditions such as HCl/EtOH reflux and calcination,<sup>47</sup> therefore it is thought that EtOH will not remove the surfactant. But, surprisingly, CTAB is removed in EtOH. By following 3-azidopropionic acid succinimidyl ester reaction in FT-IR, it can be clearly observed the azido band formation at  $2100\text{ cm}^{-1}$ , but also that the tensioactive bands disappear at 2900 and 2850

$\text{cm}^{-1}$  ( $\text{MSN}-(\text{NH}_2-\text{N}_3)\text{EtOH}$ ) (Figure 4.12). When EtOH is used, azide moiety is both present at the inner and at the outer surface.

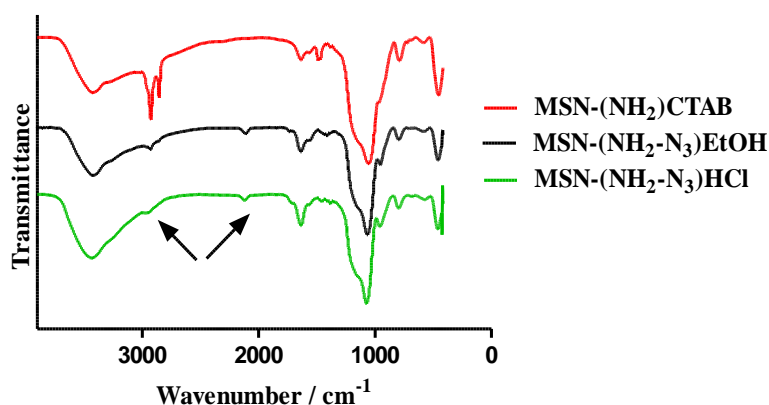


Figure 4.12. FT-IR spectra of MSN-(NH<sub>2</sub>)CTAB initial, MSN-(NH<sub>2</sub>-N<sub>3</sub>)CTAB(EtOH) and MSN-(NH<sub>2</sub>-N<sub>3</sub>)HCl.

Since EtOH is removing CTAB while azido moiety is introduced, the solvent must be changed. Another possibility was to use water. Since MSNs are synthesized in water and CTAB is still present in that solvent, it is highly believed that H<sub>2</sub>O is not able to remove CTAB. To test this hypothesis, tensioactive bands are followed by FT-IR. CTAB tensions are still present at 2900-2850  $\text{cm}^{-1}$  as well as typical N<sub>3</sub> band at 2100  $\text{cm}^{-1}$ , confirming that only the external surface have been functionalized with azido moieties (Figure 4.13).

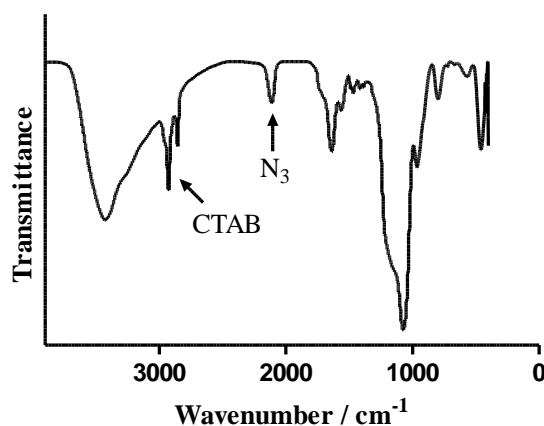


Figure 4.13. FT-IR of bifunctionalized amino-azido MSNs with CTAB.

CTAB removal can also be followed by OEA and BET analysis. For OEA, in Table 4.1, it can be observed that MSN-(NH<sub>2</sub>-N<sub>3</sub>)EtOH, when stirred with EtOH, have more or less the same C, H and N quantity as MSN-(NH<sub>2</sub>), whose tensioactive has been removed by acidic treatment. On the contrary, when MSN-(NH<sub>2</sub>)<sub>i</sub>(N<sub>3</sub>)<sub>o</sub>(CTAB) are stirred in water, MSNs present the same values that MSN-(NH<sub>2</sub>)CTAB. Moreover, when MSN-(NH<sub>2</sub>)<sub>i</sub>(N<sub>3</sub>)<sub>o</sub> tensioactive is removed by



acidic treatment C, H and N values are higher than control MSN-(NH<sub>2</sub>), showing that N<sub>3</sub> functionality has been correctly introduced and bifunctionalized amine-azido-MSNs have been obtained. Then, it can be concluded that regioselective amine-azido MSNs can be obtained since water does not remove the surfactant.

Table 4.1. OEA study of CTAB removal.

OEA	Solvent	C (%)	H (%)	N (%)
MSN-NH <sub>2</sub>	EtOH	12.4	3.2	3.9
MSN-(NH <sub>2</sub> )CTAB	H <sub>2</sub> O	25.9	5.9	2.8
MSN-(NH <sub>2</sub> -N <sub>3</sub> )-EtOH	EtOH	14.2	2.9	4.6
MSN-(NH <sub>2</sub> ) <sub>i</sub> (N <sub>3</sub> ) <sub>o</sub> (CTAB)	H <sub>2</sub> O	23.3	3.9	5.2
MSN-(NH <sub>2</sub> ) <sub>i</sub> (N <sub>3</sub> ) <sub>o</sub>	HCl/EtOH	13.5	3.2	4.6

Concerning BET studies, in Figure 4.14 it is presented the isothermal linear plots of MSN-(NH<sub>2</sub>), MSN-NH<sub>2</sub>(CTAB), MSN-(NH<sub>2</sub>-N<sub>3</sub>)EtOH and MSN-(NH<sub>2</sub>)<sub>i</sub>(N<sub>3</sub>)<sub>o</sub>CTAB. BET surface areas are near 600 m<sup>2</sup>·g<sup>-1</sup> for both control MSN-(NH<sub>2</sub>) and MSN-(NH<sub>2</sub>-N<sub>3</sub>)(EtOH), which clearly indicates that EtOH procedure removes CTAB, 599.8 ± 27.3 m<sup>2</sup>·g<sup>-1</sup> and 584.8 ± 43.16 m<sup>2</sup>·g<sup>-1</sup> respectively. Additionally, the pore volume for MSN-(NH<sub>2</sub>-N<sub>3</sub>)EtOH was 0.505 cm<sup>3</sup>·g<sup>-1</sup> in comparison to 0.550 cm<sup>3</sup>·g<sup>-1</sup> MSN-(NH<sub>2</sub>), which are very similar values and therefore demonstrates that there is no remaining tensioactive in MSNs porous (Table 4.2). On the other hand, when MSNs reaction is performed in water (MSN-(NH<sub>2</sub>)<sub>i</sub>(N<sub>3</sub>)<sub>o</sub>(CTAB) surface areas decrease from 600 m<sup>2</sup>·g<sup>-1</sup> to 272.07 ± 7.8 m<sup>2</sup>·g<sup>-1</sup>, which means that CTAB is still present inside MSNs porous and the regioselective functionalization take place.

Table 4.2. BET results of CTAB removal.

	MSN-(NH <sub>2</sub> ) (CTAB)	MSN-(NH <sub>2</sub> )	MSN-(NH <sub>2</sub> ) <sub>i</sub> (N <sub>3</sub> ) <sub>o</sub> (CTAB)(H <sub>2</sub> O)	MSN-(NH <sub>2</sub> ) <sub>i</sub> (N <sub>3</sub> ) <sub>o</sub> (EtOH)
<b>BET surface area (m<sup>2</sup>/g)</b>	70.6 ± 7.8	599.8 ± 27.3	272.1 ± 7.8	584.8 ± 43.1
<b>BJH pore volume (cm<sup>3</sup>/g)</b>	0.245	0.55	0.24	0.50
<b>Pore size (nm)</b>	--	2.4	--	2.4

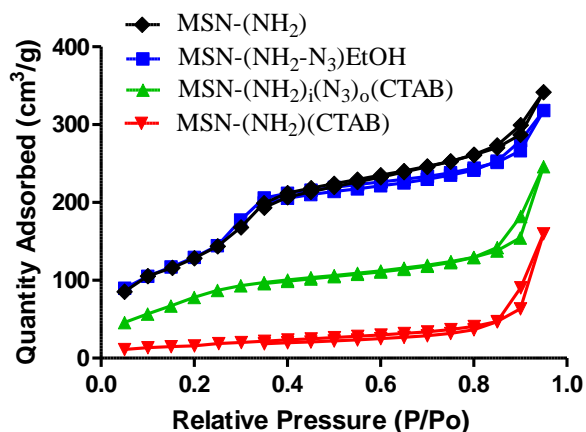


Figure 4.14. Isothermal linear plots of CTAB removal study.

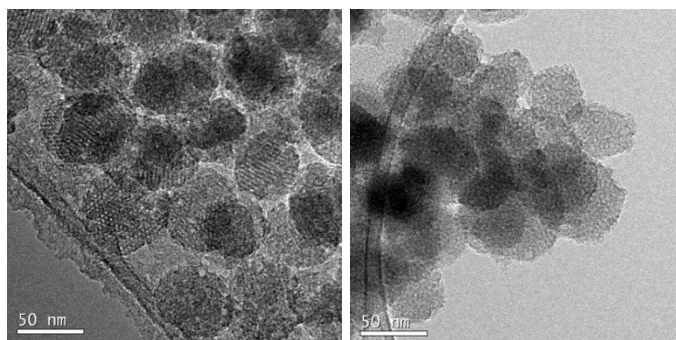
### 4.3.3. Amino-azido MSN characterization

MSN-(NH<sub>2</sub>)<sub>i</sub>(N<sub>3</sub>)<sub>o</sub> have been characterized by standard techniques (DLS, BET, IR, TEM and powder XRD) and clearly demonstrates its regioselective bifunctionalization with no morphological changes. In addition, these nanoparticles present a good chemical stability and can be kept at room temperature. In this case, MSNs of 50 nm have been chosen for uptake applications.<sup>12</sup>

No significant size and  $\zeta$ -potential differences were obtained between initial aminated-MSNs and amine-azido-MSNs. MSN-(NH<sub>2</sub>)<sub>i</sub>(N<sub>3</sub>)<sub>o</sub> have a size around 150 nm by DLS analysis (Table 4.3), which corresponds to a real TEM size around 50 nm (Figure 4.15). This difference in size between DLS and TEM is mostly due to the hydrodynamic radius effect.<sup>48</sup> Moreover, TEM micrographs confirm mesoporous structure and uniform porous size.

Table 4.3. MSN(NH<sub>2</sub>)<sub>i</sub>(N<sub>3</sub>)<sub>o</sub> size and  $\zeta$ -potential values.

Size / nm	TEM	DLS	pdl	$\zeta$ -pot / mV
MSN-(NH <sub>2</sub> )	50	142	0.070	-11
MSN-(NH <sub>2</sub> ) <sub>i</sub> (N <sub>3</sub> ) <sub>o</sub>	50	153	0.409	-18

Figure 4.15. TEM micrographs of MSN-(NH<sub>2</sub>)<sub>i</sub>(N<sub>3</sub>)<sub>o</sub> of 50 nm.

The successful MSNs regioselective bifunctionalization is supported by the presence of azido characteristic absorption band at  $2100\text{ cm}^{-1}$  along with CTAB bands at  $2850$  and  $2900\text{ cm}^{-1}$  in the FT-IR spectrum, which reveals that CTAB is still present inside the inner surface when external functionalization is carried out (Figure 4.16).

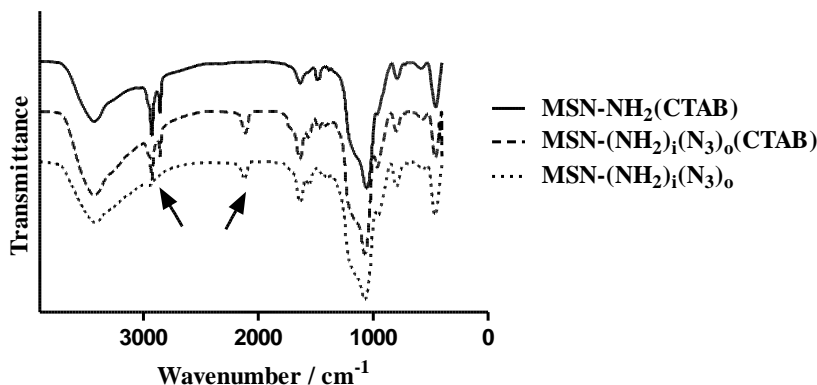


Figure 4.16. FT-IR of regioselective bifunctionalization  $\text{MSN}-(\text{NH}_2)_i(\text{N}_3)_o$ .

The  $\text{N}_2$  adsorption/desorption measurements (Figure 4.17, a and Table 4.4) for  $\text{MSN}-(\text{NH}_2)_i(\text{N}_3)_o$  show type IV isotherms, which clearly display H1 hysteresis loop, characteristic of mesoporous materials. BET surface areas are near  $600\text{ m}^2\cdot\text{g}^{-1}$  for both  $\text{MSN}-(\text{NH}_2)$  and  $\text{MSN}-(\text{NH}_2)_i(\text{N}_3)_o$ ,  $599.8 \pm 27.3\text{ m}^2/\text{g}$  and  $627.7 \pm 34.2\text{ m}^2/\text{g}$  respectively. Additionally, the pore volume for  $\text{MSN}-(\text{NH}_2)_i(\text{N}_3)_o$  is  $0.550\text{ cm}^3\cdot\text{g}^{-1}$  in comparison to  $0.669\text{ cm}^3\cdot\text{g}^{-1}$  for  $\text{MSN}-(\text{NH}_2)$ , which are very similar values. Both, MSNs present a very narrow pore size distribution centered at  $2.4\text{ nm}$  (Figure 4.17, b). These values demonstrate that  $\text{MSN}-(\text{NH}_2)_i(\text{N}_3)_o$  morphology has been well retained during the modification procedure (Table 4.4).

Table 4.4. BET results of regioselective  $\text{MSN}-(\text{NH}_2)_i(\text{N}_3)_o$ .

	$\text{MSN-NH}_2(\text{CTAB})$	$\text{MSN}-(\text{NH}_2)$	$\text{MSN}-(\text{NH}_2)_i(\text{N}_3)_o$
<b>BET surface area (<math>\text{m}^2/\text{g}</math>)</b>	$78.6 \pm 7.8$	$599.8 \pm 27.3$	$627.7 \pm 34.2$
<b>BJH pore volume (<math>\text{cm}^3/\text{g}</math>)</b>	0.249	0.55	0.669
<b>Pore size (nm)</b>	--	2.4	2.4

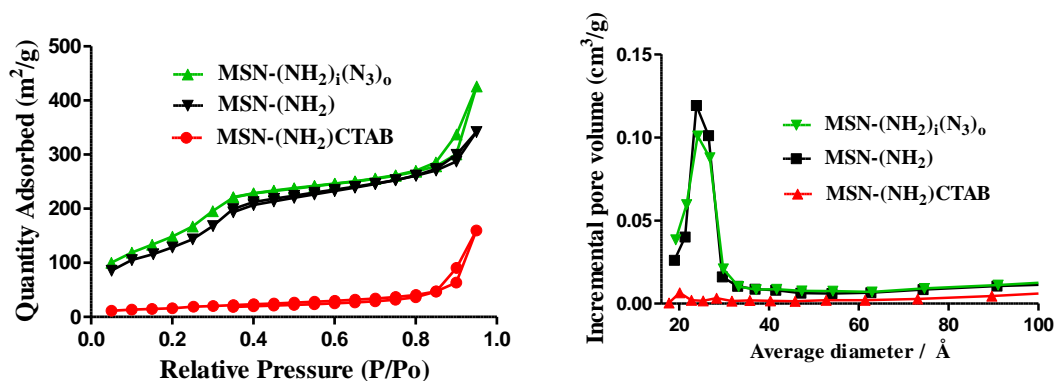


Figure 4.17. a) Isothermal linear plot and b) pore volume of regioselective MSN-(NH<sub>2</sub>)<sub>1</sub>(N<sub>3</sub>)<sub>0</sub>.

Powder XDR analysis indicates ordered structures with d100 at 2.3 and very lightly faceted hexagon-shape at 4.1 (d110) and 4.2 (d200) (Figure 4.18).

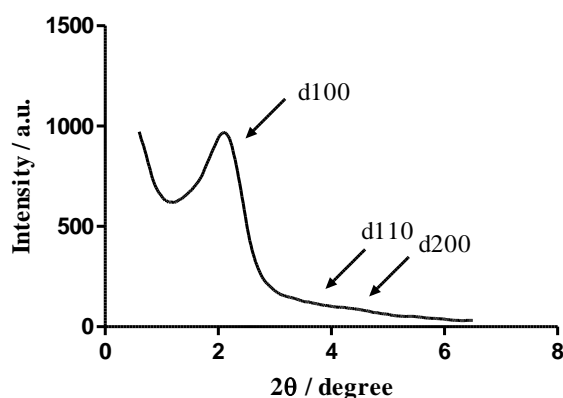


Figure 4.18. Powder XDR of MSN-(NH<sub>2</sub>)<sub>1</sub>(N<sub>3</sub>)<sub>0</sub>.

In conclusion, 3-azidopropionic acid succinimidyl ester reaction with outer amino-MSNs in water, allows the obtaining of orthogonal regioselective MSN-(NH<sub>2</sub>)<sub>1</sub>(N<sub>3</sub>)<sub>0</sub> without damaging amino MSNs morphology.

#### 4.4. MSNs functionalization with alkyne-foldamer (24)

##### 4.4.1. Synthesis of alkyne-foldamer-MSNs

In order to monitor foldamer-MSNs uptake, a fluorescent tag is used. A widely used fluorescent tag that reacts efficiently with amines is isothiocyanate fluorescein (FITC).<sup>12,14,15,17,25</sup> Moreover, FITC present green fluorescence, which do not interfere with nuclear (DAPI=blue) or cytoplasmic (phalloidin=red) dyes.

Therefore, for the synthesis of foldamer-MSNs, firstly,  $\text{MSN}-(\text{NH}_2)_i(\text{N}_3)_o$  are reacted with FITC (**23**) in a 1:1 (mg FITC/ mg MSNs) proportion. Then octamer alkyne quinoline foldamer (**24**) is added in a mixture of ACN/ $\text{H}_2\text{O}$ , CuI and DIPEA (Figure 4.19).

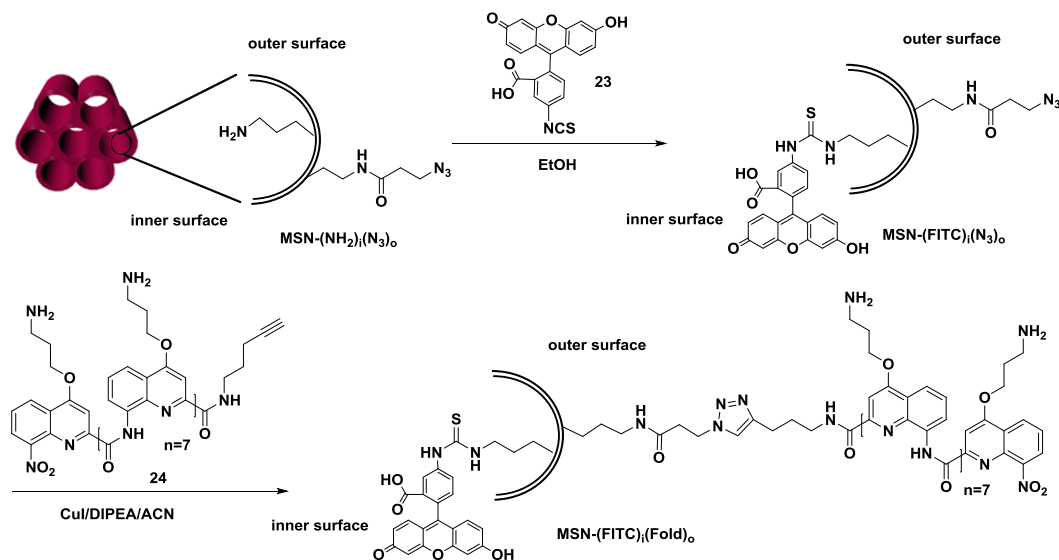


Figure 4.19. FITC (**23**) and alkyne quinoline foldamer **24** functionalization with  $\text{MSN}-(\text{NH}_2)_i(\text{N}_3)_o$ .

Due to the fact that, it is the first time that a quinoline foldamer is functionalized to nanoparticles, the functionalization protocol of MSNs was inspired in Limin Pan *et al.*<sup>12</sup> work, where TAT was functionalized to MSNs. In this case, a proportion of 10:1 (mg TAT/mg MSN) which corresponds to a 1:1 (mg alkyne-foldamer/mg MSN) equivalents was used. Therefore, 20 mg of alkyne-foldamer **24** were added to 20 mg of  $\text{MSN}-(\text{FITC})_i(\text{N}_3)_o$  in a CuI, DIPEA, ACN/ $\text{H}_2\text{O}$  solution. MSNs were washed several times with ACN, water and 0.1 M EDTA or 0.1 M *N,N*-diethyldithiocarbamate solution. CuEDTA or CuDTTC complex removal is monitored by their absorbance band at 730 nm and 430 nm respectively. MSNs were also dialyzed in water during 24 h in order to remove any residue. Finally,  $\text{MSN}-(\text{FITC})_i(\text{Fold})_o$  were obtained.

A key step in CuAAC cycloaddition is the correct removal of remaining copper either with *N,N*-diethyldithiocarbamate<sup>49</sup> or EDTA solution.<sup>41</sup> In fact, it has been reported that more than ten washings, during 3 days, are needed to completely eliminate copper.<sup>49</sup> It is worth nothing to mention that after extensive washings, MSNs yield is tremendously reduced. Moreover, EDTA is able to solubilize MSNs,<sup>41</sup> which led to the loss of a significant amount of nanoparticles.

Nevertheless, an increase in solubility and stability of the nanoparticles is clearly observed since  $\text{MSN}-(\text{FITC})_i(\text{Fold})_o$  are very well dispersed in water. Moreover,  $\text{MSN}-(\text{FITC})_i(\text{Fold})_o$  color change rapidly from yellow to orange. Cationic alkyne quinoline foldamer **24** is capable of

increasing MSN-(FITC)<sub>i</sub>(Fold)<sub>o</sub> solubilization in comparison with control MSN-(FITC). At first glance, both MSN-(FITC) and MSN-(FITC)<sub>i</sub>(Fold)<sub>o</sub> solution seem stable and well dispersed, but 24 h later MSN-(FITC) precipitate while MSN-(FITC)<sub>i</sub>(Fold)<sub>o</sub> continue in solution (Figure 4.20). MSN-(FITC)<sub>i</sub>(Fold)<sub>o</sub> are better dispersed in water than control MSN-(FITC). This process could also explain why MSN-(FITC)<sub>i</sub>(Fold)<sub>o</sub> yield is so low; alkyne-foldamer might be solubilizing MSNs too.

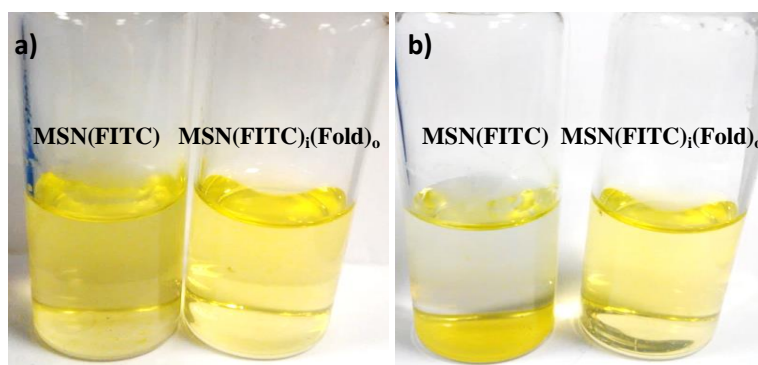


Figure 4.20. MSN-(FITC) and MSN-(FITC)<sub>i</sub>(Fold)<sub>o</sub> a) before b) and after 24 h.

MSN-(FITC)<sub>i</sub>(Fold)<sub>o</sub> stability is studied by DLS measurements. The size of a water solution of MSN-(FITC)<sub>i</sub>(Fold)<sub>o</sub> is measured at different times 1 h, 2 h and 5 h. The same intensity, volume and number value is obtained for all cases. With a zeta potential of + 30 mV the hydrodynamic radius measured is higher than “the real” size value, but measures are stable (Figure 4.21).

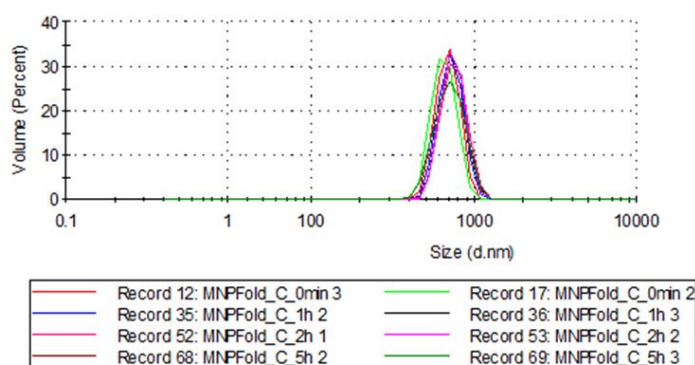


Figure 4.21. Size distribution of a solution of MSN (FITC)<sub>i</sub>(Fold)<sub>o</sub>.

This enhancement in the dispersion stability can be understood in terms of zeta potential. In fact, there is a huge increase in zeta potential from initial amine-MSN (-11 mV) to foldamer-MSN (+ 30 mV) (Figure 4.22). This high positive zeta potential could explain why final MSN-(FITC)<sub>i</sub>(Fold)<sub>o</sub> are so stable in water.

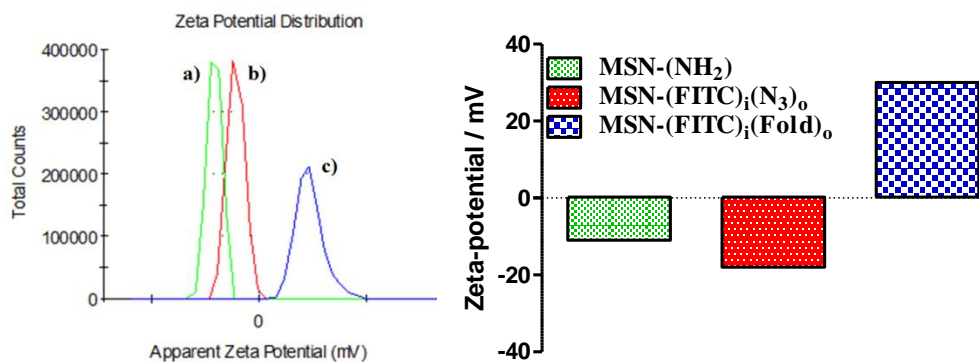


Figure 4.22. Zeta potential distribution of a) MSN-NH<sub>2</sub>, b) MSN-(FITC)<sub>1</sub>(N<sub>3</sub>)<sub>0</sub> and c) MSN-(FITC)<sub>1</sub>(Fold)<sub>0</sub>.

Furthermore, in MSN-(FITC)<sub>1</sub>(Fold)<sub>0</sub> absorption spectrum it can be clearly identified FITC absorbance band at 492 nm and alkyne quinoline foldamer band at 325 nm (Figure 4.23).

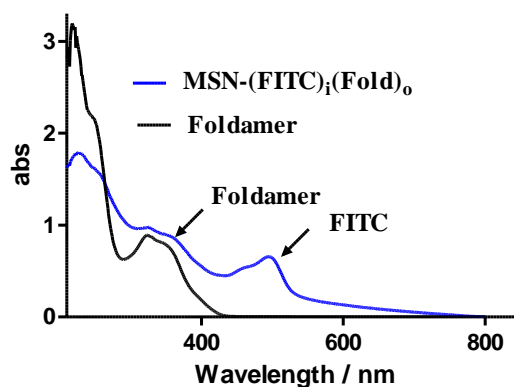


Figure 4.23. Absorption spectrum of MSN-(FITC)<sub>1</sub>(Fold)<sub>0</sub>.

The correct functionalization of alkyne-foldamer can also be verified by FT-IR spectrum, where alkyne-foldamer band appears at 1546 cm<sup>-1</sup>, while azido band at 2118 cm<sup>-1</sup> disappears after CuAAC reaction (Figure 4.24).

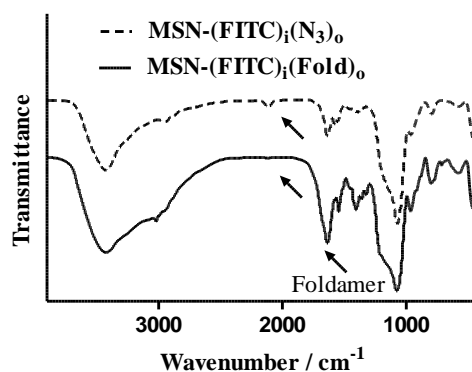


Figure 4.24. FT-IR of MSNs before (MSN-(FITC)<sub>1</sub>(N<sub>3</sub>)<sub>0</sub>) and after (MSN-(FITC)<sub>1</sub>(Fold)<sub>0</sub>) reaction with alkyne-foldamer 24.

Once alkyne-foldamer functionalization in MSNs was successfully achieved, it was though interesting to also functionalize externally a polyethylene glycol chain, in order to enhance the final biodistribution of the system. To this end,<sup>50,51</sup> tetraethyleneglycol is chosen, where one end is functionalized with an alkyne moiety and the other with FITC. Thus, the alkyne-PEG-FITC **30** moiety is also useful as a marker for MSNs. Alkyne-PEG-FITC **30** linker was synthesized as follows (Figure 4.25).

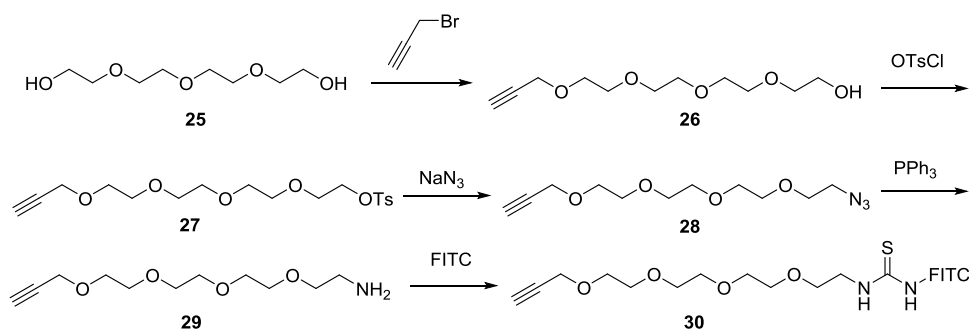


Figure 4.25. Alkyne-PEG-FITC **30** synthetic scheme.

At first, NaH and propargyl bromide were added to a tetraethyleneglycol (**25**) THF solution, to yield product **26**. Then, 1.2 eq. of tosyl chloride in DCM was added, which by a nucleophilic substitution of NaN<sub>3</sub> followed by tosylate elimination gave product **28**. Afterwards, **28** was reduced to give 3,6,9,12-tetraoxapentadec-14-yn-amine (**29**). Then an equimolar reaction of **29** with FITC gave the final alkyne-PEG-FITC **30**, which is directly added to MSN-(FITC)<sub>i</sub>(N<sub>3</sub>-Fold)<sub>o</sub> to give MSN-(FITC)<sub>i</sub>(Fold-PEG-FITC)<sub>o</sub> (Figure 4.26). Control MSN-(FITC)<sub>i</sub>(PEG-FITC)<sub>o</sub> were also synthesized.

MSN-(FITC)<sub>i</sub>(Fold-PEG-FITC)<sub>o</sub> are identically characterized as MSN-(FITC)<sub>i</sub>(Fold)<sub>o</sub>. There is a large increase in zeta potential (+ 30 mV) in comparison with initial MSNs (-11 mV) and by FT-IR a new alkyne-foldamer band at 1570 cm<sup>-1</sup> can be detected, as well as azido band elimination at 2100 cm<sup>-1</sup>. Regarding absorption spectrum, both FITC and alkyne-foldamer bands at 500 and 380 nm respectively, are observed. By OEA it is estimated the quantity of alkyne-foldamer **24** that it is functionalized in MSNs. For 1 mg of MSNs there are 0.5 mg of alkyne-foldamer, functionalization is 50 %.



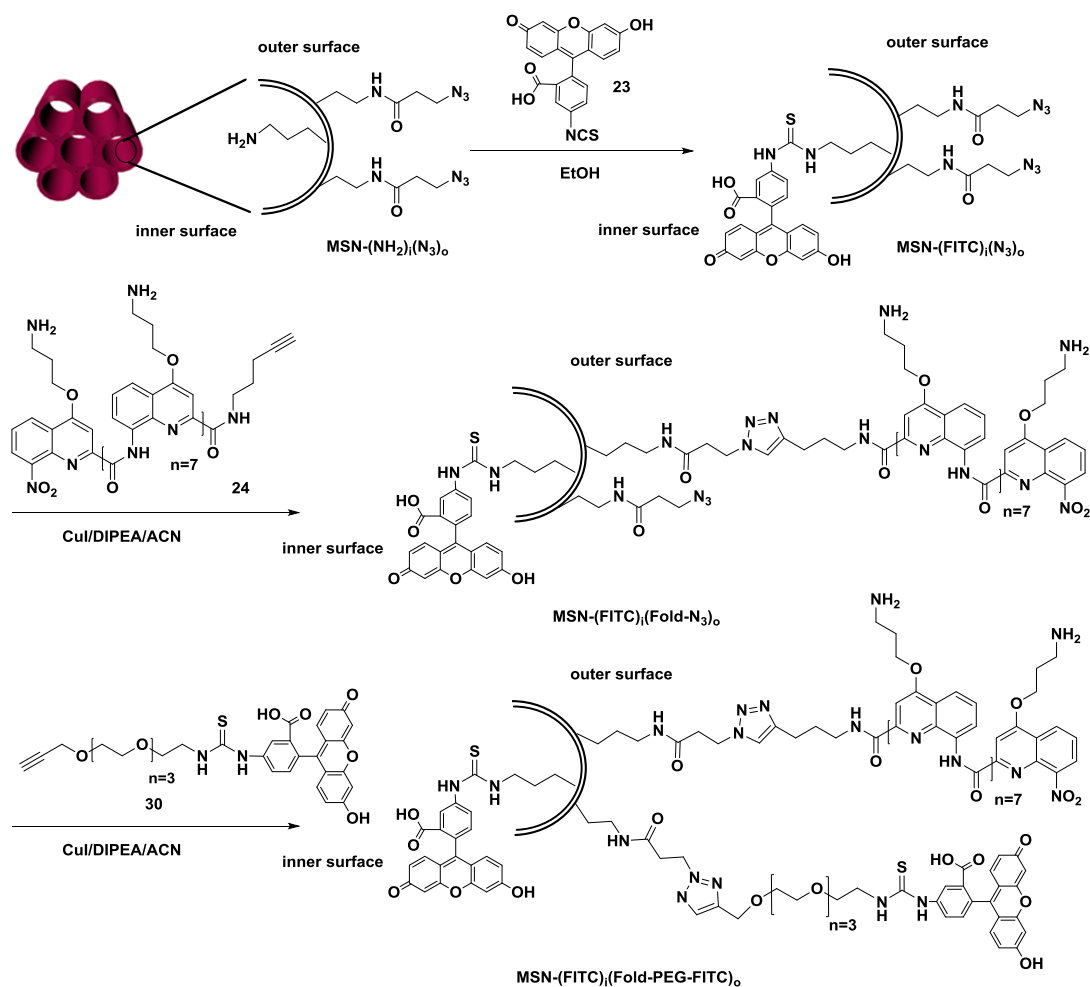


Figure 4.26. Functionalization of foldamer-MSNs ( $\text{MSN}-(\text{FITC})_1(\text{Fold}-\text{N}_3)_o$ ) with fluorescent alkyne PEG 30.

## 4.4.2. Biological experiments

### 4.4.2.1. Experimental conditions

Prior to viability and uptake experiments, the suitable conditions for biological experiments must be studied. After a wide range of proofs, the conclusions of biological experiments are summarized as follows:

- For viability experiments, COS-7 cells were used in a 10000, 2000 and 5000 cells/well concentration, 24 h and 72 h, demonstrating that 24 h 10000 cells/well were the best conditions for this cellular line.
- Nevertheless, COS-7 viability results were heterogeneous between replicates and presented a high variability.<sup>52</sup>

- MSNs washed with *N,N*-diethyldithiocarbamate presented a low viability. *N,N*-diethyldithiocarbamate is toxic,<sup>53</sup> even if it works very well for Cu removal it cannot be used for biological assays.
- Hela cells are good candidate for uptake results,<sup>12,13,15,24,25</sup> being 10000 cell/well the best concentration for viability assays and 100000 cells/well for uptake experiments. Biological experiments are reproducible and homogeneous.
- Viable MSNs concentration ranges between 0.01 and 0.16 mgMSN/mL.
- More reproducible results are obtained if MSNs are seeded directly in solution, instead of in solid state.
- Uptake experiments are more homogeneous if MSNs are seeded with an orbital agitator.

#### 4.4.2.2. Viability experiments

For viability experiments, a concentration of 10000 cells per well is chosen.<sup>12-15,24</sup> Viability assays are carried out in a 96 well plate (100  $\mu$ L/well), where cells are seeded for 24 h. Then, control MSN-(FITC) and foldamer MSN-(FITC)<sub>i</sub>(Fold)<sub>o</sub> are added and seeded for 24 h. Cells are washed with PBS and 100  $\mu$ L of MTT dissolution is added. Cells are seeded for 3 h and purple formazan crystals are suspended in DMSO. Finally, formazan absorbance is recorded in a microplate reader at 560 nm. No FITC interference is observed between 550 and 600 nm.

MSN-(FITC)<sub>i</sub>(Fold)<sub>o</sub> viability is tested for a wide range of concentrations, ranging from 0.01 mgMSN/mL to 0.16 mgMSN/mL. Relative cell viability of MSN-(FITC)<sub>i</sub>(Fold)<sub>o</sub> and MSN-(FITC) is higher than 85 %, even at high concentration doses (Figure 4.27). These results are coherent with control reported MSNs viability in Hela cells.<sup>12,14,24,54</sup>

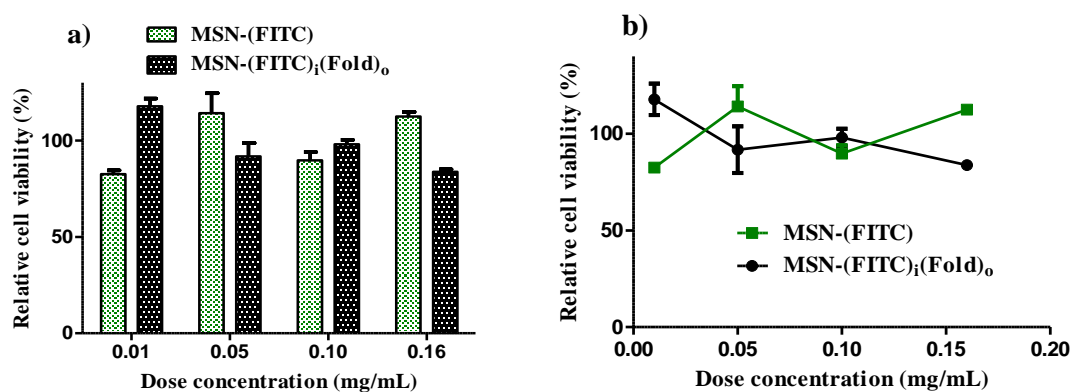


Figure 4.27. Relative cell viability for MSN(FITC)<sub>i</sub>(Fold)<sub>o</sub> and MSN(FITC) a) in bars and b) in lines.

As for foldamer-MSNs, where fluorescent-alkyne-PEG **30** has been functionalized, MTT assays demonstrated a viability of 75 % (Figure 4.28).

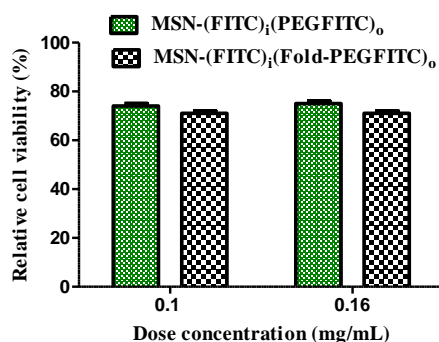


Figure 4.28. Relative cell viability of MSN(FITC)<sub>1</sub>(PEGFITC)<sub>0</sub> and MSN(Fold-PEGFITC)<sub>0</sub>.

#### 4.4.2.3. Uptake experiments

An extensive search in literature revealed that MSNs uptake experiments are normally carried out between 0 and 1 mg MSN/mL, been 0.1 mg MSN/mL the average concentration for biological applications.<sup>12–15,24</sup> Since, it is the first time that cationic quinoline foldamers are attached to a nanoparticle, it is not known if either MSNs or alkyne-foldamer will interact with the proteins present in a complete cellular medium, DMEM (Dubecco's modified Eagle's medium). This is the reason why, at the first, uptake experiment is carried out with and without LFBS proteins (LFBS: bovine serum protein 10 %).

MSN-(FITC)<sub>1</sub>(Fold)<sub>0</sub> cellular uptake is tested in Hela cells (100000 cells/well) by adding MSNs in solution. In addition, an orbital shaker is used to homogenize the uptake. Uptake experiments are carried out in a 12 well plate (1 mL/well) where clean covers have been added. Cells are seeded for 24 h and then, control MSN-(FITC) and MSN-(FITC)<sub>1</sub>(Fold)<sub>0</sub> are added and seeded for 24 h. Cells are washed with PBS and fixed to the covers. Finally, DAPI is added to stain the nucleus in blue. The resulting fluorescence was evaluated in a fluorescent microscope. Samples were visualized with a Zeiss Axiovert inverted fluorescence microscope (Axiovert 200M; Carl Zeiss Inc.) equipped with zeiss ApoTome system and with an inverted fluorescent Nikon microscope (Nikon Eclipse TS100).

MSN-(FITC)<sub>1</sub>(Fold)<sub>0</sub> did not aggregate in FBS medium, which is an excellent property, since the vast majority of nanoparticles tend to aggregate in these conditions. No differences between a rich or a poor FBS medium are observed. Therefore, FBS medium will be used for further biological experiments, since these conditions are similar to physiological medium.

On the other hand, concerning uptake results, both control-MSN and foldamer-MSN presented fluorescence in Hela cells and therefore seemed to be internalized. Whereas MSN-(FITC) fluorescence is more punctual, (Figure 4.29, b and c), MSN-(FITC)<sub>i</sub>(Fold)<sub>o</sub> fluorescence is less intense but more spread over the cells (Figure 4.29, e and f). These results are comparable with TAT and Arginine reported results.<sup>12,14</sup> The same pattern is observed, little dots for control MSN-(FITC) and blurred fluorescence for MSN-(FITC)<sub>i</sub>(Fold)<sub>o</sub>.

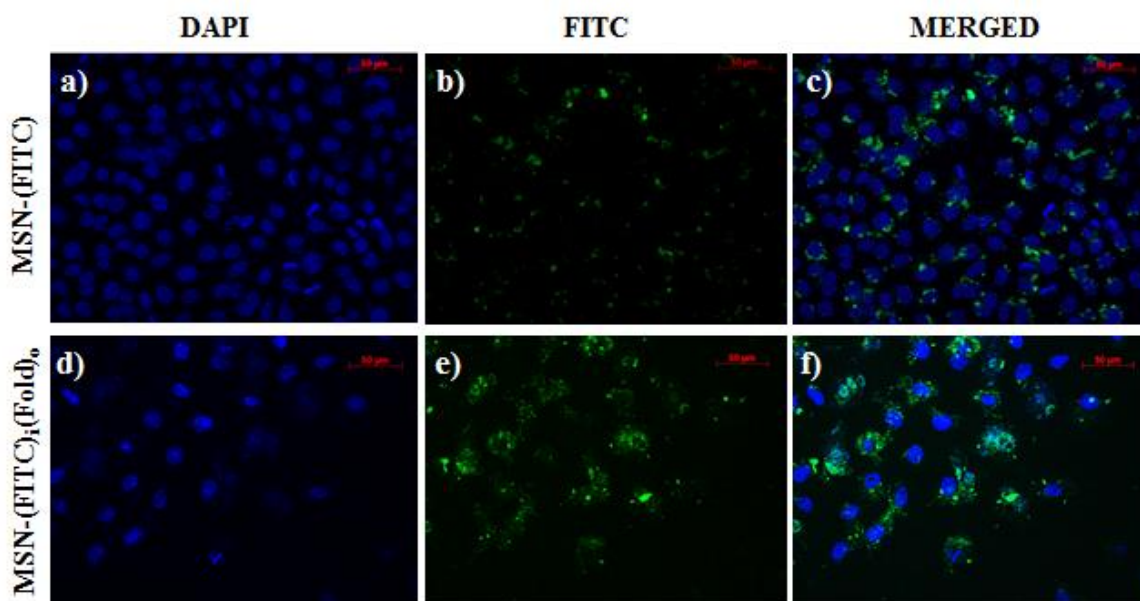


Figure 4.29. Control-MSN and foldamer-MSN uptake

As for foldamer-MSN it seems that MSN-(FITC)<sub>i</sub>(Fold)<sub>o</sub> internalize mostly in a specific area of the cytoplasm, very near to the nucleus. In addition, it seems that alkyne-foldamer could be capable of penetrating the nucleus, but it is not possible to confirm this hypothesis without any quantification method.

In order to co-localize MSN-(FITC)<sub>i</sub>(Fold)<sub>o</sub> with the nucleus and the cytoplasm, Hela cells are stained with DAPI (for the nucleus) and phalloidine (for the cytoplasm). However, it cannot be quantified, it can be confirmed that the vast majority of MSN-(FITC)<sub>i</sub>(Fold)<sub>o</sub> are clearly located in a specific area of the cytoplasm, while few MSN-(FITC)<sub>i</sub>(Fold)<sub>o</sub> seem to penetrate the nucleus (Figure 4.30).

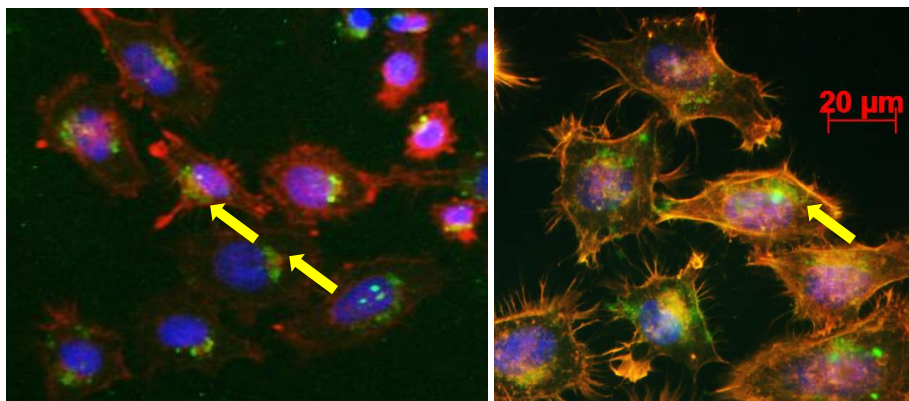


Figure 4.30. MSN-(FITC)<sub>i</sub>(Fold)<sub>o</sub> uptake stained with DAPI and phalloidin.

By studying cellular uptake in the microscope, it is possible to observe that both MSN-(FITC) and MSN-(FITC)<sub>i</sub>(Fold)<sub>o</sub> internalize cytoplasmic cells and that more quantity of MSN-(FITC)<sub>i</sub>(Fold)<sub>o</sub> is detected. Nevertheless, further experiments are needed in order to quantify the cellular and nuclear uptake.

Uptake quantification is usually carried out by cytometry measurements by monitoring FITC signal. Unfortunately, in this case it is not possible to compare FITC signal between control MSN-(FITC) and foldamer MSN-(FITC)<sub>i</sub>(Fold)<sub>o</sub>, since FITC seems to be quenched during foldamer addition. While control MSNs present fluorescence at 254 nm, when alkyne-foldamer **24** is added, foldamer-MSNs present very little fluorescence signal. MSNs fluorescence, after alkyne-foldamer **24** addition, is dramatically quenched (Figure 4.31).

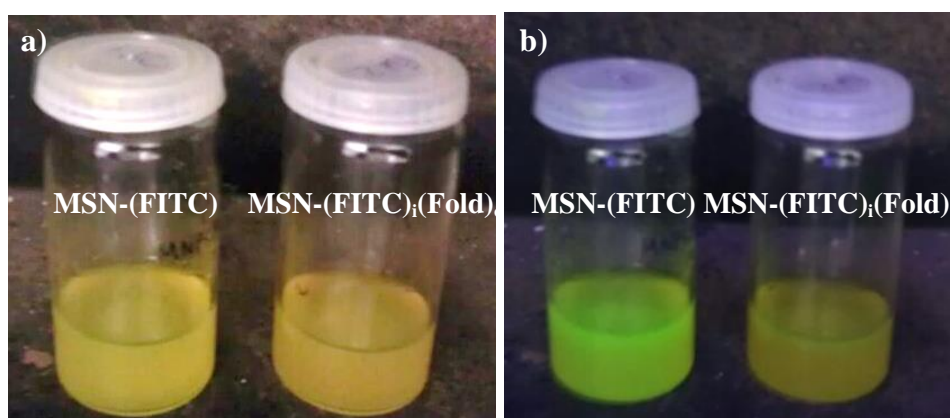


Figure 4.31. MSN(FITC) and MSN(FITC)<sub>i</sub>(Fold)<sub>o</sub> at a) visible light and at b) 254 nm.

A flow cytometry analysis is carried out for MSN-(FITC) and MSN-(FITC)<sub>i</sub>(Fold)<sub>o</sub> indicating that in both cases, 100 % of detected cells are fluorescent, which corroborates the fact that both control and foldamer-MSNs can penetrate the cells (Figure 4.32). Unfortunately, an intensity comparison between control MSN-(FITC) and MSN-(FITC)<sub>i</sub>(Fold)<sub>o</sub> cannot be done because of FITC quenching effect.

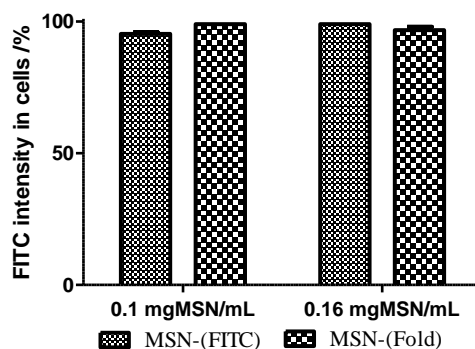
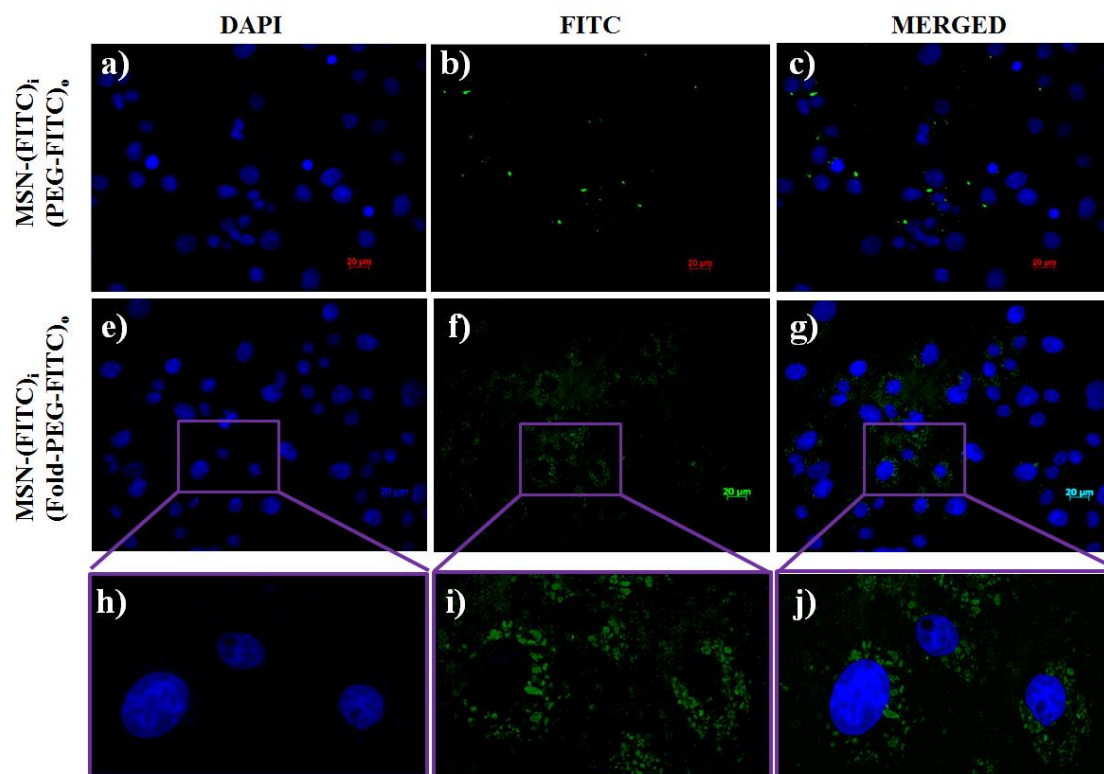


Figure 4.32. Cytometry Bars of MSN-(FITC) and MSN-(Fold).

FITC quenching can be triggered by two factors: the presence of the terminal alkyne-foldamer NO<sub>2</sub> group<sup>25</sup> and/or traces of Cu.<sup>55,56</sup> A search in literature revealed that FITC quenching has also been reported with tryptophan and guanosine moieties,<sup>57</sup> peptides similar to quinoline foldamers.<sup>57,58</sup>

In order to reduce the quenching effects of FITC, MSNs with less quantity of alkyne-foldamer **24** (five times less) and more quantity of FITC were synthesized. But, FITC was still quenched and no comparison could be done. Control MSN-(FITC) presented always more fluorescence than foldamer MSN-(FITC)<sub>i</sub>(Fold)<sub>o</sub>.

Concerning foldamer-MSNs, where fluorescent-alkyne-PEG **30** has been functionalized, a clearly difference between control MSN-(FITC)<sub>i</sub>(PEG-FITC)<sub>o</sub> and foldamer MSN-(FITC)<sub>i</sub>(Fold-PEG-FITC)<sub>o</sub> uptake is observed. Control MSNs present little and punctual fluorescence (Figure 4.33, a-c), while foldamer-MSNs show a very spread fluorescence signal (Figure 4.33, e-j). Foldamer-MSNs have been more internalized than control MSNs. Moreover, MSN-(FITC)<sub>i</sub>(Fold-PEG-FITC)<sub>o</sub> are internalized near the nucleus. Nevertheless, it does not seem that they can penetrate the nucleus. As discussed before, further studies must be carried out in order to test this hypothesis.



**Figure 4.33. Control MSN-(FITC)<sub>1</sub>(PEG-FITC)<sub>0</sub> and alkyne-PEG-FITC-foldamer MSN-(FITC)<sub>1</sub>(Fold-PEG-FITC)<sub>0</sub> uptake**

In this case, control MSN-(FITC)<sub>1</sub>(PEG-FITC)<sub>0</sub> have penetrated less than previous control MSN-(FITC)<sub>1</sub>, where no fluorescent PEG was used. One explanation to this effect could be that the external fluorescent PEG would reduce the ability of MSNs to penetrate cells compared to MSN-(FITC)<sub>1</sub>, since MSN-(FITC)<sub>1</sub> have been described in literature as penetrating systems.<sup>51</sup> Therefore, control MSN-(FITC)<sub>1</sub> would be penetrating the membrane, while control MSN-(PEG-FITC)<sub>0</sub> would not, and thus PEG-foldamer-MSNs uptake is more marked and contrasted with control MSN-(PEG-FITC)<sub>0</sub> than foldamer-MSNs with control MSN-(FITC)<sub>1</sub>. Another possibility could be that FITC, in this case, is less quenched, since an extra FITC-PEG is added and therefore the difference between foldamer-MSN and control-MSN is more contrasted.

If a 3D reconstruction with Zeiss ApoTome system is carried out in the amplified area (Figure 4.34), it can be observed that foldamer-MSNs have efficiently internalized the cells, since MSNs are present in each level of the 3D plane and therefore, MSNs are not just at the surface of the cells, but inside.

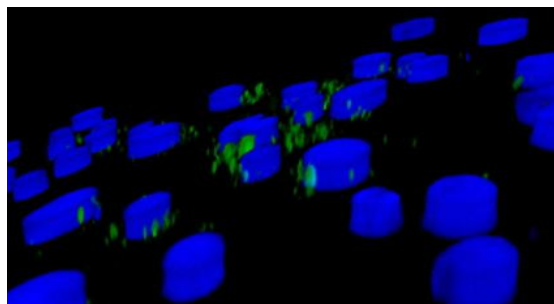


**Figure 4.34.** 3D ApoTome reconstruction of internalized MSN-(FITC)<sub>i</sub>(PEG-FITC)<sub>o</sub>.

To sum up, MSN-(FITC)<sub>i</sub>(Fold-PEG-FITC)<sub>o</sub> are non-toxic and can be internalized as well as foldamer-MSN, which is an excellent property in order to use these nanoparticles for *in vivo* applications.

#### **4.4.2.4. Uptake quantification assays**

As explained before, uptake quantification cannot be carried out by cytometry since FITC is quenched in MSN-(FITC)<sub>i</sub>(Fold)<sub>o</sub>. Another possibility, is the quantification of internalized silicon by treating MSNs in the cellular medium with HF/HNO<sub>3</sub> or NaOH (4 M) and detect silicon by atomic emission spectroscopy.<sup>15</sup> To this end, uptake experiments with a high quantity of cells in a Petri dish were carried out and after been trypsinized and centrifuged, cells with MSNs were extracted. Then, cells with MSNs were treated with HF and sonicated with both regular and ultrasonic cell disruption ultrasound to disrupt cells and solubilize silica. HNO<sub>3</sub> was also added to eliminate organic materials. Nevertheless, and after hard tries, it was not possible to solubilize the mixture. Even low concentrations of MSNs could not be dissolved in HF.

#### **4.5. Intracellular delivery of DOX with foldamer-MSN**

Due to the excellent properties of foldamer-MSNs to penetrate the cell membrane, these MSNs could be used to enhance the cellular internalization of a payload. Moreover, since quinoline foldamers are large and elongated molecules, they will easily block MSNs porous entrance. Therefore, by adding different quantities of foldamer it is possible to control the payload release. Thus, quinoline foldamers are both used as a penetrating agent and as a capping agent, for controlled release. Moreover, cationic quinoline foldamer will be better dispersed in acidic environments, than in neutral pH, acting similarly to a polymeric chain. At low pH, the alkyne-foldamer will be swelled and well dispersed, not blocking the porous, while at higher pH quinoline foldamers will be less dispersed and therefore will block more the entrance.



Therefore, it is believed that  $\text{MSN-(FITC)}_i(\text{Fold})_o$  can be used as a delivery vehicle for the release of an anticancer drug such as doxorubicin (DOX), towards cancerous cells and enhance its nuclear release. Moreover, by varying the amount of alkyne-foldamer **24** added in MSNs it is possible to modulate the quantity of DOX that can be released.

DOX is a widely studied anticancer drug that shows a pharmacodynamic effect in the nuclei by damaging the DNA structure.<sup>12,59</sup> By and large, DOX functionalization in MSNs is usually achieved on the inner porous surface by two strategies. It is either chemically absorbed in the surface or covalently linked into the pores. Nevertheless, while typical loading for absorbed DOX is near 30 %, hydrazone cleavable loading ranges from 0.2 to 2 %.<sup>60</sup> Moreover, in the case of covalent strategy, cleavable pH linkers must be introduced to MSNs surface adding synthetic steps.

Therefore, since quinoline foldamers will partially block DOX release and larger quantities of DOX can be added by absorption processes, DOX will be loaded instead of being covalently attached. Moreover, in this case, where aminated MSNs are used, by adding DOX in a basic medium, DOX loading can be enhanced.<sup>39,40,61</sup> Amino-MSNs present an excellent advantage which is that at basic pH, amino moieties would not be protonated (amino  $\text{pK}_a < 11$ ) and cationic DOX would be easily absorbed. While in an acid pH, amines will protonate preventing the electrostatic binding from happening and as consequence, DOX release will be boosted.<sup>39,40,61</sup> To this end, first of all, DOX absorption inside MSNs porous must be studied.

#### 4.5.1. DOX loading in $\text{MSN-(NH}_2)_i(\text{N}_3)_o$

In this case, DOX is absorbed in a basic trimethylamine solution, with a loading yield of 30 %. No release is obtained at  $\text{pH}=7$  (incolor supernatants), while a 60 % of release is obtained at  $\text{pH}=4$  (red supernatants). DOX is only released at  $\text{pH}=4$  (Figure 4.35).

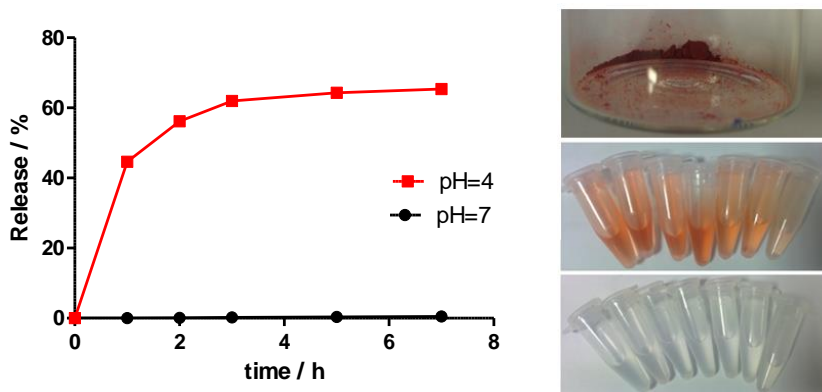


Figure 4.35. Absorbed MSN-(DOX) release.

### 4.5.2. DOX loading in foldamer-MSN

By varying the amount of alkyne-foldamer **24** added in MSNs it is possible to change the quantity of DOX that can be released. To do so, two different quantities of alkyne-foldamer **24** are functionalized in MSNs structure: a **low** density of alkyne-foldamer (0.1 mg Fold/ mg MSN) and a **high** density (0.4 mg Fold/ mg MSN) to form MSN-(DOX)(**l**-Fold)<sub>o</sub> and MSN-(DOX)(**h**-Fold)<sub>o</sub> (Figure 4.36) These MSNs are loaded with the same quantity of DOX (30 %) but with a different proportion of alkyne-foldamer . By EOA the estimated quantity of alkyne-foldamer is 16 % and 21 % for low and high density respectively.

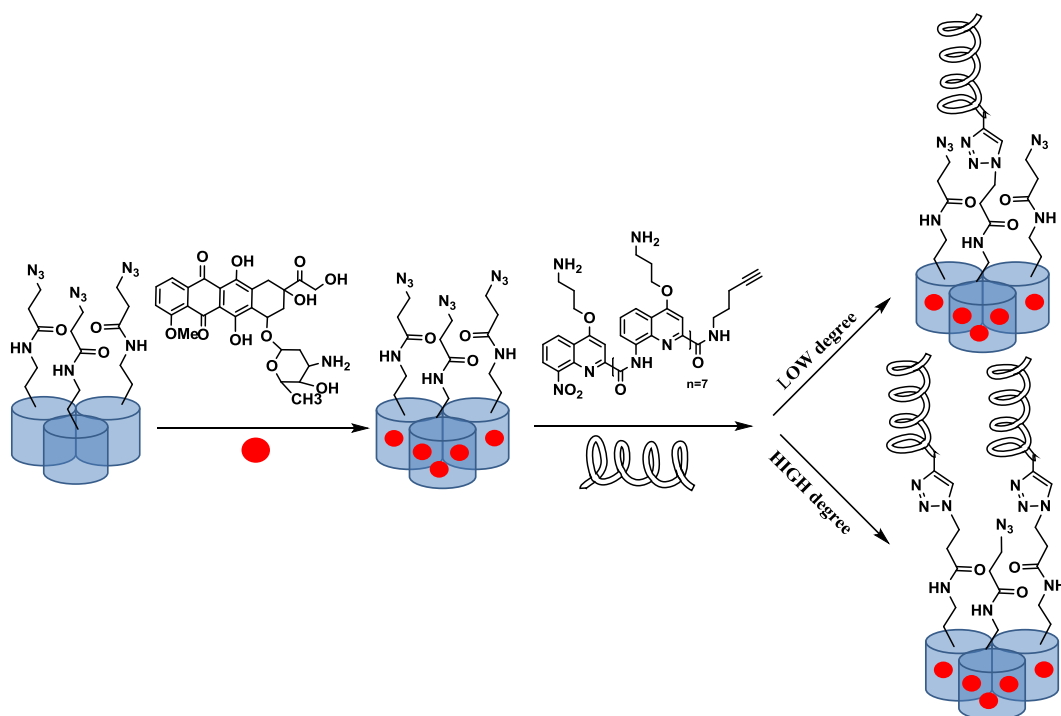
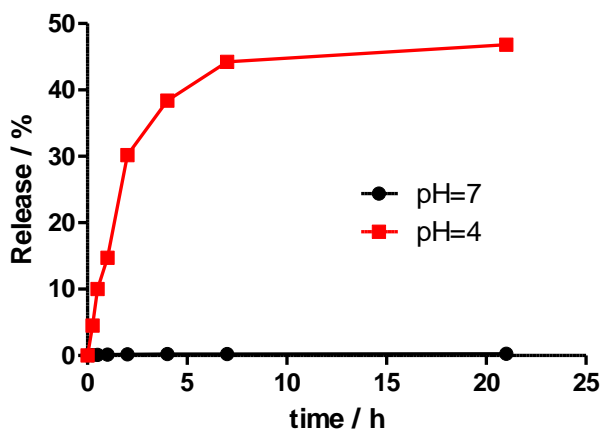
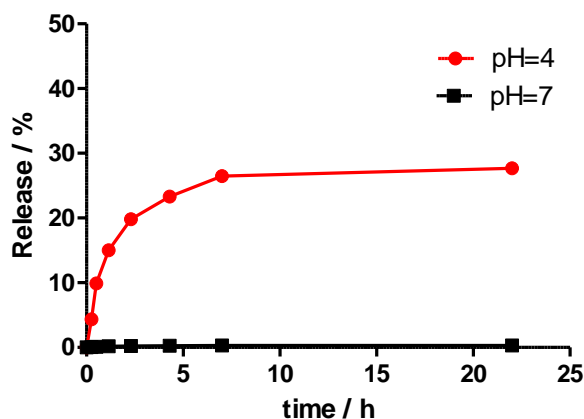


Figure 4.36. DOX loading in MSNs with low and high density of alkyne-foldamer at the outer surface.

MSN-(DOX)(**l**-Fold)<sub>o</sub> and MSN-(DOX)(**h**-Fold)<sub>o</sub> release is performed. Clearly, from the inspection of the graphic, DOX release in MSN with a lower density of alkyne-foldamer (MSN-(DOX)(**l**-Fold)<sub>o</sub>), is higher than with a high density of alkyne-foldamer (MSN-(DOX)(**h**-Fold)<sub>o</sub>) (Figure 4.37 and 4.38). Therefore, quinoline foldamer is acting as capping agent, controlling DOX release.

Figure 4.37. MSN-(DOX)(l-Fold)<sub>0</sub> release.Figure 4.38. MSN-(DOX)(h-Fold)<sub>0</sub> release.

With a high density of alkyne-foldamer, DOX release is prevented and less quantity of the drug is released. Low density of alkyne-foldamer allow a total release of 50 %, were a high density of alkyne-foldamer brings about 30 % (Table 4.5).

Table 4.5. DOX loading and release values.

MSNs	No alkyne-foldamer	Low density alkyne-foldamer	High density alkyne-foldamer
DOX Loading (%)	30	30	30
DOX Release (%)	65	47	27

For biological experiments, it is expected that MSNs with a high density of alkyne-foldamer would release less quantity of DOX and therefore will be less toxic than control-MSNs and low density alkyne-foldamer MSNs. Nevertheless, high density of alkyne-foldamer MSNs are

expected to internalize better than its counterpart and therefore could also present a higher cytotoxic effect.<sup>14</sup>

### 4.5.3. Viability and uptake experiments of MSN-(Fold)<sub>0</sub>DOX

For viability experiments, the previous later conditions were used. A 10000 cells per well concentration of Hela cells were chosen. Control MSN-(NH<sub>2</sub>)<sub>i</sub>(N<sub>3</sub>)<sub>o</sub>DOX, MSN-(DOX)(I-Fold)<sub>o</sub> and MSN-(DOX)(h-Fold)<sub>o</sub> in a 0.2, 0.1, 0.01 and 0.001 mgMSN/mL or 0.12, 0.06, 0.006 and 0.0006 mgDOX/mL concentration were added and seeded for 24 h. Viability results are presented in Figure 4.39.

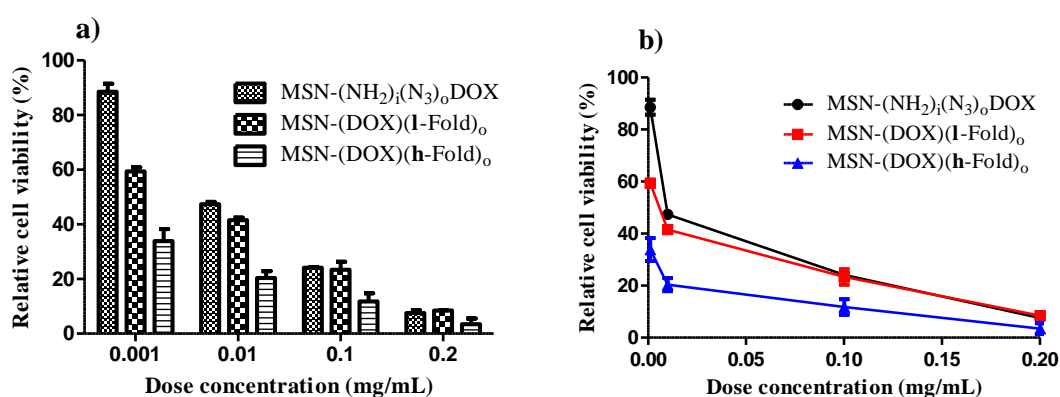


Figure 4.39. Control MSN-(NH<sub>2</sub>)<sub>i</sub>(N<sub>3</sub>)<sub>o</sub>DOX, MSN-(DOX)(I-Fold)<sub>o</sub> and MSN-(DOX)(h-Fold)<sub>o</sub> viability represented a) in bars and b) in lines.

MSN-(DOX)(h-Fold)<sub>o</sub> present a higher toxicity, considering that DOX release is the lowest (27 %), followed by MSN-(DOX)(I-Fold)<sub>o</sub> with a higher DOX release (45 %) and control MSN(NH<sub>2</sub>)<sub>i</sub>(N<sub>3</sub>)<sub>o</sub>DOX, with a DOX release of 65 %. This effect is clearer at 0.001 mgMSN/mL where MSN-(DOX)(h-Fold)<sub>o</sub> kills 66 %, MSN-(DOX)(I-Fold)<sub>o</sub> 40 % and MSN-(NH<sub>2</sub>)<sub>i</sub>(N<sub>3</sub>)<sub>o</sub>DOX only 20 % of the cells. Therefore, in all likelihood, the quantity of alkyne-foldamer increase cell mortality due to the intracellular release of DOX. Moreover, these results are in good agreement with published results,<sup>14</sup> where instead of quinoline foldamer, lysine was used as an internalizing vector. MSNs with more quantity of alkyne-foldamer are more toxic, because MSNs is more internalized and therefore DOX present a higher intracellular release and toxicity.

In order to determine if this effect is related with the quantity of MSNs and DOX that can be internalized, uptake experiments are carried out. Again, 100000 cells per well of Hela cells were used. In this case, uptake experiments were carried out with a high viability concentration, 0.01 mgMSN/mL or 0.006 mgDOX/mL was chosen. For control MSN-(NH<sub>2</sub>)<sub>i</sub>(N<sub>3</sub>)<sub>o</sub>DOX uptake images are presented in Figure 4.40 a, b and c. As it can be concluded from control MSN-

$(\text{NH}_2)_i(\text{N}_3)_o\text{DOX}$ , little quantity of DOX was detected even by saturating doxorubicin/ rhodamine red channel. Whereas, for  $\text{MSN}-(\text{DOX})(\text{l-Fold})_o$  and  $\text{MSN}-(\text{DOX})(\text{h-Fold})_o$  (Figure 4.40 e, f, g and h, i, j respectively) more quantity of DOX is observed. It seems that in comparison with control MSNs, more DOX is internalized by using quinoline foldamers. This effect has been observed both by viability and uptake experiments. Furthermore, DOX seems to internalize in the nucleus since DOX and the nucleus stained with DAPI seems to co-localize. This effect is expected since DOX is able to internalize the nucleus.<sup>62</sup> However, this hypothesis should be proven.

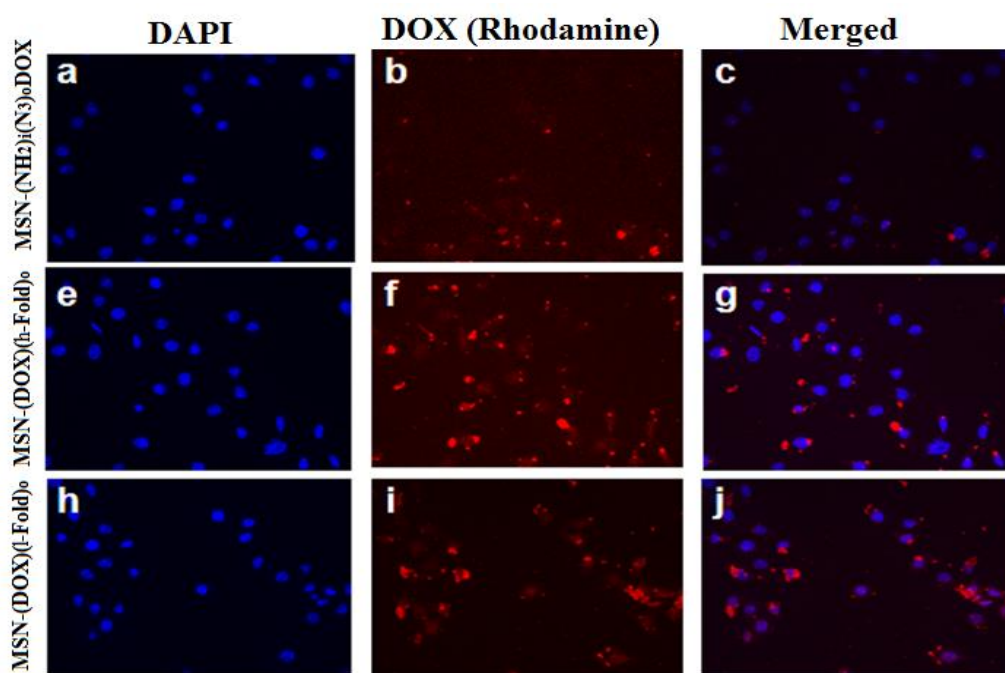


Figure 4.40. Uptake images of control  $\text{MSN}(\text{NH}_2)_i(\text{N}_3)_o\text{DOX}$  (a, b, c), of  $\text{MSN}-(\text{DOX})(\text{l-Fold})_o$  (d, e, f) and  $\text{MSN}-(\text{DOX})(\text{h-Fold})_o$  (g, h, j).

Therefore, it can be concluded that foldamer-MSN nanocarrier enhance the intracellular release of DOX and moreover, by tuning the quantity of functionalized alkyne-foldamer a controlled DOX release can be obtained.

#### 4.6. Conclusions and Outlook

- A complete regioselective methodology for the synthesis of bifunctionalized amino-azido MSNs has been carried out.
- The resulting MSNs can react with cationic quinoline foldamer allowing its complete functionalization through a CuAAC coupling. Novel foldamer-MSNs present a positive zeta potential, a good solubility in water, are non-toxic at a maximum concentration of

0.16 mgMSN/mL and are internalized better in Hela than control MSNs. Nevertheless, further experiments need to be carried out in order to quantify this effect.

- In addition, MSNs with an alkyne-foldamer moiety and a polyethylene glycol chain were also synthesized (MSN-(FITC)<sub>i</sub>(Fold-PEG-FITC)<sub>o</sub>). These Foldamer-PEG-MSNs showed a positive zeta potential, were nontoxic at a maximum concentration of 0.16 mgMSN/mL and are better internalized in Hela cells than control MSNs and foldamer-MSN. These Foldamer-PEG-MSNs could be useful for *in vivo* applications.
- Nevertheless, CuAAC coupling protocol has proven to be challenging. Cu must be completely removed before cellular experiments. This process has been difficult to achieve since Cu complexing species such as EDTA and *N,N*-diethyldithiocarbamate either solubilize MSNs or are toxic, and therefore need to be carefully removed as well. These difficulties highlight the fact that a better reaction must be used in order to functionalize cationic quinoline foldamers into MSNs.
- A quantitative determination of foldamer-MSNs uptake has not been possible to achieve since FITC is mostly quenched by the alkyne-foldamer and thus fluorescence intensity comparison cannot be done. Nevertheless, it seems clear that quinoline foldamer enhance MSNs internalization.
- Moreover, foldamer-MSNs have been proven to enhance intracellular DOX release, since MSNs with a high concentration of alkyne-foldamer, (MSN-(DOX)(h-Fold)<sub>o</sub>) are more toxic and present more quantity of DOX internalized in the cells, than low alkyne-foldamer MSN-(DOX)(l-Fold)<sub>o</sub> and control MSN(NH<sub>2</sub>)<sub>i</sub>(N<sub>3</sub>)<sub>o</sub>DOX.

Due to the excellent properties of foldamer-MSNs as cell penetrating nanoplatfoms for the delivery of active drugs, a quantitative uptake determination must be performed. Therefore, in order to quantify the uptake, another fluorophore could be used, which would not be quenched either by NO<sub>2</sub> group or by Cu. An siRNA transfection agent could also be used to express a fluorescent signal such as luciferase<sup>25</sup> or mcherry<sup>14</sup> in order to detect and compare the intensity between control and foldamer-MSNs. Moreover in this case, intensity signal would be more contrasted since control MSN would have no signal. Nevertheless, since quenching effects seem to be related with both alkyne-foldamer and CuAAC chemistry, the better course of action is to change the fluorophore as well as the click chemistry approach. Moreover, in order to enhance foldamer nuclear uptake, a foldamer with arginine moieties could be used.<sup>63</sup>

Changing both the fluorophore and the chemistry strategy would not affect the promising properties that present quinoline foldamers as penetrating agents. Quinoline foldamer structure will be preserved, since only the propargyl moiety will be changed for another suitable functional group.

New bifunctionalized amino-isothiocyanate MSNs (Chapter 5) could be an excellent approach for quinoline foldamer conjugation, since isothioureia formation is an easy, clean and fast reaction, which does not present any subproduct formation. For example, an amine BOC protected foldamer that would react at the external surface of isothiocyanate-MSN could be used (Figure 4.41).

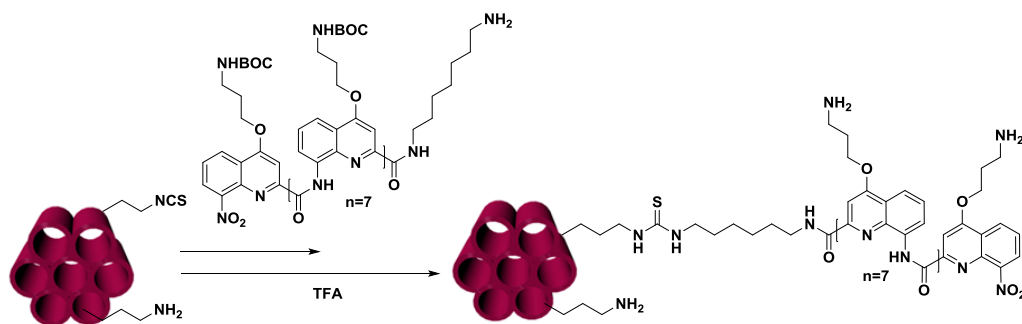


**Figure 4.41. New strategy functionalization.**

With this new strategy and a new fluorophore, foldamer MSNs uptake could be compared with other penetrating peptides such as TAT,<sup>12</sup> arginines<sup>14</sup> or amphiphilic peptides virus-like.<sup>64</sup>

#### 4.7. Bibliography

- (1) <http://biology.tutorvista.com/animal-and-plant-cel> 09/2015.
- (2) Torchilin, V. P. *Biopolym. Pept. Sci. Sect.* **2008**, *90* (5), 604–610.
- (3) Gu, Z.; Biswas, A.; Zhao, M.; Tang, Y. *Chem. Soc. Rev.* **2011**, *40* (7), 3638–3655.
- (4) Li, H.; Tsui, T.; Ma, W. *Int. J. Mol. Sci.* **2015**, *16* (8), 19518–19536.
- (5) Munyendo, W. L.; Lv, H.; Benza-Ingoula, H.; Baraza, L. D.; Zhou, J. *Biomolecules* **2012**, *2* (2), 187–202.
- (6) Stewart, K. M.; Horton, K. L.; Kelley, S. O. *Org. Biomol. Chem.* **2008**, *6* (13), 2242–2255.
- (7) Morris, M. C.; Deshayes, S.; Heitz, F.; Divita, G. *Biol. Cell* **2008**, *100* (4), 201–217.
- (8) Delehanty, J.B.; Boeneman, K.; Bradburne, C.E.; Robertson, K.; Bongard, J.E.; Medintz, I. L. . *Ther. Deliv.* **2010**, *1* (3), 411–433.
- (9) Bagashev, A.; Sawaya, B. E. *Viol. J.* **2013**, *10* (358), 1–10.
- (10) Trabulo, S.; Cardoso, A. L.; Mano, M.; de Lima, M. C. P. *Pharmaceuticals* **2010**, *3* (4), 961–993.
- (11) Mishra, A.; Lai, G. H.; Schmidt, N. W.; Sun, V. Z.; Rodriguez, A. R.; Tong, R.; Tang, L.; Cheng, J.; Deming, T. J.; Kamei, D. T.; Wong, G. C. L. *Proc. Natl. Acad. Sci.* **2011**, *108* (41), 16883–16888.
- (12) Pan, L.; He, Q.; Liu, J.; Chen, Y.; Ma, M.; Zhang, L.; Shi, J. *J. Am. Chem. Soc.* **2012**, *134* (13), 5722–5725.
- (13) Pan, L.; Liu, J.; He, Q.; Wang, L.; Shi, J. *Biomaterials* **2013**, *34* (11), 2719–2730.
- (14) Kar, M.; Tiwari, N.; Tiwari, M.; Lahiri, M.; Gupta, S. *Part. Part. Syst. Charact.* **2013**, *30* (2), 166–179.
- (15) Lu, F.; Wu, S. H.; Hung, Y.; Mou, C. Y. *Small* **2009**, *5* (12), 1408–1413.
- (16) Chou, L. Y. T.; Ming, K.; Chan, W. C. W. *Chem. Soc. Rev.* **2011**, *40* (1), 233–245.
- (17) Slowing, I.; Trewyn, B. G.; Lin, V. S. Y. *J. Am. Chem. Soc.* **2006**, *128* (46), 14792–14793.
- (18) Ma, M.; Zheng, S.; Chen, H.; Yao, M.; Zhang, K.; Jia, X.; Mou, J.; Xu, H.; Wu, R.; Shi, J. *J. Mater. Chem. B* **2014**, *2* (35), 5828–5836.
- (19) Townson, J. L.; Lin, Y. S.; Agola, J. O.; Carnes, E. C.; Leong, H. S.; Lewis, J. D.; Haynes, C. L.; Brinker, C. J. *J. Am. Chem. Soc.* **2013**, *135* (43), 16030–16033.
- (20) Meng, H.; Li, Z.; Angeles, L.; Liong, M.; Xue, M. US 2012/0207795A1, 2012.
- (21) Liu, R.; Liao, P.; Liu, J.; Feng, P. *Langmuir* **2011**, *27* (6), 3095–3099.
- (22) Manuscript, A.; Nanoparticles, M. S. *ACS Nano* **2009**, *3* (10), 3273–3286.
- (23) Baù, L.; Selvestrel, F.; Arduini, M.; Zamparo, I.; Lodovichi, C.; Mancin, F. *Org. Lett.* **2012**, *14* (12), 2984–2987.
- (24) Lee, C. H.; Cheng, S. H.; Huang, I. P.; Souris, J. S.; Yang, C. S.; Mou, C. Y.; Lo, L. W. *Angew. Chemie Int. Ed.* **2010**, *49* (44), 8214–8219.
- (25) Gillies, E. R.; Deiss, F.; Staedel, C.; Schmitter, J. M.; Huc, I. *Angew. Chemie Int. Ed.* **2007**, *46* (22), 4081–4084.
- (26) Guichard, G.; Huc, I. *Chem. Commun.* **2011**, *47* (21), 5933–5941.
- (27) Iriondo-Alberdi, J.; Laxmi-Reddy, K.; Bouguerne, B.; Staedel, C.; Huc, I. . *ChemBioChem* **2010**, *11*, 1679–1685.
- (28) Sánchez-García, D.; Kauffmann, B.; Kawanami, T.; Ihara, H.; Takafuji, M.; Delville, M. H.; Huc, I. *J. Am. Chem. Soc.* **2009**, *131* (24), 8642–8648.
- (29) Benoît, B.; Douat-Casassus, C.; Laxmi-Reddy, K.; Godde, F.; Huc, I. *J. Org. Chem.* **2010**, *75* (21), 7175–7185.



- 
- (30) Huc, I.; Hecht, S. *Foldamers: Structure, Properties, and Applications*, WileyVCH.; 2007.
- (31) Shirude, P. S.; Gillies, E. R.; Ladame, S.; Godde, F.; Shin-ya, K. **2007**, *10*, 1–10.
- (32) Müller, S.; Laxmi-Reddy, K.; Jena, P. V.; Baptiste, B.; Dong, Z.; Godde, F.; Ha, T.; Rodriguez, R.; Balasubramanian, S.; Huc, I. *ChemBioChem* **2014**, *15* (17), 2563–2570.
- (33) Delauriere, L.; Dong, Z.; Laxmi-Reddy, K.; Godde, F.; Toulme, J. J.; Huc, I. *Angew. Chemie - Int. Ed.* **2012**, *51* (2), 473–477.
- (34) Chandramouli, N.; Ferrand, Y.; Lautrette, G.; Kauffmann, B.; Mackereth, C. D.; Laguerre, M.; Dubreuil, D.; Huc, I. *Nat. Chem.* **2015**, *7* (4), 334–341.
- (35) Kar, M.; Malvi, B.; Das, A.; Panneri, S.; Gupta, S. *Sen. J. Mater. Chem.* **2011**, *21* (18), 6690–6697.
- (36) Moitra, N.; Trens, P.; Raehm, L.; Durand, J. O.; Cattoën, X.; Chi Man, M. W. *J. Mater. Chem.* **2011**, *21* (35), 13476–13482.
- (37) Dickschat, A. T.; Behrends, F.; Bühner, M.; Ren, J.; Weiß, M.; Eckert, H.; Studer, A. *Chem. Eur. J.* **2012**, *18* (52), 16689–16697.
- (38) Chandran, S.P.; Hotha, S.; Prasad, B. L. V. *Curr. Sci.* **2008**, *95* (9), 1327–1333.
- (39) Meng, H.; Xue, M.; Xia, T.; Zhao, Y. L.; Tamanoi, F.; Stoddart, J. F.; Zink, J. I.; Nel, A. E. *J. Am. Chem. Soc.* **2010**, *132* (36), 12690–12697.
- (40) Muhammad, F.; Guo, M.; Qi, W.; Sun, F.; Wang, A.; Guo, Y.; Zhu, G. *J. Am. Chem. Soc.* **2011**, *133*, 8778–8781.
- (41) Malvi, B.; Sarkar, B. R.; Pati, D.; Mathew, R.; Ajithkumar, T. G.; Sen Gupta, S. *J. Mater. Chem.* **2009**, *19* (10), 1409–1416.
- (42) Wan, X.; Yao, S.; Liu, H.; Yao, Y. *J. Mater. Chem. A* **2013**, *1* (35), 10505–10512.
- (43) Hara, K.; Akahane, S.; Wiench, J. W.; Burgin, B. R.; Ishito, N.; Lin, V. S.-Y.; Fukuoka, A.; Pruski, M. *J. Phys. Chem. C* **2012**, *116* (12), 7083–7090.
- (44) Huang, Y.; Xu, S.; Lin, V. S. Y. *Angew. Chemie Int. Ed.* **2011**, *50* (3), 661–664.
- (45) Grandjean, C.; Boutonnier, A.; Guerreiro, C.; Fournier, J. M.; Mulard, L. a. *J. Org. Chem.* **2005**, *70* (18), 7123–7132.
- (46) Huang, Y.; Xu, S.; Lin, V. S. Y. *Angew. Chemie Int. Ed.* **2011**, *50* (3), 661–664.
- (47) Vallet-Regí, M. *ISRN Mater. Sci.* **2012**, *2012*, 1–20.
- (48) Chiang, Y. D.; Lian, H. Y.; Leo, S. Y.; Wang, S. G.; Yamauchi, Y.; Wu, K. C. W. *J. Phys. Chem. C* **2013**, *115* (27), 13158–13165.
- (49) Gao, J.; Zhang, X.; Xu, S.; Tan, F.; Li, X.; Zhang, Y.; Qu, Z.; Quan, X.; Liu, J. *Chem. Eur. J.* **2014**, *20* (7), 1957–1963.
- (50) Cui, J.; Rose, R. De; Alt, K.; Alcantara, S.; Paterson, B. M.; Liang, K.; Hu, M.; Richardson, J. J.; Yan, Y.; Jeffery, C. M.; Price, R. I.; Peter, K.; Hagemeyer, C. E.; Donnelly, P. S.; Kent, S. J.; Caruso, F. *ACS Nano* **2015**, *9* (2), 1571–1580.
- (51) He, Q.; Zhang, Z.; Gao, F.; Li, Y.; Shi, J. *Small* **2011**, *7* (2), 271–280.
- (52) Quianjun He, Zhiwen Zhang, Yu Gao, J. S. and Y. L. *Small* **2009**, *5* (23), 2722–2729.
- (53) Tonkin, E. G.; Valentine, H. L.; Milatovic, D. M.; Valentine, W. M. *Toxicol. Sci.* **2004**, *81* (1), 160–171.
- (54) Fan, J.; Fang, G.; Wang, X.; Zeng, F.; Xiang, Y.; Wu, S. *Nanotechnology* **2011**, *22* (455102), 1–11.
- (55) Wang, S.; Wang, X.; Zhang, Z.; Chen, L. *Colloids Surfaces A Physicochem. Eng. Asp.* **2015**, *468* (09), 333–338.
- (56) Liu, Z. C.; Yang, Z. Y.; Li, T. R.; Wang, B. D.; Li, Y.; Qin, D. D.; Wang, M. F.; Yan, M. H. *Dalt. Trans.* **2011**, *40* (37), 9370–9373.

- (57) Togashi, D. M.; Szczupak, B.; Ryder, A. G.; Calvet, A.; O'Loughlin, M. *J. Phys. Chem. A* **2009**, *113* (12), 2757–2767.
- (58) Test, F.; Studied, O. *Integr. DNA Technol.* **2011**, 1–3.
- (59) <http://www.cancerresearchuk.org/about-cancer/cancers-in-general/treatment/cancer-drugs/doxorubicin> 09/2015.
- (60) Fan, J.; Fang, G.; Wang, X.; Zeng, F.; Xiang, Y.; Wu, S. *Nanotechnology* **2011**, *22* (455102), 1–11.
- (61) Cheng, Z.; Ma, P.; Hou, Z.; Wang, W.; Dai, Y.; Zhai, X.; Lin, J. *Dalt. Trans.* **2012**, *41* (5), 1481–1489.
- (62) Goto, S.; Ihara, Y.; Urata, Y.; Izumi, S.; Abe, K.; Koji, T.; Kondo, T. *FASEB J.* **2001**, *15* (14), 2702–2714.
- (63) Melikov, K.; Chernomordik, L. V. *Cell. Mol. Life Sci.* **2005**, *62* (23), 2739–2749.
- (64) Li, Z.; Liu, Y.; Hu, J.; Xu, Q.; Liu, L.; Jia, H.; Chen, W.; Lei, Q.; Rong, L.; Zhang, X. *ACS Appl. Mater. Interfaces* **2014**, *6*, 14568–14575.

## Chapter 5. Amino-isothiocyanate MSNs for the controlled release of Ataluren.

---

A simple and straightforward protocol to prepare isothiocyanate functionalized MSNs is described. The synthetic methodology is general and can be applied, in principle, to all type of aminated MSNs. The efficiency of the functionalization is comparable to the copper cycloaddition (CuAAC) avoiding isolation and copper removal protocols. Following this methodology, new amino-isothiocyanate regioselective functionalized MSNs have been prepared for the design of a nano-container able to release the drug Ataluren in a controlled manner for the treatment of Duchenne Muscular Dystrophy (DMD).



## Chapter 5. Amino-isothiocyanate MSNs for the controlled release of Ataluren.

### 5.1. Introduction

MSNs have proven to exhibit outstanding properties for its application as carriers in drug delivery.<sup>1,2</sup> However, different anchoring synthetic strategies are needed in order to functionalize multiple substituents to MSNs domains and confer complexity to the system. A quick, clean, high yield and selective chemistry is necessary to functionalize different agents with efficient protocols.<sup>3</sup> Typical coupling strategies that have been widely studied are CuAAC chemistry<sup>4</sup> and the formation of amides,<sup>5,6</sup> disulfide bonds,<sup>7</sup> thioureas<sup>8</sup> and isothiureas<sup>9</sup> (Chapter 1). Nevertheless, some reactions such as amide and disulfide bond formation, although being very efficient, present the disadvantage of using activating agents such as succinimidyl or maleimide groups, which necessarily need to be incorporated to the system.<sup>10</sup> As for isocyanate moiety, although it readily reacts with amines without the liberation of any by-product, it is prone to hydrolysis, not allowing its use with non-anhydrous solvents and precluding their storage.<sup>11</sup> Moreover, in Chapter 4, the problems derived from using CuAAC reactions for cellular applications have clearly underlined that strict protocols for the removing of transition metal catalysts are needed. As an example, EDTA or *N,N*-diethyldithiocarbamate complexants must be used for this end. Nevertheless, these complexing agents present more drawbacks than advantages. EDTA solubilizes MSNs<sup>12</sup> and *N,N*-diethyldithiocarbamate is highly toxic.<sup>13</sup> Moreover, Cu can be held in amino-MSNs channels by Cu-NH<sub>2</sub> interactions<sup>14</sup> at the same time that it can enhance fluorophore quenching processes.<sup>15</sup> As a result, a large quantity of washing cycles are needed,<sup>4</sup> which diminish final yields. Therefore, even if CuAAC chemistry is a selective and efficient reaction, it is crucial to find easy, fast and high yield chemistry that does not require the presence of any activating agent or transition metal catalyst removal.

On the other hand, although isocyanate is not suitable for bioconjugation, its sulphur-containing counterpart, isothiocyanate easily overcomes isocyanate downsides. Isothiocyanate present a high stability and selectivity at the same time that is amino selective and stable in mild solvents.<sup>16</sup> The fact that thiourea reactions are fast, specific, selective, water tolerant, with high yield reactions and that does not add any metal catalyst, highlights the idea that isothiocyanate is an optimal moiety to use for MSNs bioconjugation. In fact, bioconjugations involving thiourea formation has been widely used, for example in the case of FITC functionalization.<sup>9</sup>

Thiourea formation in nanoparticles has been usually carried out by using aminated nanoparticles and an isothiocyanate linker.<sup>9</sup> Nevertheless, most of the bioactive molecules such

as proteins, amino acids, peptides and drugs, present amine moieties instead of isothiocyanates groups in their structure. Therefore, in order to introduce these active molecules onto MSNs surface, amine moiety must be turned into isothiocyanate functionality. Yet, instead of synthesizing isothiocyanate moieties in every active molecule, it is proposed to prepare isothiocyanate MSNs and directly add any primary amine reagent.

Moreover, in order to attain the level of complexity needed for the design of “smart” nanocarriers, it is vital to develop, stable and ready-to-use clickable MSNs that will incorporate different and orthogonal functional groups. Therefore, by using the same regioselective methodology that has been applied in Chapter 4, regioselective bifunctionalized amino-isothiocyanate MSNs can be synthesized and used for the synthesis of excellent drug release nanocarriers. While inner amino moieties would enhance drug loading and drug release,<sup>17-19</sup> the external isothiocyanate domain will be suitable for installing stimulus-responsive systems, opening or capping the nanochannels of MSNs through different stimuli. For example, these outer isothiocyanate groups would be able to react with primary amines, ranging from simple alkyl amines, short PEGs to polymers. Once attached to the MSNs, their presence could modulate the release profile of a payload. Furthermore, the chemical nature of these chains is a key factor to optimize not only the drug release but also the characteristics of MSNs corona that define their biodistribution and clearance from the body.<sup>20</sup>

A search in literature revealed that there are no examples of aminated-isothiocyanate MSNs. Regarding isothiocyanates in mesoporous silica nanoparticles in general, only two authors reported the use of isothiocyanate in non-functionalized MSNs<sup>21-23</sup> but in just one case isothiocyanate was added for bioconjugation applications.<sup>23</sup> In the case of Li and Lui *et al.*,<sup>21,22</sup> isothiocyanate was added by grafting a isothiocyanate silane in non-functionalized MSNs and these MSNs were only used for the detection of Cu and Hg. The result is the obtaining of monofunctionalized isothiocyanate MSNs, where functional moiety is present in MSNs surface without any regioselectivity. Alternatively, Faure *et al.*<sup>23</sup> exposed aminated MSNs to *p*-diisothiocyanatophenylene, providing MSNs with phenyl isothiocyanate moiety on their surface.<sup>23</sup> In this case, these MSNs are used for bioconjugation applications but again isothiocyanate is present in MSNs surface without any regioselectivity. In addition, this strategy adds phenyl moieties in MSNs structure, which impart a hydrophobic coating to the MSNs. Therefore, a new way of adding isothiocyanate moieties without using *p*-diisothiocyanatophenylene and that would allow regioselective bifunctionalization must be studied.

In this case, since initial MSNs present amino groups, isothiocyanate silanization cannot be achieved if amino moieties are present in MSNs surface area. By using grafting procedures it is

not possible to give bifunctionalized amino-isothiocyanate MSNs. Isothiocyanate functionality can only be introduced into MSNs surface if amino moieties are directly transformed to isothiocyanate moiety. Therefore, the only possibility to introduce isothiocyanate functionality is by chemically transforming all the outer amino moieties into isothiocyanate groups. Since isothiocyanate and amine react, it is not possible to introduce the final moiety by any linker, as it was done in Chapter 4, for azido moiety. Consequently, it is proposed to transform directly the outer amino groups in isothiocyanate moieties, while the tensioactive is still present in the porous to give inner amino, outer isothiocyanate MSNs (MSN-(NH<sub>2</sub>)<sub>i</sub>(NCS)<sub>o</sub>). Furthermore, the ability of these new MSNs as a drug release nanocarrier will be tested for the delivery of Ataluren drug, as a treatment of Duchenne muscular dystrophy (DMD).

## 5.2. Synthesis and characterization of Isothiocyanate-MSNs

First, the study of the synthesis and characterization of monofunctionalized isothiocyanate-MSNs is carried out.

A search in the literature reveals that, the typical procedure for the preparation of isothiocyanates from amines consists in a two-step methodology.<sup>24,25</sup> In the main, isothiocyanate formation from amine moieties proceeds through the reaction between amines and carbon disulfide in aqueous ammonia or NaOH. This results in the precipitation of the ammonium dithiocarbamate salt, which is then treated with lead nitrate or cyanuric chloride to yield the corresponding isothiocyanate.<sup>26,27</sup> Another possibility of forming isothiocyanates is using a tosyl chloride mediated decomposition of dithiocarbamate salts.<sup>25</sup> Nevertheless, both synthesis are not straightforward and are difficult to apply in MSNs conjugation.

An alternative and straightforward protocol is the use of the “thiocarbonyl transfer reagents” such as 1,1'-thiocarbonyldi-2(1*H*)-pyridone.<sup>28</sup> This commercially available reagent reacts smoothly with primary amines under neutral conditions to give high yields of the corresponding isothiocyanate in a single step. The only by-product formed is the water soluble 2-pyridone.<sup>29</sup> This reaction is straightforward, easy and fast, with high yields, does not require the presence of any activating agent or any transition metal catalyst and therefore can be easily applied in MSNs functionalization. 1-1'-thiocarbonyldi-2(1*H*)-pyridone has never been used for isothiocyanate formation in MSNs.

As a result, first of all, MSNs isothiocyanate formation with 1-1'-thiocarbonyldi-2(1*H*)-pyridone (**5**) must be tested. Since amine and isothiocyanate moieties are not compatible in the

same surface, first the concept of converting all amino moieties into isothiocyanates must be proven. For this reason, CTAB must be completely removed before any reaction. As proof of concept, aminated MSNs of two different sizes (50 and 100 nm), prepared by the co-condensation method were reacted with 12 eq. of 1,1'-thiocarbonyldi-2(1*H*)-pyridone (**5**) in anhydrous dichloromethane for 24 h. Previously, MSNs were treated with toluene to dry any remained water inside the channels. The resulting material was washed with ethanol and dried at 60 °C (Figure 5.1).

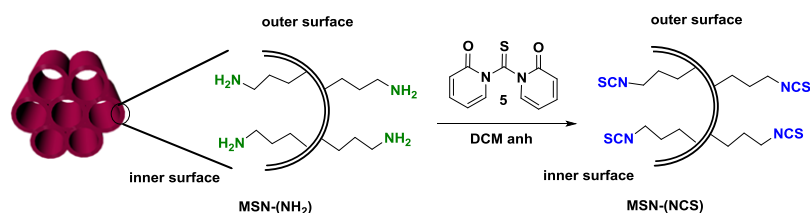


Figure 5.1. Synthetic approach of monofunctionalized isothiocyanate MSNs (MSN-(NCS)).

The successful functionalization of MSN-(NCS) is supported by the presence of two characteristic absorption bands around 2100  $\text{cm}^{-1}$  in the FT-IR spectrum, characteristic of isothiocyanate tensions (Figure 5.2).

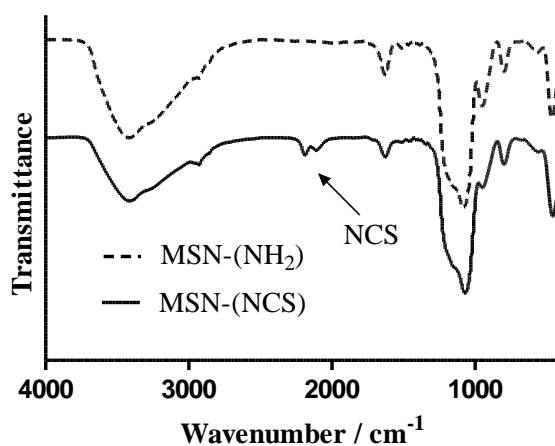


Figure 5.2. FTIR spectra of MSN-(NH<sub>2</sub>) and MSN-(NCS).

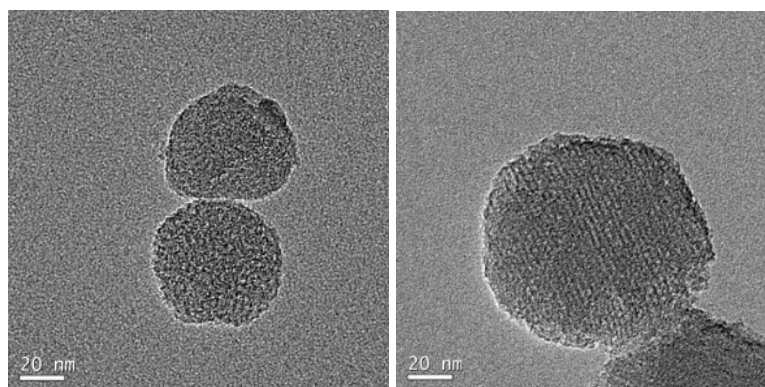
MSN-(NCS) nanoparticles were characterized by DLS, TEM, BET and powder XRD analysis. No significant size and  $\zeta$ -potential differences were obtained between initial aminated MSNs (MSN-(NH<sub>2</sub>)) and isothiocyanate-MSNs (MSN-(NCS)) (Table.5.1). These data suggest that the mild conditions used for the functionalization do not erode the structural features of MSNs. These nanoparticles show good chemical stability and can be stored at room temperature indefinitely.



**Table 5.1. Dynamic light scattering (DLS) size and  $\zeta$ -potential values of MSN-(NH<sub>2</sub>) and MSN-(NCS) of 50 and 100 nm.**

Size / nm	TEM	DLS	pDI	$\zeta$ -pot / mV
MSN-(NH <sub>2</sub> )	50	129	0.19	-1.7
	100	142	0.07	-12
MSN-(NCS)	50	152	0.09	-1.4
	100	215	0.50	-11

As expected, no significant size, shape and morphology differences were obtained for MSN-(NCS) in comparison with aminated MSNs. MSN-(NCS) are regular, homogeneous and round shaped as it can be observed in TEM micrographs (Figure 5.3).

**Figure 5.3. TEM micrographs of MSN-(NCS) of 50nm (a) and 100 nm (b).**

Regarding N<sub>2</sub> adsorption/desorption measurements, MSN-(NCS) showed type IV isotherms, which display clear H1 hysteresis loop characteristic of mesoporous materials. BET surface areas are over 600 m<sup>2</sup>·g<sup>-1</sup> and 1100 m<sup>2</sup>·g<sup>-1</sup> for MSN-(NH<sub>2</sub>) (50 nm) and (100 nm) respectively, whereas for MSN-(NCS) (50 nm) were 554 m<sup>2</sup>·g<sup>-1</sup> and 849 m<sup>2</sup>·g<sup>-1</sup> for MSN-(NCS) (100 nm) (Figure 5.4). Additionally, the pore volume for MSN-(NCS) (50nm) was 0.45 cm<sup>3</sup>·g<sup>-1</sup> and 0.53 cm<sup>3</sup>·g<sup>-1</sup> for the MSN-(NCS) (100 nm). As a reference, the values recorded for MSN-(NH<sub>2</sub>) were 0.55 cm<sup>3</sup>·g<sup>-1</sup> and 0.72 cm<sup>3</sup>·g<sup>-1</sup> respectively. MSN present a very narrow pore size distribution centered at 2.5 nm (Table 5.2). These data also suggest that the mild conditions used for the functionalization do not erode the structural features of the MSNs.

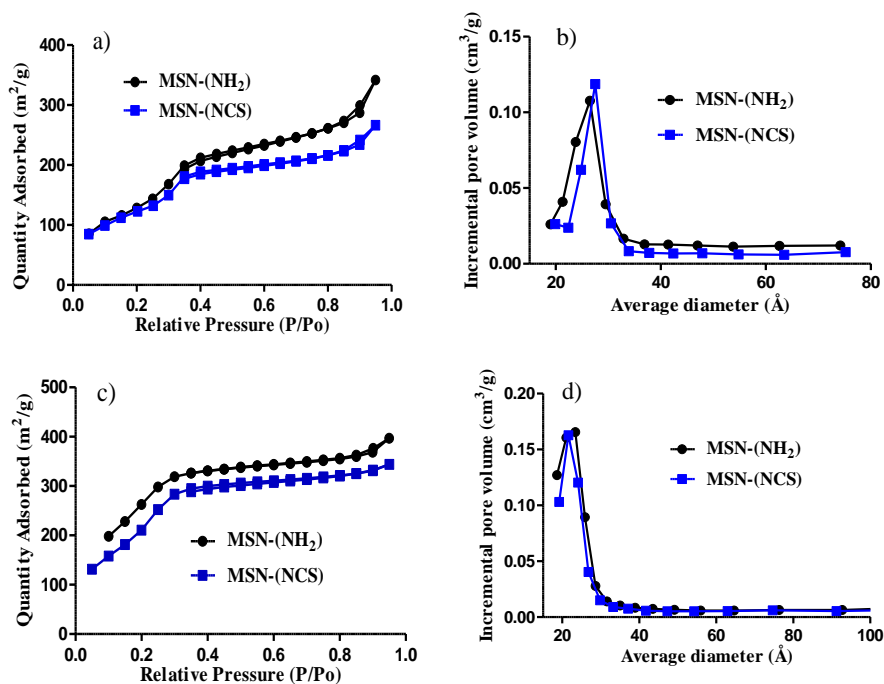


Figure 5.4.  $N_2$  adsorption-desorption and BJH pore size distribution plots of MSN-( $NH_2$ ) and MSN-(NCS) of 50 nm (a,b) and 100 nm (c,d).

Table 5.2.  $N_2$  adsorption-desorption and BJH pore size distribution values of MSN-( $NH_2$ ) and MSN-(NCS) of 50 and 100 nm.

	MSN-( $NH_2$ )		MSN-(NCS)	
	(50 nm)	(100 nm)	(50 nm)	(100 nm)
<b>BET Surface area (<math>m^2/g</math>)</b>	599.80	1120.90	554.54	849.20
<b>BJH pore volume (<math>cm^3/g</math>)</b>	0.55	0.72	0.45	0.53
<b>Pore size (nm)</b>	2.50	2.20	2.75	2.20

Powder XDR analysis indicates highly ordered structures with d100 at 2.3 and lighter faceted hexagon-shape at 4.1 (d110) and 4.2 (d200) (Figure 5.5).

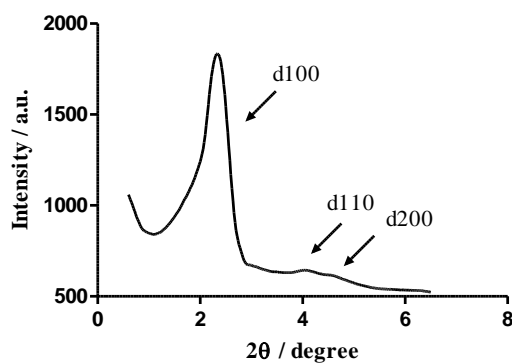


Figure 5.5. SXDR of MSN-(NCS) of 100 nm.

It can be concluded that isothiocyanate formation from amino MSNs can be successfully carried out without affecting MSNs morphology.

### 5.3. Assessment of MSN-(NCS) functionalization

Once MSN-(NCS) have been synthesized, its reactivity must be assessed. To prove that isothiocyanate-MSNs can react with amino moieties rapidly, efficiently, with quantitative yields and without further purifications, this reaction is compared with the CuAAC. Therefore, azido and isothiocyanate MSNs are synthesized, reacted with a comparable reagent and its performance studied by OEA analysis. By these means, a fluorescent naphthalimide bearing an alkyne and aliphatic primary amine was chosen. CuAAC cycloaddition is carried out by the reaction of amino MSNs with the activated azido-propionic acid, *N*-succinidyl 3-azidopropionate (**22**). Then, both azido and isothiocyanate MSNs are reacted with alkyne **32** and amino **11** naphthalimides respectively (Figure 5.6 and 5.8). MSNs were synthesized using the same equivalents of azide linker **22** and 1,1'-thiocarbonyldi-2(1*H*)-pyridone (**5**), as well as adding the same amount of suitable naphthalimide (**11** and **32**) for each case.

First, mono-functionalized MSN-(NCS) were exposed to primary amine **11** for 48 h, using ethanol as a solvent (Figure 5.6). The reacting mixture was washed five times with the same solvent and centrifuged to render a yellow solid.

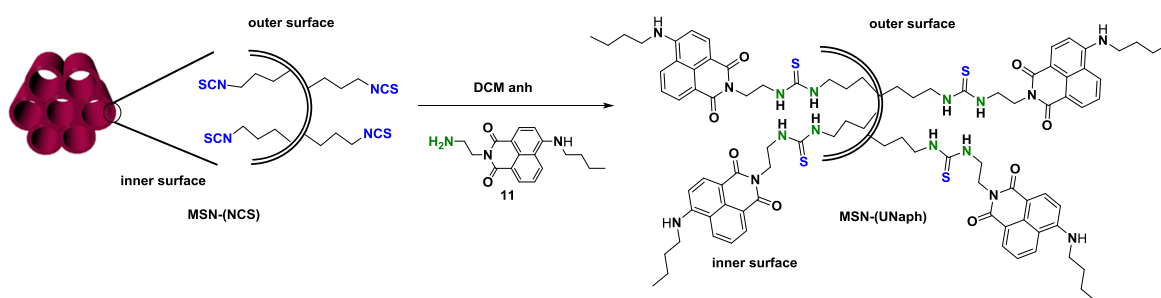


**Figure 5.6. MSN-(NCS) functionalization with amine naphthalimide 11 (MSN-(UNaph)).**

The disappearance of the two bands around  $2100\text{ cm}^{-1}$  indicates the completion of the reaction demonstrating that MSN-(NCS) can react with amino moieties forming isothioureas (Figure 5.7).

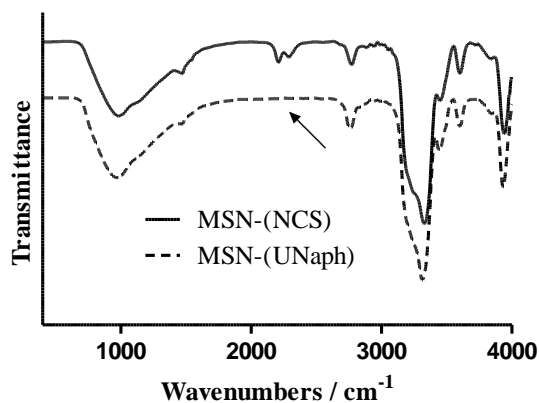


Figure 5.7. FTIR spectra of MSN-(NCS) functionalization with naphthalimide MSN-(UNaph).

To assess the performance of this new functionalization methodology, CuAAC coupling was used as standard. Therefore, the corresponding azido monofunctionalized MSNs (MSN-(N<sub>3</sub>)) were coupled with an alkyne butylnaphthalimide **32** (Figure 5.8).

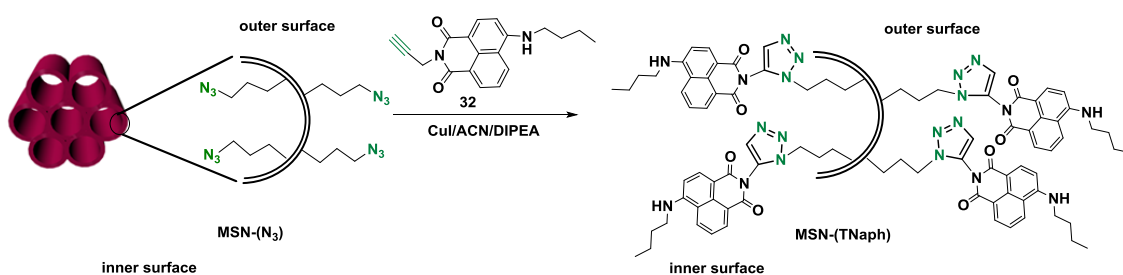


Figure 5.8. MSN-(N<sub>3</sub>) functionalization with alkyne naphthalimide **32** (MSN-(TNaph)).

In this case, the disappearance of the azido band around 2100 cm<sup>-1</sup> indicates the completion of the reaction (Figure 5.9).

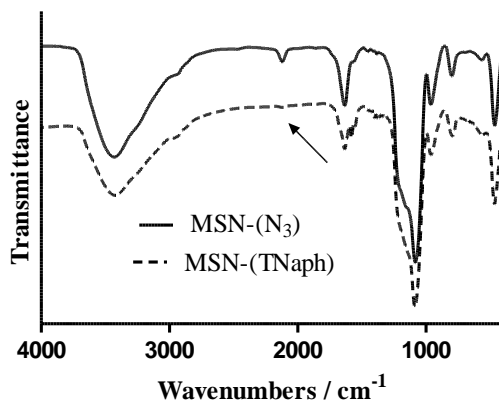


Figure 5.9. FTIR spectra of MSN-(N<sub>3</sub>) functionalization with alkyne naphthalimide (**32**) (MSN-(TNaph)).

Both MSN-(NCS) and MSN-(N<sub>3</sub>) nanoparticles are successfully functionalized with naphthalimide moieties presenting yellow coloration and a maximum band in the absorption spectrum of approximately 450 nm (Figure 5.10).

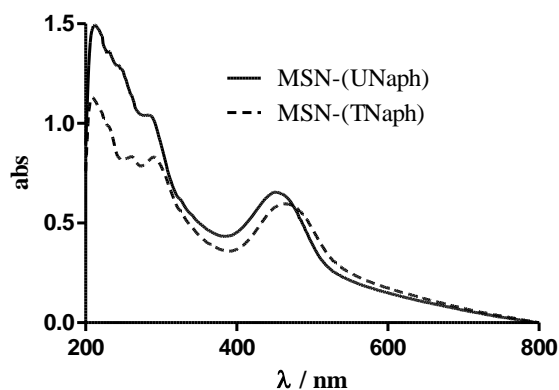


Figure 5.10. Absorption spectra of MSN-(UNaph) and MSN-(TNaph).

Finally, the functionalization capacity of both MSNs was determined by organic elemental analysis (OEA) (Table 5.3). Naphthalimide loading turned out to be comparable in both cases; 4.6 % of naphthalimide loading was achieved when the CuAAC protocol is used, while a 4.8 % is obtained when using isothiocyanate chemistry. As anticipated, these results confirm the suitability of the isothiocyanate group to participate in the functionalization of MSNs.

Table 5.3. OEA analysis of MSN-(NCS), MSN-(UNapht), MSN-(N<sub>3</sub>) and MSN-(TNaph).

MSNs	C (%)	H (%)	N (%)
MSN-(NCS)	9.78	1.87	1.92
MSN-(UNapht)	14.59	2.59	2.32
MSN-(N <sub>3</sub> )	7.22	2.56	2.64
MSN-(TNaph)	11.79	2.56	3.08

The resulting MSNs easily react with primary amines and are compatible with aqueous media. The efficiency of the functionalization is comparable to the CuAAC. However, in stark contrast with the CuAAC protocols, the isolation of the derivatized MSNs is simple and there is no need to remove any by-product or toxic catalysts. While the thiourea-containing MSNs are easily isolated, the removal of copper species from the CuAAC reaction requires tedious and extensive washings. More than twelve washings with dithiocarbamate were needed,<sup>4</sup> in order to remove

Cu traces, when alkyne-azide reaction was used; while, four washings in EtOH were only needed to remove amine-naphthalimide in MSN-(NCS). Moreover, this large number of washings in CuAAC synthesis leads to a high loss of MSNs, whereas with isothioureia formation quantitative yields are obtained. In addition, isothiocyanate chemistry can be carried out in alcohol and water solvents. Therefore, any supernatant quantification of drug loading can be achieved by absorbance determination, while in the case of cycloaddition, due to extensive washings in different solutions such as EDTA, dithiocarbamate, ACN and water, supernatant quantification cannot be achieved. These CuAAC disadvantages make isothiocyanate reaction an excellent approach for “click chemistry” synthesis in nanoparticles.

#### 5.4. Orthogonal regioselective bifunctionalization of MSN-(NH<sub>2</sub>)<sub>i</sub>(NCS)<sub>o</sub>

Amino MSNs can be easily converted into isothiocyanate moieties and isothioureia “click chemistry” is reactively comparable with CuAAC protocol. Therefore, bifunctionalized amino-isothiocyanate nanoparticles (MSN-(NH<sub>2</sub>)<sub>i</sub>(NCS)<sub>o</sub>) are synthesized as a ready-to-use system derived from aminated MSNs.

As mentioned before, regioselective bifunctionalization is based on a co-condensation process, followed by an external reaction, while tensioactive is still present in MSNs porous. Generally, in order to preserve the surfactant inside MSNs porous, toluene is used as a solvent for external functionalization processes.<sup>30</sup> In this case 1-1'-thiocarbonyldi-2(1*H*)-pyridone (**5**) is soluble in toluene and this procedure can be easily applied.

Briefly, the synthesis follows a similar scheme as described before. The aminated nanoparticles (50 nm and 100 nm) containing the surfactant (CTAB) were reacted with 12 eq. of 1,1'-thiocarbonyldi-2(1*H*)-pyridone (**5**) in toluene for 24 h (Figure 5.11).

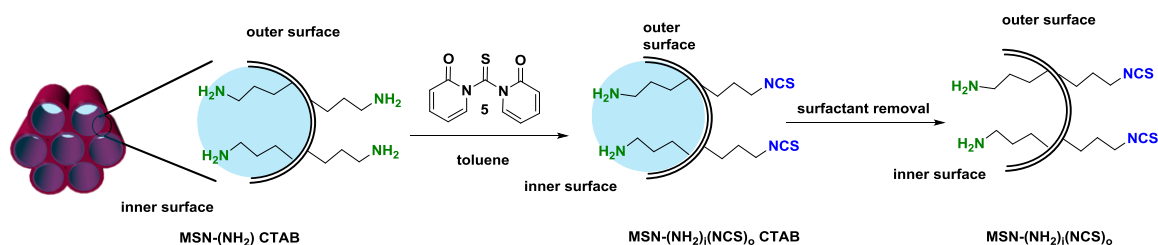


Figure 5.11. MSNs orthogonal bifunctionalization (MSN-(NH<sub>2</sub>)<sub>i</sub>(NCS)<sub>o</sub>).

Once functionalized, and prior to tensioactive removal, the resulting solid was washed once with toluene and EtOH. Then the surfactant was removed by refluxing the nanoparticles in a mixture of HCl/EtOH or NH<sub>4</sub>NO<sub>3</sub>/EtOH. The successful regioselective functionalization of

MSNs is supported by the presence of two isothiocyanate absorption bands around  $2100\text{ cm}^{-1}$  with the presence of the tensioactive blocking the porous at  $2990\text{ cm}^{-1}$  in the FT-IR spectrum (Figure 5.12). In this case, external aminated nanoparticles with tensioactive (MSN(NH<sub>2</sub>)-CTAB) are transformed into isothiocyanate moieties, while tensioactive is still present, preserving inner amino groups from reaction (MSN(NH<sub>2</sub>)<sub>i</sub>(NCS)<sub>o</sub>-CTAB). Tensioactive removal at  $2990\text{ cm}^{-1}$  finally gives MSN-(NH<sub>2</sub>)<sub>i</sub>(NCS)<sub>o</sub>.

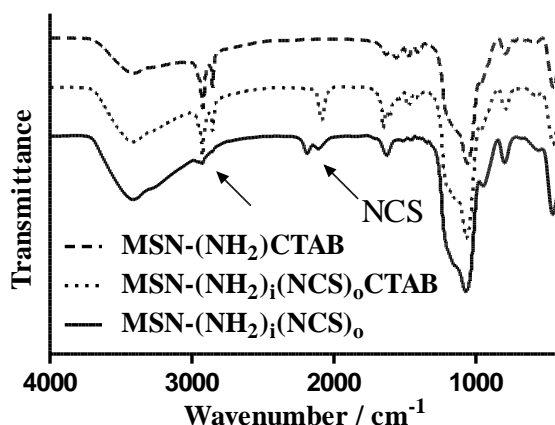


Figure 5.12. FTIR spectra of bifunctionalized MSN-(NH<sub>2</sub>)<sub>i</sub>(NCS)<sub>o</sub>.

Bifunctionalized amino-isothiocyanate nanoparticles were characterized by DLS, TEM, BET and powder XRD analysis. As expected, no significant size and  $\zeta$ -potential differences were obtained between initial aminated nanoparticles (MSN-(NH<sub>2</sub>)) and bifunctionalized amino-isothiocyanate nanoparticles (MSN-(NH<sub>2</sub>)<sub>i</sub>(NCS)<sub>o</sub>) (Table.5.4). Again, these data suggest that the mild conditions used for the functionalization do not erode the structural features of the MSNs. These nanoparticles show good chemical stability and can be stored at room temperature indefinitely. Again, MSN-(NH<sub>2</sub>)<sub>i</sub>(NCS)<sub>o</sub> are regular, homogeneous and round shaped as it can be observed in TEM micrographs (Figure 5.13).

Table 5.4. Dynamic light scattering (DLS) size and  $\zeta$ -potential values of MSN-(NH<sub>2</sub>) and MSN-(NH<sub>2</sub>)<sub>i</sub>(NCS)<sub>o</sub> of 50nm and 100 nm.

Size / nm	TEM	DLS	pDI	$\zeta$ -pot / mV
MSN-(NH <sub>2</sub> )	50	129	0.19	-1.7
	100	142	0.07	-12
MSN-(NH <sub>2</sub> ) <sub>i</sub> (NCS) <sub>o</sub>	50	141	0.29	-1.7
	100	173	0.04	-13

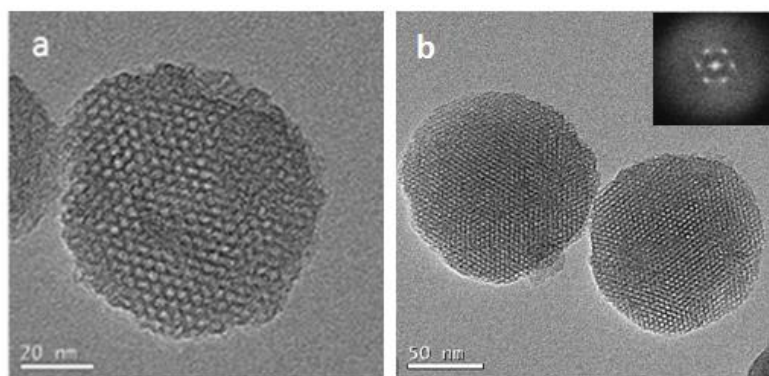


Figure 5.13. TEM micrographs of MSN-(NH<sub>2</sub>)<sub>i</sub>(NCS)<sub>o</sub> of 50 nm (a) and 100 nm (b).

As for N<sub>2</sub> adsorption/desorption measurements, MSN-(NH<sub>2</sub>)<sub>i</sub>(NCS)<sub>o</sub> showed type IV isotherms, which display clear H<sub>1</sub> hysteresis loop characteristic of mesoporous materials. BET surface areas are over 600 m<sup>2</sup>·g<sup>-1</sup> and 1100 m<sup>2</sup>·g<sup>-1</sup> for MSN-(NH<sub>2</sub>) (50 nm) and MSN-(NH<sub>2</sub>) (100 nm) respectively, whereas for MSN-(NH<sub>2</sub>)<sub>i</sub>(NCS)<sub>o</sub> (50 nm) were 554 m<sup>2</sup>·g<sup>-1</sup> and 1000 m<sup>2</sup>·g<sup>-1</sup> for MSN-(NH<sub>2</sub>)<sub>i</sub>(NCS)<sub>o</sub> (100 nm) (Figure 5.14). Additionally, the pore volume for MSN-(NH<sub>2</sub>)<sub>i</sub>(NCS)<sub>o</sub> (50 nm) was 0.45 cm<sup>3</sup>·g<sup>-1</sup> and 0.63 cm<sup>3</sup>·g<sup>-1</sup> for the MSN-(NH<sub>2</sub>)<sub>i</sub>(NCS)<sub>o</sub> (100 nm). As a reference, the values recorded for MSN-(NH<sub>2</sub>) were 0.55 cm<sup>3</sup>·g<sup>-1</sup> and 0.72 cm<sup>3</sup>·g<sup>-1</sup> respectively. The MSN present a very narrow pore size distribution centered at 2.6 and 2.2 nm respectively (Table 5.4).

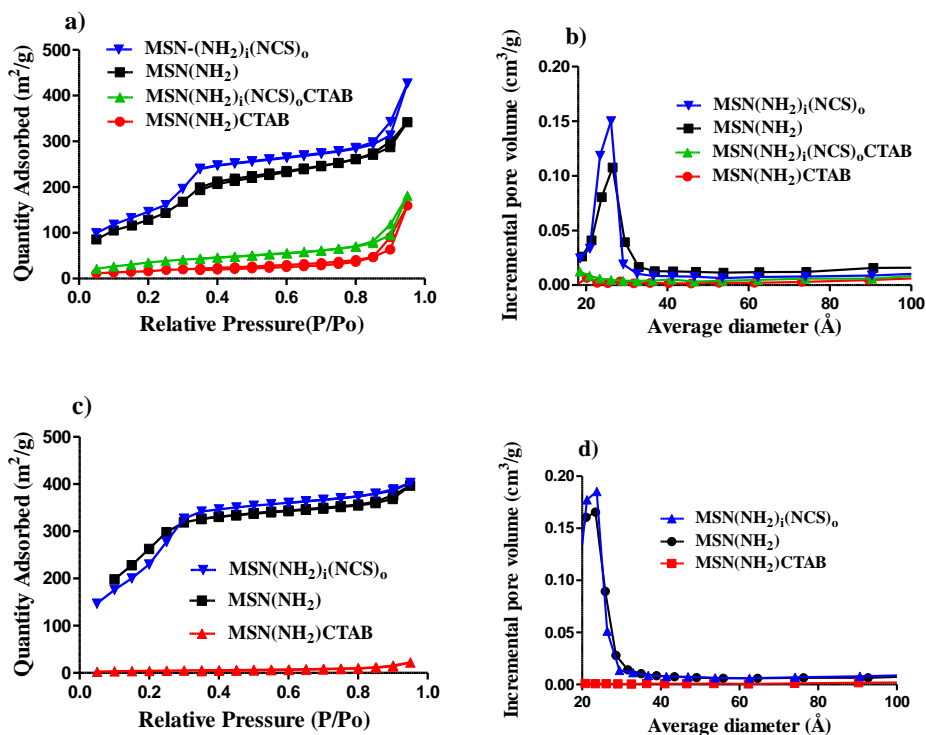


Figure 5.14. N<sub>2</sub> adsorption-desorption and BJH pore size distribution plots of MSN-NH<sub>2</sub>(CTAB), MSN-(NH<sub>2</sub>) and MSN-(NH<sub>2</sub>)<sub>i</sub>(NCS)<sub>o</sub> of 50 nm (a/b) and 100 nm (c/d).



Only external surface functionalization with 1-1'-thiocarbonyldi-2(1*H*)-pyridone (**5**) was successfully achieved, since MSNs mesoporous were blocked by the surfactant during the reaction process. BET surface area for bifunctionalized MSNs with surfactant in its matrix (MSN-(NH<sub>2</sub>)<sub>i</sub>(NCS)<sub>o</sub>(CTAB)) was 133.71 (m<sup>2</sup>/g), which means that porous were completely blocked and no reaction took place in inner amino moieties (Figure 5.14 and Table 5.5).

**Table 5.5.** N<sub>2</sub> adsorption-desorption and BJH pore size values of MSN-NH<sub>2</sub>(CTAB), MSN-(NH<sub>2</sub>) and MSN-(NH<sub>2</sub>)<sub>i</sub>(NCS)<sub>o</sub> of 50 nm and 100 nm.

	MSN-NH <sub>2</sub> (CTAB)		MSN-(NH <sub>2</sub> )		MSN-(NH <sub>2</sub> ) <sub>i</sub> (NCS) <sub>o</sub>		MSN-(NH <sub>2</sub> ) <sub>i</sub> (NCS) <sub>o</sub> (CTAB)
	(50 nm)	(100 nm)	(50 nm)	(100 nm)	(50 nm)	(100 nm)	(50 nm)
<b>BET surface area (m<sup>2</sup>/g)</b>	78.60	17.30	599.80	1120.90	554.50	1000.70	133.71
<b>BJH pore volume (cm<sup>3</sup>/g)</b>	0.25	0.03	0.55	0.72	0.45	0.63	0.28
<b>Pore size (nm)</b>	--	--	2.60	2.20	2.60	2.20	--

Powder XDR analysis indicates highly ordered structures with d100 at 2.3 and faceted hexagon-shape at 4.1 (d110) and 4.2 (d200) (Figure 5.15).

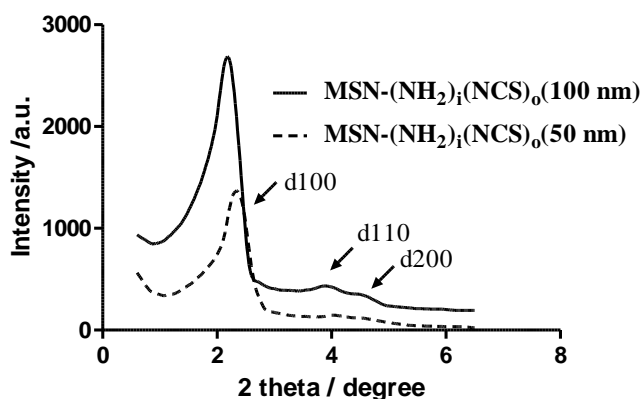


**Figure 5.15.** SXDR of MSN-(NH<sub>2</sub>)<sub>i</sub>(NCS)<sub>o</sub> of 50 and 100 nm.

Thus, it is concluded that bifunctional amino-isothiocyanate formation from amino MSNs can be successfully achieved without affecting MSNs morphology. A successfully one-step conversion of amino MSNs into bifunctionalized amino-isothiocyanate MSNs has been achieved.

## 5.5. Controlled release of Ataluren

Duchenne muscular dystrophy (DMD) is a degenerative disease, which is generally associated with a nonsense mutation in the gene dystrophin, responsible for structural stability of muscle tissue. Therefore, without dystrophin protein, mutation results in muscle degeneration of young children. Even if still today there are no effective treatments for this disease, Ataluren has been recently approved by the FDA as a promising drug for DMD treatment.<sup>31–33</sup> Nevertheless, Ataluren present some disadvantages, such as being little soluble in water and non-selective for muscles. This is the reason why it is believed that the use of nanoparticles for Ataluren release could overcome these problems.

Recently, Bibee *et al.*,<sup>34</sup> have developed perfluorocarbons polymeric nanoparticles where drug rapamycin has been encapsulated for the treatment of Duchenne Muscular Dystrophy. They have reported that drug encapsulation in polymeric nanoparticles provide greater therapeutic effect than oral administration of the drug, since more quantity of the drug can be supplied. At the same time, they have proven that nanoparticles accumulate in organs affected by DMD due to inflammation processes. Therefore, it seems that nanoparticles can be applied as nanovectors to passively deliver drugs in muscles.

Bearing in mind these results, aminated-MSNs were proposed for the delivery of Ataluren for the treatment of DMD. In collaboration with Francina Munell at *Institut de recerca de la Vall d'Hebron* aminated MSNs were administered to mice affected by DMD disease, in order to study MSNs accumulation. Preliminary *in vivo* experiments revealed that MSNs were able to selectively accumulate in the muscle of model mice affected with DMD, while they did not accumulate in control mice (Figure 5.16). Even if the *in vivo* experiments are preliminary and need to be repeated, these results are very encouraging since to date, no MSNs have been described as targeted muscle nanocarriers.

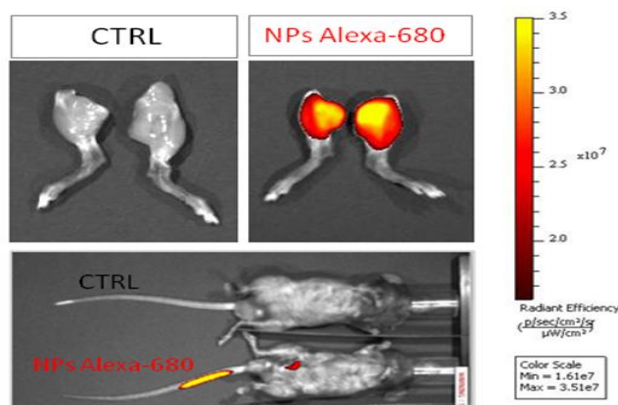


Figure 5.16. Accumulation of Alexa-680-MSNs in mice affected by DMD.

Given these encouraging results, it is proposed the use of MSN-(NH<sub>2</sub>)<sub>i</sub>(NCS)<sub>o</sub> for the design of nanocarriers useful for the passive targeting of Ataluren.<sup>17,19,35,36</sup>

### 5.5.1. Design of the nanocarrier

As mention in Chapter 1, it is possible to achieve MSN-based controlled release systems by applying mechanical controls over the pore openings. By capping and opening the entrance porous it is possible to build nanogates that would allow selective transport and efficient release of a payload. Among all possible stimuli such as pH, enzymatic activity, reductive environment, light, ultrasound or magnetic field, the more suitable stimuli for Duchenne muscular dystrophy applications seems to be reductive environment. pH stimulus is normally used in cancer processes due to the difference of acidity in cancerous cells in comparison with normal cells,<sup>37</sup> but it is not clear if there are any pH changes in inflammation processes.<sup>38,39</sup> On the other hand, enzymes are very specific. So, the only stimulus that could be used in this case is general intracellular signal. Redox-responsive glutathione (GSH) stimulus is one of the most used intracellular signal, since it exist a high redox potential gradient between intra and extra cellular media. This redox potential is due to the difference of GSH concentration between the extracellular (10 μM) and the intracellular (10 mM) media. Therefore, this difference is high enough to release a cargo intracellularly.<sup>40,41</sup> Moreover, glutathione is capable of reducing disulfide bonds by being oxidized to glutathione disulfide.

Recently, many studies on glutathione-mediated-MSNs controlled release have been reported.<sup>40-43</sup> In these cases, it is used glutathione ability to reduce and split disulfide bonds to open the gates of the nanoparticles. Disulfide bonds therefore work as a switch, in response to the redox-potential gradient. Then, when drug-loaded MSNs enter the cells, the capping agent is split away from the outlet of the pores to facilitate drug release inside the cells. Normally, a hindered large chain with a disulfide bond in its structure is used as capping agent.<sup>40-44</sup>

In this case, a PEG chain is proposed as a capping agent since it has been described that coating polyethylene chains on silica nanoparticles provides a nontoxic, biocompatible, and protective covering for *in vivo* applications, slowing the action of the reticuloendothelial system (RES).<sup>20</sup> Therefore, it is expected that using PEG as a mechanical gate will give MSNs additional physiological stability. To begin with, two different PEG, with different size, are used. On the one hand, a short PEG (**n=3**, **S-PEG**) such as tetraethyleneglycol is chosen, as it is neither too short nor too long, and consequently it is relatively easy to functionalize in MSNs surface. Moreover, tetraethyleneglycol polymer has been described as capping agent in literature.<sup>45</sup> On

the other hand, a long PEG ( $n=15$ , L-PEG) is chosen to compare the delivery of the payload with a small and a long chain.

To add the disulfide bond into PEG structure, in the main, two strategies are used. The first one is to add a thiol moiety into PEG structure and functionalize it to thiol-MSNs.<sup>40</sup> On the other hand, cleavable disulfide bond could be added by using cystamine (**34**). Since introducing another moiety to bifunctionalized amino-isothiocyanate MSNs, such as thiol moiety, seems difficult to achieve, the use of cystamine is preferred. Moreover cystamine approach has been widely studied in literature.<sup>45</sup>

Generally, capping agents are introduced at the porous entrance of MSNs directly through silanization,<sup>46</sup> by just one step reaction,<sup>40</sup> or sequently,<sup>41</sup> fragment by fragment. Nevertheless, grafting PEG process is not recommended since it can erode MSNs surface,<sup>47</sup> while a step by step reaction with MSNs can affect MSNs purification. Therefore, the best option would be to add the final polymer directly to the MSNs and confirm that the cleavable disulfide bond has been successfully formed.

In order to release the maximum quantity of PEG, cystamine (**34**) must be added as close as possible to MSNs entrances. It is not desired to have any remaining, non-reduced, PEG moieties that would block the porous entrance while the drug is released. A large size reduction in the appended gate is needed in order to enable the total release of the drug.

So, the three key components needed for a scissile disulfide PEG functionalization in MSNs are tetraethyleneglycol monomethyl ether (**33**), cystamine (**34**) and amino-isothiocyanate MSNs (Figure 5.17).

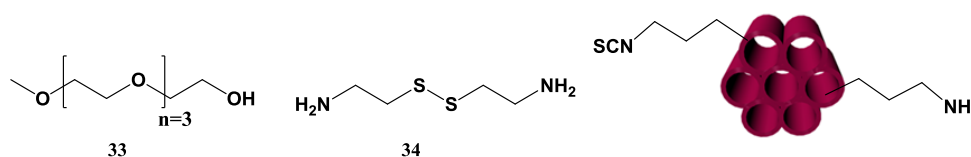


Figure 5.17. Key components for drug release capping system.

If the dithiol bond needs to be as close as possible to MSNs surface, one of the amines of cystamine (**34**) must react with the isothiocyanate moieties of bifunctionalized MSNs. Therefore, at one point monoprotected cystamine **35** must be synthesized. In addition, the other amine moiety of cystamine molecule must react with the tetraethyleneglycol chain. As a consequence, the synthetic approach that is proposed is to introduce an amine moiety to the

methoxy tetraethylene glycol **33**, giving **39**, and react it with a monoprotected isothiocyanate cystamine **36** (Figure 5.18).

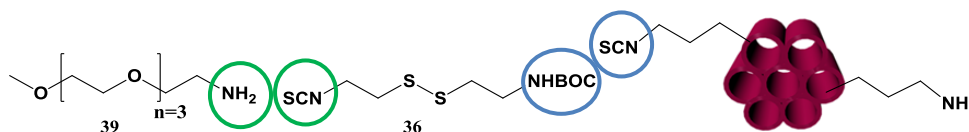


Figure 5.18. Key functional groups for capping agent synthesis.

To synthesize the monoprotected cystamine isothiocyanate, commercial cystamine (**34**) is used. One of the two amino groups is monoprotected with BOC and this reaction leads to product *tert*-butyl(2-((2-aminoethyl)disulfanyl)ethyl)carbamate (**35**). Remaining group  $\text{NH}_2$  is reacted with 1,1'-tiocarbonildi-2(1*H*)-pyridone (**5**) to give final product *tert*-butyl(2-((2-isothiocyanatoethyl)disulfanyl)ethyl)carbamate (**36**) Figure 5.19.

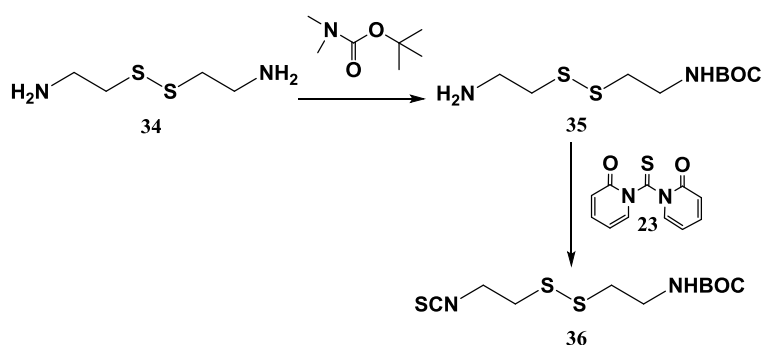


Figure 5.19. Synthesis of *tert*-butyl(2-((2-isothiocyanatoethyl)disulfanyl)ethyl)carbamate (**36**).

As for (S-PEG), to synthesize triethylene glycol 2-methyl amino methyl ether (**39**) commercial methoxy triethylene glycol monomethyl ether (**33**) is used (Figure 5.20). The reaction begins with a nucleophilic substitution between the alcohol group and chloride tosylate, which generates triethylene glycol 2-methyl tosylate methyl ether (**37**). A second nucleophilic substitution between tosylate molecule and sodium azide give product triethylene glycol 2-methyl azide methyl ether (**38**). Finally, triethylene glycol 2-methyl amino methyl ether (**39**) is synthesized by Staudinger reaction, where azide is reduced to amine moiety with triphenylphosphine followed by hydrolysis.

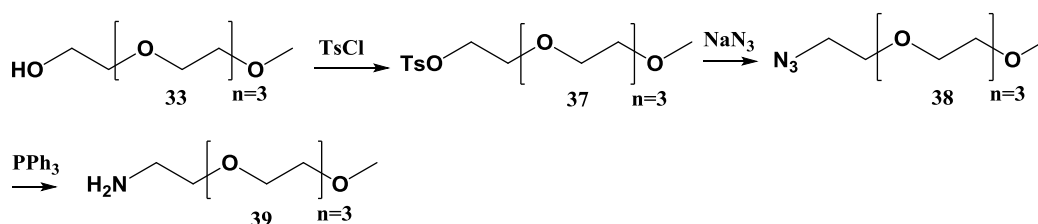


Figure 5.20. Synthesis of triethylene glycol 2-methyl amino methyl ether (**39**).

For (**L**-PEG), a commercially available methoxypolyethylene glycol amine **n=15** [PM=750 g·mol<sup>-1</sup>] is directly chosen.

Finally, monoprotected cystamine-isothiocyanate (**36**) and triethylene glycol 2-methyl amino methyl ether (**39**, **n=3**) or methoxypolyethylene glycol amine (**39**, **n=15**) give the disulfide PEG *tert*-butyl(15-thioxo-2,5,8,11-tetraoxa-19,20-dithia-14,16-diazadocosan-22-yl)carbamate (**40**, **n=3** and **n=15**). The product **40** (**n=3** and **n=15**) is purified with a silica gel column chromatography using as eluent a mixture of 50:50 (DCM:AcOEt). Once purified, final BOC deprotection with TFA gives 1-(2-((2-aminoethyl)disulfanyl)ethyl)-3-(2,5,8,11-tetraoxatrideca-13-yl)thiourea (**41**, **n=3** and **n=15**) (Figure 5.21). Product **41** (**n=3** and **n=15**) is directly added to the MSNs.

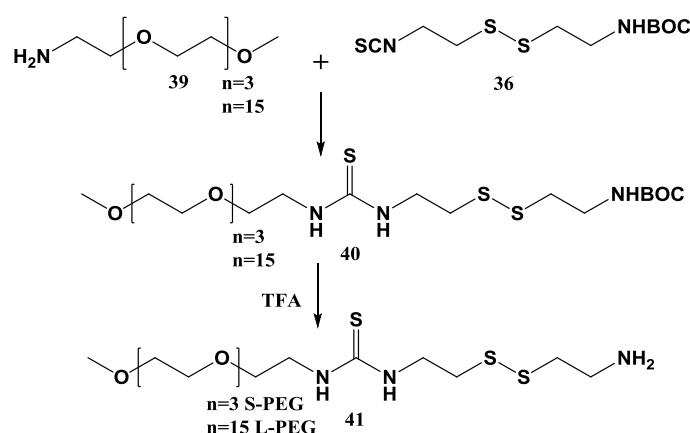


Figure 5.21. Synthetic approach of capping agent **41**.

### 5.5.2. Controlled Ru(bipy)<sub>3</sub><sup>2+</sup> release

For the sake of simplicity Ru(bipy)<sub>3</sub><sup>2+</sup> was chosen as a proof of concept dye. Ru(bipy)<sub>3</sub><sup>2+</sup> was added to the MSNs by absorption process and following the procedure described by Sancenon *et al.*<sup>48,49</sup> Ru(bipy)<sub>3</sub><sup>2+</sup> loading was achieved in a 8 % loading, similar to the typical value found in the literature.<sup>40</sup> When Ru(bipy)<sub>3</sub><sup>2+</sup> release is carried out in bifunctionalized MSN-(NH<sub>2</sub>)<sub>i</sub>(NCS)<sub>o</sub> without any capping agent, release is almost completed in 1 h. Complete Ru(bipy)<sub>3</sub><sup>2+</sup> release (100 %) is achieved at 3 h.

There is no control of Ru(bipy)<sub>3</sub><sup>2+</sup> release when no capping agent is added. In order to functionalize a mechanized stimulus in MSNs, MSNs are functionalized with disulfide-PEG **41** (**n=3** and **n=15**) (S-PEG) and (L-PEG). Before adding the redox responsive PEG linker (**41**) to the nanoparticles, MSNs must be filled with the drug.

Typically, 18 mg ( $2.45 \cdot 10^{-5}$  mol) of  $\text{Ru}(\text{bipy})_3^{2+}$  were added to a solution of 30 mg of bifunctionalized MSNs in 5 mL of ACN. After 24 h, 60 mg ( $1.49 \cdot 10^{-4}$  mol) of disulfide-PEG **41** (**L**-PEG and **S**-PEG) were added in 15 mL of ACN for 24 h (Figure 5.22). Finally, after washing with EtOH,  $\text{Ru}(\text{bipy})_3^{2+}$  supernatant was measured at 451 nm to estimate the loading of  $\text{MSN}(\text{NH}_2)_i(\text{S}\text{-PEG})_o\text{Ru}$  and  $\text{MSN}(\text{NH}_2)_i(\text{L}\text{-PEG})_o\text{Ru}$ . In order to assess the total amount of  $\text{Ru}(\text{bipy})_3^{2+}$  that can be released, MSNs are treated with HCl (c) for 12 h and the supernatant is measured at 451 nm.

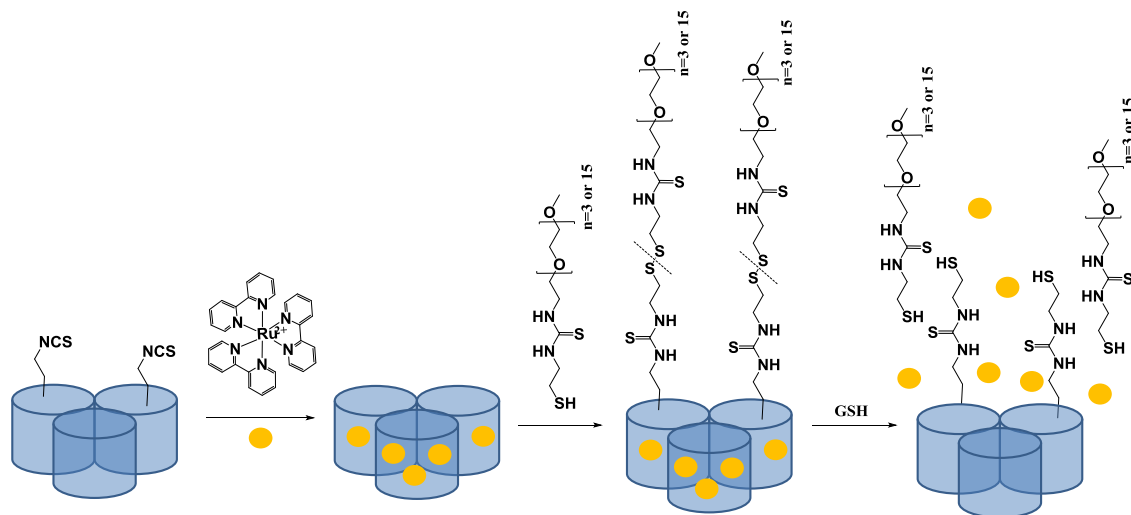


Figure 5.22. General scheme for  $\text{MSN}(\text{NH}_2)_i(\text{S}\text{-PEG})_o\text{Ru}$  and  $\text{MSN}(\text{NH}_2)_i(\text{L}\text{-PEG})_o\text{Ru}$  synthesis.

*In vitro* release experiments were performed at pH 7.4 and 10 mM GSH solution. For each release study, 1.5 mL of buffer solution was first added to 10 mg of  $\text{MSN}(\text{NH}_2)_i(\text{S}\text{-PEG})_o\text{Ru}$  and  $\text{MSN}(\text{NH}_2)_i(\text{L}\text{-PEG})_o\text{Ru}$  and maintained at  $37^\circ\text{C}$ , while being stirred at 100 rpm. Release medium was removed for analysis at specific time intervals by centrifuging at 12000 rpm for 13 min and placing solid residues into identical volumes of fresh buffer solution. The amount of released  $\text{Ru}(\text{bipy})_3^{2+}$  was analyzed with a UV–Vis absorption spectrophotometer at 451 nm.  $\text{Ru}(\text{bipy})_3^{2+}$  release curves are shown in Figure 5.22 and Figure 5.23.

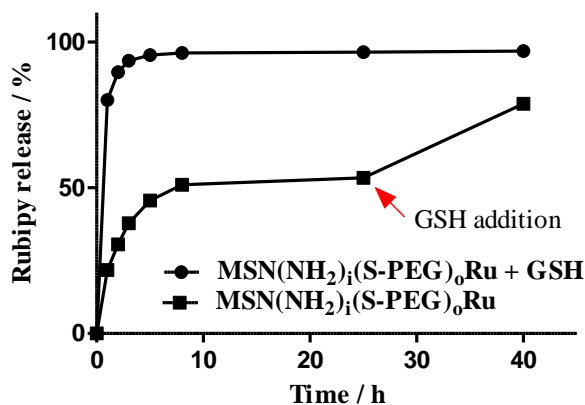


Figure 5.23. Release of  $\text{MSN}(\text{NH}_2)_i(\text{S}\text{-PEG})_o\text{Ru}$  in the absence and presence of GSH .

Regarding the short PEG (S-PEG) (Figure 5.23), when GSH is added in the medium, Ru(bipy)<sub>3</sub><sup>2+</sup> release follows the same pattern as if there was no capping agent, approximately 90 % of Ru(bipy)<sub>3</sub><sup>2+</sup> is released in the first hour. When GSH is not added, there is a high remaining release. It seems that this S-PEG (**41**, n=3) is not blocking enough the entrance of the porous, because without stimulus, half of the payload is released. Nonetheless, when GSH is added to regular PBS medium, release percentage increases considerably which demonstrates the fact that it is really the disulfide split triggered by GSH and consequent size reduction of the PEG, that brings about Ru(bipy)<sub>3</sub><sup>2+</sup> release.

Nevertheless, when the large PEG (L-PEG) is used as a capping agent, the difference between Ru(bipy)<sub>3</sub><sup>2+</sup> release at pH=7 and in GSH medium is quite marked. Ru(bipy)<sub>3</sub><sup>2+</sup> release supernatants in pH=7 present no coloration, while supernatants in GSH medium are yellow due to higher Ru(bipy)<sub>3</sub><sup>2+</sup> release (Figure 5.24).

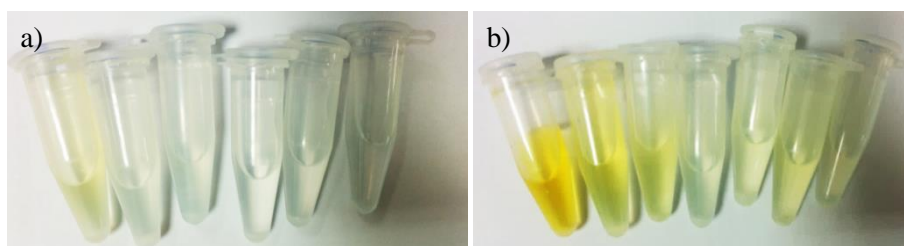


Figure 5.24. Ru(bipy)<sub>3</sub><sup>2+</sup> release of MSN(NH<sub>2</sub>)<sub>i</sub>(L-PEG)<sub>o</sub>Ru without GSH (a) and with GSH (b).

With the long PEG (L-PEG) in a GSH medium, approximately the vast majority of Ru(bipy)<sub>3</sub><sup>2+</sup> is released in the first hour, while just 15 % of Ru(bipy)<sub>3</sub><sup>2+</sup> is free in normal conditions. These results meet with described releases for other systems.<sup>40,46</sup> In this case, a controlled release with long disulfide PEG (**34**, n=15) is obtained (Figure 5.25). Again, when GSH is added to regular PBS medium, the quantity of Ru(bipy)<sub>3</sub><sup>2+</sup> released is enhanced.

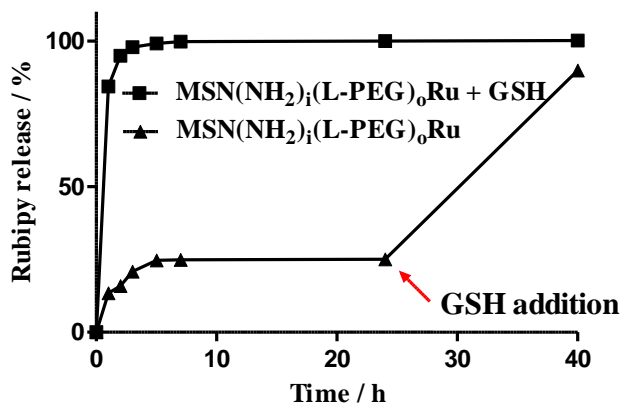


Figure 5.25. Release of MSN(NCS)(L-PEG)Ru in the absence and presence of GSH.



Even though remaining release at pH=7 is low, this value could maybe become lower with the addition of a larger or more ramified PEG.

Although it has been reported that small tetraethyleneglycol can seal MSNs entrance,<sup>45</sup> long PEG (L-PEG) is able to cap more efficiently than small PEG (S-PEG). To sum up, Ru(bipy)<sub>3</sub><sup>2+</sup> loading and release percentages are summarized in table 5.6.

**Table 5.6. Loading and release of Ru(bipy)<sub>3</sub><sup>2+</sup>**

	No PEG		S-PEG		L-PEG	
		No GSH	GSH	No GSH	GSH	
<b>Ru(bipy)<sub>3</sub><sup>2+</sup></b>	--					
<b>Loading (%)</b>	7	7			7	
<b>Release (%)</b>	104	53	96	25	100	

Now that it has been proven that it is possible to control Ru(bipy)<sub>3</sub><sup>2+</sup> release by using a disulfide-PEG, the payload is changed for Ataluren drug.

### 5.5.3. Ataluren Release

As a possible therapeutic application of this new methodology for Duchenne disease, a very simple nanovehicle for the delivery of Ataluren (**43**) (Translarna™) has been designed (Figure 5.26).<sup>50</sup>

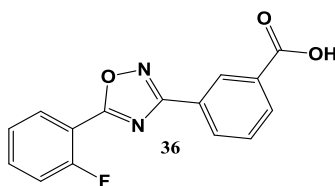


**Figure 5.26. Chemical structure of Ataluren.**

First, MSNs pores must be filled with Ataluren drug. Since there are no references of MSNs loaded with Ataluren, the same protocol used for Ibuprofen and Captopril loading have been used.<sup>51-54</sup> Bifunctional MSN-(NH<sub>2</sub>)<sub>i</sub>(NCS)<sub>o</sub> nanoparticles were loaded with the drug in a proportion (2:1.5) respectively, by exposing MSNs to a solution of Ataluren in ethanol. Finally, after washing with EtOH once, Ataluren supernatant was measured at 255 nm, to assess the loading. Ataluren loading was obtained between 4-6 %, similar to described first impregnations results for Ibuprofen.<sup>54</sup> Ataluren release in pH=7, without any capping gate is presented in Figure 5.27.

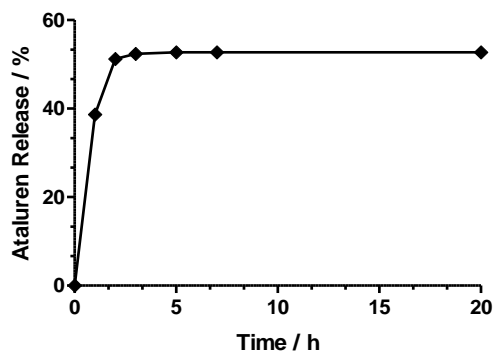


Figure 5.27. MSN-Ataluren release.

No control of Ataluren release is obtained when no capping agent is added. More or less 40 % of Ataluren is released in the first 1 h. These results correspond to described values for Captopril release in the literature.<sup>53</sup> While, in the case of  $\text{Ru}(\text{bipy})_3^{2+}$  a 100 % of the payload was released, in this case part of Ataluren drug is still present in the MSNs pores and has been not released. This is probably due to the interactions between the carboxylic acid of Ataluren and the amino moieties of MSNs. This interaction has also been described in the case of Ibuprofen,<sup>52,54</sup> whereas for  $\text{Ru}(\text{bipy})_3^{2+}$  no interactions were found, since  $\text{Ru}(\text{bipy})_3^{2+}$  present no functional group able to interact with MSNs.

Ataluren release can be divided in two clearly differentiated parts. The former, can be explained as a fast release due to Ataluren molecules that neither have been absorbed nor interact with MSNs. The latter is attributed to a slow release due to strong interactions between amino functional groups of the pores and the carboxylic acid of Ataluren. Nevertheless, when no capping agent is added, no control of Ataluren release is obtained. In order to control Ataluren release, these nanoparticles are functionalized with **S-PEG** and **L-PEG** (**41**, **n=3** and **n=15**) following the same procedure as before. First Ataluren is added to bifunctionalized MSNs in a 1.5:2 proportion and then after 24 h small (**n=3**) and long (**n=15**) methoxypolyethylene glycol amine (**41**, **n=3** (**S-PEG**) and **41**, **n=15** (**L-PEG**)) were added to seal the porous. The suspension was stirred for 24 h. Finally, the mixture was centrifuged and washed twice with ethanol to obtain  $\text{MSN}-(\text{NH}_2)_i(\text{S-PEG})_o\text{Ata}$  and  $\text{MSN}-(\text{NH}_2)_i(\text{L-PEG})_o\text{Ata}$  (Figure 5.28).

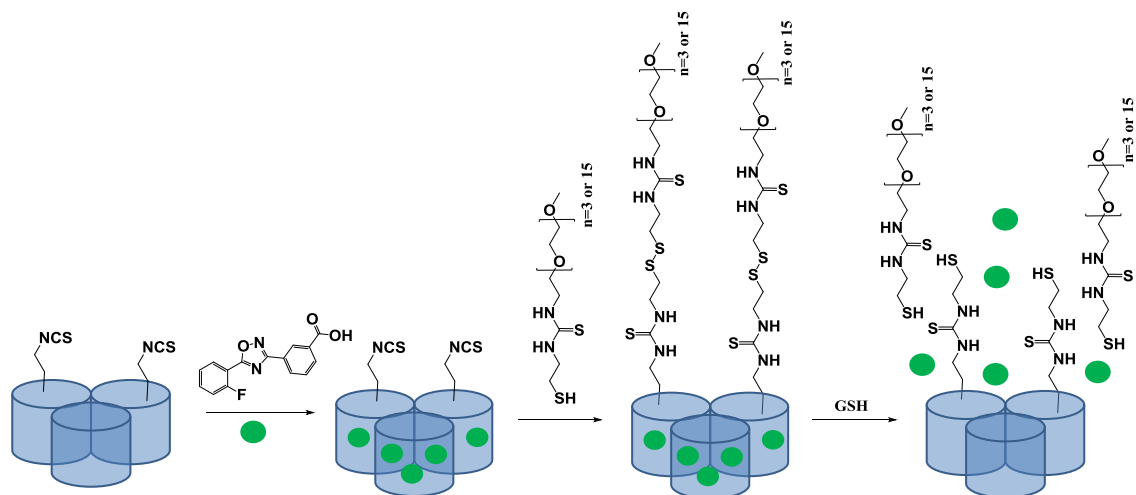


Figure 5.28.  $\text{MSN}(\text{NH}_2)_i(\text{S-PEG})_o\text{Ata}$  and  $\text{MSN}(\text{NH}_2)_i(\text{L-PEG})_o\text{Ata}$  functionalization.

Again, release profile clearly demonstrates the blocking action of both small and long PEG, although L-PEG blocking effect is more pronounced (Figure 5.29 and 5.30).

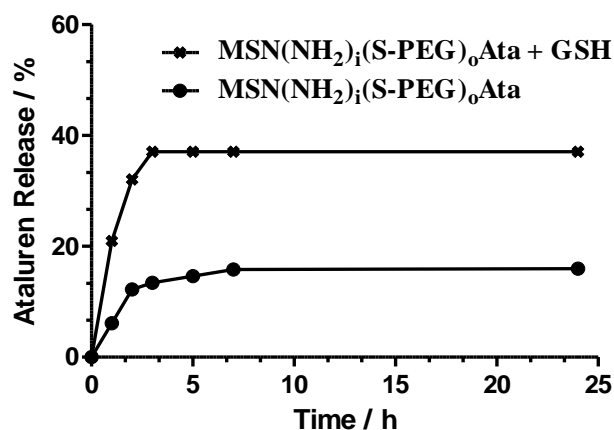


Figure 5.29.  $\text{MSN}-(\text{NH}_2)_i(\text{S-PEG})_o\text{Ata}$  release.

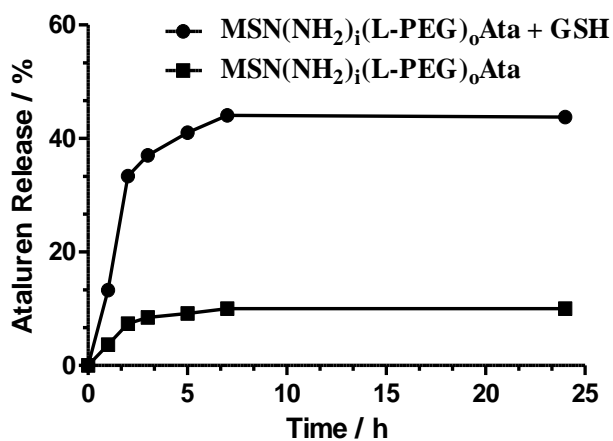


Figure 5.30.  $\text{MSN}-(\text{NH}_2)_i(\text{L-PEG})_o\text{Ata}$  release.

Long polymer is able to seal more efficiently MSNs channels than small PEG. Ataluren release with L-PEG without GSH stimulus is just 10 %, while with S-PEG uncontrolled release is more than 18 %. In fact, when PEG polymer is added to MSNs, Ataluren release is less abrupt. At 1 h, for both small and large PEG, Ataluren release is less than 15 %, whereas for MSNs without any capping agents was 40 %. PEG addition at the outside surface enhances a controlled Ataluren release over time. Therefore, the functionalization of a scissile PEG is an excellent strategy to control drug release and diminish Ataluren abrupt liberation.

Nevertheless, with PEG addition, the final quantity of Ataluren that can be released is inferior to the quantity obtained when no PEG is added. Related with that, Jadzinsky *et al*<sup>55</sup> have described that thiols moieties are capable of forming hydrogen bond interactions with molecules that present phenyl and carboxylic acids in their structure, which is exactly the case of Ataluren molecule. These assumptions may explain why Ataluren release in pegylated MSNs is lower than initial non pegylated MSNs. In all likelihood, Ataluren phenyl and carboxylic acid moieties interact with thiol scissile groups of PEG chains. Moreover, it is highly probable that this interaction could be responsible for the gradual release of Ataluren, when the gate is opened. When thiols are present in the external surface, Ataluren interactions might slow the release profile reaching 50 % at five hours, while without PEG, Ataluren release reached 50 % at 1h.

On the other hand, it is worth mentioning that desirable drug release profile depends on MSNs biodistribution and blood clearance. If MSNs are excreted rapidly it is not interesting to delay Ataluren release over time, but instead a fast release in the first hours would be needed. For similar nanoparticles, it has been described that blood clearance is reached in less than 4 h.<sup>20</sup> Therefore it is believed that a drug release profile, where the maximum quantity of drug is released at 5 h, as the one obtained in Figure 5.30 is desirable. There is no point in having a long release profile in 24 h if blood clearance is reached at 4 h.

Ataluren maximum release in all cases has been approximately  $7 \cdot 10^{-8}$  mol Ataluren/ mg MSN or 0.02 mg Ataluren/mg MSN. Ataluren loading and release values are summarized in table 5.7.

**Table 5.7. Loading and release of Ataluren.**

Ataluren	No PEG		S-PEG		L-PEG	
	pH=7	No GSH	GSH	No GSH	GSH	
<b>Loading (%)</b>	4	4		4		
<b>Release (%)</b>	53	16	37	10	44	
<b>Loading (molAta/mgMSN)</b>	$1.4 \cdot 10^{-7}$		$1.4 \cdot 10^{-7}$		$1.4 \cdot 10^{-7}$	
<b>Release (molAta/mgMSN)</b>	$7.4 \cdot 10^{-8}$	$2.2 \cdot 10^{-8}$	$5.2 \cdot 10^{-8}$	$1.3 \cdot 10^{-8}$	$6.1 \cdot 10^{-8}$	

Typically, the concentration of Ataluren that is used for *in vitro* experiments is 10  $\mu\text{M}$  per well (500 $\mu\text{L}$ ), which corresponds to  $5 \cdot 10^{-9}$  mol Ataluren/well. Knowing that with L-PEG in a GSH medium, the quantity of Ataluren that is released is  $6.1 \cdot 10^{-8}$  molAta/mgMSN, in order to have a  $5 \cdot 10^{-9}$  mol Ataluren per well, a concentration of 0.16 mgMSN/mL will be needed. This concentration can be added to the cells without expecting any toxicity intrinsic to the MSNs. Therefore the quantity of Ataluren released seems good enough to study this system *in vivo* for the treatment of DMD.

## 5.6. Conclusions and Outlook

- A straightforward protocol to prepare isothiocyanate functionalized MSNs from aminated MSNs has been achieved. The resulting MSNs easily react with primary amines and are compatible with aqueous media. The efficiency of the functionalization is comparable to the CuAAC cycloaddition, while presenting a simple isolation with no need to remove any by-product or toxic catalysts.
- Following this methodology, amino-isothiocyanate regioselective functionalized MSNs have been prepared for the first time. These MSNs present external isothiocyanates ready to react with amines, whereas inner amino groups are available for subsequent manipulations.
- The chemical stability of new bifunctionalized amine-isothiocyanate MSNs, along with the clean reactivity and easy purification of the particles, endows these systems with ideal properties to be used in the design of drug carriers.
- These regioselective functionalized nanoparticles have been used for the design of a nanocontainer able to release the drug Ataluren in a controlled, manner when using a long PEG polymer (**34**, **n=15**). The quantity of Ataluren that can be released with this system is high enough to start *in vivo* experiments with MSNs loaded with the drug.

Due to the promising results obtained with this responsive glutathione system, the next step is to use amine-isothiocyanate MSNs for *in vivo* experiments. Nevertheless prior to use this system in mice, it is crucial to prove that Ataluren, loaded in MSNs, is more effective than the drug itself. Should this hypothesis be proven, the optimization of MSNs biodistribution, solubility and enhancement of the payload loading and release will be carried out.

One of the greatest advantages of regioselective amino-isothiocyanate MSNs is that they are extremely versatile, and therefore a wide range of drugs, apart from Ataluren, can be used for the treatment of Duchenne dystrophy.

## 5.7. Bibliography

- (1) Argyo, C.; Weiss, V.; Bräuchle, C.; Bein, T. *Chem. Mater.* **2014**, *26* (1), 435–451.
- (2) Vallet-Regí, M.; Balas, F.; Arcos, D. *Angew. Chemie Int. Ed.* **2007**, *46* (40), 7548–7558.
- (3) Thanh, N. T. K.; Green, L. a W. *Nano Today* **2010**, *5* (3), 213–230.
- (4) Gao, J.; Zhang, X.; Xu, S.; Tan, F.; Li, X.; Zhang, Y.; Qu, Z.; Quan, X.; Liu, J. *Chem. Eur. J.* **2014**, *20* (7), 1957–1963.
- (5) Cheng, S. H.; Lee, C. H.; Yang, C. S.; Tseng, F. G.; Mou, C. Y.; Lo, L. W. *J. Mater. Chem.* **2009**, *19* (9), 1252–1257.
- (6) Pan, L.; He, Q.; Liu, J.; Chen, Y.; Ma, M.; Zhang, L.; Shi, J. *J. Am. Chem. Soc.* **2012**, *134* (13), 5722–5725.
- (7) Li, L. Le; Yin, Q.; Cheng, J.; Lu, Y. *Adv. Healthc. Mater.* **2012**, *1* (5), 567–572.
- (8) Zhang, Q.; Neoh, K. G.; Xu, L.; Lu, S.; Kang, E. T.; Mahendran, R. *Langmuir* **2014**, *30*, 6151–6161.
- (9) Clarke, O. J.; Boyle, R. W. *Chem. Commun.* **1999**, *21*, 2231–2232.
- (10) Khung, Y. L.; Narducci, D. *Adv. Colloid Interface Sci.* **2015**, *226*, 166–186.
- (11) Malti, W. El; Mongin, O.; Blanchard-Desce, M.; Raehm, L.; Durand, J. O. *Comptes Rendus Chim.* **2011**, *14* (12), 1055–1058.
- (12) Malvi, B.; Sarkar, B. R.; Pati, D.; Mathew, R.; Ajithkumar, T. G.; Sen Gupta, S. *J. Mater. Chem.* **2009**, *19* (10), 1409–1416.
- (13) Tonkin, E. G.; Valentine, H. L.; Milatovic, D. M.; Valentine, W. M. *Toxicol. Sci.* **2004**, *81* (1), 160–171.
- (14) Parida, K.; Mishra, K. G.; Dash, S. K. *Methods* **2012**, 2235–2246.
- (15) Liu, Z. C.; Yang, Z. Y.; Li, T. R.; Wang, B. D.; Li, Y.; Qin, D. D.; Wang, M. F.; Yan, M. H. *Dalt. Trans.* **2011**, *40* (37), 9370–9373.
- (16) Wiberg, K. B.; Wang, Y.; Miller, S. J.; Puchlopek, A. L. a; Bailey, W. F.; Fair, J. D. *J. Org. Chem.* **2009**, *74* (10), 3659–3664.
- (17) Natarajan, S. K.; Selvaraj, S. *RSC Adv.* **2014**, *4* (28), 14328–14334.
- (18) Gu, H.; Guo, Y.; Wong, S. Y.; Zhang, Z.; Ni, X.; Zhang, Z.; Hou, W.; He, C.; Shim, V. P. W.; Li, X. *Microporous Mesoporous Mater.* **2013**, *170*, 226–234.
- (19) Kamarudin, N. H. N.; Jalil, A.; Triwahyono, S.; Salleh, N. F. M.; Karim, A. H.; Mukti, R. R.; Hameed, B. H.; Ahmad, A. *Microporous Mesoporous Mater.* **2013**, *180*, 235–241.
- (20) He, Q.; Zhang, Z.; Gao, F.; Li, Y.; Shi, J. *Small* **2011**, *7* (2), 271–280.
- (21) Li, C.; Liu, J.; Alonso, S.; Li, F.; Zhang, Y. *Nanoscale* **2012**, *4* (19), 6065.
- (22) Liu, J.; Li, C.; Li, F. *J. Mater. Chem.* **2011**, *21* (20), 7175–7181.
- (23) Faure, A. C.; Hoffmann, C.; Bazzi, R.; Goubard, F.; Pauthe, E.; Marquette, C. a.; Blum, L. J.; Perriat, P.; Roux, S.; Tillement, O. *ACS Nano* **2008**, *2* (11), 2273–2282.
- (24) Faure, A. C.; Hoffmann, C.; Bazzi, R.; Goubard, F.; Pauthe, E.; Marquette, C.; Blum, L. J.; Perriat, P.; Roux, S.; Tillement, O. *Nanoscale* **2012**, *4* (11), 2273–2282.
- (25) Wong, R.; Dolman, S. J. *J. Org. Chem.* **2007**, *72* (10), 3969–3971.
- (26) F. B. Dains, R. Q. Brewster, C. P. O. *Org. Synth.* **2014**, *6* (09), 1–3.
- (27) Sun, N.; Li, B.; Shao, J.; Mo, W.; Hu, B.; Shen, Z.; Hu, X. *Beilstein J. Org. Chem.* **2012**, *8*, 61–70.

- (28) Harpp, D. N.; MacDonald, J. G.; Larsen, C. *Can. J. Chem.* **1985**, *63* (4), 951–957.
- (29) Kim, S.; Yi, K. Y. *J. Org. Chem.* **1986**, *51*, 2613–2615.
- (30) F. de Juan and E. Ruiz-Hitzky. *Adv. Mater.* **2000**, *12* (6), 430–432.
- (31) PTC therapeutics <http://www.ptcbio.com/en/pipeline/ataluren-translarna/> 09/2015.
- (32) Cure Duchenne Organization <http://www.cureduchenne.org/researcharticles/ataluren-becomes-the-worlds.html> 09/2015.
- (33) ClinicalTrials.gov. <https://clinicaltrials.gov/ct2/show/NCT02106598> 09/2015.
- (34) Bibee, K. P.; Cheng, Y. J.; Ching, J. K.; Marsh, J. N.; Li, J.; Keeling, R. M.; Connolly, M.; Golumbek, P. T.; Myerson, J. W.; Hu, G.; Chen, J.; Shannon, W. D.; Lanza, G. M.; Weihl, C. C.; Wickline, S. *FASEB J.* **2014**, *28* (5), 2047–2061.
- (35) Wang, G.; Otuonye, A. N.; Blair, E. a.; Denton, K.; Tao, Z.; Asefa, T. *J. Solid State Chem.* **2009**, *182* (7), 1649–1660.
- (36) Muhammad, F.; Guo, M.; Qi, W.; Sun, F.; Wang, A.; Guo, Y.; Zhu, G. *J. Am. Chem. Soc.* **2011**, *133*, 8778–8781.
- (37) G. Mattheolabakis, B. Rigas, P. C. *Nanomedicine* **2012**, *7* (10), 1577–1590.
- (38) Punnia-Moorthy. *J. Oral Pathol.* **1987**, *16* (1), 36–44.
- (39) Steen, K. H.; Steen, A. E.; Reeh, P. W. *J. Neurosci.* **1995**, *15* (5), 3982–3989.
- (40) Cui, Y.; Dong, H.; Cai, X.; Wang, D.; Li, Y. *ACS Appl. Mater. Interfaces* **2012**, *4* (6), 3177–3183.
- (41) Guo, R.; Li, L. Le; Zhao, W. H.; Chen, Y. X.; Wang, X. Z.; Fang, C.-J.; Feng, W.; Zhang, T. L.; Ma, X.; Lu, M.; Peng, S. Q.; Yan, C. H. *Nanoscale* **2012**, *4* (11), 3577–3583.
- (42) Yuan, L.; Chen, W.; Hu, J.; Zhang, J. Z.; Yang, D. *Langmuir* **2013**, *29*, 734–743.
- (43) Chang, B.; Chen, D.; Wang, Y.; Chen, Y.; Jiao, Y.; Sha, X.; Yang, W. *Chem. Mater.* **2013**, *25* (4), 574–585.
- (44) El Sayed, S.; Giménez, C.; Aznar, E.; Martínez-Máñez, R.; Sancenón, F.; Licchelli, M. *Org. Biomol. Chem.* **2015**, *13* (4), 1017–1021.
- (45) Luo, Z.; Cai, K.; Hu, Y.; Zhao, L.; Liu, P.; Duan, L.; Yang, W. *Angew. Chemie Int. Ed.* **2011**, *50* (3), 640–643.
- (46) Agostini, A.; Mondragón, L.; Pascual, L.; Aznar, E.; Coll, C.; Martínez-Máñez, R.; Sancenón, F.; Soto, J.; Marcos, M. D.; Amorós, P.; Costero, A. M.; Parra, M.; Gil, S. *Langmuir* **2012**, *28* (41), 14766–14776.
- (47) Lim, M. H.; Stein, A. *Chem. Mater.* **1999**, *11* (11), 3285–3295.
- (48) Agostini, A.; Mondragón, L.; Coll, C.; Aznar, E.; Marcos, M. D.; Martínez-Máñez, R.; Sancenón, F.; Soto, J.; Pérez-Payá, E.; Amorós, P. *Chem. Open* **2012**, *1*, 17–20.
- (49) Mondragón, L.; Mas, N.; Ferragud, V.; de la Torre, C.; Agostini, A.; Martínez-Máñez, R.; Sancenón, F.; Amorós, P.; Pérez-Payá, E.; Orzáez, M. *Chem. Eur. J.* **2014**, *20* (18), 5271–5281.
- (50) López-Hernández, L.; Gómez-Díaz, B.; Luna-Angulo, A.; Anaya-Segura, M.; Bunyan, D.; Zúñiga-Guzman, C.; Escobar-Cedillo, R.; Roque-Ramírez, B.; Ruano-Calderón, L.; Rangel-Villalobos, H.; López-Hernández, J.; Estrada-Mena, F.; García, S.; Coral-Vázquez, R. *Int. J. Mol. Sci.* **2015**, *16* (3), 5334–5346.
- (51) Rámila, A.; Muñoz, B.; Pérez-Pariente, J.; Vallet-Regí, M. *J. Sol-Gel Sci. Technol.* **2003**, *26*, 1199–1202.

- (52) Vallet-Regi, M.; Rámila, a.; Del Real, R. P.; Pérez-Pariente, J. *Chem. Mater.* **2001**, *13* (2), 308–311.
- (53) Qu, F.; Zhu, G.; Huang, S.; Li, S.; Sun, J.; Zhang, D.; Qiu, S. *Microporous Mesoporous Mater.* **2006**, *92* (1-3), 1–9.
- (54) Charnay, C.; Bégu, S.; Tourné-Péteilh, C.; Nicole, L.; Lerner, D. a.; Devoisselle, J. M. *Eur. J. Pharm. Biopharm.* **2004**, *57* (3), 533–540.
- (55) Jadzinsky, P. D.; Calero, G.; Ackerson, C. J.; Bushnell, D. a.; Kornberg, R. D. *Science* (80-. ). **2007**, *318* (5849), 430–433.



## Chapter 6. Amino-aldehyde MSNs for their application as dual drug delivery system

---

Regioselective bifunctionalized  $\text{MSN}(\text{NH}_2)_i(\text{CHO})_o$  nanoparticles have been synthesized. These MSNs have been applied as a versatile nanoplatform able to release dual synergistic CPT/DOX mixture for cancer treatment, by using pH stimuli. While CPT is absorbed at the inner surface, DOX is covalently linked to the external domain acting both as an active and a capping agent. This system responds to pH stimuli and both CPT and DOX drugs are only released in an acidic media (pH=4).



## **Chapter 6. Amino-aldehyde MSNs for their application as dual drug delivery system**

### **6.1. Introduction**

Over the past few years, next generation multiplatforms have been considered as combined vehicles for the detection and treatment of aggressive diseases.<sup>1</sup> In this field, multifunctional drug delivery systems (DDS) have emerged as a promising multiplatform able to combine the release of multiple therapeutic agents in one vehicle.<sup>2,3</sup> DDS are designed to overcome unspecific uptake, rapid clearance, poor water solubility and reduce secondary effects related problems.<sup>4-6</sup> So far, dual DDS have been used for the combined treatment and reduction of drug resistance effect,<sup>7,8</sup> for the dual combination of chemotherapy and PDT,<sup>9</sup> chemotherapy and imaging,<sup>10</sup> as a targeted controlled drug release<sup>11</sup> and for the combined release of synergetic chemotherapeutic agents.<sup>12</sup> Nevertheless, even if combined nanoplatforms have been used in different applications,<sup>1</sup> it is in the field of cancer treatment that dual combined nanoplatforms are being widely studied.<sup>13</sup>

Among a large number of diseases, cancer is still the most common and aggressive disease present in the first global world.<sup>14</sup> Nevertheless, despite the phenomenal advancement in molecular genetics, tumor biology and chemical therapy, adequate treatment of cancer is far from satisfactory.<sup>15</sup> The therapeutic effect of chemical approach remains quite poor due to insufficient drug dosage to the diseased regions, rapid blood clearance, severe side effects and drug resistance.

To sweep out these obstacles, combination of different chemotherapeutic agents has attracted increasing attention because of its enhanced therapeutic efficiency compared with the unsatisfactory results of single agents in the treatment of advanced tumors.<sup>16,17</sup> By this means, the application of nanocarriers for dual drug release is of great interest. As an example of success, recently Celator Pharmaceutical Inc has been awarded with the Nanomedicine 2015 award for the development of a combined Cytarabine-Daunorubicin (VYXEOS™) nanoplatform (CombiPlex®) for the treatment of myeloid leukemia (AML).<sup>18-20</sup> This discovery clearly highlights the fact that even if the development of effective multi-cargo-loaded systems remains a challenge,<sup>13</sup> great encouraging improvements are being done to apply these systems in the near future.

In this field, mesoporous silica materials present promising properties for drug delivery applications due to their ability to encapsulate different types of cargo molecules within their pore channels and control payloads release, by adding triggered gates at the external surface.<sup>6,21</sup> Among different stimuli, pH-sensitivity promises to be one of the most powerful tools for the development of smart nanovalves in cancer therapy. Taking into account that pH values at the vicinity of cancerous tissues (pH=6.5) and in endo/lysosomes (pH=4-6) are lower than in blood and normal tissues (pH=7.4), pH sensitivity can be used to control release systems in cancer applications.<sup>22,23</sup>

Therefore, the synthesis of a combined MSN nanoplatform for a dual synergistic drug release in an acidic media would be of great interest.

The general principle of combination chemotherapy is the delivery of the maximum tolerated dose of different drugs with independent mechanisms of action.<sup>24</sup> In this regard, many antitumor drugs without overlapping toxicities and cross-resistance have been used together to afford a remarkable synergistic effect to enhance cancer cell killing.<sup>13</sup> Among them (5-fluorouracil, methotrexate, cisplatin, camptothecin, doxorubicin, etoposide, paclitaxel, carboplatin, and vincristine), a combination of camptothecin (CPT) with doxorubicin (DOX) has attracted great interest, due to its effective synergistic effect (Figure 6.1).<sup>25-30</sup>

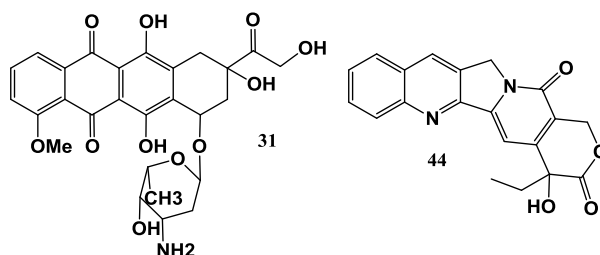


Figure 6.1. DOX and CPT chemical structure.

DOX and CPT derivatives are considered to be two of the most promising anticancer drugs of the 21st century. Although studies have demonstrated their effectiveness against many different types of cancer *in vitro*, clinical application of CPT and DOX is difficult to achieve due to their poor water solubility and their high secondary effects.<sup>25-30</sup> Both CPT and DOX are DNA-damaging drugs that result in the unwinding of DNA transcription, by inhibiting the progression of the topoisomerase I (CPT) and II (DOX) enzymes, enhancing the DNA-damaging efficiency.<sup>25-30</sup>

A search in literature revealed that dual DOX-CPT-MSNs have been only scarcely described in the literature. To our knowledge, there are just two examples where MSNs have been used to deliver dual DOX-CPT drugs.<sup>28,29</sup>

On the one hand, Ze-Yong Li *et al.*,<sup>28</sup> proposed to functionalize DOX with an hydrolysable linker into mercaptopropyl MSN and then, absorption of CPT. As a consequence DOX is released only in an acid pH, but no control of CPT release is obtained, since it is only present at the external surface of MSNs. As a consequence, CPT release is not affected by the linker split at pH=4 and is equally released at any pH. In addition, CPT release at pH=7 is not desired since at these physiological conditions CPT is hydrolyzed, leading to the opening of the lactone ring forming the inactive carboxylate.<sup>31</sup>

Moreover, Ze-Yong Li *et al.* approach is chemically complex and not versatile, since the hydrolysable linker is attached to the drug. Instead of adding the scissile linker directly to the nanoparticles and then add DOX, the authors functionalize the DOX structure, which could change the action mechanism of the drug and therefore its therapeutic effect. Thus, this approach is not only difficult to carry out but also not general. If another drug is used, the linker must be synthesized again. On the contrary, by adding directly to the MSN a suitable hydrolysable linker, any drug with a carbonyl group could be added afterwards, without any chemical reaction in its structure.

On the other hand, Muhammad *et al.*<sup>29</sup> proposed to use DOX as a capping agent by a coordination interaction. Channels in this case are capped with cadmium disulfide CdS quantum dots and DOX is absorbed at the entrance of the porous by the interaction between the amino group of DOX and Cd<sup>2+</sup>. In an acid environment this interaction is not present and therefore, DOX is released with inner CPT. Nevertheless, in this case CPT was only released at pH=7 (80 %).

Although in none of the reports, a blocking effect is attributed to DOX itself, it has been described that similar structures are able to block the outer surface.<sup>32,33</sup> Therefore, it seems that either by linking DOX covalently or electrochemically, the drug would be capable of blocking the pores. Moreover, it is firmly believed that by combining the two strategies it could be possible to control CPT and DOX release in different pH media.

Thus, the synthesis of MSNs with CPT loaded at the inner porous and DOX covalently linked at the surface of MSNs through a scissile bond is envisaged for the delivery of a dual synergistic pH triggered system. Typical cleavable pH sensitive bonds are hidrazones,<sup>28,34</sup> hidrazides,<sup>35</sup> or imines<sup>36</sup>. Among them, hidrazones have been widely studied.<sup>34,35,37-39</sup> By absorbing CPT drug

inside the channels and therefore adding a capping DOX-linker system at basic pH the entrance of the porous will be blocked, having a controlled release of CPT and DOX .

## 6.2. Strategy for dual drug release

MSNs nanoplatform is designed as a versatile system, where a same drug would act both as a capping linker and as a therapeutic agent. To our knowledge, no examples of drugs acting both as a therapeutic agent as well as a capping gate in MSNs or other similar systems have been described. This strategy is not commonly used in the literature.

To this end, a drug A is loaded in MSNs porous, in this case CPT, then the blocking hydrolysable linker is introduced and finally the second drug B (DOX) is added. By pH stimulus drug B (DOX) and capping linker would be hydrolyzed and the gates would open. Therefore no release is expected at pH=7 while a high drug A and B release is expected at pH=4 (Figure 6.2).

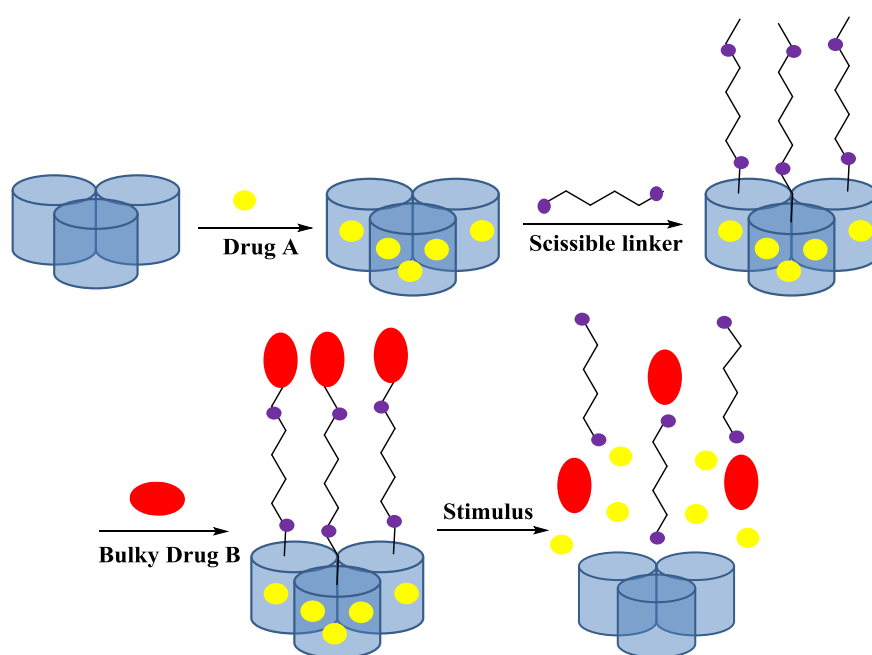


Figure 6.2. Dual drug release system scheme.

Both drug A and B are added to the system without any chemical reaction to their structure. Therefore it is proposed a versatile, one-pot approach where any carbonyl drug could be used as a capping agent.

Consequently, a linker that would react with MSNs and DOX is needed. Therefore, this strategy presents the advantage of using a linker with two scissile points, and therefore it will enable DOX to be released even if one of the two points is not hydrolyzed.

In this case, it is proposed to use a polyethylene glycol chain, that apart from blocking MSNs porous, would also increase MSNs biodistribution and time clearance.<sup>40</sup> Small and similar compounds have shown to be able to block the porous entrance.<sup>35,41,42</sup>

Moreover, the cytotoxicity of hydrazone-linked polymer–drug conjugates, for different applications, have been studied<sup>43</sup> and they do not induce cytotoxicity. Therefore hydrazine moieties are a suitable group to use for *in vitro* and *in vivo* applications.

Then, a dihydrazide PEG (**34**) that could be easily synthesized from tetraethylene glycol is proposed as a suitable linker. Thus the components proposed to carry out the final systems are presented in Figure 6.3, which are aminated-MSNs; 3,6,9,12,5-pentaoxaheptadecanedihydrazide (**34**) and DOX (**22**).

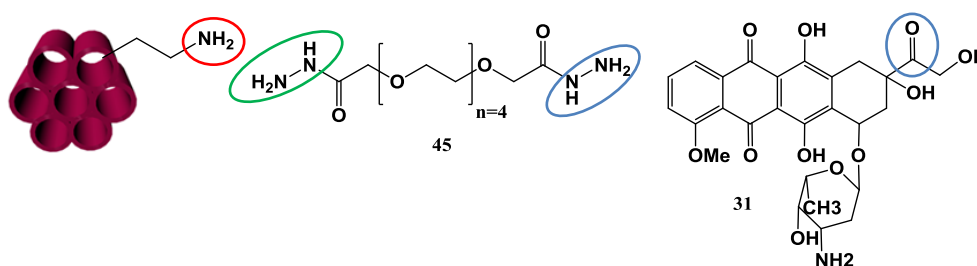


Figure 6.3. Proposed components for dual system application.

One extremity of PEG (**45**), 3,6,9,12,5-pentaoxaheptadecanedihydrazide, is reacted with the ketone moiety presented in DOX structure and the other with MSNs. Therefore proper functionality in MSNs that would directly react with the hydrazide moiety is needed. An easy possibility is to introduce an aldehyde moiety into the MSNs surface. Thus, the synthesis of amine-aldehyde regioselective MSNs is needed. In addition, while aldehyde moiety would react with the linker, amino functionality will enhance drug loading.

A search in literature revealed that, there are few examples of aldehyde-MSNs<sup>35,39,44,45</sup> and in all the cases, aldehyde is added by silanization through triethoxysilylbutyraldehyde. Nevertheless, to our knowledge, there are no amine-aldehyde MSNs, not to mention regioselective amino-aldehyde MSNs.

Aldehyde-MSNs can be synthesized by using amino reactivity. MSN must react with a linker holding a functionality that would react with aminated-MSNs and the other that would give an

aldehyde moiety. A linker bearing an activated acid or an isothiocyanate moiety with an aldehyde could be used, but since amine-acetal, 2,2-dimethoxyethan-1-amine (**47**), is commercially available and accessible in the laboratory, it is believed that using isothiocyanate reaction would be easier. Amine-acetal **47**, can be easily transformed to the isothiocyanate-acetal linker **46**, 2-isothiocyanate-1,1-dimethoxyethane, which after deprotection in acidic media will give aldehyde-MSNs (Figure 6.4.) .

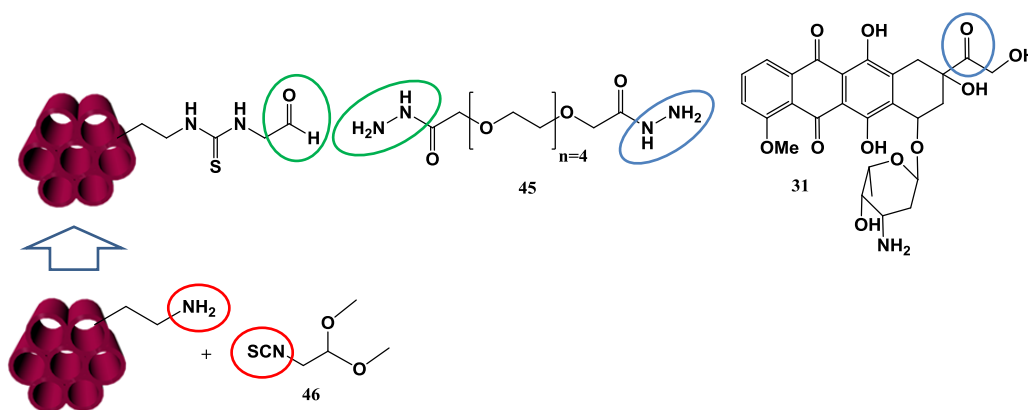


Figure 6.4. Components for dual system application.

Therefore aldehyde MSNs and the capping dihydrazide linker must be synthesized and then, the entire system proved.

### 6.3. Synthesis of aldehyde-MSNs

First, a study of the synthesis and reactivity of monofunctionalized aldehyde-MSNs must be carried out. Therefore, MSNs aldehyde formation with 2-isothiocyanate-1,1-dimethoxyethane (**46**) must be tested. Since amino and aldehyde moieties are not compatible in the same surface, first the concept must be proven by converting all amino moieties into aldehyde functionality. For that, CTAB must be completely removed before any reaction. As proof of concept, 28 eq. of 2-isothiocyanate-1,1-dimethoxyethane (20 mg,  $1.36 \cdot 10^{-4}$  mol) (**46**) in 20 mL of EtOH were added to 40 mg of aminated-MSNs of 100 nm. 24 h later, the resulting material was then treated with acid ethanol for 4 hours in order to deprotect the acetal moiety and form the aldehyde moiety (Figure 6.5).



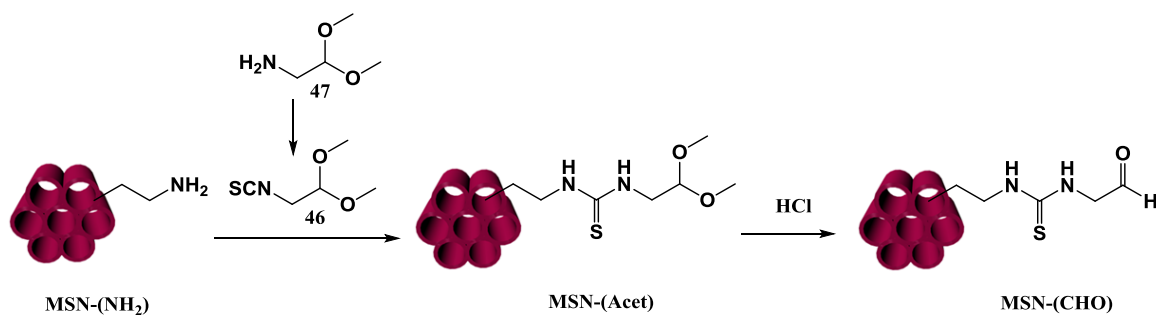


Figure 6.5. Synthesis of aldehyde MSNs.

MSN-(CHO) nanoparticles were characterized by IR and DLS. No further characterization was carried out since the aim of this nanoparticles MSN-(CHO) is just to prove that the use of 2-isothiocyanate-1,1-dimethoxyethane (46) can yield aldehyde reactive MSNs. The successful functionalization of MSN-(CHO) is supported by the presence of two characteristic absorption bands around  $2900\text{ cm}^{-1}$  and  $1400\text{ cm}^{-1}$  in the FT-IR spectrum (Figure 6.6). Moreover, acetal formation (MSN-(Acet)) can be clearly observed by the widen signals at  $3000\text{ cm}^{-1}$  and  $1200\text{ cm}^{-1}$ .

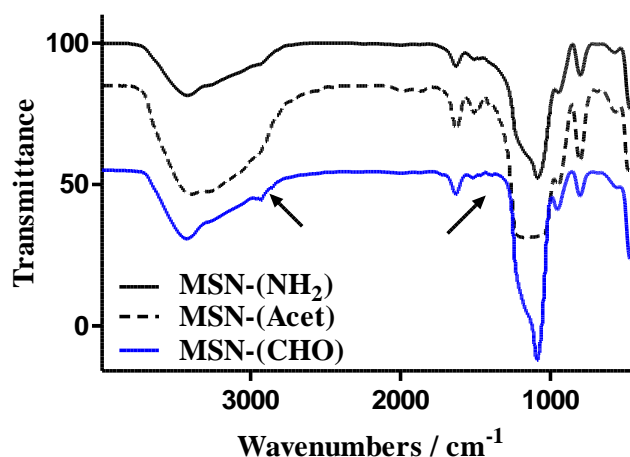


Figure 6.6. FTIR of MSN-(CHO).

As expected, no significant size and  $\zeta$ -potential differences were obtained between initial MSNs-(NH<sub>2</sub>) and MSN-(CHO) (Table.6.1). These data suggest that aldehyde functionalization do not erode the structural features of the MSNs.

Table 6.1. MSN-(CHO) size.

Size / nm	TEM	DLS	pDI	$\zeta$ -pot / mV
MSN-(CHO)	100	190	0.148	-15

#### 6.4. Functionalization test of MSN-(CHO)

Once MSN-(CHO) have been synthesized, its reactivity must be checked. To prove that aldehyde-MSNs can react with hydrazine moieties rapidly, efficiently, in quantitative yields and without further purifications, the reaction is carried out with (2,4-dinitrophenyl)hydrazine (**47**) which gives a yellow colored product and thus, MSNs functionalization can be easily detected (Figure 6.7).

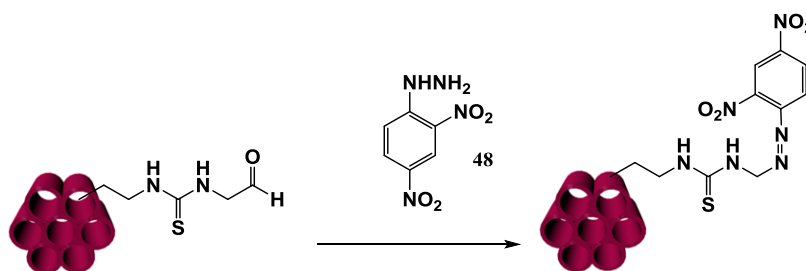


Figure 6.7. 2,4-dinitrophenylhydrazine (**38**) reaction with MSN-(CHO).

20 mg ( $1.056 \cdot 10^{-4}$  mol) of 2,4-dinitrophenylhydrazine (**48**) were added to a solution of 5 mg amino-MSNs in 5 mL of MeOH and were left for 24 h. MSNs were washed with MeOH until supernatant presented no color. The yellow coloration of MSNs corroborates that MSN-(CHO) have indeed reacted with 2,4-dinitrophenylhydrazine (**48**) and that aldehyde moiety has been correctly introduced to MSNs. 13 % of 2,4-(dinitrophenyl)hydrazine was finally attached to the MSNs.

#### 6.5. Synthesis of bifunctionalized amino-aldehyde MSNs

Now that it has been proved that amino-MSNs can be easily converted into aldehyde moieties, regioselective bifunctionalized ( $\text{MSN}-(\text{NH}_2)_i(\text{CHO})_o$ ) must be synthesized.

As mentioned before, regioselective bifunctionalization is based on a co-condensation process, followed by an external reaction, while tensioactive is still present in MSNs porous. Generally, in order to preserve the surfactant inside MSNs porous, toluene is used as a solvent in external functionalization processes. In this case isothiocyanate-acetal linker **46** is soluble in toluene and this procedure can be easily applied.

Briefly, the synthesis follows a similar scheme as described before. 0.2 g of aminated-MSNs containing the surfactant (CTAB) were reacted with 4 eq. of 2-isothiocyanate-1,1-dimethoxyethane (**46**) (0.1 g,  $6.8 \cdot 10^{-4}$  mol) in 50 mL of toluene. 24 h later, MSNs were washed twice with toluene and ethanol and then the tensioactive was eliminated.  $\text{MSN}-(\text{NH}_2)_i(\text{Acet})_o$

were treated in 40 mL solution of EtOH, where 0.5 g of  $\text{NH}_4\text{NO}_3$  were dissolved. 24 h later, MSNs were washed with EtOH and acetal protecting group was removed by stirring MSNs in HCl solution for 6 h (Figure 6.8).

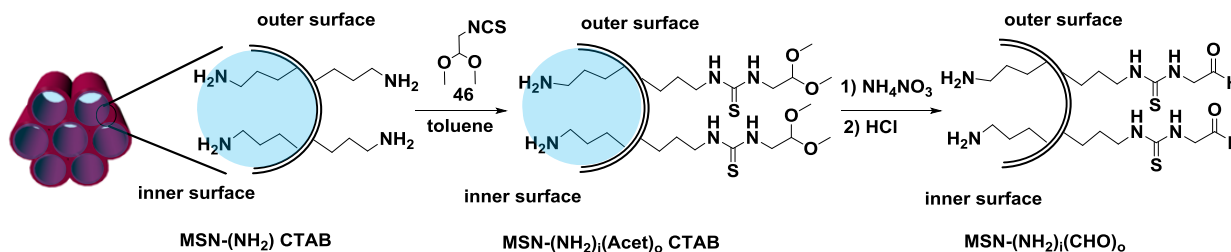


Figure 6.8. Bifunctionalized  $\text{MSN}-(\text{NH}_2)_i(\text{CHO})_o$  scheme.

The successful functionalization of MSNs is supported again by the presence of three small aldehyde absorption bands, two around  $2990\text{ cm}^{-1}$  and one at  $1400\text{ cm}^{-1}$  in the FT-IR spectrum (Figure 6.9). In this case, amine moieties of aminated nanoparticles with tensioactive ( $\text{MSN}-(\text{NH}_2)\text{CTAB}$ ) are transformed into acetal ( $\text{MSN}-(\text{NH}_2)_i(\text{Acet})_o\text{CTAB}$ ) while tensioactive is still present as it is clear from the absorption band at  $2990\text{ cm}^{-1}$ , preserving inner amino groups from reaction. Tensioactive removal gives  $\text{MSN}-(\text{NH}_2)_i(\text{Acet})_o$  that present widen acetal bands at  $3000\text{ cm}^{-1}$  and  $1200\text{ cm}^{-1}$ . Finally, treatment with HCl gives the final  $\text{MSN}-(\text{NH}_2)_i(\text{CHO})_o$ ,

The regioselective bifunctionalization of  $\text{MSN}-(\text{NH}_2)_i(\text{CHO})_o$  was successfully achieved since MSNs mesoporous were blocked by the surfactant ( $\text{MSN}-(\text{NH}_2)_i(\text{Acet})_o\text{CTAB}$ ), during the reacting process ( $2900\text{ cm}^{-1}$ ) and no reaction was carried at inner amino moieties.

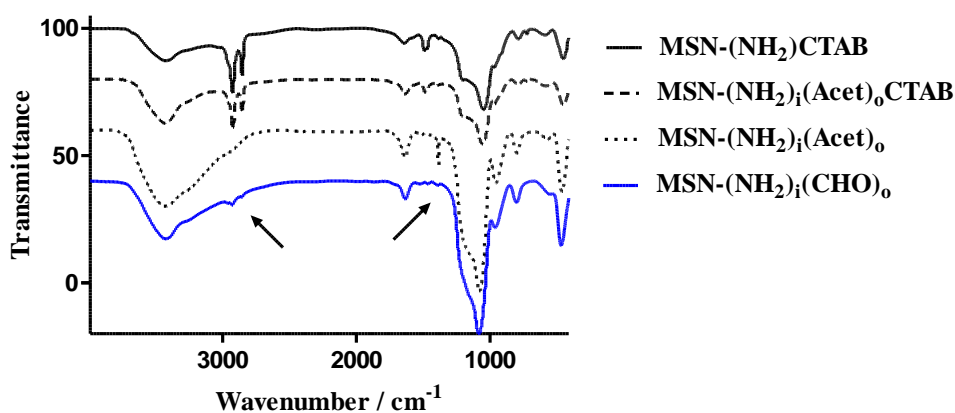


Figure 6.9. FTIR of bifunctionalized  $\text{MSN}-(\text{NH}_2)_i(\text{CHO})_o$ .

Bifunctionalized amino-aldehyde MSNs were characterized by DLS, TEM, BET and powder XRD analysis. As expected, no significant size and  $\zeta$ -potential differences were obtained between initial aminated nanoparticles (MSNs-(NH<sub>2</sub>)) and bifunctionalized amino-aldehyde nanoparticles (MSNs-(NH<sub>2</sub>)<sub>i</sub>(NCS)<sub>o</sub>) (Table.6.2). Again, these data suggest that aldehyde introduction does not erode the structural features of the MSNs. Moreover, MSN-(NH<sub>2</sub>)<sub>i</sub>(CHO)<sub>o</sub> are regular, homogeneous and round shaped (Figure 6.10).

Table 6.2. MSN-(NH<sub>2</sub>)<sub>i</sub>(CHO)<sub>o</sub> size.

Size / nm	TEM	DLS	pdl	$\zeta$ -pot / mV
MSN-(NH <sub>2</sub> )	100	140	0.040	-13
MSN-(NH <sub>2</sub> ) <sub>i</sub> (CHO) <sub>o</sub>	100	148	0.608	-17

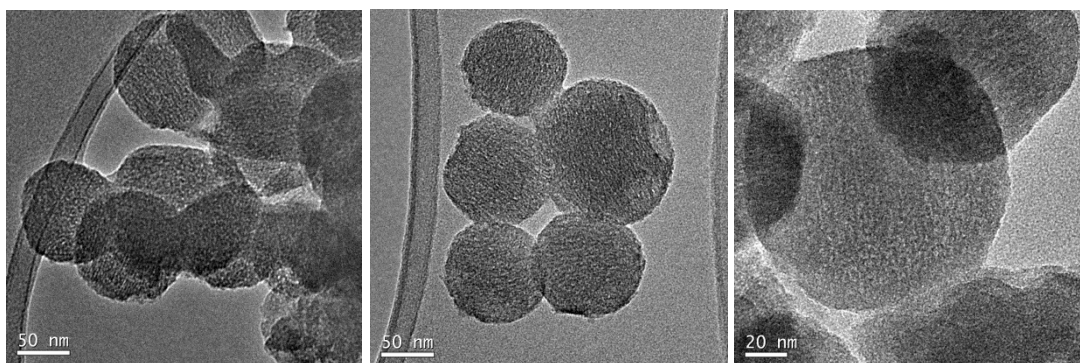


Figure 6.10. TEM micrographs of monodispersed MSN-(NH<sub>2</sub>)<sub>i</sub>(CHO)<sub>o</sub>.

Powder XDR analysis indicates highly ordered structures with d100 at 2.3 and lightly faceted hexagon-shape at 4.1 (d110) and 4.2 (d200) (Figure 6.11).

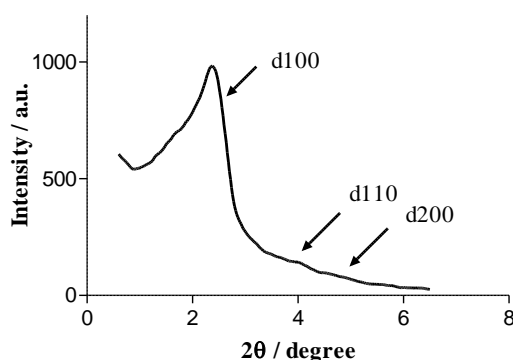


Figure 6.11. SXDR of MSN-(NH<sub>2</sub>)<sub>i</sub>(CHO)<sub>o</sub>.

N<sub>2</sub> adsorption/desorption measurements, MSN-(NH<sub>2</sub>)<sub>i</sub>(CHO)<sub>o</sub> showed type IV isotherms, which display clear H<sub>1</sub> hysteresis loop characteristic of mesoporous materials. BET surface areas are over 1006.86 m<sup>2</sup>·g<sup>-1</sup> for MSN-(NH<sub>2</sub>) and 989.67 m<sup>2</sup>·g<sup>-1</sup> for MSN-(NH<sub>2</sub>)<sub>i</sub>(CHO)<sub>o</sub> (Figure 6.12).

Additionally, the pore volume for MSN-(NH<sub>2</sub>)<sub>i</sub>(CHO)<sub>o</sub> was 0.56 cm<sup>3</sup>·g<sup>-1</sup> and 0.67 cm<sup>3</sup>·g<sup>-1</sup> for reference MSN-(NH<sub>2</sub>). The MSN present a very narrow pore size distribution centered at 2.4 nm (Table 6.3).

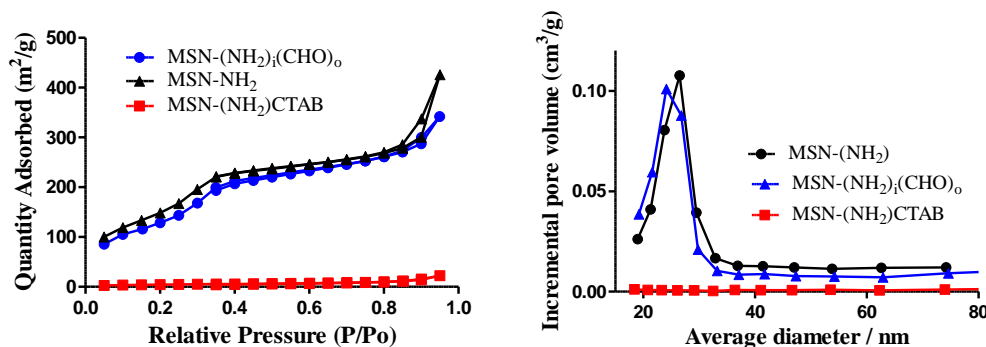


Figure 6.12. N<sub>2</sub> adsorption-desorption and BJH pore size distribution plots of MSN-(NH<sub>2</sub>)<sub>i</sub>(CHO)<sub>o</sub>.

Table 6.3. N<sub>2</sub> adsorption-desorption and BJH pore size distribution values of MSN-(NH<sub>2</sub>)<sub>i</sub>(CHO)<sub>o</sub>.

	MSN-NH <sub>2</sub> (CTAB)	MSN-(NH <sub>2</sub> )	MSN-(NH <sub>2</sub> ) <sub>i</sub> (CHO) <sub>o</sub>
BET surface area (m <sup>2</sup> /g)	50.07	1006.86	989.67
BJH pore volume (cm <sup>3</sup> /g)	0.03	0.67	0.56
Pore size (nm)	--	2.40	2.40

It can be concluded that bifunctional amino-aldehyde formation from amino-MSNs can be successfully achieved without affecting MSNs morphology.

## 6.6. Synthesis of capping dihydrazide PEG linker

As explained before, a long PEG dihydrazide linker (**45**) is believed to be an excellent blockage linker capable of opening and capping the porous by pH stimuli. Moreover, similar hydrazone linkers have been reported as non-cytotoxic species.<sup>43</sup> In order to synthesize this product **45**, tetraethylene glycol (**25**) is used, which by a nucleophilic substitution with bromo ethylacetate would give diester PEG (**49**). A final substitution with hydrazine results in the formation of dihydrazide PEG (**45**) (Figure 6.13).

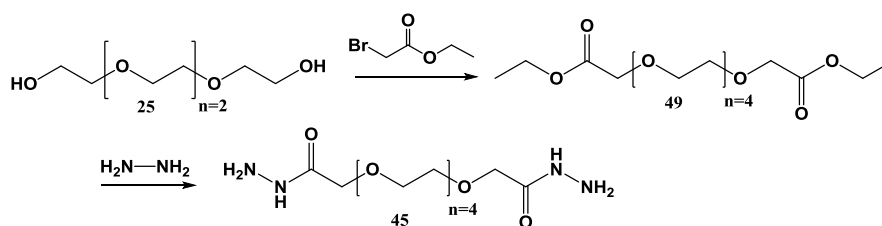


Figure 6.13. Schematic synthesis of the capping gate linker.

## 6.7. Dual MB and DOX drug release nanocarrier

Before using CPT/DOX approach, the mechanism of the platform must be tested. As proof of concept, MB is chosen as a suitable dye. MB maximum absorbance is centered at 650 nm very different from DOX at 490 nm maximum absorbance. Moreover, MB presents an intense blue-violet coloration, while DOX is red.

### 6.7.1. MB Loading

MB is reported to have been loaded in MSNs using EtOH<sup>46</sup> and water solutions.<sup>47</sup> Since MB is a cationic dye, its absorption and release depend on the acidity of the medium. Maximum absorption has been achieved in basic media, while maximum release takes place in acid pH.<sup>47</sup> In this case, since aminated MSNs have a pKa=10, a higher pH (pH>10) is needed in order to load the cationic dye. Therefore, first of all, the best conditions of MB loading must be studied. MB was loaded in EtOH and a basic solution of 0.44 M and 0.88 M of triethylamine in EtOH. MB loading increased from 2 %, to 4 % and 7 % respectively when more trimethylamine was added. This effect can be followed by the intensity of MSNs color (Figure 6.14).

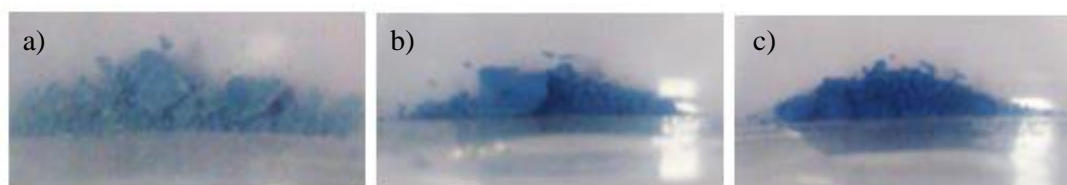


Figure 6.14. MSN-(MB) color a) in EtOH, b) 0.44 M triethylamine and c) 0.88 M triethylamine in EtOH.

Triethylamine enhances MB loading and a concentration of approximately 0.88 M is the better option to improve MB loading. This effect can also be observed by monitoring MB release. In EtOH, very little quantity of MB is loaded and therefore, little release is obtained, while when triethylamine is added to the media, MB loading and release increase (Figure 6.15). Consequently, to enhance MB loading, MB must be added at basic pH.



Figure 6.15. MSN-(MB) release a) in MeOH, b) 0.44 M triethylamine in MeOH and c) 0.88 M triethylamine in MeOH.

### 6.7.2. DOX/MB release

The first step to synthesize dual MB/DOX system is to load MB inside amine-aldehyde MSNs porous at basic pH. Then, 3,6,9,12,5-pentaoxaheptadecanedihydrazide (**45**) is added in excess to the solution. An excess must be added in order to promote aldehyde MSNs reaction with only one of the terminal moieties of the linker. Afterwards, remaining PEG **45** must be removed to avoid any reaction with DOX. Finally, DOX in a basic pH is added to the solution to give MSN-(NH<sub>2</sub>)<sub>1</sub>(PEGDOX)<sub>0</sub>MB (Figure 6.16).

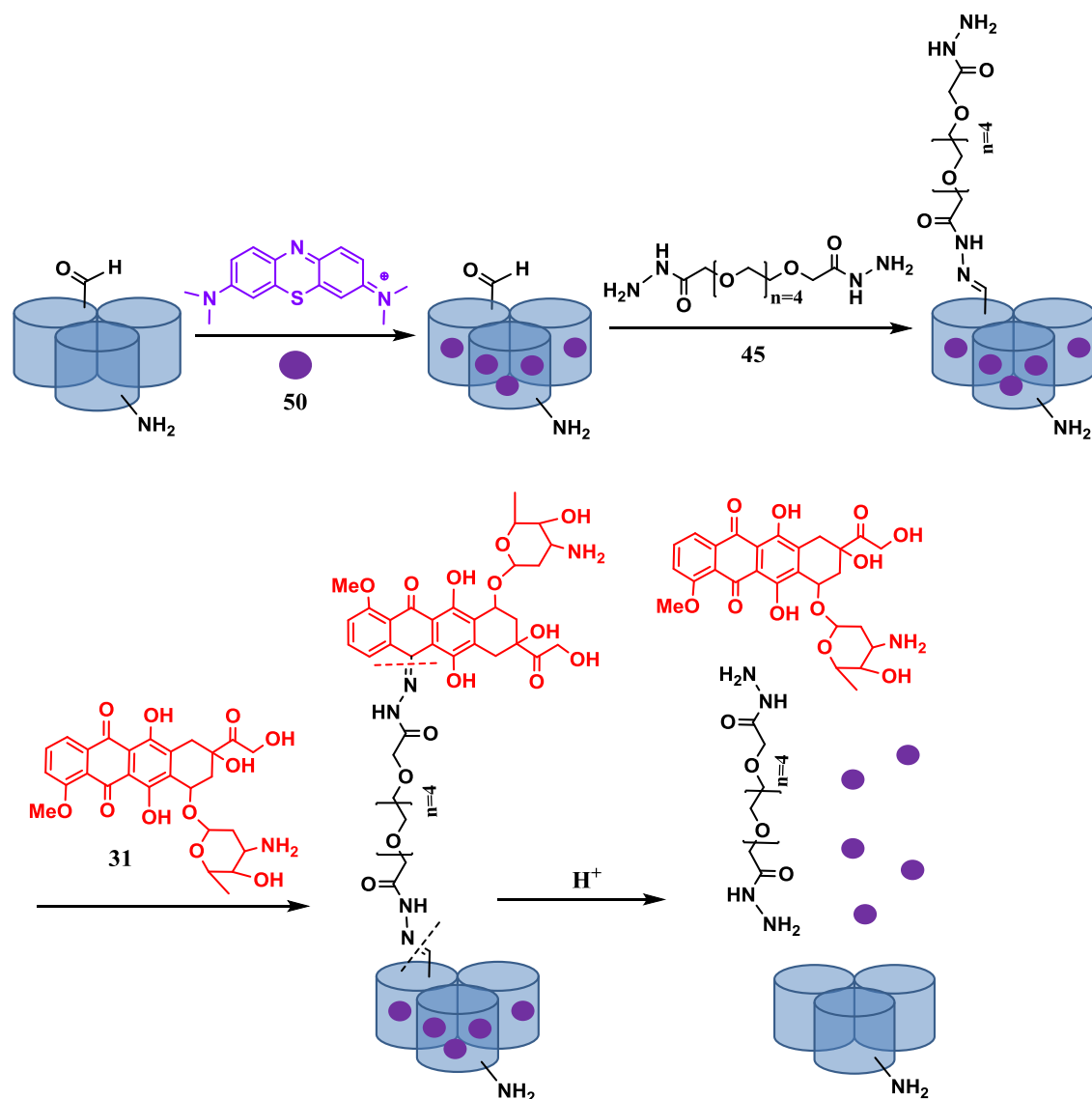


Figure 6.16. Schematic reaction of dual MB/DOX loading.

Absorption spectra of the supernatants at pH=7 (Figure 6.17, a) and at pH=4 (Figure 6.17, b) clearly demonstrate that no MB and DOX release is observed in a neutral pH, while high absorption DOX and MB bands at 490 and 650 nm are present in pH=4 supernatants. Moreover, MB release increases with time, the higher absorption band intensity of MB is observed at 22 h,

which led to believe that more MB is released when the large quantity of capping PEG-DOX system is hydrolyzed.

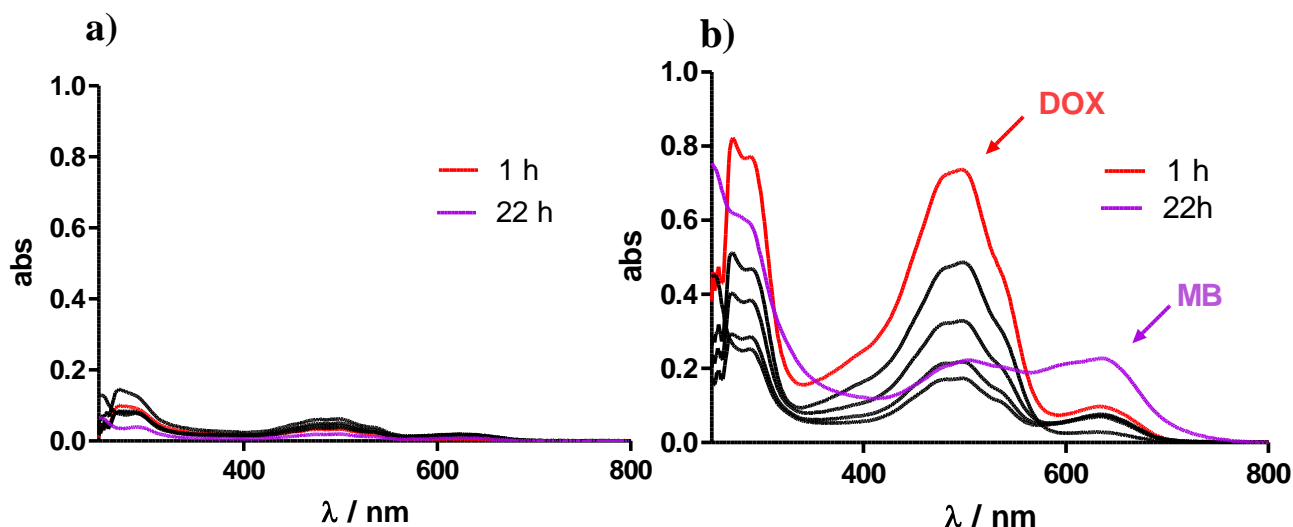


Figure 6.17. Absorption supernatants of MB and DOX at a) pH=7 and b) pH=4.

This effect can also be observed by naked eye, at pH=4 supernatants present a red color, whereas at pH=7 supernatants are colorless (Figure 6.18). DOX release decrease with time, as well as red coloration.

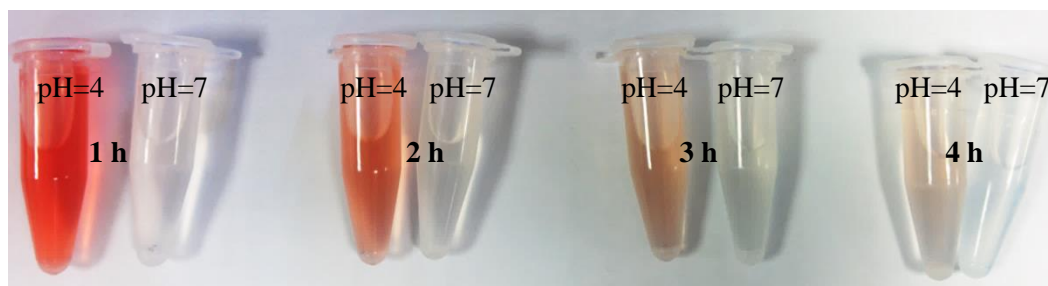


Figure 6.18. Visual release of MSN-(NH<sub>2</sub>)<sub>4</sub>(PEGDOX)<sub>6</sub>MB supernatants at 1 h, 2 h, 3 h and 4 h, at pH=4 and pH=7.

Regarding DOX release curves (Figure 6.19), it can be clearly seen that no DOX release is observed at pH=7 while a 45 % DOX release is observed after 30 h, at pH=4. Moreover, DOX release at pH=4 is quite fast, since half of the maximum quantity (25 %) that can be released, is released at 1 h. The incomplete release of DOX may be mainly attributed to the physical adsorption of DOX in MSN.<sup>48</sup> The different behavior of DOX release at pH=4 and pH=7 confirms the fact that this system respond to pH stimuli. Furthermore, when MSN-(NH<sub>2</sub>)<sub>4</sub>(PEGDOX)<sub>6</sub>MB nanoparticles at pH=7 are treated with acid (pH=4), DOX release starts to increase from 0 % to 35 %, which demonstrates that it is really the acidic medium that triggers DOX release.



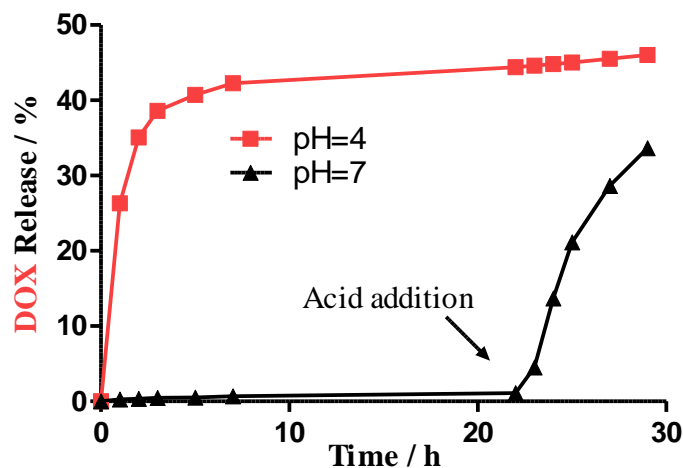


Figure 6.19. DOX Release at pH=4 and pH=7.

As for MB release (Figure 6.20), it can be observed that little MB release is achieved at pH=7 while a 50 % of MB release is observed after 30 h, at pH=4. Moreover, in this case, MB release at pH=4 is not as fast as DOX release, since only 10 % of MB is released at 1 h. MB release increases with time, since maximum MB release (50 %) is observed at 22 h. This effect emphasizes the fact that prior to MB release; capping linker DOX must be removed.

Again, the incomplete release of MB may be mainly attributed to the physical adsorption of MB in MSN.<sup>48</sup> The difference in MB release at pH=4 and pH=7 confirms the fact that this system respond to pH stimuli. As well as with DOX release, when MSN-(NH<sub>2</sub>)<sub>i</sub>(PEGDOX)<sub>o</sub>MB nanoparticles at pH=7 are treated with acid (pH=4), MB release starts to increase reaching the same release value obtained at pH=4. This demonstrates that it is really the acid medium that triggers both MB and DOX release.

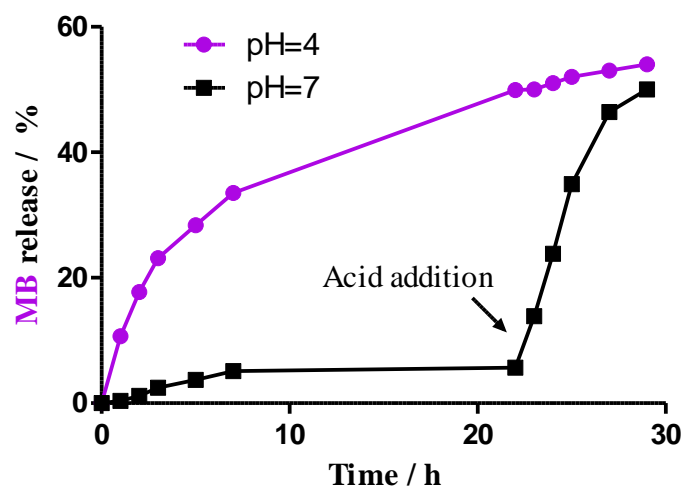
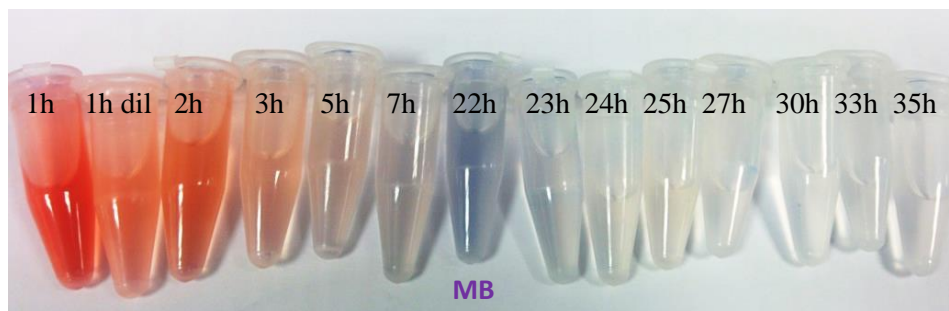


Figure 6.20. CPT release at pH=4 and pH=7.

MB maximum release at 22 h in pH=4 can also be monitored by naked eye (Figure 6.21). First DOX is released, which corresponds to the red supernatants, and after the capping agent is removed; MB is mostly released, which can be observed in the blue supernatant at 22 h.



**Figure 6.21. Supernatants release at pH=4 at different times.**

When acid medium at 22 h is added to MSN-(NH<sub>2</sub>)<sub>i</sub>(PEGDOX)<sub>o</sub>MB at pH=7 both DOX and MB release start to increase (Figure 6.22). Hence, it can be concluded that only pH has a strong effect on dual MB/DOX release.

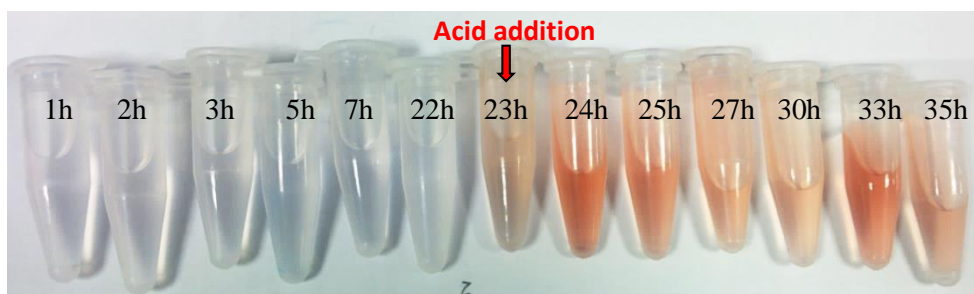


**Figure 6.22. Supernatants release at pH=7 at different times before and after acid addition.**

The total quantity of DOX and MB that can be released with this system has been calculated as  $7.2 \cdot 10^{-8}$  molDOX/mgMSN and  $8.5 \cdot 10^{-10}$  molMB/mgMSN. DOX is two orders of magnitude more released than MB, mostly due to the fact that DOX present a higher loading percentage than MB. DOX loading by positive interactions and covalent attachment is typically 25-30 % while MB loading is not higher than 7 % in the best case (Table 6.4). This difference can be explained as it is much easier to release a drug that is present only at the external surface than at the inner porous channels. Drug matrix interactions are higher inside the nanochannels than at the external surface, not to mention that drugs inside the inner surface have to diffuse through the exit.<sup>49</sup>

**Table 6.4. Loading and release values of MB and DOX.**

	<b>MB</b>	<b>DOX</b>
<b>Loading (%)</b>	7	25
<b>Release (%)</b>	50	46
<b>Release (molDRUG/mgMSN)</b>	$8.5 \cdot 10^{-10}$	$7.2 \cdot 10^{-8}$

The concept of dual drug release controlled by pH stimuli is validated; therefore MB dye is substituted by CPT.

## 6.8. Dual CPT and DOX drug release nanocarrier

### 6.8.1. CPT loading

CPT has been described as a very insoluble product. A research in literature revealed that CPT loading has been carried out in MeOH,<sup>42</sup> CHCl<sub>3</sub>/MeOH,<sup>50</sup> ACN/EtOH,<sup>51</sup> DMSO<sup>29</sup> and DMF.<sup>28</sup> Therefore, in order to determine which mixture could increase the quantity of absorbed CPT, some of these solvents were proven (Figure 6.23).

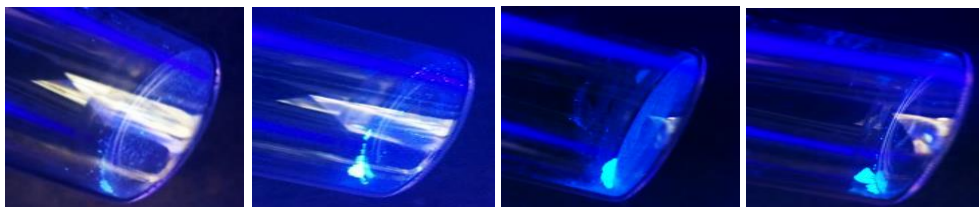


**Figure 6.23. MSN(CPT) fluorescence depending on the solvent, MeOH, CHCl<sub>3</sub>/MeOH, ACN/MeOH and DMSO.**

In all the cases, MeOH, CHCl<sub>3</sub>/MeOH, ACN/EtOH and DMSO, loading and release results were very low and difficult to measure. Loadings ranged between 0.5 and 3 % (Table 6.5).

**Table 6.5. OEA Loadings of CPT depending on the solvent.**

<b>OEA</b>	<b>MeOH</b>	<b>CHCl<sub>3</sub>/MeOH</b>	<b>ACN/MeOH</b>	<b>DMSO</b>
<b>CPT Loading (%)</b>	1.9	3.1	2.8	0.5

Nevertheless, above all the solvents, CHCl<sub>3</sub>/MeOH mixture was chosen since CPT was better dissolved and presented the better loading result (3.1 %).

### 6.8.2. CPT-DOX release

As in MB/DOX dual release, the first step to build this system is the addition of CPT into the porous of MSN-(NH<sub>2</sub>)<sub>i</sub>(CHO)<sub>o</sub>. Then, an excess of 3,6,9,12,5-pentaoxaheptadecanedihydrazide (**45**) is added to the solution. Afterwards, remaining PEG **45** must be removed to avoid any reaction with DOX. Finally, DOX is added to the solution in a basic medium (Figure 6.24).

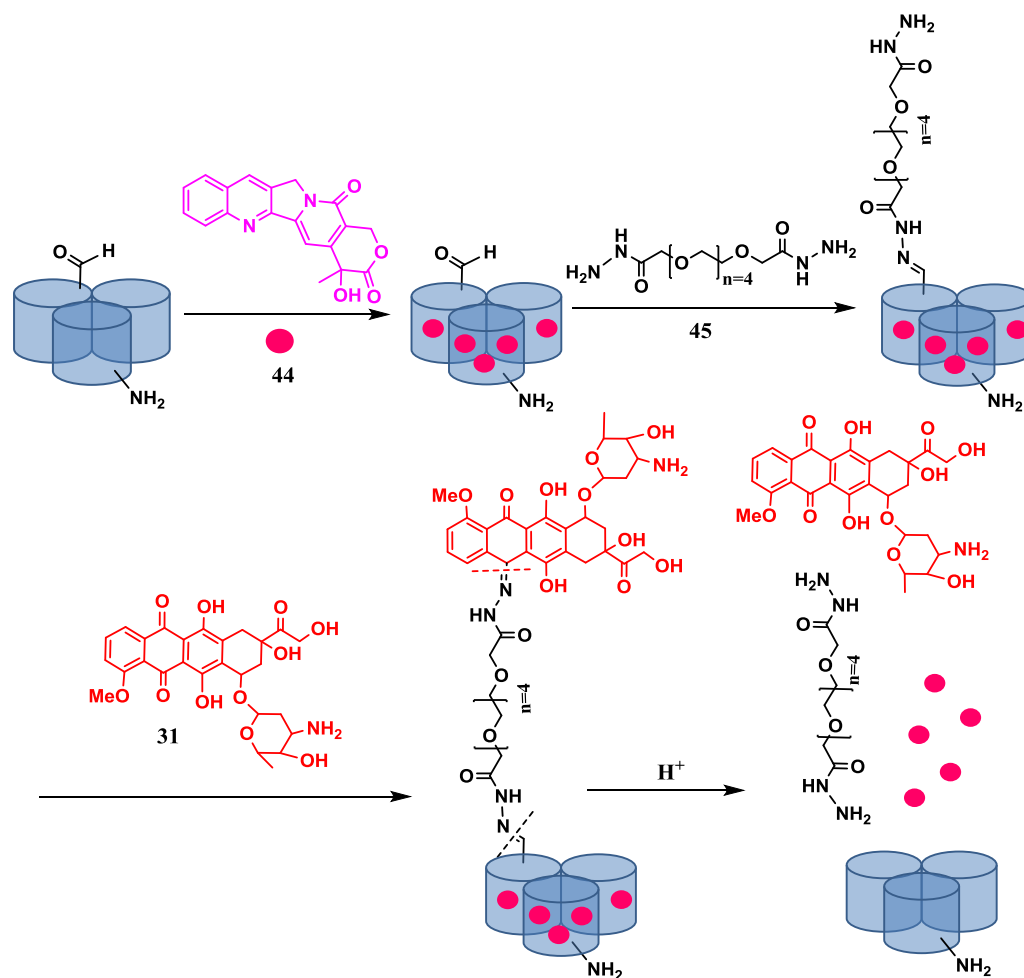


Figure 6. 24. Schematic synthesis of dual CPT/DOX system release.

Maximum loading for CPT, assessed either by absorption spectroscopy or by OEA, was obtained as  $1.36 \cdot 10^{-8}$  molCPT/mgMSN, which corresponds to a 2.3 % loading. This loading is very similar to reference CPT values ranging from 2 and 5 %.<sup>28</sup>

Regarding DOX loading, approximately  $7.06 \cdot 10^{-7}$  molDOX/mg MSN were incorporated to the MSNs, which corresponds to 25 %.

Release quantification was followed by both CPT and DOX absorption bands at 354 nm and 490 nm respectively. Even if CPT and DOX maximum absorption bands are separate enough and do not interfere between each other, CPT absorption intensity has been quantified by

subtracting to CPT maximum absorption band (354 nm) the intensity of DOX band at that same wavelength. Therefore, the resulting absorption can only be attributed to CPT. A standard curve that relates 490 nm DOX maximum band with 354 nm intensity was carried out.

Absorption spectra of the supernatants at pH=7 (Figure 6.25, a) and at pH=4 (Figure 6.25, b) clearly demonstrates that no CPT and DOX release is observed in a neutral pH, while high absorption DOX and CPT bands, at 490 and 354 nm, are presented in pH=4 supernatants. Moreover, CPT higher absorption band is observed at 7 h, which led to believe that more quantity of CPT is released when the large quantity of capping PEG-DOX system is hydrolyzed.

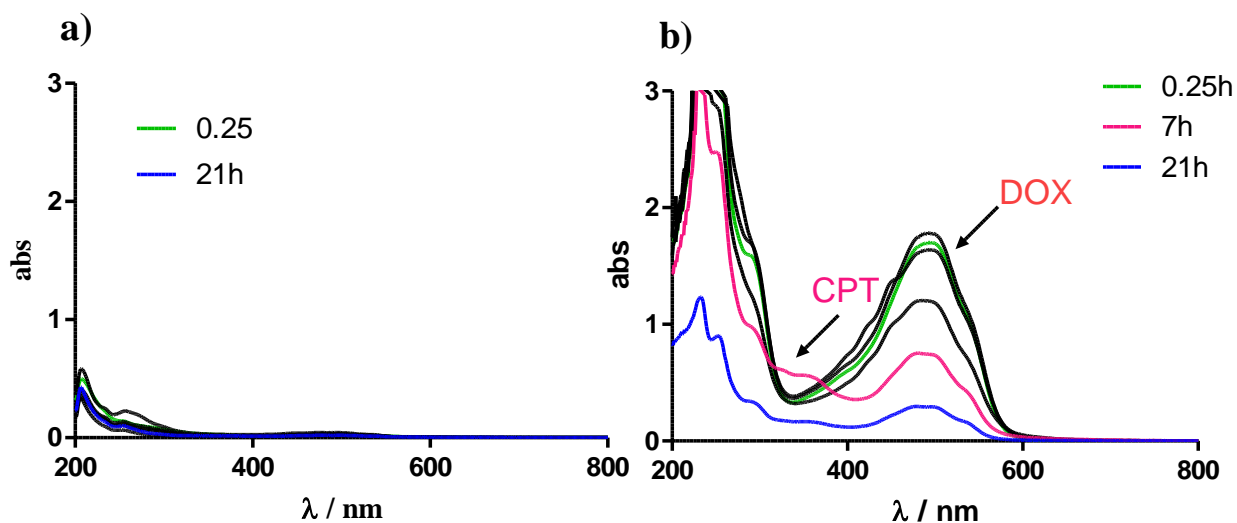


Figure 6.25. Absorption supernatants of CPT and DOX at a) pH=7 and b) pH=4.

This phenomenon can also be observed by naked eye, where at pH=7 supernatants are colorless, whereas at pH=4 supernatants present a red coloration (Figure 6.26).

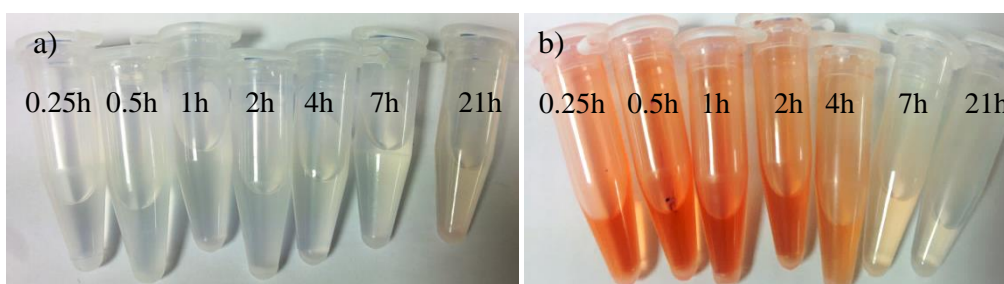


Figure 6.26. Supernatants of MSN-(NH<sub>2</sub>)<sub>1</sub>CPT(PEGDOX)<sub>0</sub> a) pH=7 and b) pH=4 at visible light.

CPT maximum release at 7 h (pH=4) can also be monitored by observing the supernatants in a UV lamp at 366 nm (Figure 6.27). First DOX is released, which corresponds to the red

supernatants, and after the capping agent is removed; CPT is mostly released, which can be attributed to the blue fluorescence at 7 h.

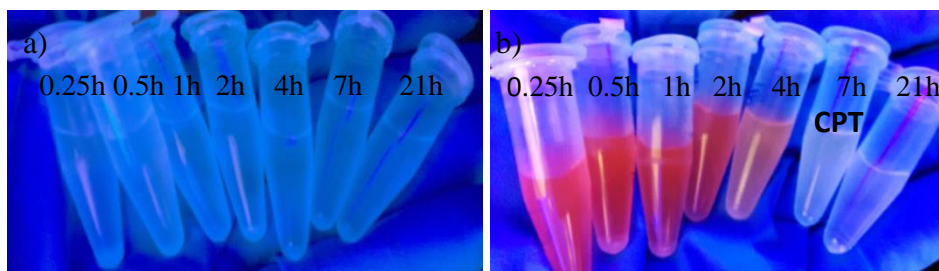


Figure 6.27. Supernatants of MSN-(NH<sub>2</sub>)<sub>1</sub>CPT(PEGDOX)<sub>0</sub>, a) pH=7 and b) pH=4 at 366 nm.

Regarding DOX release curves (Figure 6.28), it can be clearly observed that there is no DOX release at pH=7, while a 50 % of DOX release is observed after 20 h, at pH=4. Moreover, DOX release at pH=4 is quite fast, since more than a half of the maximum quantity that can be released (30 %) is released at 1 h. Again, the difference in DOX release at pH=4 and pH=7 confirms the fact that this system respond to pH stimuli.

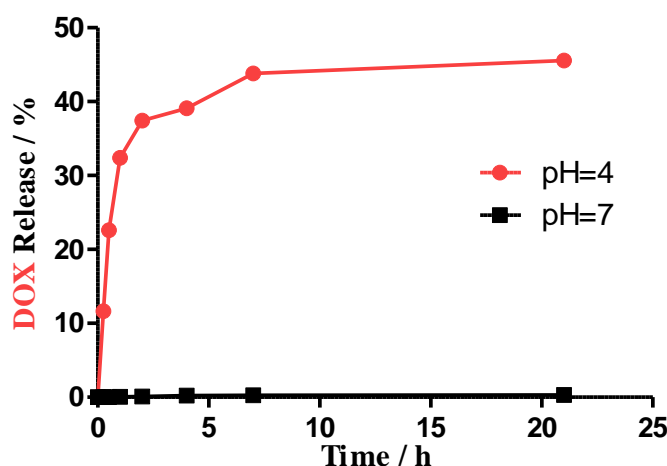


Figure 6.28. DOX release at pH=4 and pH=7.

As for CPT release (Figure 6.29), it can be pointed out that very little CPT release is observed at pH=7, while a 30 % of CPT release is observed after 20 h, at pH=4. Moreover, in this case, CPT release at pH=4 is not as fast as DOX release, since only 10 % of CPT is freed at 1 h. Again, the incomplete release of CPT may be attributed to the physical adsorption of CPT in MSN<sup>48</sup> or to its high insolubility in the medium. Again, the difference in CPT release at pH=4 and pH=7 confirms the fact that this system respond to pH stimuli and that DOX-dihydrazidePEG linker **45** was acting as a capping agent. No CPT release at pH=7 was observed, highlighting the fact that this system works better than reported CPT-DOX-MSNs systems.<sup>28,29</sup>

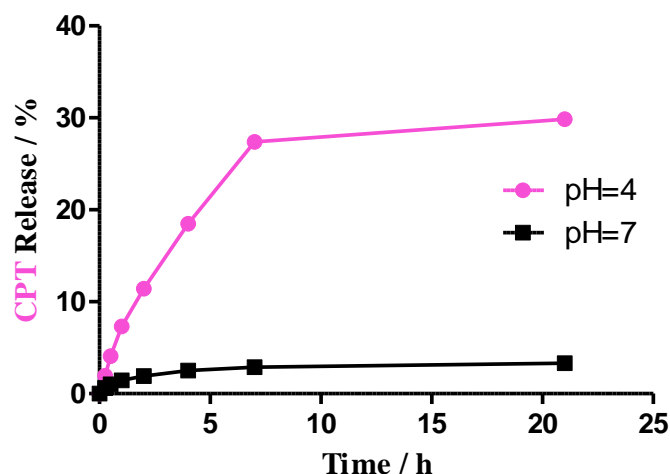


Figure 6.29. CPT release at pH=4 and pH=7.

It is worth nothing that this system possesses two different release profiles. Hydrophobic CPT is sustainably released from mesoporous channels, whereas DOX follows a fast burst-like release in acidic medium.

Even if a 30 % of CPT release seems a very low percentage, it is in fact a high number since described CPT release is around 20 %.<sup>52</sup> By and large, in the literature, when CPT is absorbed in MSNs, CPT release curves are not presented,<sup>42,50,51,53</sup> since in most of the cases, CPT loading and release are very low. In fact, Zink *et al* carried out CPT release experiments in DMSO because they could not detect CPT release in water.<sup>53</sup>

In this case, the concept of dual drug release controlled by pH stimuli is proven. Both CPT and DOX drugs can be controlled by pH stimuli. In table 6.6, it is summarized the maximum release of CPT and DOX that has been obtained with this system.

Table 6.6. Maximum release of CPT and DOX in MSN-(NH<sub>2</sub>)<sub>i</sub>(PEGDOX)<sub>o</sub>CPT.

Maximum Release	Percentage (%)	mol Drug /mg MSN	mg drug /mg MSN
CPT	20	$3.34 \cdot 10^{-9}$	0.014
DOX	50	$1.4 \cdot 10^{-7}$	0.088

The total quantity of DOX and CPT that can be released with this system has been calculated as  $1.4 \cdot 10^{-7}$  molDOX/mgMSN and  $3.34 \cdot 10^{-9}$  molCPT/mgMSN or 0.088 mgDOX/mgMSN and 0.014 mgMB/mg MSN. CPT value is very similar to described loadings since literature values are near  $5.79 \cdot 10^{-9}$  molCPT/mg<sup>52</sup>,  $2.9 \cdot 10^{-8}$  molCPT/mgMSN<sup>53</sup> and  $1.6 \cdot 10^{-8}$  molCPT/mgMSN.<sup>54</sup>

DOX is two orders of magnitude more released than CPT mostly because DOX present a higher loading than CPT most probably due to its better solubility in water.

## 6.9. Preliminary biological experiments

For viability experiments, control MSN-(NH<sub>2</sub>)<sub>i</sub>(DOX)<sub>o</sub> and MSN-(NH<sub>2</sub>)<sub>i</sub>(DOX)<sub>o</sub>CPT, in a 100, 50, 5, 0.5 μgMSN/mL or 30, 15, 1.5 and 0.15 μgDOX/mL concentration, were added and seeded for 24 h. Viability results are presented in Figure 6.30, where it can be observed that when DOX concentration is high, there is little difference between control MSN-(NH<sub>2</sub>)<sub>i</sub>(DOX)<sub>o</sub> and dual MSN-(NH<sub>2</sub>)<sub>i</sub>(DOX)<sub>o</sub>CPT, while at low DOX concentrations (0.5 μgMSN/mL) the combination of CPT/DOX is more toxic than with only DOX. These results can be rationalized, since the quantity of CPT that has been functionalized is little in comparison with the quantity of DOX, and therefore, only at a low concentration of DOX, CPT effect can be observed. Moreover, this phenomenon has also been reported by Ze-Yong Li *et al.*<sup>28</sup> and Muhammad *et al.*,<sup>29</sup> where CPT/DOX dual effect was more evident at diluted concentrations than at higher

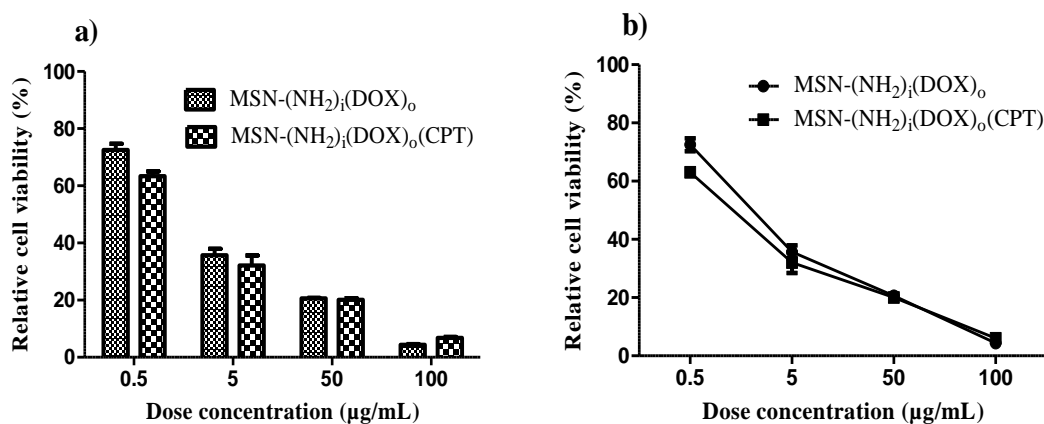


Figure 6.30. Control MSN-(NH<sub>2</sub>)<sub>i</sub>(DOX)<sub>o</sub> and MSN-(NH<sub>2</sub>)<sub>i</sub>(DOX)<sub>o</sub>CPT viability represented a) in bars and b) in lines.

To provide a qualitative information of the drug interaction, the combinatorial index (CI) of the diluted concentrations (0.5 and 5 μgMSN·mL<sup>-1</sup> or 0.15 and 1.5 μgDOX·mL<sup>-1</sup> respectively) of control MSN-(NH<sub>2</sub>)<sub>i</sub>(DOX)<sub>o</sub> and MSN-(NH<sub>2</sub>)<sub>i</sub>(DOX)<sub>o</sub>CPT is calculated. For 0.5 μgMSN·mL<sup>-1</sup> or 0.15 μgDOX·mL<sup>-1</sup> CI=0.38, while for 5 μgMSN·mL<sup>-1</sup> or 1.5 μgDOX·mL<sup>-1</sup> CI=0.51. In both cases, CI<1, which highlights the synergetic effect of CPT and DOX, previously described in the literature.<sup>[55]</sup> In addition, this system is very efficient in killing Hela cells since for 100 μgMSN/mL, where normally control MSNs are 100 % viable, in this case either with control MSN-(NH<sub>2</sub>)<sub>i</sub>(DOX)<sub>o</sub> or dual MSN-(NH<sub>2</sub>)<sub>i</sub>(DOX)<sub>o</sub>CPT, viability reaches 4 %. Therefore the system works and synergistic effects are observed at low concentrations.



To verify the release of both drugs, an uptake experiment of control MSN-(NH<sub>2</sub>)<sub>i</sub>(DOX)<sub>o</sub> and dual MSN-(NH<sub>2</sub>)<sub>i</sub>(DOX)<sub>o</sub>CPT is carried out. Again, the same conditions of Chapter 4 have been used for uptake experiments (100000 cells per well of Hela cells). In this case, since it is at low concentrations where CPT effect is observed, uptake experiments are carried out at 5 μgMSN/mL or 1.5 μgDOX/mL for 4 h. No staining protocols have been used, blue and red fluorescence correspond to DOX and CPT signal. As it can be observed for control MSN-(NH<sub>2</sub>)<sub>i</sub>(DOX)<sub>o</sub> (Figure 6.31, a-f), when a blue filter is used, cells present no signal. Whereas, for dual MSN-(NH<sub>2</sub>)<sub>i</sub>(DOX)<sub>o</sub>CPT, blue spots are observed, which indicates that CPT has been efficiently released and internalized in the cells (Figure 6.31, g-l). For dual MSNs blue spots correspond to the release of CPT molecules from the pores, whereas intense red spots relate to the release of DOX. Therefore, both drugs have been efficiently internalized in Hela cells.

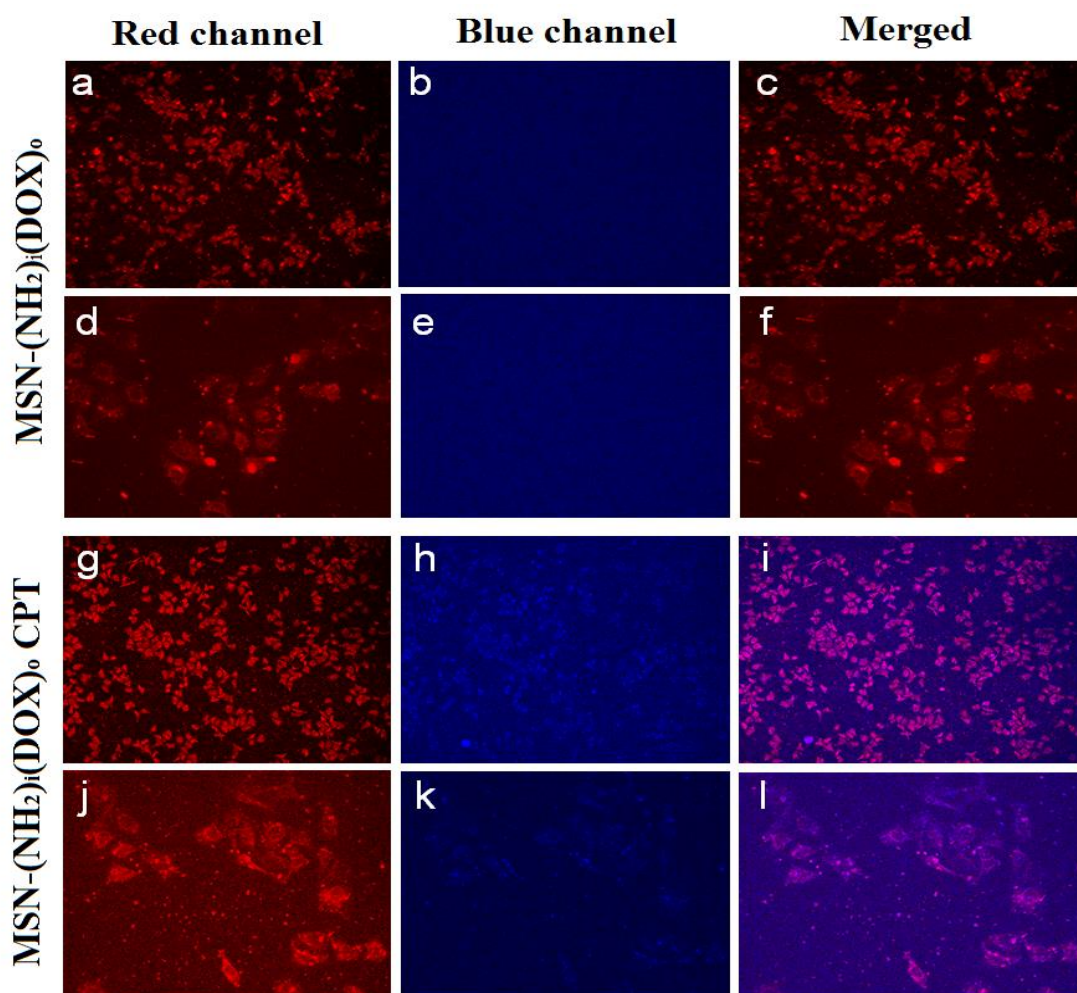


Figure 6.31. Uptake images of control MSN-(NH<sub>2</sub>)<sub>i</sub>(DOX)<sub>o</sub> (a-f) and MSN-(NH<sub>2</sub>)<sub>i</sub>(DOX)<sub>o</sub> CPT (g-l) at x10 and x40 objective.

## 6.10. Conclusions and Outlook

- Regioselective bifunctionalized MSN-(NH<sub>2</sub>)<sub>i</sub>(CHO)<sub>o</sub> nanoparticles have been synthesized. These MSNs have been applied as a nanoplatform for the controlled release of dual synergistic CPT/DOX. While CPT is loaded at the inner surface, DOX is covalently functionalized to a pH scissile dihydrazide-PEG-linker, acting both as an active and a capping agent.
- The system respond to pH stimuli and both CPT and DOX drugs are only released in an acidic media (pH=4). The system is versatile and therefore can be used for a variety of drug combinations.
- This strategy only presents three synthetic steps, avoiding any chemical reaction to the drug which could damage its active site or reactivity.
- MSN-(NH<sub>2</sub>)<sub>i</sub>(DOX)<sub>o</sub>CPT are toxic and CPT/DOX synergistic effect is detected at low concentrations of MSNs.

This versatile nanocarrier has been proven to respond to pH stimuli, while a dual controlled drug release has been achieved. This system allows a high release of DOX, but, although CPT maximum release (30 %) is comparable with other reported releases, CPT loading and release curves must be enhanced, in order to translate this system for *in vivo* experiments.

Just by enhancing CPT loading, this system could offer an excellent way to release two different drugs without any burst or premature release. It is worth nothing to mention again how easy is to use this strategy in comparison with published approaches<sup>28,29</sup> where a large quantity of chemical reactions were carried out directly to the drug. With this methodology and only in three steps, virtually any drug with a carbonyl moiety can be used, and therefore this system could be extended for the use of other drugs.

## 6.11. Bibliography

- (1) Ma, L.; Kohli, M.; Smith, A. *ACS Nano* **2013**, *7* (11), 9518–9525.
- (2) Hu, C.-M. J.; Zhang, L. *Biochem. Pharmacol.* **2012**, *83* (8), 1104–1111.
- (3) Hu, C.-M. J.; Aryal, S.; Zhang, L. *Ther. Deliv.* **2010**, *1* (2), 323–334.
- (4) Rosenholm, J.; Sahlgren, C.; Lindén, M. *J. Mater. Chem.* **2010**, *20* (14), 2707–2713.
- (5) Wang, A. Z.; Langer, R.; Farokhzad, O. C. *Annu. Rev. Med.* **2012**, *63* (1), 185–198.
- (6) Choi, K. Y.; Liu, G.; Lee, S.; Chen, X. *Nanoscale* **2012**, *4* (2), 330–342.
- (7) Meng, H.; Mai, W. X.; Zhang, H.; Xue, M.; Xia, T.; Lin, S.; Wang, X.; Zhao, Y. *ACS Nano* **2013**, *7* (2), 994–1005.
- (8) Bertucci, A.; Prasetyanto, E. A.; Septiadi, D.; Manicardi, A.; Brognara, E.; Gambari, R.; Corradini, R.; Cola, L. De. *Small* **2015**, *11* (42), 5687–5695.
- (9) Gary-Bobo, M.; Hocine, O.; Brevet, D.; Maynadier, M.; Raehm, L.; Richeter, S.; Charasson, V.; Looock, B.; Morère, A.; Maillard, P.; Garcia, M.; Durand, J.-O. *Int. J. Pharm.* **2012**, *423* (2), 509–515.
- (10) He, L.; Lai, H.; Chen, T. *Biomaterials* **2015**, *51*, 30–42.
- (11) Bharti, C.; Gulati, N.; Nagaich, U.; Pal, A. *Int. J. Pharm. Investig.* **2015**, *5* (3), 124–133.
- (12) Wang, W.; Wen, Y.; Xu, L.; Du, H.; Zhou, Y.; Zhang, X. *Chem. Eur. J.* **2014**, *20* (25), 7796–7802.
- (13) Mignani, S.; Bryszewska, M.; Klajnert-Maculewicz, B.; Zablocka, M.; Majoral, J. P. *Biomacromolecules* **2015**, *16* (1), 1–27.
- (14) Siegel RL, Miller KD, J. A. *CA Cancer J Clin* **2015**, *65*, 5–29.
- (15) Heagerty, M. *Br. J. Anaesth.* **2010**, *61* (3), 279–283.
- (16) Shah, M.; Schwartz, G. K. *Drug Resist. Updat.* **2000**, *3* (6), 335–356.
- (17) DeVita, V. T.; Young, R. C.; Canellos, G. P. *Cancer* **1975**, *35*, 98–110.
- (18) El Mundo: <http://www.elmundo.es/economia/2015/11/05/563a4561ca-4741c1788b4689.html> 11/2015.
- (19) CelatorPharma: <http://ir.celatorpharma.com/releasedetail.cfm?releaseid=938560> 11/2015.
- (20) CelatorPharma: <http://www.celatorpharma.com/> 11/2015.
- (21) Gan, Q.; Zhu, J.; Yuan, Y.; Liu, H.; Qian, J.; Li, Y.; Liu, C. *J. Mater. Chem. B* **2015**, *3* (10), 2056–2066.
- (22) Yang, K. N.; Zhang, C. Q.; Wang, W.; Wang, P. C.; Zhou, J. P.; Liang, X. J. *Cancer Biol. Med.* **2014**, *11* (1), 34–43.
- (23) Vivero-Escoto, J. L.; Slowing, I. I.; Trewyn, B. G.; Lin, V. S. Y. *Small* **2010**, *6* (18), 1952–1967.
- (24) Cancer Progress: <http://www.cancerprogress.net/> 2015.
- (25) Pavillard, V.; Kherfellah, D.; Richard, S.; Robert, J.; Montaudon, D. *Br. J. Cancer* **2001**, *85* (7), 1077–1083.
- (26) Shen, Y.; Jin, E.; Zhang, B.; Murphy, C. J.; Sui, M.; Zhao, J.; Wang, J.; Tang, J.; Fan, M.; Van Kirk, E.; Murdoch, W. J. *J. Am. Chem. Soc.* **2010**, *132* (12), 4259–4265.
- (27) Kathryn M. Camacho, Sunny Kumar, Stefano Menegatti, Douglas R. Vogus, Aaron C.

- Anselmo, S. M. *J. Control. Release* **2015**, *210*, 198–207.
- (28) Li, Z. Y.; Liu, Y.; Wang, X. Q.; Liu, L. H.; Hu, J. J.; Luo, G. F.; Chen, W. H.; Rong, L.; Zhang, X. Z. *ACS Appl. Mater. Interfaces* **2013**, *5* (16), 7995–8001.
- (29) Muhammad, F.; Guo, M.; Wang, A.; Zhao, J.; Qi, W.; Guo, Y.; Zhu, G. *J. Colloid Interface Sci.* **2014**, *434*, 1–8.
- (30) Schmid, B.; Chung, D. E.; Warnecke, A.; Fichtner, I.; Kratz, F. *Bioconjug. Chem.* **2007**, *18* (3), 702–716.
- (31) Scrivener, M.; Carmical, P. In *Chapter 16, Nanomedicine for Drug Delivery and therapeutics*; Mishra, A. K., Ed.; Beverly, MA, US, 2013.
- (32) Bernardos, A.; Mondragón, L.; Aznar, E.; Marcos, M. D.; Martínez-Máñez, R.; Sancenón, F.; Soto, J.; Barat, J. M.; Pérez-Payá, E.; Guillem, C.; Amorós, P. *ACS Nano* **2010**, *4* (11), 6353–6368.
- (33) Bernardos A, Mondragón L, Javakhishvili I, M. N.; Martínez-Máñez R, Sancenón F, Barat JM, Hvilsted S, Pérez- Payá E, A. P. *Chem. Eur. J.* **2012**, *18*, 13068–13078.
- (34) Lee, J. E.; Lee, D. J.; Lee, N.; Kim, B. H.; Choi, S. H.; Hyeon, T. *J. Mater. Chem.* **2011**, *21* (42), 16869–16872.
- (35) Lee, C. H.; Cheng, S. H.; Huang, I. P.; Souris, J. S.; Yang, C. S.; Mou, C. Y.; Lo, L. W. *Angew. Chemie Int. Ed.* **2010**, *49* (44), 8214–8219.
- (36) Gao, W.; Chan, J.; Farokhzad, O. C. *Mol. Pharm.* **2010**, *7* (6), 1913–1920.
- (37) Kar, M.; Tiwari, N.; Tiwari, M.; Lahiri, M.; Gupta, S. Sen. *Part. Part. Syst. Charact.* **2013**, *30* (2), 166–179.
- (38) Fan, J.; Fang, G.; Wang, X.; Zeng, F.; Xiang, Y.; Wu, S. *Nanotechnology* **2011**, *22* (455102), 1–11.
- (39) Cheng, Y; Morshed, R.; Cheng, S.H; Tobias, A; Auffinger, B; Wainwright, D.A.;Zhang, L.; Yunis, C; Han, Y.; Chen, C.T; Lo, L. W.; Aboody, K. S.; Ahmed, A. U.; Lesniak, M. . *Small* **2013**, *9* (14), 4123–4129.
- (40) Ohno, K.; Akashi, T.; Tsujii, Y.; Yamamoto, M.; Tabata, Y. *Biomacromolecules* **2012**, *13* (3), 927–936.
- (41) El Sayed, S.; Giménez, C.; Aznar, E.; Martínez-Máñez, R.; Sancenón, F.; Licchelli, M. *Org. Biomol. Chem.* **2015**, *13* (4), 1017–1021.
- (42) Agostini, A.; Mondragón, L.; Pascual, L.; Aznar, E.; Coll, C.; Martínez-Máñez, R.; Sancenón, F.; Soto, J.; Marcos, M. D.; Amorós, P.; Costero, A. M.; Parra, M.; Gil, S. *Langmuir* **2012**, *28* (41), 14766–14776.
- (43) Zhang, Y.; Gao, M.; Chen, C.; Wang, Z.; Zhao, Y. *RSC Adv.* **2015**, *5* (44), 34800–34802.
- (44) Cheng, S. H.; Liao, W. N.; Chen, L. M.; Lee, C. H. *J. Mater. Chem.* **2011**, *21*, 7130–7137.
- (45) Kuthati, Y.; Kankala, R. K.; Lin, S. X.; Weng, C. F.; Lee, C. H. *Mol. Pharm.* **2015**, *12* (7), 2289–2304.
- (46) Planas, O.; Bresolí-Obach, R.; Nos, J.; Gallavardin, T.; Ruiz-González, R.; Agut, M.; Nonell, S. *Molecules* **2015**, *20* (4), 6284–6298.
- (47) Peng, X.; Huang, D.; Odoom-Wubah, T.; Fu, D.; Huang, J.; Qin, Q. *J. Colloid Interface Sci.* **2014**, *430* (0), 272–282.
- (48) Luo, G.-F.; Chen, W. H.; Liu, Y.; Zhang, J.; Cheng, S. X.; Zhuo, R. X.; Zhang, X. Z. *J. Mater. Chem. B* **2013**, *1* (41), 5723–5732.

- (49) Ukmara, T.; Maverá, U.; Planinšek, O.; Kaučiča, V.; Gaberščeka, M.; Godec, A. *J. Control. Release* **2011**, *155*, 409–417.
- (50) Mondragón, L.; Mas, N.; Ferragud, V.; de la Torre, C.; Agostini, A.; Martínez-Mañez, R.; Sancenón, F.; Amorós, P.; Pérez-Payá, E.; Orzáez, M. *Chem. Eur. J.* **2014**, *20* (18), 5271–5281.
- (51) Agostini, A.; Mondragón, L.; Coll, C.; Aznar, E.; Marcos, M. D.; Martínez-Mañez, R.; Sancenón, F.; Soto, J.; Pérez-Payá, E.; Amorós, P. *Chem. Open* **2012**, *1* (1), 17–20.
- (52) Ritenberg, M.; Kolusheva, S.; Ganin, H.; Meijler, M. M. *Chempluschem* **2012**, *200* (2), 1–8.
- (53) Lu, J.; Liong, M.; Zink, J. I.; Tamanoi, F. *Small* **2007**, *3* (8), 1341–1346.
- (54) Lu, J.; Liong, M.; Li, Z.; Zink, J. I.; Tamanoi, F. *Small* **2010**, *6* (16), 1794–1805.
- (55) Xu, Z.; Liu, S.; Kang, Y.; Wang, M. *Nanoscale* **2015**, *7* (13), 5859–5868.



## Chapter 7. Experimental Part

---





---

## Chapter 7. Experimental Part

### 7.1. Instrumentation

**TEM Microscopy** was carried out using a JEOL microscope model JEM 2011 in *Universidad Autónoma de Barcelona* (UAB).

**Porous surface nitrogen physisorption** analysis was conducted on a Micromeritics Gemini V surface area and pore size analyzer. Pore size distribution curves were obtained from analysis of the absorption portion of the isotherms using the BJH (Barrett-Joyner-Halenda) method.

**Dynamic Light scattering (DLS)** size and  $\zeta$ -potential measurements were obtained by Malvern Zetasizer Nano Series ZEN 3600.

**Small angle powder X-ray diffraction (SXR)** were performed with a Philips X'Pert diffractometer equipped with Cu K $\alpha$  radiation (wavelength 1.5406 Å) at *Centro de asistencia a la investigación de rayos X en la Universidad complutense de Madrid*. XRD patterns were collected in the 2 $\theta$  range between 0.6° and 6.5 with a step size of 0.02° and counting time of 5 s per step.

**Infrared Spectra (FTIR)** was recorded in a Thermo Scientific Nicolet iS10 FTIR spectrometer with Smart iTr. Values are reported in wavenumbers (cm<sup>-1</sup>).

**Organic combustion Elemental Analysis (OEA)** were obtained in a EuroVector Instruments Euro EA elemental analyzer.

**UV-Vis Absorption and Fluorescence** spectra were recorded in a Thermo Scientific 300 UV-Vis spectrophotometer. Fluorescence excitation spectra were recorded in a Hitachi F2500 fluorescence spectrophotometer.

**Nuclear Magnetic Resonance spectra (<sup>1</sup>H-NMR and <sup>13</sup>C-NMR)** were recorded on a Varian 400-NMR spectrometer with frequency generators for ranges <sup>1</sup>H-<sup>19</sup>F and <sup>15</sup>N-<sup>31</sup>P, temperature control system, automatic tuning probe and sample introduction robot 50 positions (<sup>1</sup>H-NMR at 400 MHz and <sup>13</sup>C-NMR at 100.6 MHz). Chemical shifts are reported in part per million (ppm) on the  $\delta$  scale, and are referenced to tetramethylsilane (TMS) in <sup>1</sup>H-NMR spectra and to solvent signal of CDCl<sub>3</sub> (77.0 ppm), DMSO-d<sub>6</sub> (39.5 ppm), or methanol-d<sub>4</sub> (49.0 ppm) in <sup>13</sup>C-NMR spectra. Coupling constants are reported in Hertz (Hz). Spectral splitting patterns are designed as: s (singlet), d (doublet), t (triplet), q (quartet), dd (doublet of doublets), ddd (doublet of doublets), m (complex multiplet) and brs (broad signal).

**High Resolution Mass Spectrometry (HRMS)** was conducted on a VG AutoSpec (Micromass Instruments) Trisector EBE of high resolution spectrometer operating in FAB or EI mode and on Biotoff II (Bruker) apparatus in ESI-TOF mode at *Servicio de Espectroscopía de Masas (Universidad de Santiago de Compostela)*.

**Fluorescence Microscopy** was conducted on a Zeiss Axiovert inverted fluorescence microscope (Axiovert 200M; Carl Zeiss Inc.) equipped with zeiss ApoTome system and with a Nikon fluorescence microscope (Nikon Eclipse TS100).

## 7.2. Protocols

### TEM Microscopy

Samples were ultrasonically dispersed in EtOH for 1 h at a concentration of  $0.1 \text{ mg}\cdot\text{mL}^{-1}$  and deposited on an amorphous, porous carbon grid. Sometimes, initial concentration is too high and 1/10 or 1/100 dilutions need to be carried out. Sonication must be applied 15 min before using the microscope.

### Porous surface

After numerous tests processes it was determined that:

- CTAB removal must be completely achieved.
- MSNs must be washed several times with water and ethanol and final ethanol solutions must be removed under reduced pressure.
- Final solid samples must be sonicated until the formation of a free powdered solid.
- MSNs must be treated in a lyophilizer at 0.05 mBar,  $-0.759 \text{ }^{\circ}\text{C}$ , 24 h, prior to conduct adsorption experiments directly inside BET tubs.
- More or less 15 mg of MSNs are needed to obtain a correct measure.

### Dynamic Light scattering (DLS)

Samples were prepared at a concentration of  $0.1 \text{ mg}\cdot\text{mL}^{-1}$  in EtOH for size measurements and  $0.05 \text{ mg}\cdot\text{mL}^{-1}$  in  $\text{H}_2\text{O}$  for the zeta measurements. Better results are obtained if MSNs have just been synthesized and have not been dried. Sonication must be applied 1 h before using DLS. Sometimes, samples need to be filtered in a  $0.45 \text{ }\mu\text{m}$  nylon filter. Normally, in order to adjust concentration range, the initial concentration must be diluted 1/10 or 1/3. No results can be achieved by DLS measurements if CTAB is still present in MSNs matrix or if there is any fluorescent molecule attached to MSNs.

### SXRD

This technique needs perfectly well dried and dispersed powdered nanoparticles. By this means, the same procedure for nitrogen physisorption analysis has been applied.

### Infrared Spectra (FTIR) and Organic combustion Elemental Analysis (OEA)

Well dried MSNs need to be obtained. To do so, final solvent is evaporated under reduced pressure and samples have been placed in a vacuum desiccator at  $60 \text{ }^{\circ}\text{C}$  for 24 h.

### UV-Vis Absorption and Fluorescence

For titrations experiments, since MSNs precipitate very easily, the following procedure has been applied for the obtaining of a stable solution. First a well known quantity of MSNs is weighed, dispersed in the proper solvent and sonicated for 1 h. Then, an aliquot of the supernatant is taken. This aliquot is generally stable enough to work with. Absorbance needs to be less than 0.1 to perform acid and fluoride titrations.

### Uptake experiments

Uptake experiments are carried out in a 12 well plate (1 mL/well) where clean covers have been added. Normally, a concentration of 100000 cells per well is used with a cellular medium of DMEM (Dubecco's modified Eagle's medium) with LFBS (LFBS: bovine serum protein 10%).

The following procedure has been used:

- Cells are seeded for 24 h.
- MSNs are added and seeded for 24 h in incubator at 37 °C.
- Cells are washed with PBS and fixed to the covers.
- Fixation procedure is done by vectashield mounting medium with DAPI to stain the nucleus in blue color.
- MSNs are observed in fluorescence microscope.

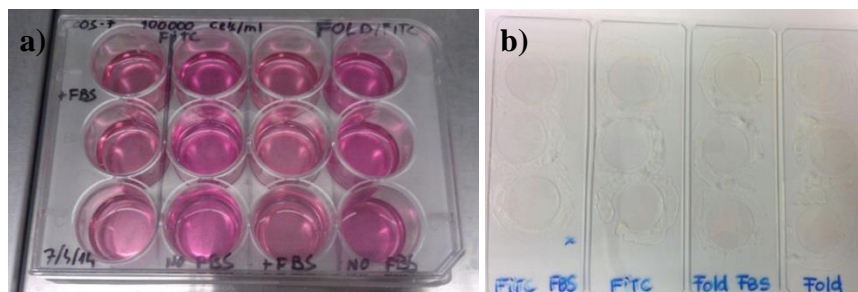


Figure 7.1. a) Twelve well plate of MSNs incubated in Hela cells and b) cells fixed in covers.

### MTT experiments

Viability assays are generally based on MTS or MTT approach. Since MTS absorbance is read at the same wavelength that FITC absorbs (490 nm), it is better to use MTT assay, which maximum absorbance at 550 nm does not interfere with FITC absorption or fluorescence. MTT assay is a colorimetric assay based on the reduction of MTT (3-(4,5-dimethylthiazol-2-yl)-2,5-diphenyltetrazolium bromide) to formazan crystals that present an intense violet color. This reaction only occurs when the oxidoreductase enzymes, present in cells, are active, which is the same as saying that cells are alive. Therefore, to measure the amount of formazan crystals that

have been formed is equivalent to know how many cells are still alive, which allows to estimate the viability of the cellular medium.

MTT experiments are carried out in a 96 well plate (0.1 mL/well) where a concentration of 10000 cells per well is prepared. Cellular medium, DMEM (Dubecco's modified Eagle's medium) with LFBS (LFBS: bovine serum protein 10 %) is used. The following procedure has been used:

- Cells are seeded for 24 h.
- MSNs are added and seeded for 24 h at 37 °C.
- Cells are washed with PBS and filtered MTT solution at final 0.5 mg/mL is added (25 mg MTT in 5 mL of PBS at 5 mg/mL).
- A 1/10 dilution is performed in culture medium (0.5 mg / mL).
- Cells are seeded for 3 h at 37 °C.
- MTT is removed and 0.1 mL of DMSO is added. Formazane crystals are suspended by up and down.
- Cells are seeded 10 min by stirring.
- Formazan absorbance is recorded in a microplate reader at 560 nm.
- Viability is calculated by the following equation.

$$\% \text{ cellular viability} = \frac{Abs_{sample} - Abs_{blank}}{Abs_{control} - Abs_{blank}} \cdot 100$$

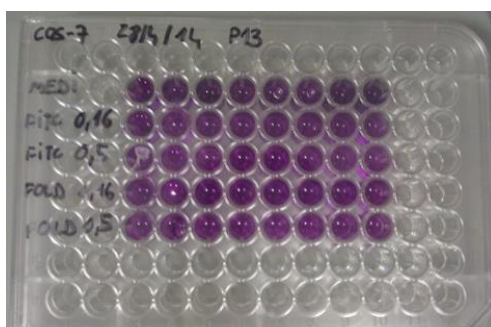


Figure 7.2. Ninety six well plate of MSNs incubated in Hela cells.

***In vitro* release experiments of MSN-(DOX), MSN-(DOX)(l-Fold)<sub>o</sub>, MSN-(DOX)(h-Fold)<sub>o</sub>, MSN-(MB), MSN-(CPT), MSN-(NH<sub>2</sub>)<sub>i</sub>(PEG-DOX)<sub>o</sub>MB and MSN-(NH<sub>2</sub>)<sub>i</sub>(PEG-DOX)<sub>o</sub>CPT)**

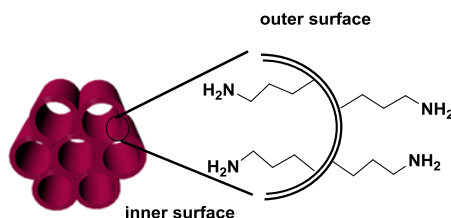
*In vitro* release experiments were performed at pH=7.4 and pH=4. For each release study, 1.5 mL of buffer solution was first added to 10 mg of MSNs and maintained at 37 °C, while being stirred at 100 rpm. Release medium was removed for analysis at specific time intervals by centrifuging at 12000 rpm for 13 min and placing solid residues into identical volumes of fresh buffer solution. The amount of released was analyzed with a UV–Vis absorption spectrophotometer at 490 nm for DOX, 650 nm for MB and 354 nm for CPT.

***In vitro* release experiments of MSN-(Ru), MSN-(Ata), MSN-(NH<sub>2</sub>)<sub>i</sub>(S-PEG)<sub>o</sub>Ru, MSN-(NH<sub>2</sub>)<sub>i</sub>(L-PEG)<sub>o</sub>Ru, MSN-(NH<sub>2</sub>)<sub>i</sub>(S-PEG)<sub>o</sub>Ata and MSN-(NH<sub>2</sub>)<sub>i</sub>(L-PEG)<sub>o</sub>Ata.**

*In vitro* release experiments were performed at pH=7.4 and 10 mM GSH solution. For each release study, 1.5 mL of buffer solution was first added to 10 mg of MSNs and maintained at 37 °C, while being stirred at 100 rpm. Release medium was removed for analysis at specific time intervals by centrifuging at 12000 rpm for 13 min and placing solid residues into identical volumes of fresh buffer solution. The amount of released Ru(bipy)<sub>3</sub><sup>2+</sup> and Ataluren were analyzed with a UV–Vis absorption spectrophotometer at 451 nm and 255 nm respectively.

### 7.3. Synthesis Chapter 2

#### 7.3.1. General procedure for the synthesis of MSNs<sup>1,2</sup>



To a solution of 0.1 g of CTAB and 50 mL of  $\text{NH}_3$  (A M), at B °C temperature, was added dropwise by an automatic injector, 0.8 mL of 0.2 M TEOS, diluted in EtOH. The solution was stirred at C rpm. Five hours later, it was added dropwise 0.8 mL of 12 % v/v APTES in EtOH and 0.8 mL of 1 M TEOS in EtOH. The solution was stirred at the same temperature for another 1 h. Then, the solution was aged, without stirring, at B °C temperature, for 24 h. Solid samples were collected via centrifuging at 12000 rpm for 20 min, washing and dispersing with deionized  $\text{H}_2\text{O}$  and EtOH, twice. Surfactant templates were removed by extraction in acidic ethanol, 0.17 g of HCl in 9 mL of EtOH at 65 °C for 24 h. Again, samples were collected via centrifuging at 12000 rpm for 20 min, washing and dispersing with deionized  $\text{H}_2\text{O}$  and EtOH, twice.

Samples	A / M	B / °C	C / rpm
MSN <sub>2</sub>	0.5	50	600
MSN <sub>6</sub>	0.5	70	600
MSN <sub>1</sub>	0.5	50	1100
MSN <sub>4</sub>	0.5	70	1100
MSN <sub>11</sub>	0.25	50	1100
MSN <sub>13</sub>	0.25	60	1100
MSN <sub>2</sub>	0.5	50	1100
MSN <sub>7</sub>	0.5	60	1100
MSN <sub>REF</sub>	0.2	60	1100
MSN <sub>A</sub>	0.25	60	1100
MSN <sub>B</sub>	0.2	60	1000
MSN <sub>C</sub>	0.2	65	1100
MSN <sub>100nm</sub>	0.5	60	1100
MSN <sub>50-70nm</sub>	0.2	60	1100

### **7.3.2. FITC functionalization for NH<sub>2</sub> determination**

#### **External NH<sub>2</sub> determination**

To a solution of 10 mg amino-surfactant nanoparticles MSN-(NH<sub>2</sub>)CTAB in 10 mL of toluene, were added 5 mg of FITC. Solution was left 24 h at room temperature. Samples were collected by centrifugation at 12000 rpm for 20 min, washing and dispersing with toluene and EtOH. To eliminate the surfactant, MSNs were treated with HCl (c) in 5 mL of EtOH. Solid samples were collected by centrifugation at 12000 rpm for 20 min, washing and dispersing with deionized water and EtOH, twice. Finally, supernatant is measured at 495 nm to assess the quantity of FITC that has been functionalized at the external surface of amino-MSNs, which can be attributed to the quantity of amino groups that are present at the outer surface.

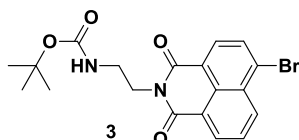
#### **Total NH<sub>2</sub> determination**

To a solution of 10 mg amino-nanoparticles MSN-(NH<sub>2</sub>), where tensioactive has been previously removed, in 10 mL of EtOH, were added 5 mg of FITC. Solution was left 24 h at room temperature. Samples were collected by centrifugation at 12000 rpm for 20 min, washing and dispersing several times with EtOH. Finally, supernatant is measured at 495 nm to assess the quantity of FITC that has been functionalized in both internal and external surface of amino-MSNs, which can be attributed to the total quantity of amino groups present in MSNs surface. Inner amino quantification is carried out by the subtracting difference between total and external quantification.



## 7.4. Synthesis Chapter 3

### 7.4.1. Synthesis of *tert*-butyl(2-(6-bromo-1,3-dioxo-1H-benzoisoquinolin-2(3H)-yl)ethyl)carbamate, EdaBOCNapht (3).

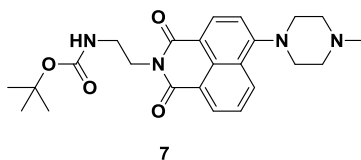


4-bromo-1,8-naphthalic anhydride (**1**) (15 g, 3.6 mmol) was dissolved in 50 mL of EtOH, and 1-(*tert*-butyloxycarbonyl)ethyldiamine, (EdaBoc, **2**), (0.8 g, 5 mmol) was added. The mixture was heated at reflux overnight. After cooling to room temperature, 50 ml of water were added and the precipitated solid was filtered after 1 h in the fridge. The solid was washed with H<sub>2</sub>O, (1:1) H<sub>2</sub>O/EtOH, EtOH and vacuum-dried to yield 1.5 g (97 %) of the product EdaBocNaftBr (**3**).

<sup>1</sup>H-NMR (400 MHz, CDCl<sub>3</sub>) δ 8.63 (d, *J* = 7.2 Hz, 1H), 8.52 (d, *J* = 8.4 Hz, 1H), 8.38 (d, *J* = 7.8 Hz, 1H), 8.01 (d, *J* = 7.8 Hz, 1H), 7.82 (t, *J* = 7.8 Hz, 1H), 4.99 (brs, 1H), 4.34 (brs, 2H), 3.54 (brs, 2H), 1.28 (s, 9H). <sup>13</sup>C-NMR (100 MHz, CDCl<sub>3</sub>) δ 163.9, 156.0, 133.4, 132.2, 131.4, 131.1, 130.6, 129.1, 128.0, 122.9, 122.0, 40.0, 39.5, 28.2 IR (KBr) ν<sub>max</sub>: 3386, 2976, 1703-1653, 1366-1346, 778 cm<sup>-1</sup> **Calculated OEA**: C: 54.43 %, H: 4.57 %, N: 6.68 % **Experimental OEA**: C: 54.63 % H: 4.42 % N: 6.56 %.

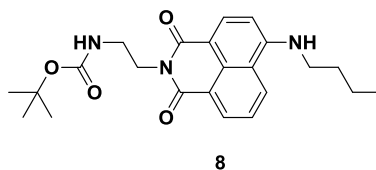
### 7.4.2. General procedure for synthesis of EdaBOC-naphthalimides (7-9)

Compound **3**, (0.7 mmol) was dissolved in 10 mL DMSO and *N*-methylpiperazine, butyl amine and methylpropyl amine (4.5 mmol) were added to the mixture. The suspension was heated to 80 °C for 24 h. Then, 100 mL of DCM were added. The solvent was washed three times with saturated lithium chloride and water and was finally removed under reduced pressure. To assure total elimination of DMSO, the solid was also washed with Cy/AcOEt and cleaned with LiCl and water. Compounds **7-9**, were obtained as a yellow solid.

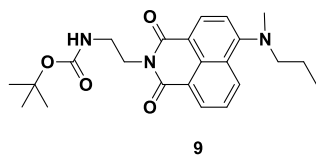


(**7**) <sup>1</sup>H-NMR (400 MHz, CDCl<sub>3</sub>) δ 8.59 (d, *J* = 7.2 Hz, 1H), 8.52 (d, *J* = 8.0 Hz, 1H), 8.41 (d, *J* = 8.4 Hz, 1H), 7.69 (t, *J* = 7.8 Hz, 1H), 7.22 (d, *J* = 8.1 Hz, 1H), 5.02 (brs, 1H), 4.35 (brs, 2H), 3.53 (brs, 2H), 3.31 (brs, 4H), 2.75 (brs, 4H), 2.44 (s, 3H), 1.31 (s, 9H). <sup>13</sup>C-NMR (100 MHz, CDCl<sub>3</sub>) δ 164.4, 163.8, 133.1, 131.6, 130.8, 130.0, 126.2, 125.7, 122.7, 116.2, 115.1, 55.0, 52.8, 46.0, 42.9, 38.9. IR (KBr) ν<sub>max</sub>: 3387,

2971-2796, 1697-1654, 1589, 1387-1366, 84-759  $\text{cm}^{-1}$  **HRMS** (EI):  $m/z$  **calculated** for  $\text{C}_{24}\text{H}_{30}\text{N}_4\text{O}_4$  438.2267; **found** 438.2260.



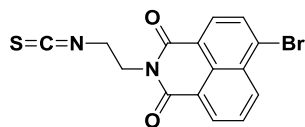
(8)  $^1\text{H-NMR}$  (400 MHz,  $\text{CDCl}_3$ )  $\delta$  8.59 (d,  $J = 7.2$  Hz, 1H), 8.47 (d,  $J = 8.4$  Hz, 1H), 8.08 (d,  $J = 8.3$  Hz, 1H), 7.62 (t,  $J = 7.9$  Hz, 1H), 6.73 (d,  $J = 8.5$  Hz, 1H), 5.11 (brs, 1H), 4.35 (brs, 2H), 3.52 (brs, 2H), 3.42 (brs, 2H), 1.87 – 1.75 (m, 2H), 1.56 – 1.49 (m, 2H), 1.33 (s, 9H), 1.03 (t,  $J = 7.3$  Hz, 3H).  $^{13}\text{C-NMR}$  (100 MHz,  $\text{CDCl}_3$ )  $\delta$  165.0, 164.5, 156.0, 149.6, 134.7, 131.3, 129.9, 125.9, 124.6, 122.9, 120.1, 109.8, 104.3, 43.4, 39.4, 31.0, 28.3, 20.3, 13.8. **IR** (KBr)  $\nu_{\text{max}}$ : 3365, 2958-2855, 1685-1639, 1579, 1394-1363, 773  $\text{cm}^{-1}$  **Calculated OEA**: C: 67.13 %, H: 7.10 %, N: 10.21 % **Experimental OEA**: C: 67.27 %, H: 7.23 %, N: 10.11 %.



(9)  $^1\text{H-NMR}$  (400 MHz,  $\text{CDCl}_3$ )  $\delta$  8.58 (d,  $J = 7.1$  Hz, 1H), 8.48 (d,  $J = 8.2$  Hz, 1H), 8.42 (d,  $J = 8.3$  Hz, 1H), 7.66 (t,  $J = 7.8$  Hz, 1H), 7.16 (d,  $J = 8.2$  Hz, 1H), 5.04 (brs, 1H), 4.36 (brs, 2H), 3.52 (brs, 2H), 3.30 (t,  $J = 7.4$  Hz, 2H), 3.06 (s, 3H), 1.85-1.70 (m, 2H), 1.32 (s, 9H), 0.94 (t,  $J = 7.4$  Hz, 3H).  $^{13}\text{C-NMR}$  (100 MHz,  $\text{CDCl}_3$ )  $\delta$  165.0, 164.4, 157.1, 156.0, 132.7, 131.2, 131.1, 130.3, 125.8, 124.9, 122.8, 114.8, 114.5, 58.8, 58.4, 41.5, 40.0, 39.5, 28.2, 28.2, 20.7, 18.4, 11.4. **IR** (KBr)  $\nu_{\text{max}}$ : 3365, 2966-2874, 1693-1647, 1389-1367, 781-760  $\text{cm}^{-1}$  **Calculated OEA**: C: 67.13 %, H: 7.10 %, N: 10.21 % **Experimental OEA**: C: 67.39 %, H: 7.25 %, N: 9.98 %.

### 7.4.3. General procedure for synthesis of isothiocyanate-naphthalimides (6;13-15)

Compounds **3**; **7-9** were dissolved (0.37 mmol) in 10 mL of DCM, then 3 mL of TFA were added. The mixture was stirred and monitored by TLC (AcOEt:MeOH = 20:1). After completion of the reaction, the solvent was washed twice with bicarbonate and removed under reduced pressure to give deprotected ethylenediamine-naphthalimide (**4**; **10-12**). The crude compound was dissolved in 10 mL of DCM. Then, 0.9 mmol of 1,1'-thiocarbonyldi-2(1*H*)-pyridone (**5**) was added. The mixture was stirred and monitored by TLC (DCM:MeOH = 90:10). After completion of the reaction, the solvent was washed, twice with saturated bicarbonate, and removed under reduced pressure. The crude product was purified by column chromatography on silica gel (DCM) to give compound **6;13-15**.

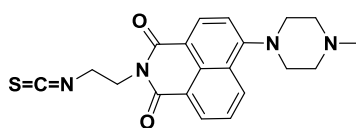


6

(6)  $^1\text{H-NMR}$  (400 MHz,  $\text{CDCl}_3$ )  $\delta$  8.66 (d,  $J = 7.3$  Hz, 1H), 8.58 (d,  $J = 8.5$  Hz, 1H), 8.42 (d,  $J = 7.9$  Hz, 1H), 8.05 (d,  $J = 7.9$  Hz, 1H), 7.85 (t,  $J = 7.9$  Hz, 1H), 4.51 (t,  $J = 6.3$  Hz, 2H), 3.92 (t,  $J = 6.3$  Hz, 2H).

$^{13}\text{C-NMR}$  (100 MHz,  $\text{CDCl}_3$ )  $\delta$  163.5, 163.4, 133.8, 132.5, 131.6, 131.2, 130.9, 130.7, 129.0, 128.2, 122.5, 121.6, 42.8, 39.1. **IR** (KBr)  $\nu_{\text{max}}$ : 2924-2853, 2207-2108, 1702-1659, 1361-1345, 778  $\text{cm}^{-1}$

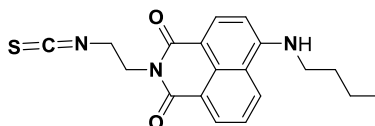
**Calculated OEA:** C: 49.88 % H: 2.51 %, N: 7.76 %, S: 8.88 % **Experimental OEA:** C: 49.86 %, H: 2.58 %, N: 7.55 %, S: 8.49 % .



13

(13)  $^1\text{H-NMR}$  (400 MHz,  $\text{CDCl}_3$ )  $\delta$  8.60 (d,  $J = 7.0$  Hz, 1H), 8.54 (d,  $J = 8.1$  Hz, 1H), 8.43 (d,  $J = 8.1$  Hz, 1H), 7.71 (t,  $J = 7.8$  Hz, 1H), 7.23 (d,  $J = 8.1$  Hz, 1H), 4.51 (t,  $J = 6.4$  Hz, 2H), 3.90 (t,  $J = 6.4$  Hz, 2H), 3.33 (brs, 4H), 2.76 (brs, 4H), 2.45 (s, 3H).  $^{13}\text{C-NMR}$  (100 MHz,  $\text{CDCl}_3$ )  $\delta$  164.4, 163.8, 133.1, 131.6,

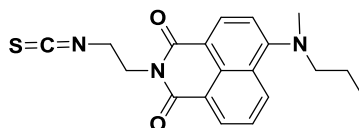
130.8, 130.0, 126.2, 125.7, 122.7, 116.2, 115.1, 55.0, 52.8, 46.0, 42.9, 38.9. **IR** (KBr)  $\nu_{\text{max}}$ : 2926-2795, 2199-2109, 1696-1656, 1588, 1385-1360, 784-758  $\text{cm}^{-1}$ . **HRMS** (EI):  $m/z$  **calculated** for  $\text{C}_{20}\text{H}_{20}\text{N}_4\text{O}_2$   $S_1$  380.1370; **found** 380.1307.



14

(14)  $^1\text{H-NMR}$  (400 MHz,  $\text{CDCl}_3$ )  $\delta$  8.59 (d,  $J = 7.3$  Hz, 1H), 8.47 (d,  $J = 8.4$  Hz, 1H), 8.10 (d,  $J = 8.3$  Hz, 1H), 7.62 (t,  $J = 7.9$  Hz, 1H), 6.73 (d,  $J = 8.5$  Hz, 1H), 4.50 (t,  $J = 6.5$  Hz, 2H), 3.89 (t,  $J = 6.5$  Hz, 2H), 3.42 (q,  $J = 7.0$  Hz, 2H), 1.81 (p,  $J = 7.3$  Hz, 2H), 1.59-1.50 (m, 2H), 1.03 (t,  $J = 7.3$  Hz, 3H).  $^{13}\text{C-NMR}$

(100 MHz,  $\text{CDCl}_3$ )  $\delta$  164.5, 163.7, 149.8, 134.9, 131.0, 130.0, 126.2, 124.7, 122.6, 120.1, 109.4, 104.4, 43.4, 42.9, 38.8, 31.0, 20.3, 13.8. **IR** (KBr)  $\nu_{\text{max}}$ : 3413, 2958-2868, 2197-2134, 1682-1639, 1588-1572, 1382-1358, 768-756  $\text{cm}^{-1}$ . **HRMS** (EI):  $m/z$  **calculated** for  $\text{C}_{19}\text{H}_{19}\text{N}_3\text{O}_2\text{S}_1$  353.1198; **found** 353.1194.



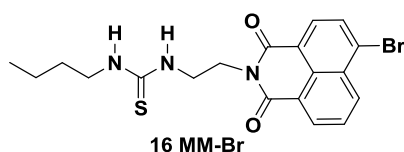
15

(15)  $^1\text{H-NMR}$  (400 MHz,  $\text{CDCl}_3$ )  $\delta$  8.58 (d,  $J = 7.2$  Hz, 1H), 8.48 (d,  $J = 8.2$  Hz, 1H), 8.43 (d,  $J = 8.3$  Hz, 1H), 7.66 (t,  $J = 7.9$  Hz, 1H), 7.15 (d,  $J = 8.3$  Hz, 1H), 4.50 (t,  $J = 6.4$  Hz, 2H), 3.89 (t,  $J = 6.4$  Hz, 2H), 3.31 (t,  $J = 7.4$  Hz, 2H), 3.07 (s, 3H), 1.83-1.73 (m, 2H), 0.94 (t,  $J = 7.4$  Hz, 3H).  $^{13}\text{C-NMR}$  (100 MHz,

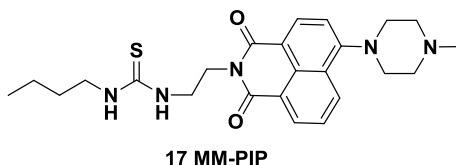
CDCl<sub>3</sub>)  $\delta$  164.5, 163.8, 157.4, 133.0, 131.5, 131.5, 130.5, 125.9, 125.0, 122.6, 114.5, 114.3, 58.8, 42.9, 41.5, 38.9, 20.7, 11.4 **IR** (KBr)  $\nu_{\max}$ : 2960-2852, 2202-2105, 1695-1652, 1391-1364, 781-758 cm<sup>-1</sup>  
**HRMS** (EI):  $m/z$  **calculated** for C<sub>19</sub>H<sub>19</sub>N<sub>3</sub>O<sub>2</sub>S<sub>1</sub> 353.1198; **found** 353.1196.

#### 7.4.4. General procedure for model naphthalimides (16-19)

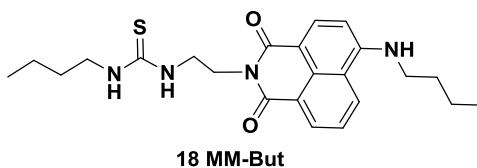
Compounds **6**; **13-15** (0.287 mmol) were dissolved in 15 mL of EtOH, then 0.1 mL (25 mmol) of *n*-butylamine were added. The mixture was stirred and monitored by TLC (DCM:MeOH; 9:1). After completion of the reaction, the solvent was removed under reduced pressure, reconstituted with DCM, and washed several times with ethanol. Product **16-19** (MM-Br, MM-PIP, MM-But and MM-MetProp) were obtained as a yellowish solid (96 %).



(**16**) <sup>1</sup>H-NMR (400 MHz, CDCl<sub>3</sub>)  $\delta$  8.68 (dd,  $J$  = 7.3, 1.0 Hz, 1H), 8.63 (dd,  $J$  = 8.5, 1.0 Hz, 1H), 8.44 (d,  $J$  = 7.9 Hz, 1H), 8.08 (d,  $J$  = 7.9 Hz, 1H), 7.88 (dd,  $J$  = 8.5, 7.4 Hz, 1H), 6.53 (brs, 1H), 4.44 (brs, 2H), 3.81 (brs, 2H), 3.39 (brs, 2H), 1.69-1.56 (m, 2H), 1.42 (h,  $J$  = 7.3 Hz, 2H), 0.95 (t,  $J$  = 7.3 Hz, 3H). <sup>13</sup>C-NMR (100 MHz, CDCl<sub>3</sub>)  $\delta$  181.7, 164.4, 134.0, 132.5, 131.7, 131.3, 131.1, 130.8, 129.1, 128.2, 122.5, 121.6, 52.1, 39.0, 38.9, 30.8, 20.1, 13.7. **IR** (KBr)  $\nu_{\max}$ : 3382-3253, 2954-2869, 1698-1651, 1568, 1231, 782 cm<sup>-1</sup> **AEO predicted**: C: 52.54 %, H: 4.64 %, N: 9.67 %, S: 7.38 % **AEO obtained**: C: 52.41 %, H: 4.61 %, N: 9.50 %, S: 7.65 %.

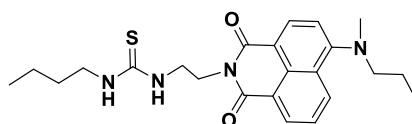


(**17**) <sup>1</sup>H-NMR (400 MHz, DMSO-*d*<sub>6</sub>)  $\delta$  8.47 (t,  $J$  = 7.8 Hz, 1H), 8.40 (d,  $J$  = 8.1 Hz, 1H), 7.82 (t,  $J$  = 7.8 Hz, 1H), 7.36 (d,  $J$  = 8.1 Hz, 1H), 7.27 (brs, 1H), 4.23 (t,  $J$  = 5.9 Hz, 2H), 3.82- 3.69 (m, 2H), 3.27 (brs, 4H), 2.67 (brs, 4H), 2.33 (s, 3H), 1.45-1.35 (m, 2H), 1.29- 1.21 (m, 2H), 0.84 (t,  $J$  = 7.3 Hz, 3H). <sup>13</sup>C-NMR (100 MHz, CDCl<sub>3</sub>)  $\delta$  181.5, 165.2, 164.7, 156.6, 133.1, 131.6, 131.0, 130.0, 126.1, 125.7, 122.6, 115.0, 55.0, 52.9, 46.0, 30.8, 29.7, 20.1, 13.7. **IR** (KBr)  $\nu_{\max}$ : 3341, 2929-2795, 1692-1651, 1588, 1551, 1454-1424, 1388-1361, 1142, 785-759 cm<sup>-1</sup> **HRMS** (EI):  $m/z$  **calculated** for C<sub>24</sub>H<sub>31</sub>N<sub>5</sub>O<sub>2</sub>S<sub>1</sub> 453.2198; **found** 453.2191.



(**18**) <sup>1</sup>H-NMR (400 MHz, CDCl<sub>3</sub>)  $\delta$  8.60 (d,  $J$  = 7.3 Hz, 1H), 8.47 (d,  $J$  = 8.4 Hz, 1H), 8.11 (d,  $J$  = 8.3 Hz, 1H), 7.65 (t,  $J$  = 7.9 Hz, 1H), 6.74 (d,  $J$  = 8.5 Hz, 1H), 5.33 (brs, 2H), 4.42 (brs, 2H), 3.61 – 3.38 (m, 4H),

1.82 (dt,  $J = 14.8, 7.3$  Hz, 2H), 1.64 (brs, 2H), 1.61- 1.55 (m, 2H), 1.48- 1.38 (m, 2H), 1.04 (t,  $J = 7.3$  Hz, 3H), 0.95 (t,  $J = 7.3$  Hz, 3H).  $^{13}\text{C-NMR}$  (100 MHz,  $\text{CDCl}_3$ )  $\delta$  181.5, 165.3, 164.7, 157.6, 133.1, 131.7, 131.5, 130.4, 125.6, 124.9, 122.4, 114.3, 113.9, 58.8, 41.4, 20.7, 20.1, 13.7, 11.4. **IR** (KBr)  $\nu_{\text{max}}$ : 3379-3286, 2953-2868, 1673-1641, 1581, 1547, 1358, 770-757  $\text{cm}^{-1}$  **HRMS** (EI):  $m/z$  **calculated** for  $\text{C}_{23}\text{H}_{30}\text{N}_4\text{O}_2\text{S}_1$  426.2089; **found** 426.2089.



**19 MM-MetProp**

(**19**)  $^1\text{H-NMR}$  (400 MHz,  $d_6$ -dms $\text{o}$ )  $\delta$  8.48 (t,  $J = 7.4$  Hz, 1H), 8.36 (d,  $J = 8.2$  Hz, 1H), 7.77 (t,  $J = 7.9$  Hz, 1H), 7.32 – 7.25 (m, 2H), 4.23 (t,  $J = 6.0$  Hz, 2H), 3.76 (brs, 2H), 3.37 – 3.30 (m, 2H), 3.30 – 3.23 (m, 2H), 3.06 (s, 3H), 1.80 – 1.67 (m, 2H), 1.46 – 1.33 (m, 2H), 1.32 – 1.19 (m, 2H), 0.90 (t,  $J = 7.4$  Hz, 2H), 0.85 (t,  $J = 7.3$  Hz, 2H).  $^{13}\text{C-NMR}$  (100 MHz,  $\text{CDCl}_3$ )  $\delta$  181.5, 165.3, 164.7, 157.6, 133.1, 131.7, 131.5, 130.4, 125.6, 124.9, 122.4, 114.3, 113.9, 58.8, 41.4, 20.7, 20.1, 13.7, 11.4. **IR** (KBr)  $\nu_{\text{max}}$ : 3334, 2958-2871, 1690-1647, 1585, 1387-1361, 1202, 781-759  $\text{cm}^{-1}$  **HRMS** (EI):  $m/z$  **calculated** for  $\text{C}_{23}\text{H}_{30}\text{N}_4\text{O}_2\text{S}_1$  426.2089; **found** 426.2089.

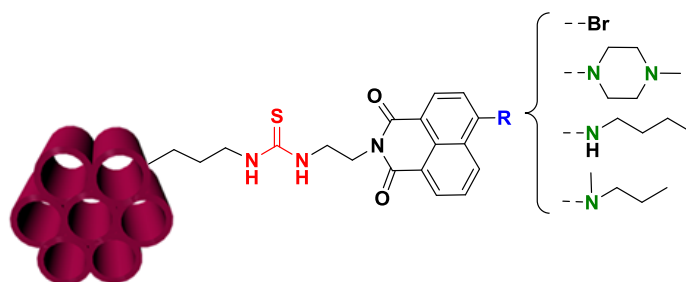
#### 7.4.5. Absorption and fluorescent properties of MSN and MM naphthalimides

Systems	$\lambda_{\text{abs}}/\text{nm}$	$\lambda_{\text{em}}/\text{nm}$	$\epsilon/\text{M}^{-1}\cdot\text{cm}^{-1}$	$\tau_f/\text{ns}$	$\Phi_f$
MSN-(NaphBr)	340	424	15000	2.38 ns $\chi^2 = 1.058$	0.004*
MSN-(NaphPIP)	400	529	11250	6.563 ns $\chi^2 = 1.140$	0.06
MSN-(NaphBut)	442	529	15108	8.095 ns $\chi^2 = 1.099$	0.196
MSN-(NaphMetProp)	428	529	10883	7.413 ns $\chi^2 = 1.046$	0.023
MM-Br	340	380	15000	--	0.001*
MM-PIP	400	525	11250	0.78 ns $\chi^2 = 1.269$	0.01
MM-But	435	529	15108	11.70 ns $\chi^2 = 1.085$	0.46
MM-MetProp	422	537	10883	6.86 ns $\chi^2 = 1.137$	0.055

Naphthalimide as standard ( $\Phi_f = 0.45$  in ACN)

\* Quinine sulphate as standard ( $\Phi_f = 0.546$  in 0.05 M  $\text{H}_2\text{SO}_4$ )

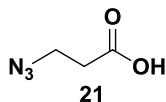
#### 7.4.6. MSNs functionalization with naphthalimides



Typically, 0.20 mmol of isothiocyanate naphthalimides **6**; **13-15** were added in 5 mL of MSN-(NH<sub>2</sub>) (1.6 mg/mL). The solution was covered from light, and stirred at 60 °C for 48 h. Solid samples were collected via centrifuging at 12000 rpm for 20 min, washing and dispersing with EtOH twice. Finally, solvent was removed under reduced pressure. Functionalization was checked by TLC (CH<sub>2</sub>Cl<sub>2</sub>:THF; 9:1) and UV-Vis giving the resulting MSN-(NaphBr), MSN-(NaphPIP), MSN-(NaphBut) and MSN-(NaphMetProp).

## 7.5. Synthesis Chapter 4

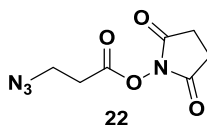
### 7.5.1. Synthesis of 3-azidopropionic acid (**21**)<sup>3</sup>



To a stirred solution of 3-bromopropionic acid (**20**) (2.7 g, 18 mmol) in CH<sub>3</sub>CN (8 mL) was added sodium azide (3.48 mg, 53 mmol), and the mixture was heated at reflux for 3 h. The brown crude reaction mixture was diluted in CH<sub>2</sub>Cl<sub>2</sub>, and the solution was washed with 0.1 N HCl. The organic layer was dried over anhydrous MgSO<sub>4</sub>, filtered and concentrated under reduced pressure to furnish 3-azidopropionic acid (**21**) (6 %). Spectroscopic data were in good agreement with reported data.

<sup>1</sup>H-NMR (400 MHz, CDCl<sub>3</sub>) δ 11.4 (br s, 1H), δ 3.60 (t, *J* = 6.5 Hz, 2H), 2.65 (t, *J* = 6.4 Hz, 2H). <sup>13</sup>C-NMR (100 MHz, CDCl<sub>3</sub>) δ 33.6, 46.3, 176.9.

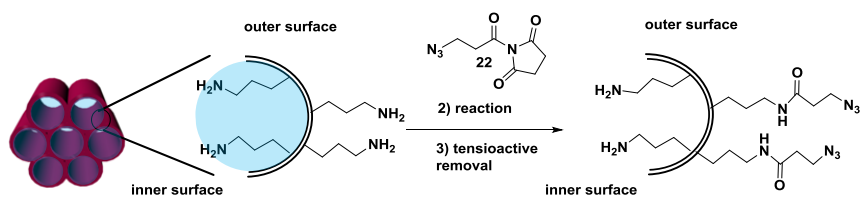
### 7.5.2. Synthesis of 3-azidopropionic acid succinimidyl ester (**22**)<sup>3</sup>



To a stirred solution of 3-azidopropionic acid (**21**) (0.17 g, 1.4 mmol) and *N*-hydroxysuccinimide (0.21 g, 2.2 mmol) in anhydrous CH<sub>2</sub>Cl<sub>2</sub> (2 mL) was added EDC (0.31 g, 1.9 mmol), and the mixture was allowed to stir at room temperature overnight. The crude reaction mixture was poured into a saturated aqueous NaCl solution and extracted with CH<sub>2</sub>Cl<sub>2</sub>. The organic layer was dried over anhydrous MgSO<sub>4</sub>, filtered and concentrated under reduced pressure to furnish the succinimidyl ester **22**. Spectroscopic data were in good agreement with reported data.

<sup>1</sup>H-NMR (400 MHz, CDCl<sub>3</sub>) δ 3.68 (t, *J* = 6.5 Hz, 2H), 2.89 (t, *J* = 6.7 Hz, 2H), 2.87- 2.81 (br s, 4H). <sup>13</sup>C-NMR (100 MHz, CDCl<sub>3</sub>) δ 169.6, 169.0, 46.4, 31.4, 25.9.

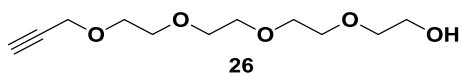
### 7.5.3. Synthesis of bifunctionalized amino-azide nanoparticles (MSN-(NH<sub>2</sub>)<sub>i</sub>(N<sub>3</sub>)<sub>o</sub>)



0.028 g of amine nanoparticles with CTAB (MSN-(NH<sub>2</sub>)CTAB) were suspended into 10 mL of H<sub>2</sub>O. Then, a solution of 0.035 g (0.164 mmol, 10 eq.) of 3-azidopropionic acid succinimidyl ester (**22**) was dissolved in 50 mL of water and afterwards was added to MSNs solution. The mixture was stirred in the dark for 24 h at room temperature. Solid samples were collected via centrifuging at 12000 rpm for 20 min, washing and dispersing with deionized water. To eliminate the surfactant, MSNs were treated with HCl (c) in 5 mL of EtOH. Solid samples were collected via centrifuging at 12000 rpm for 20 min, washing and dispersing with deionized water and EtOH, twice.

### 7.5.4. Synthesis of alkyne-FITC-PEG<sup>4</sup>

#### 7.5.4.1. Synthesis of 3,6,9,12-tetraoxapentadec-14-yn-1-ol (**26**)

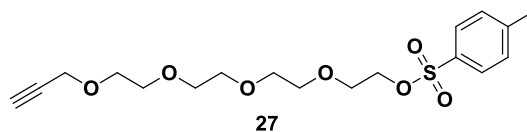


To 20 mL of tetraethylene glycol (**25**) (0.11 mol), 70 mL of THF anhydrous were added. Then, 0.90 g (0.022 mol) of a 60 % suspension in oil at 0 °C were added to the solution. The resulting mixture was stirred at 0 °C for 30 min and then held at 80 °C for 2 h under nitrogen atmosphere. When the solution turned dark brown, 3 mL (0.034 mol) of propargyl bromide was added to the solution, and the resulting mixture was stirred at 80 °C for 12 h. The resulting solution was cooled to room temperature and extracted with DCM (500 mL). The organic layer was washed with brine, dried over anhydrous MgSO<sub>4</sub>, concentrated *in vacuo* to give product **26** in 80 % yield. Spectroscopic data were in good agreement with reported data.

<sup>1</sup>H-NMR (400 MHz, CDCl<sub>3</sub>) δ 4.21 (d, *J* = 2.3 Hz, 2H), 3.74-3.65 (m, 14H), 3.62 (d, *J* = 4.8 Hz, 2H), 2.86 (s, 1H), 2.48 (t, *J* = 2.2 Hz, 1H). <sup>13</sup>C-NMR (100 MHz, CDCl<sub>3</sub>) δ 79.6, 74.5, 72.5, 70.5, 70.3, 69.1, 61.7, 58.3. IR (KBr) ν<sub>max</sub>: 3457, 3249, 2870, 2112, 1458, 1350, 1292, 1249, 1103, 1032, 942, 885, 842, 682 cm<sup>-1</sup>.



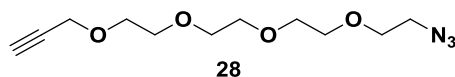
#### 7.5.4.2. Synthesis of 3,6,9,12-Tetraoxapentadec-14-yn-1-yl-4-methylbenzenesulfonate (27)



Product **26**, 3,6,9,12-tetraoxapentadec-14-yn-1-ol (3.37 g, 0.014 mol) was dissolved in 20 mL of DCM anh. Tosyl chloride (4 g, 0.020 mol) was added, and the mixture was cooled to 0 °C on an ice bath. KOH (3.2 g, 0.057 mol) was added slowly, and the mixture was stirred vigorously for 2 h. The mixture was then poured on ice water and extracted with DCM (3 x 50 mL). The combined organic phase was washed with brine, dried over MgSO<sub>4</sub>, and evaporated under reduced pressure to give **27** as a yellowish oil in 60 % yield. Spectroscopic data were in good agreement with reported data.

<sup>1</sup>H-NMR (400 MHz, CDCl<sub>3</sub>) δ 7.79 (d, 2H, *J* = 8.2 Hz), 7.35 (d, 2H, *J* = 8.2 Hz), 4.20 (d, *J* = 3.2 Hz, 2H), 4.15 (t, *J* = 3.9 Hz, 2H), 3.71-3.660 (m, 6H), 3.63 (m, 4H), 3.58-3.56 (m, 4H), 2.45 (s, 3H), 2.43 (t, *J* = 2.3 Hz, 1H). <sup>13</sup>C-NMR (100 MHz, CDCl<sub>3</sub>) δ 144.7, 133.0, 129.8, 127.9, 79.6, 74.5, 70.7, 70.5, 70.4, 69.2, 69.1, 68.6, 58.3, 21.6. IR (KBr)  $\nu_{\text{max}}$ : 3279, 2922, 2856, 2113, 1597, 1458, 1356, 1292, 1250, 1177, 1097, 1017, 922, 817, 776, 633 cm<sup>-1</sup>.

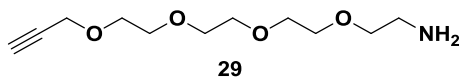
#### 7.5.4.3. Synthesis of 1-azido-3,6,9,12-tetraoxapentadec-14-yne (28)



Product **27**, 3,6,9,12-tetraoxapentadec-14-yn-1yl-(4-methylbenzenesulfonate) (5.36 g, 0.013 mol) was dissolved in DMF (40 mL). Then NaN<sub>3</sub> (1.18 g, 0.018 mol) and tetra butyl ammonium iodide (TBAI) (0.48 g, 0.0015 mol) was added, and the mixture was stirred vigorously at 45 °C overnight. The resulting mixture was diluted with AcOEt and washed with saturated NaHCO<sub>3</sub> (aq). The water phase was extracted twice with AcOEt, and the combined organic phase was washed with water and brine, and dried over MgSO<sub>4</sub>. Evaporation under reduced pressure yielded **28** of crude product in a 60 % yield. Spectroscopic data were in good agreement with reported data.

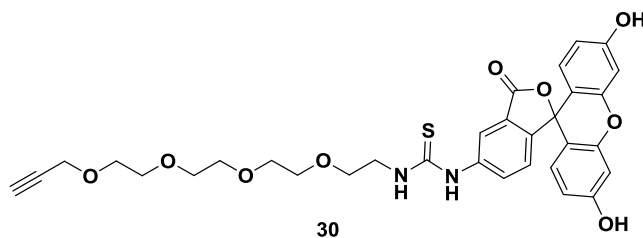
<sup>1</sup>H-NMR (400 MHz, CDCl<sub>3</sub>) δ 4.14 (d, 2H, *J*=2.4 Hz), 3.64-3.55 (m, 14H), 3.32 (t, 2H, *J*=5.1 Hz), 2.40 (t, 1H, *J*=2.4Hz). <sup>13</sup>C-NMR (100 MHz, CDCl<sub>3</sub>) δ 79.6, 74.5, 70.6, 70.6, 70.3, 70.0, 69.0, 58.3, 50.6. IR (KBr)  $\nu_{\text{max}}$ : 2954, 2924, 2853, 2100, 1462, 1377, 1110, 722 cm<sup>-1</sup>.

## 7.5.4.4. Synthesis of 3,6,9,12-tetraoxapentadec-14-yn-1-amine (29)

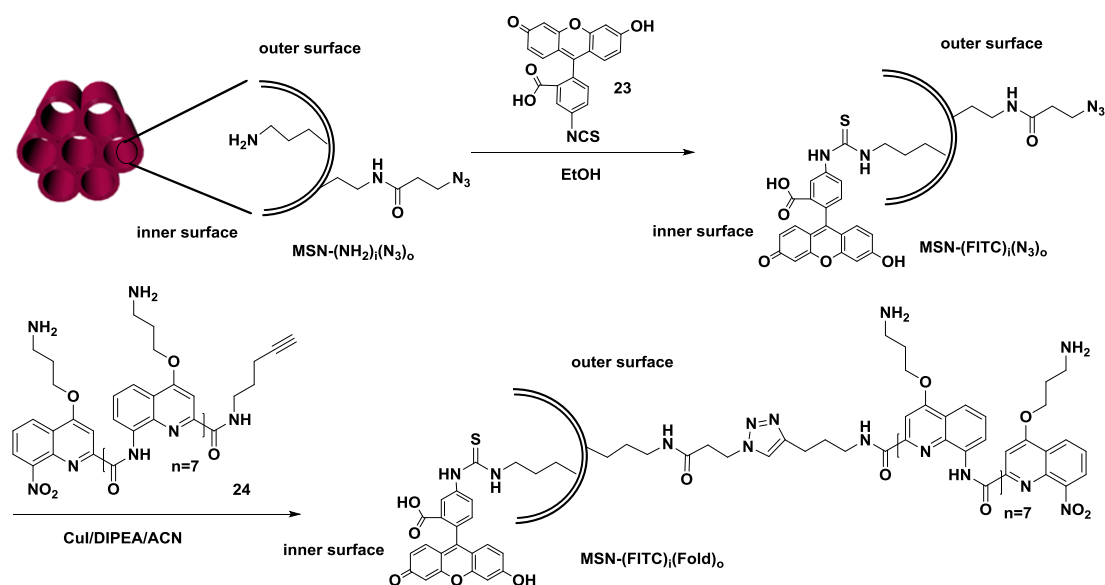


Product **28**, 1-azido-3,6,9,12-tetraoxapentadec-14-yne (0.920 g, 3.57 mmol) was dissolved in dry THF.  $\text{PPh}_3$  (1.176 g, 4.48 mmol) was added, and the mixture was stirred at room temperature for 2.5 h. The temperature was then raised to 30 °C, and the mixture was stirred at 30 °C for 25 h, after which the solvent was dissolved in AcOEt and extracted four times with 1M HCl (aq). The combined water phase was then basified with ground NaOH to basic pH and extracted four times with AcOEt. The combined organic phase was dried over  $\text{MgSO}_4$  and evaporated under reduced pressure to give the crude product, which was precipitated in diethyl ether to give product **29** with 70 % yield. Spectroscopic data were in good agreement with reported data.

$^1\text{H-NMR}$  (400 MHz,  $\text{CDCl}_3$ )  $\delta$  4.20 (s, 2H), 3.73 – 3.58 (m, 12H), 3.65 (t, 2H,  $J=5.4$  Hz.), 2.88 (t, 2H), 2.44 (t, 1H,  $J=2.4$ Hz), 1.69 (s, 2H).  $^{13}\text{C-NMR}$  (100 MHz,  $\text{CDCl}_3$ )  $\delta$  79.5, 74.6, 72.2, 70.4, 70.2, 70.1, 69.0, 58.2, 41.2. **IR** (KBr)  $\nu_{\text{max}}$ : 3247, 2868, 2111, 1665, 1576, 1457, 1350, 1292, 1248, 1103, 1034, 920, 843, 731, 646  $\text{cm}^{-1}$ .

7.5.4.5. Synthesis of 1-(3',6'-dihydroxy-3-oxo-3H-spiro[isobenzofuran-1,9'-xanthen]-5-yl)-3-(3,6,9,12-tetraoxapentadec-14-yn-1-yl)thiourea (30)<sup>5</sup>

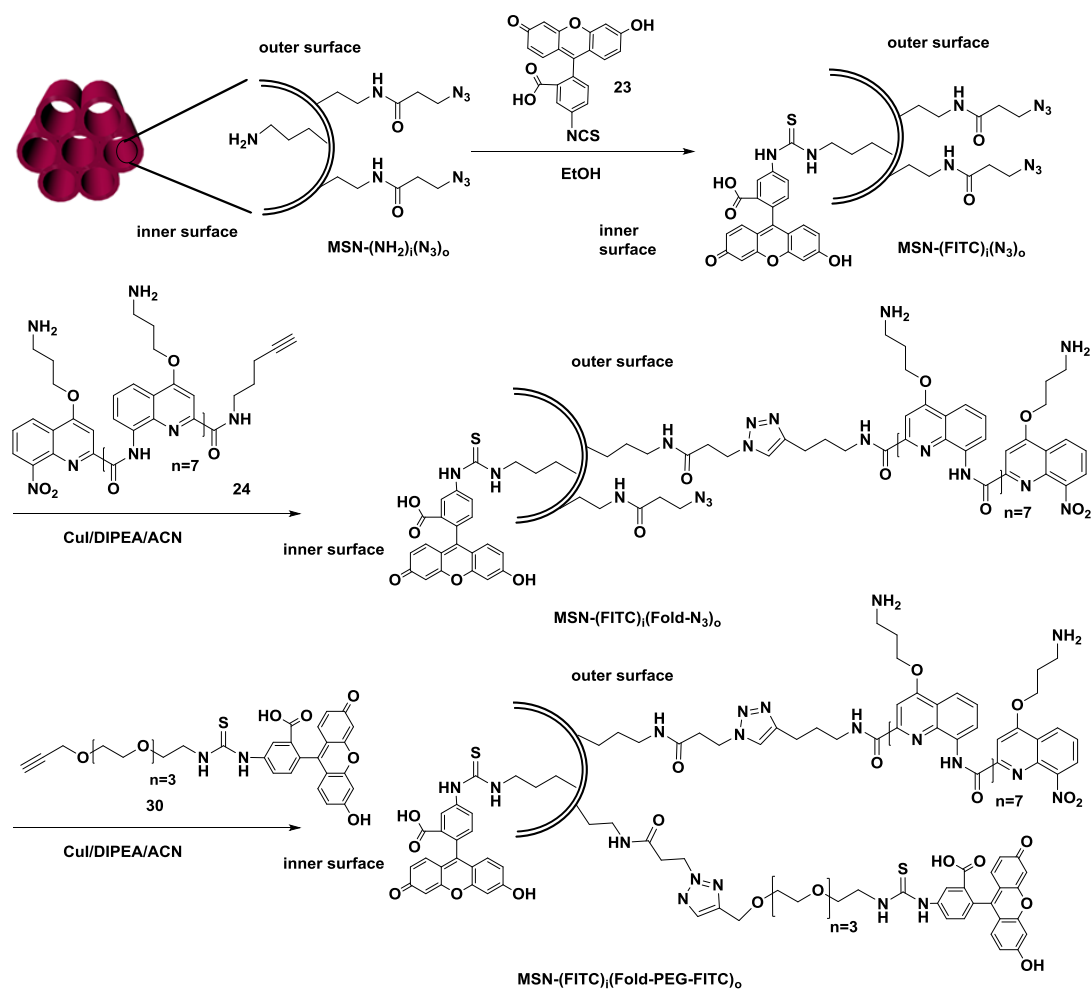
Product **39** (0.021 g, 0.9 mmol) was dissolved in 2 mL of ethanol. Then FITC (0.060 g, 0.7 mmol, 0.8 eq.) was added dropwise in 4 mL of ethanol and the mixture was stirred at room temperature for 24 h. The mixture was evaporated under reduced pressure and was directly added to reference  $\text{MSN}-(\text{FITC})_i(\text{N}_3)_o$  and  $\text{MSN}-(\text{FITC})_i(\text{Fold-N}_3)_o$ .

7.5.5. Synthesis of MSN-(FITC)<sub>i</sub>(Fold)<sub>o</sub>

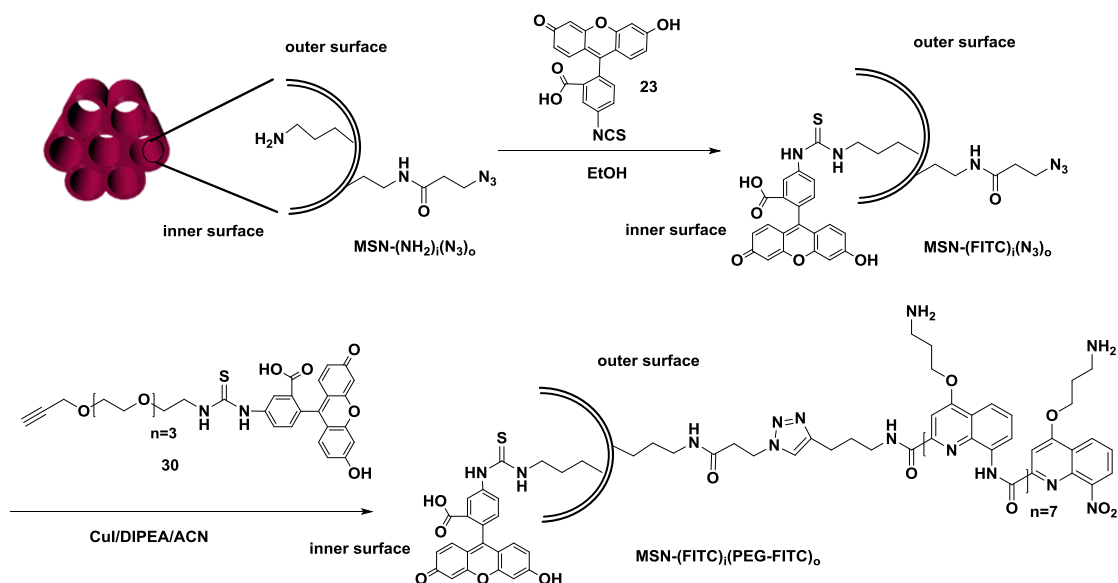
To 96 mg of MSN-(NH<sub>2</sub>)(CTAB), 7.6 mg of 3-azidopropionic acid succinimidyl ester (**22**) in 60 mL of water were added. The mixture was stirred in the dark for 24 h at room temperature. Solid samples were collected via centrifuging at 12000 rpm for 20 min, washing and dispersing with deionized water. To eliminate the surfactant, MSNs were treated with HCl (c) in 50 mL of EtOH. Solid samples were collected via centrifuging at 12000 rpm for 20 min, washing and dispersing with deionized water and EtOH, twice.

0.036 g of MSN-(NH<sub>2</sub>)<sub>i</sub>(N<sub>3</sub>)<sub>o</sub>, without surfactant at the porous, were suspended in 20 mL of EtOH and sonicated during 1 h. Then, 0.016 g (0.04 mmol, 4 eq.) of FITC were added. The solution was left at room temperature for 48 h. Again, samples were collected via centrifuging at 12000 rpm for 20 min, washing and dispersing with deionized H<sub>2</sub>O and EtOH until supernatant presented no color.

After FITC conjugation, 15 mg (0.005 mmol) of quinoline foldamer were added to 15 mg of MSN-(FITC)<sub>i</sub>(N<sub>3</sub>)<sub>o</sub> solution in a H<sub>2</sub>O/ACN mixture (30 mL). MSN/Foldamer proportion is (1:1) mg Fold/mg MSN. Final MSNs were washed with EDTA 0.1 M solution, and *N,N*-diethyldithiocarbamate. CuEDTA and CuDTTC complex removal were monitored at 730 nm and 430 nm respectively. Moreover, MSNs are dialyzed in water during 24 h in order to remove any Cu or EDTA residue.

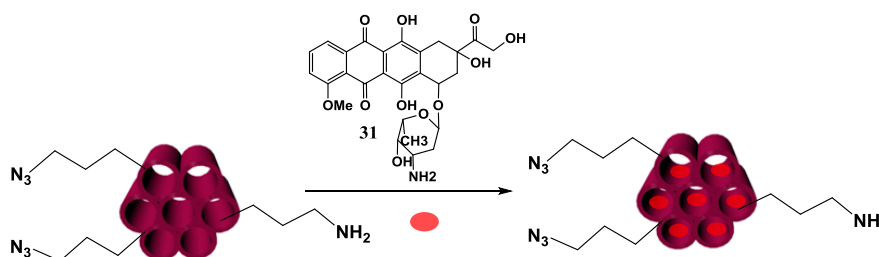
7.5.6. Synthesis of MSN-(FITC)<sub>i</sub>(Fold-FITC-PEG)<sub>o</sub>

0.034 g of MSN-(NH<sub>2</sub>)<sub>i</sub>(N<sub>3</sub>)<sub>o</sub>, without surfactant at the porous, were suspended in 5 mL of EtOH and sonicated during 1 h. Then, 0.016 g (0.04 mmol, 4 eq.) of FITC (**23**) were added. The solution was left at room temperature for 48 h. Again, samples were collected via centrifuging at 12000 rpm for 20 min, washing and dispersing with deionized H<sub>2</sub>O and EtOH until supernatant presented no color. Then, 20 mg of cationic quinoline foldamer (**24**) were added to 20 mg of MSN-(FITC)<sub>i</sub>(N<sub>3</sub>)<sub>o</sub> in a CuI (0.010 mg), DIPEA (2 drops), ACN/H<sub>2</sub>O solution (30 mL). MSN/Foldamer proportion is (1:1) mg Fold/mg MSN. The solution was left at room temperature for 48 h. MSNs were washed several times with ACN, water and 0.1 M EDTA solution to obtain MSN-(FITC)<sub>i</sub>(Fold-N<sub>3</sub>)<sub>o</sub>. Finally, to 10 mg of MSN-(FITC)<sub>i</sub>(Fold-N<sub>3</sub>)<sub>o</sub> 3 mg of alkyneFITCPEG **30** were added in 10 mL of a ACN:H<sub>2</sub>O mixture (3:1). 2 mg of CuI and two drops of DIPEA were added. The solution was left at room temperature for 48 h. MSNs were washed several times with ACN, water and 0.1 M EDTA solution to obtain MSN-(FITC)<sub>i</sub>(Fold-PEG-FITC)<sub>o</sub>.

7.5.7. Synthesis of reference MSN-(FITC)<sub>i</sub>(PEG-FITC)<sub>o</sub>

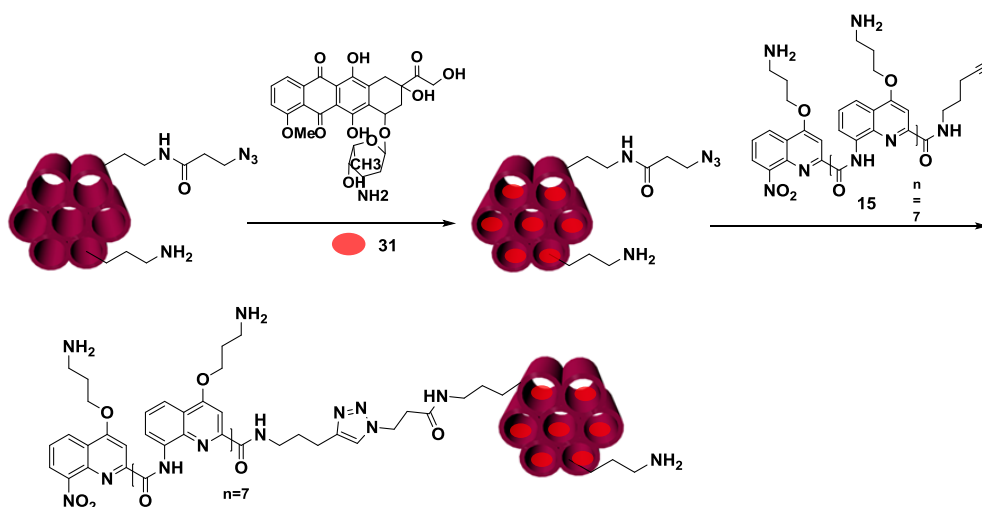
0.034 g of MSN-(NH<sub>2</sub>)<sub>i</sub>(N<sub>3</sub>)<sub>o</sub>, without surfactant at the porous, were suspended in 5 mL of EtOH and sonicated during 1 h. Then, 0.016 g (0.04 mmol, 4 eq.) of FITC (**23**) were added. The solution was left overnight at room temperature for 48 h. Again, samples were collected via centrifuging at 12000 rpm for 20 min, washing and dispersing with deionized H<sub>2</sub>O and EtOH until supernatant presented no color. Then to 10 mg of MSN-(FITC)<sub>i</sub>(N<sub>3</sub>)<sub>o</sub> 10 mg of alkyne-FITC-PEG **30** were added in 20 mL of a ACN:H<sub>2</sub>O mixture (3:1). Then, 5 mg of CuI and two drops of DIPEA were added. Finally, the solution was left at room temperature for 48 h. MSNs were washed several times with ACN, water and 0.1 M EDTA solution to obtain reference MSN-(FITC)<sub>i</sub>(FITC-PEG)<sub>o</sub>.

### 7.5.8. DOX loading in MSN-(NH<sub>2</sub>)<sub>i</sub>(N<sub>3</sub>)<sub>o</sub> (MSN-(DOX))



To 15 mg MSN-(NH<sub>2</sub>)<sub>i</sub>(N<sub>3</sub>)<sub>o</sub> in 30 mL MeOH, 7 mg (0.012 mol) of DOX (**31**) and 0.8 mL of trimethylamine were added. The solution was left 24 h at room temperature. Then, MSNs were washed extensively, until no red supernatant was obtained. Supernatant was collected and measured by UV-Vis to assess the quantity of DOX loaded at 490 nm, which was near 30 %.

### 7.5.9. DOX loading with different quantities of foldamer (MSN-(DOX)(l-Fold)<sub>o</sub> and MSN-(DOX)(h-Fold)<sub>o</sub>)



To 35 mg MSN-(NH<sub>2</sub>)<sub>i</sub>(N<sub>3</sub>)<sub>o</sub> in 45 mL MeOH were added 0.5 mL of trimethylamine and 16 mg (0.028 mmol) of DOX. The solution was left 24 h at room temperature. Then, MSNs were washed extensively, until no red supernatant was obtained. Supernatant was collected and measured to assess the quantity of DOX loaded at 490 nm, which was near 30 %. Finally, MSN-DOX-(NH<sub>2</sub>)<sub>i</sub>(N<sub>3</sub>)<sub>o</sub> were obtained.

**Synthesis of MSN-(DOX)(l-Fold)<sub>o</sub>** (0.1 mg Fold/ mg MSN)

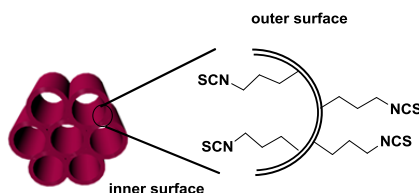
To a solution of 35 mL (ACN/H<sub>2</sub>O;3:1) of MSN-DOX(NH<sub>2</sub>)<sub>i</sub>(N<sub>3</sub>)<sub>o</sub> nanoparticles, 3.5 mg of quinoline foldamer (0.0011 mmol), 0.6 mg of CuI and two drops of DIPEA were added. Then, 24 h later, MSNs were washed extensively with water, ACN, and EDTA 0.1 M, until blue CuEDTA supernatant color disappeared. Finally, solvent was reduced under low pressure to give MSN-(DOX)(l-Fold)<sub>o</sub>.

**Synthesis of MSN-(DOX)(h-Fold)<sub>o</sub>** (0.4 mg Fold/ mg MSN)

To a solution of 35 mL (ACN/H<sub>2</sub>O;3:1) of MSN-DOX(NH<sub>2</sub>)<sub>i</sub>(N<sub>3</sub>)<sub>o</sub> nanoparticles, 13.5 mg of quinoline foldamer (0.0045 mmol), 1.5 mg of CuI and two drops of DIPEA were added. Then, 24 h later, MSNs were washed extensively with water, ACN, and EDTA 0.1 M, until blue CuEDTA supernatant color disappeared. Finally, solvent was reduced under low pressure to give MSN-(DOX)(h-Fold)<sub>o</sub>.

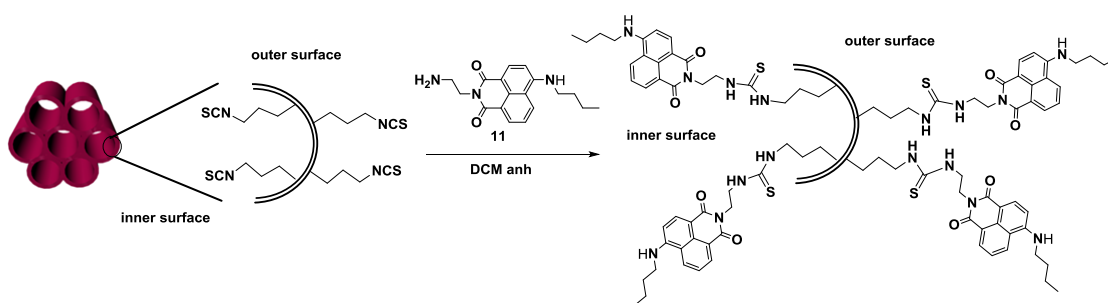
## 7.6. Synthesis Chapter 5

### 7.6.1. Synthesis of isothiocyanate MSNs ((MSN-(NCS))



200 mg of MSN-(NH<sub>2</sub>)CTAB were treated with 5 mL HCl (c) in 90 mL of EtOH for 24 h, in order to eliminate the tensioactive. Solid samples were collected by centrifugation at 13000 rpm for 13 min, washing and dispersing with deionized water and EtOH, twice. Then, MSN-NH<sub>2</sub> were treated with toluene at 50 °C for 24 h. 40 mg of the resulting MSN-(NH<sub>2</sub>) were suspended in 35 mL of toluene and 95 mg of thiocarbonyldi-2(1*H*)-pyridone (**5**) (0.409 mmol, 12 eq.) in 15 mL of dry DCM were added. The suspension was stirred for 24 h at room temperature. Solid samples were collected by centrifugation at 13000 rpm for 13 min and then were washed and dispersed with DCM and EtOH. This procedure was repeated six times and finally MSN-(NCS) were evaporated under reduced pressure and stored dry.

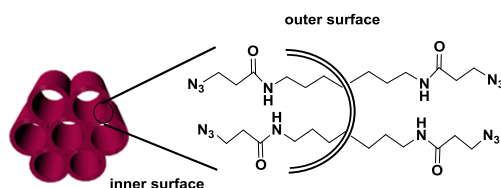
### 7.6.2. Functionalization of MSN-(NCS) with 4-(*n*-butylamino)-*N*-(2-aminoethyl)-1,8-naphthalimide (MSN-(UNaph))



20 mg of MSN-(NCS) were suspended in 15 mL of EtOH. Then 6.6 mg of 4-*n*-butylamino-*N*-(2-aminoethyl)-1,8-naphthalimide (**11**) (0.021 mmol, 2 eq.) were added. The mixture was stirred for 48 h at room temperature in the dark. Solid samples were collected by centrifugation and were washed and dispersed in EtOH until disappearance of yellow color (5 times).

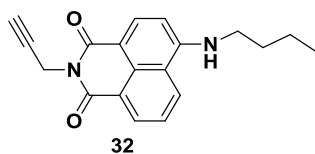


### 7.6.3. Synthesis of azido MSNs (MSN-(N<sub>3</sub>))



200 mg of MSN-(NH<sub>2</sub>)CTAB were treated with 5 mL HCl (c) in 90 mL of EtOH for 24 h, in order to eliminate the tensioactive. Solid samples were collected by centrifugation at 13000 rpm for 13 min, and were washed and dispersed with deionized water and EtOH, twice. Then, 40 mg of the resulting MSN-(NH<sub>2</sub>) were suspended into 20 mL of EtOH. Afterwards, 86 mg (0.405 mmol, 12 eq.) of 3-azidopropionic acid succinimidyl ester (**22**) in 15 mL of EtOH was added to the MSNs suspension. The mixture was stirred for 24 h at room temperature. Solid samples were collected by centrifugation at 13000 rpm for 13 min, and were washed and dispersed with EtOH six times, evaporated under reduced pressure and stored dry.

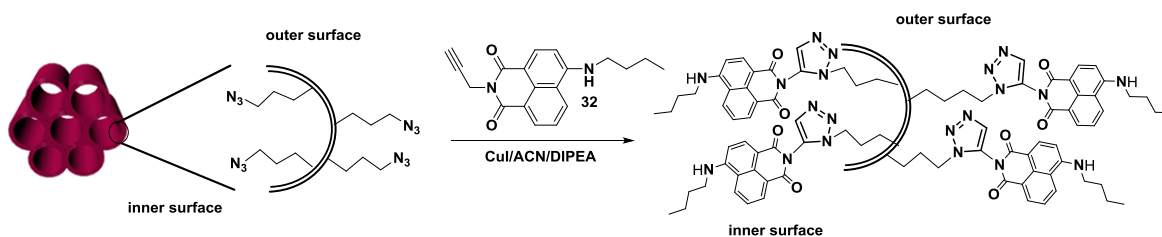
### 7.6.4. Propargyl 8-butylamine naphthalimide (**32**)<sup>6</sup>



Propargyl 8-bromo naphthalimide (0.3 g, 0.7 mmol) was dissolved in 7 mL of DMSO and *N*-butylamine (3 mL, 30 mmol) was added to the mixture. The suspension was warmed to 80 °C overnight. The resulting solution was diluted with 100 mL of DCM and washed three times with lithium chloride and water, and was removed under reduced pressure. Compound propargyl 8-butylamine naphthalimide (**32**) (0.252 g, 75 %) was obtained as a yellow solid. Spectroscopic data were in good agreement with reported data.

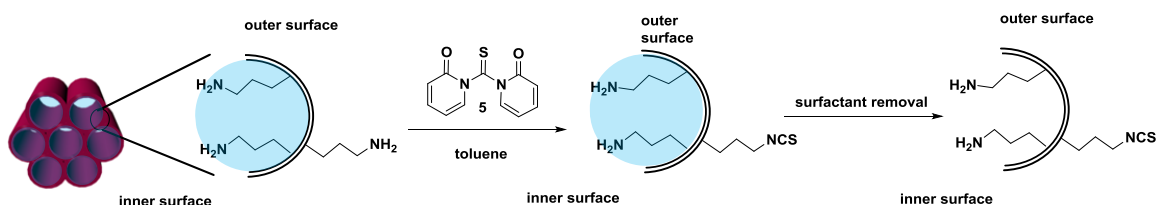
<sup>1</sup>H-NMR (400 MHz, CDCl<sub>3</sub>) δ 8.62 (dd, *J* = 7.8 Hz, 1H), 8.51 (d, *J* = 8.4 Hz, 1H), 8.09 (d, *J* = 8.3 Hz, 1H), 7.63 (dd, *J* = 7.9 Hz, 1H), 6.74 (d, *J* = 8.5 Hz, 1H), 5.27 (m, 1H), 4.95 (d, *J* = 2.3 Hz, 2H), 3.42 (d, 2H), 2.16 (t, *J* = 2.3 Hz, 1H), 1.85 – 1.77 (m, 2H), 1.54 (m, 4H), 1.04 (t, *J* = 7.4 Hz, 3H). <sup>13</sup>C-NMR (100 MHz, CDCl<sub>3</sub>) δ 163.9, 163.2, 149.7, 134.9, 131.4, 129.9, 126.1, 124.7, 122.8, 120.1, 109.7, 104.4, 79.2, 70.0, 43.4, 31.0, 29.1, 20.3, 13.8.

### 7.6.5. Functionalization of (MSN-(N<sub>3</sub>)) with 4-(*n*-butylamino)-*N*-(2-propargyl)-1,8-naphthalimide (MSN-(TNaph))



26 mg of MSN-(N<sub>3</sub>) were suspended in 20 mL of ACN. Then 7.7 mg of propargyl 8-butylamine naphthalimide (**32**) (0.025 mmol, 2 eq.) with 3 mg CuI (0.001 mmol) and 3 drops of DIPEA were added. The mixture was stirred for 48 h at room temperature in the dark. Solid samples were collected by centrifugation and were washed with diethyldithiocarbamate until yellow color disappeared. The presence of copper was monitored by UV-Vis absorbance at 430 nm. More than 10 centrifugations were needed in order to eliminate Cu-diethyldithiocarbamate complex. Afterwards, MSNs were suspended in a methanolic solution of HCl 0.1 M / MeOH for 12 h.

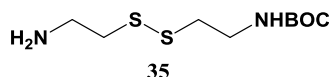
### 7.6.6. Synthesis of bifunctionalized amino-isothiocyanate (MSNs (MSN-(NH<sub>2</sub>)<sub>i</sub>(NCS)<sub>o</sub>))



44 mg of MSN-(NH<sub>2</sub>)CTAB were dissolved in 20 mL of dry toluene and stirred at 60 °C for 24 h. Then, 42 mg of thiocarbonyldi-2(1*H*)-pyridone (**5**) (0.180 mmol, 20 eq.) were added and the mixture was stirred at room temperature in the dark for 48 h. Solid samples were collected by centrifugation at 13000 rpm and then were washed with EtOH twice. Then, tensioactive was eliminated by adding to the dispersion 30 mL of a 0.1 M NH<sub>4</sub>NO<sub>3</sub> methanolic solution for 24 h. Solid samples were collected by centrifugation and then were washed and dispersed with EtOH and water. MSN-(NH<sub>2</sub>)<sub>i</sub>(NCS)<sub>o</sub> were evaporated under reduced pressure and stored dry.

### 7.6.7. Synthesis of disulfide small and long PEG (41, n=3 and n=15).

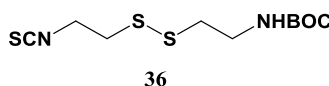
#### 7.6.7.1. Synthesis of *tert*-butyl(2-((2-aminoethyl)disulfanyl)ethyl)carbamate (35)<sup>7</sup>



2.2 g of cystamine dihydrochloride (**34**) (10.0 mmol) and 4.2 mL of triethylamine (30.0 mmol) were dissolved in MeOH (30 mL) and added to a methanolic solution (20 mL) of di-*tert*-butyl dicarbonate (1.091 g, 5.00 mmol). The reaction mixture was stirred for 6 h at 0 °C, after which the solution was evaporated, and 1 M NaH<sub>2</sub>PO<sub>4</sub> was added to the residue. The aqueous solution was washed with diethyl ether to remove di-*t*-Boc-cystamine. The aqueous solution was adjusted to pH=9 by addition of 1 M NaOH, and the solution was extracted with AcOEt. The organic phase was dried over MgSO<sub>4</sub> and then evaporated. The resulting yellow oil was dried *in vacuo* to give (**35**) with 41.7 % yield. Spectroscopic data were in good agreement with reported data.

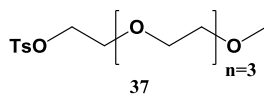
<sup>1</sup>H-NMR (400 MHz, CDCl<sub>3</sub>) δ 4.97 (b, 1 H), 3.47 (q, 2H), 3.03 (t, 2H), 2.80 (q, 4H), 1.46 (s, 9H).

#### 7.6.7.2. Synthesis of *tert*-butyl(2-((2-isothiocyanateethyl)disulfanyl)ethyl) carbamate (36)



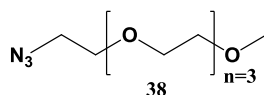
0.786 g (3.11 mmol) of product (**35**) and 0.68 g (2.95 mmol) of 1,1'-thiocarbonylbis(pyridine-2(1*H*)-one) were dissolved in 50 mL of anhydrous DCM. The reaction was stirred at 25 °C for 24 h. Then, the organic phase was washed with H<sub>2</sub>O and NaHCO<sub>3</sub> twice. Afterwards, MgSO<sub>4</sub> was used in order to dry the organic layer and then the solution was evaporated to give **36** in a 10 %.

<sup>1</sup>H NMR (400 MHz, CDCl<sub>3</sub>) δ 4.96 (s, 1H), 3.46 (brs, 2H), 3.01 (t, *J* = 6.2 Hz, 2H), 2.81 – 2.76 (m, 4H), 1.45 (s, 9H). <sup>13</sup>C NMR (100 MHz, CDCl<sub>3</sub>) δ 155.7, 132.8, 79.7, 44.0, 39.3, 38.5, 37.9, 28.4 .IR (KBr)  $\nu_{\max}$ : 3354, 2976, 2929, 2188, 2113, 2083, 1700, 1509 cm<sup>-1</sup>. Calculated OEA C: 40.79 %; H: 6.16 %; N: 9.51 %, O: 10.87 %, S: 32.66 %. Experimental OEA C: 40.71 % , H: 6.37 % , N:9.31 % , S:32.15 %.

**7.6.7.3. Synthesis of triethylene glycol 2-methyl tosylate methyl ether (37)**<sup>8,9</sup>

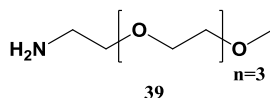
2 mL (10.0 mmol) of the commercially available tetraethyleneglycol monomethyl ether (**33**) in 10 mL THF were added to a solution of 4.5 g of KOH (80.2 mmol) in 40 mL H<sub>2</sub>O. The resulting mixture was stirred for 1 h at 0 °C. Then 1.91 g (10.0 mmol) *p*-toluensulfonyl chloride in 10 mL of THF was added drop wise to the reaction mixture during 1 h at 0 °C. The mixture was stirred for additional 3 h. The solution was poured onto 1 M HCl and the organic solvent was evaporated. The residue was extracted three times with chloroform and the organic phase dried over MgSO<sub>4</sub>, filtered and the solvent was removed under reduced pressure. A transparent incolor oil (**37**) in a 75 % yield was obtained. Spectroscopic data were in good agreement with reported data.

<sup>1</sup>H-NMR (400 MHz, CDCl<sub>3</sub>) 7.80 (d, *J*=8.3 Hz, 2H), 7.34 (d, *J*=8.9 Hz, 2H), 4.16 (t, *J*=4.8 Hz, 2H), 3.70-3.54 (overlapping multiplets, 14 H), 3.38 (s, 3 H), 2.45 (s, 3 H). <sup>13</sup>C-NMR (100 MHz, Chloroform-d) δ 144.8, 133.0, 129.9, 128.0, 72.0, 70.6, 69.3, 68.7, 59.1, 21.7.

**7.6.7.4. Synthesis of triethylene glycol 2-methyl azide methyl ether (38)**<sup>10</sup>

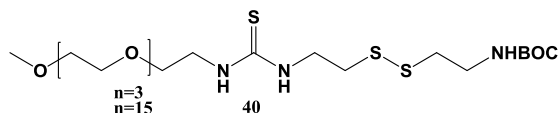
2.74 g (7.5 mmol) of triethylene glycol 2-methyl azide methyl ether (**37**) was dissolved in ethanol (50 mL) and 1.2 g of sodium azide (18.5 mmol) were added. The solution was heated under reflux overnight or until TLC (10 % MeOH in CHCl<sub>3</sub>) showed no starting material. The solvent was removed under vacuum and CH<sub>2</sub>Cl<sub>2</sub> was added to the residue. The organic layer was extracted with water (3 times) and dried (MgSO<sub>4</sub>) to give product **38** in a 58 % yield. Spectroscopic data were in good agreement with reported data.

<sup>1</sup>H-NMR (400 MHz, CDCl<sub>3</sub>) δ 3.64–3.69 (overlapping multiplets, 12H). 3.53–3.56 (m, 2H), 3.40 (brs, 2 H), 3.38 (s, 3 H). <sup>13</sup>C-NMR (100 MHz, Chloroform-d) δ 50.7, 59.0, 70.0, 70.5, 70.6, 70.6, 70.7, 72.9.

7.6.7.5. Synthesis of triethylene glycol 2-methyl amino methyl ether (**39**)<sup>11</sup>

A solution of triethylene glycol 2-methyl azide methyl ether (**38**) (1.02 g, 4.4 mmol) in dry THF (30 mL) was cooled at 0 °C. 1.2 g of triphenyl phosphine was added (5.5 mmol), after which the mixture was allowed to stand at room temperature for 24 h. Water (0.4 mL) was added, and the reaction mixture was stirred for another 24 h to hydrolyze the intermediate phosphorus adduct. The reaction mixture was diluted with water and washed with toluene. Then the aqueous layer was evaporated to give product **39** in a 40 % yield. Spectroscopic data were in good agreement with reported data.

<sup>1</sup>H-NMR (400 MHz, CDCl<sub>3</sub>) δ 3.69-3.61 (m, 10H), 3.58-3.54 (m, 2H), 3.52 (t, *J*=5.2, 2H), 3.38 (s, 3H), 2.87 (t, *J*=5.2, 2H), 1.70 (s, 2H). <sup>13</sup>C-NMR (100 MHz, Chloroform-*d*) δ 73.3, 72.0, 70.7, 70.7, 70.6, 70.4, 59.1, 41.7.

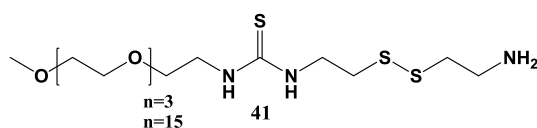
7.6.7.6. Synthesis of *tert*-butyl(15-thioxo-2,5,8,11-tetraoxa-19,20-dithia-14,16-diazadocosan-22-yl)carbamate (**40**; n=3 and n=15)

1.73 mmol of product **39** and 562 mg (1.91 mmol) of product **36** were dissolved in 50 mL of anhydrous DCM. The reaction was stirred at 20 °C for 24 h. The result product **40** was purified through a silica gel column chromatographic with DCM:ACOEt mixtures (50:50). The product **40** was collected and the solvent was removed under vacuum to yield the pure product. Yield: 27%.

(**40a**) n=3: <sup>1</sup>H-NMR (400 MHz, CDCl<sub>3</sub>) δ 7.14 (brs, 1H), 5.31 (brs, 1H), 3.66 (brs, 12H), 3.56 (brs, 2H), 3.44 (brs, 2H), 3.37 (s, 3H), 3.12 (brs, 2H), 3.04 (brs, 2H), 2.80 (brs, 4H), 1.45 (s, 9H). <sup>13</sup>C-NMR (100 MHz, Chloroform-*d*) δ 183.5, 153.7, 79.8, 71.9, 70.6, 70.5, 70.4, 70.2, 59.1, 43.1, 39.6, 38.3, 38.0, 28.6. IR (KBr) ν<sub>max</sub>: 3330, 2926, 2871, 1709, 1546, 1167, 1110 cm<sup>-1</sup> Calculated OEA C: 45.49 %, H: 7.84 %; N: 8.38 %, O: 19.13 %; S: 19.17 %. Experimental OEA C: 45.53 %, H: 7.93 %, N: 7.99 %, S: 18.88 %.

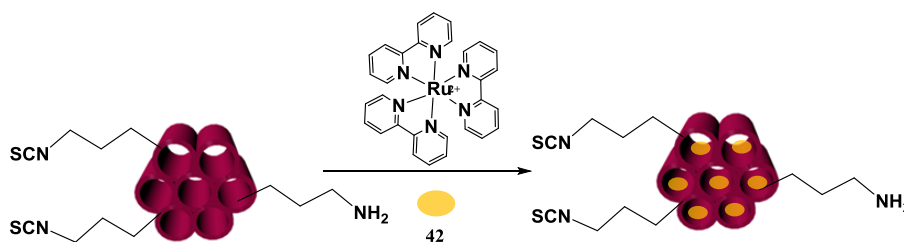
**(40b)** n=15:  $^1\text{H-NMR}$  (400 MHz,  $\text{CDCl}_3$ )  $\delta$  6.94 (brs, 1H), 5.24 (brs, 1H), 3.90 (brs, 2H), 3.74-355 (overlapping multiplets, 72H), 3.45 (brs, 2H), 3.37 (s, 3H), 2.96 (brs, 2H), 2.78 (brs, 2H), 1.45 (s, 9H).  $^{13}\text{C-NMR}$  (100 MHz, Chloroform-*d*)  $\delta$  183.2, 155.9, 79.5, 71.8, 70.5, 70.4, 70.2, 70.0, 58.9, 44.0, 39.4, 37.9, 37.8, 28.4. **IR (KBr)**  $\nu_{\text{max}}$  3517, 3335, 2871, 1709, 1542, 1454, 1107  $\text{cm}^{-1}$  **MALDI-TOF** Matrix: DHB 10 mg/mL acetone, Ratio Sample-Matrix-NaTFA: 4:20:2, Method: Reflector positive ion mode (RP\_master): 619.916, 692.848, 745.783, 736.931, 758.927, 878.043, 922.075, 965.111, 1009.188, 1053.275, 1053.275, 1097.309, 1141.357, 1185.463, 1229.516, 1273.535

#### 7.6.7.7. Synthesis of 1-(2-((2-aminoethyl)disulfanyl)ethyl)-3-(2,5,8,11-tetraoxatrideca-13-yl)thiourea (**41**; n=3 and n=15).



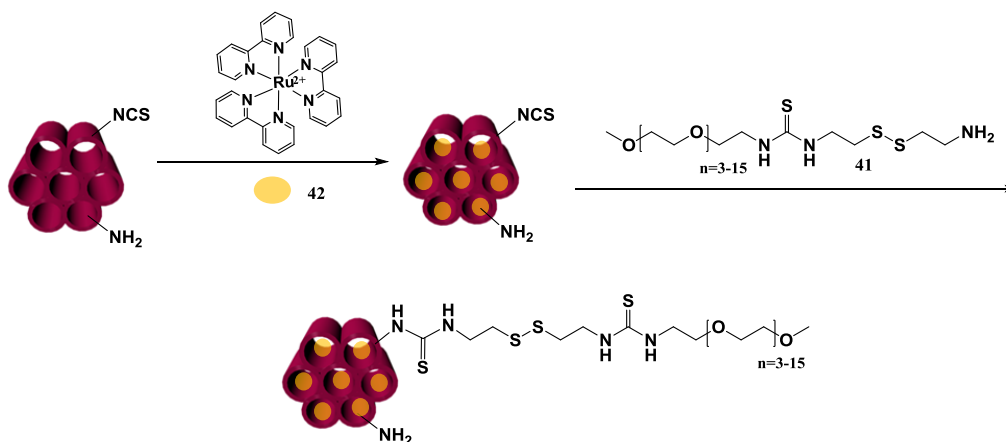
0.26 mmol of product **40**, n=3 and n=15 were dissolved in 10 mL of anhydrous DCM. The mixture was cooled at 0 °C and stirred for 30 minutes. Then, 1 mL (13 mmol) of trifluoroacetic acid (TFA) was added dropwise. Afterwards, the mixture was stirred for 1.5 h at 0 °C and the solvent was removed at vacuum. The product **41** n=3 (**41a**) and n=15 (**41b**) is directly functionalized to the nanoparticles.

#### 7.6.8. $\text{Ru}(\text{bipy})_3^{2+}$ loading in amino-isothiocyanate MSNs ( $\text{MSN}-(\text{NH}_2)_i(\text{NCS})_o\text{Ru}$ )



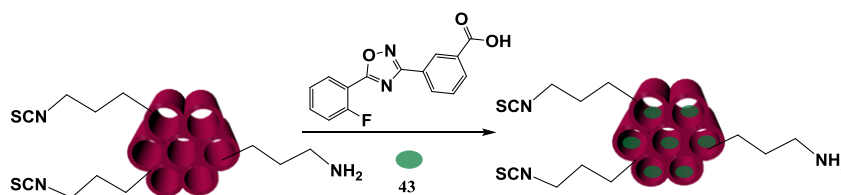
Typically, 18 mg ( $2.45 \cdot 10^{-5}$  mol) of  $\text{Ru}(\text{bipy})_3^{2+}$  (**42**) were added to a solution of 30 mg of bifunctionalized MSNs in 5 mL of ACN for 24 h. Finally, after washing with EtOH,  $\text{Ru}(\text{bipy})_3^{2+}$  supernatant was measured at 451 nm to assess the loading. In order to determine the total amount of  $\text{Ru}(\text{bipy})_3^{2+}$  that can be released, MSNs are treated with HCl (c) for 12 h and the supernatant is measured at 451 nm.

### 7.6.9. $\text{Ru}(\text{bipy})_3^{2+}$ loading in amino-isothiocyanate MSNs with small and long PEG 41 ( $n=3$ and $n=15$ ) ( $\text{MSN}-(\text{NH}_2)_i(\text{S-PEG})_o\text{Ru}$ and $\text{MSN}-(\text{NH}_2)_i(\text{L-PEG})_o\text{Ru}$ )



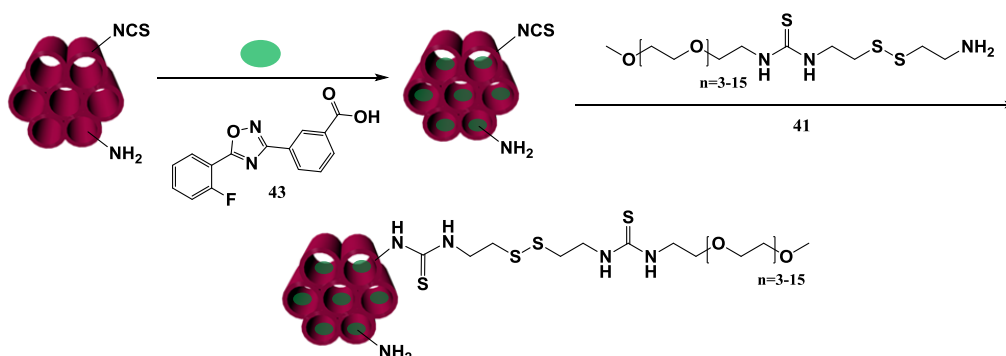
First, 18 mg ( $2.45 \cdot 10^{-5}$  mol) of  $\text{Ru}(\text{bipy})_3^{2+}$  were added to a solution of 30 mg of bifunctionalized MSNs in 5 mL of ACN. After 24 h, 60 mg ( $1.49 \cdot 10^{-4}$  mol) of S-PEG and L-PEG 41 ( $n=3$  and  $n=15$ ) were added in 15 mL of ACN for 24 h. Finally, after washing with EtOH, Rubipy supernatant was measured at 451 nm to assess the loading. In order to know the total amount of  $\text{Ru}(\text{bipy})_3^{2+}$  that can be released, MSNs are treated with HCl (c) for 12 h and the supernatant is measured at 451 nm.

### 7.6.10. Ataluren loading in amino-isothiocyanate MSNs ( $\text{MSN}-(\text{NH}_2)_i(\text{NCS})_o\text{Ru}$ )



Bifunctional  $\text{MSN}-(\text{NH}_2)_i(\text{NCS})_o$  nanoparticles were dissolved in 30 mL of ethanol and stirred vigorously for 1 h. Then 11 mg of Ataluren (0.0397 mmol) were added to the solution. The mixture was stirred at 20 °C temperature for 24 h. Ataluren (43) was loaded in a proportion (4:3). Finally, after washing with EtOH once, Ataluren supernatant was measured at 255 nm to assess the loading.

### 7.6.11. Ataluren loading in amino-isothiocyanate MSNs with small and long PEG **41** (n=3 and n=15) MSN-(NH<sub>2</sub>)<sub>i</sub>(S-PEG)<sub>o</sub>Ata and MSN-(NH<sub>2</sub>)<sub>i</sub>(L-PEG)<sub>o</sub>Ata

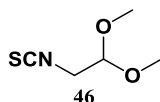


13 mg of bifunctional MSN-(NH<sub>2</sub>)<sub>i</sub>(NCS)<sub>o</sub> nanoparticles were dissolved in 30 mL of ethanol and stirred vigorously for 1 h. Then 11 mg of Ataluren (**43**) (0.0397 mmol) were added to the solution. The mixture was stirred at 20 °C temperature for 24 h. Then 60 mg (1.49·10<sup>-4</sup> mol) of S-PEG and L-PEG **41** (n=3 and n= 15) were added to the silica nanoparticles. Finally, the mixture was stirred for another 24 h. Solid samples were collected by centrifugation at 13000 rpm for 13 minutes and washed four times with EtOH and water to give MSN-(NH<sub>2</sub>)<sub>i</sub>(S-PEG)<sub>o</sub>Ata and MSN-(NH<sub>2</sub>)<sub>i</sub>(L-PEG)<sub>o</sub>Ata.



## 7.7. Synthesis Chapter 6

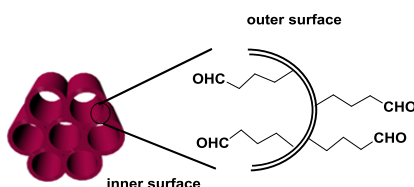
### 7.7.1. Synthesis of 2-isothiocyanate-1,1-dimethoxyethane (**46**)<sup>12</sup>



0.2 mL (1.9 mmol) of 2,2-dimethoxyethan-1-amine (**47**) was dissolved in 10 mL of DCM anh. Then, 0.1 g (2.6 mmol, 1.4 eq) of 1,1'-thiocarbonyldil-2(1*H*)-pyridone (**5**) was added. The mixture was stirred at room temperature for 24 h. The solvent was washed twice with bicarbonate, and removed under reduced pressure to give product **46** in 60 % yield. Spectroscopic data were in good agreement with reported data.

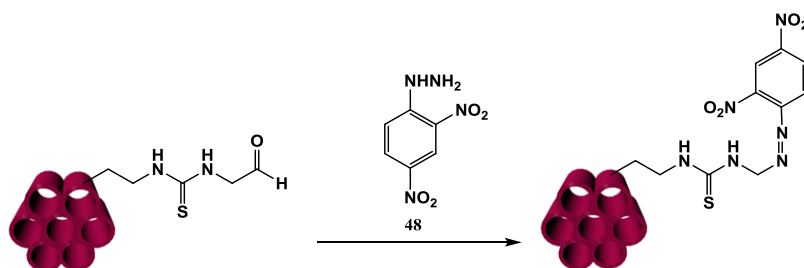
<sup>1</sup>H NMR (400 MHz, CDCl<sub>3</sub>) δ 4.46 (t, 1H), 3.60 (d, 2H), 3.43 (s, 9H). <sup>13</sup>C NMR ((100 MHz, CDCl<sub>3</sub>) : δ 130.9, 101.5, 54.1, 54.1, 46.5.

### 7.7.2. Synthesis of MSN-(CHO)



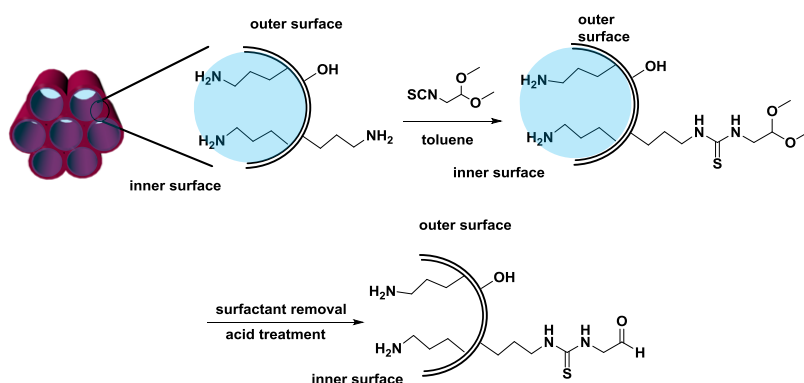
200 mg of MSN-(NH<sub>2</sub>)CTAB were treated with 5 mL HCl (c) in 90 mL of EtOH for 24 h, in order to eliminate the tensioactive. Solid samples were collected by centrifugation at 13000 rpm for 13 min, washing and dispersing with deionized water and EtOH, twice. Then, MSN-(NH<sub>2</sub>) were treated with toluene at 50 °C for 24 h. 40 mg of the resulting MSN-(NH<sub>2</sub>) were suspended in 35 mL of EtOH and 28 eq. of 2-isothiocyanate-1,1-dimethoxyethane (**46**) (20 mg, 1.36·10<sup>-4</sup> mol) (**37**) in 20 mL of EtOH were added. 24 h later, the resulting material was then treated with acid ethanol for 4 hours in order to deprotect the acetal and form the aldehyde moiety. Solid samples were collected by centrifugation at 13000 rpm for 13 min and then were washed and dispersed with DCM and EtOH. This procedure was repeated six times and finally MSN-(CHO) were evaporated under reduced pressure and stored dry.

### 7.7.3. Functionalization of MSN-(CHO) with 2,4-dinitrophenylhydrazine



20 mg ( $1.056 \cdot 10^{-4}$  mol) of 2,4-dinitrophenylhydrazine (**48**) were added to a solution of 5 mg MSN-(CHO) in 5 mL of MeOH and were left for 24 h. MSNs were washed with MeOH until supernatant had no color. The yellow coloration of MSNs corroborates that MSN-(CHO) have indeed reacted with 2,4-dinitrophenylhydrazine and that aldehyde moiety has been correctly introduced to MSNs. 13 % of 2,4-(dinitrophenyl)hydrazine was finally loaded to the MSNs.

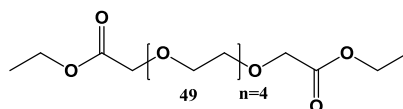
### 7.7.4. Synthesis of bifunctionalized amino-aldehyde MSNs ( $\text{MSN}-(\text{NH}_2)_i(\text{CHO})_o$ )



Briefly, the synthesis follows a similar scheme as described before. 0.2 g of MSN-(NH<sub>2</sub>) containing the surfactant (CTAB) were reacted with 4 eq. of 2-isothiocyanate-1,1-dimethoxyethane (**46**) (0.1 g,  $6.8 \cdot 10^{-4}$  mol) in 50 mL of toluene. 24 h later, MSNs were washed twice with toluene and ethanol and then the tensioactive was eliminated. MSN-(NH<sub>2</sub>)<sub>i</sub>(Acet)<sub>o</sub> were treated in 40 mL solution of EtOH, where 0.5 g of NH<sub>4</sub>NO<sub>3</sub> were dissolved. 24 h later, MSNs were washed with EtOH and acetal protecting group was removed by stirring MSNs in HCl solution for 6 h.

### 7.7.5. Synthesis of the linker

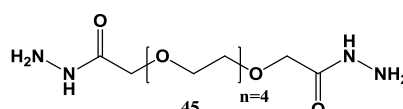
#### 7.7.5.1. Synthesis of diethyl 3,6,9,12,15-pentaoxaheptadecanedioate (**49**)<sup>13</sup>



1.7 mL ( $9.8 \cdot 10^{-3}$  mol) of tetraethyleneglycol (**25**) in 20 mL of anhydrous THF and with 1.2 g of NaH (0.05 mol, 5 eq.) were added and stirred at 0 °C for 30 min. Then the solution was heated at 80 °C until color change from yellow to brown, 6 h. Then, 3.3 mL (0.034 mol, 3.4 eq.) of ethyl bromoacetate were added to the solution and left it in reflux for 24 h. The white precipitate was filtered and the solvent was reduced under low pressure. Then, the final oil was digested for 24 h in Cy to obtain the product dimethyl-3,6,9,12,15-pentaoxaheptadecanedioate (**49**) in a yield of 40 %.

<sup>1</sup>H NMR (400 MHz, CDCl<sub>3</sub>) δ 4.26-4.17 (m, 4H), 4.15 (s, 4H), 3.78-3.6 (m, 16H), 1.29 (t,  $J=7.2$  Hz, 6H). <sup>13</sup>C NMR (100 MHz, CDCl<sub>3</sub>) δ 170.7, 70.7, 70.1, 68.8, 60.8, 14.1. IR (KBr)  $\nu_{\max}$  2873, 1752, 1449, 1381, 1350, 1282, 1205, 1122, 1032, 945, 854, 722, 665 cm<sup>-1</sup>.

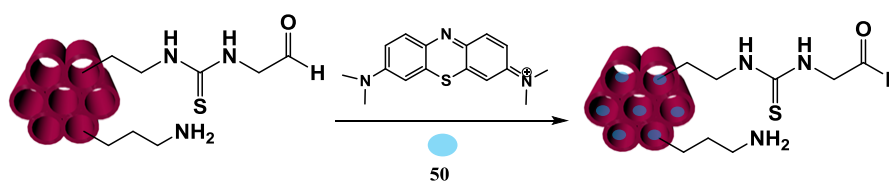
#### 7.7.5.2. Synthesis of dimethyl 3,6,9,12,15-pentaoxaheptadecanedihydrazide (**45**)<sup>14-</sup>



0.8 g ( $2.4 \cdot 10^{-3}$  mol) diester PEG **49** were dissolved in 25 mL of EtOH and 0.6 mL (2.1 eq.) of NH<sub>2</sub>NH<sub>2</sub> were added. After 24 h of reflux, the eluent is eliminated at reduced pressure to give an oil, which after being washed with EtOH/Cy/DCM gave the product 3,6,9,12,15-pentaoxaheptadecanedihydrazide **45** in a yield of 80 %. Spectroscopic data were in good agreement with reported data.

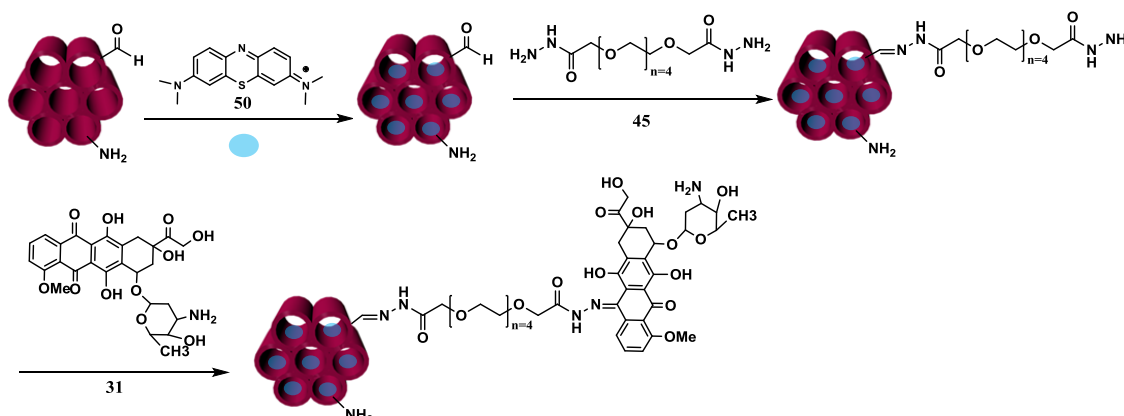
<sup>1</sup>H NMR (400 MHz, CDCl<sub>3</sub>) δ 6.81 (brs, 6H), 4.07 (s, 4H), 3.71-3.64 (m, 16H). <sup>13</sup>C NMR (100 MHz, CDCl<sub>3</sub>) δ 169.6, 77.0, 72.6, 70.1, 61.5. IR (KBr)  $\nu_{\max}$  3319, 2873, 1671, 1524, 1453, 1347, 1294, 1250, 1108, 943, 888, 852, 666 cm<sup>-1</sup>.

### 7.7.6. MB loading in amino-aldehyde nanoparticles (MSN-(NH<sub>2</sub>)<sub>i</sub>(CHO)<sub>o</sub>MB)<sup>17</sup>



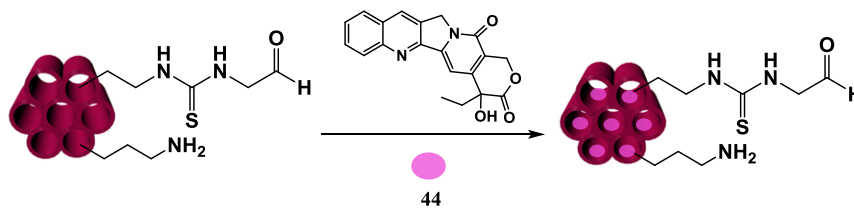
Typically, 6 mg (0.016 mmol) of MB were added to a solution of 20 mg of MSNs in 25 mL of EtOH with the addition of triethylamine. Finally, after washing with EtOH, MB supernatant was measured with a UV–Vis absorption spectrophotometer at 650 nm to assess the loading.

### 7.7.7. Dual MB-DOX nanocarrier



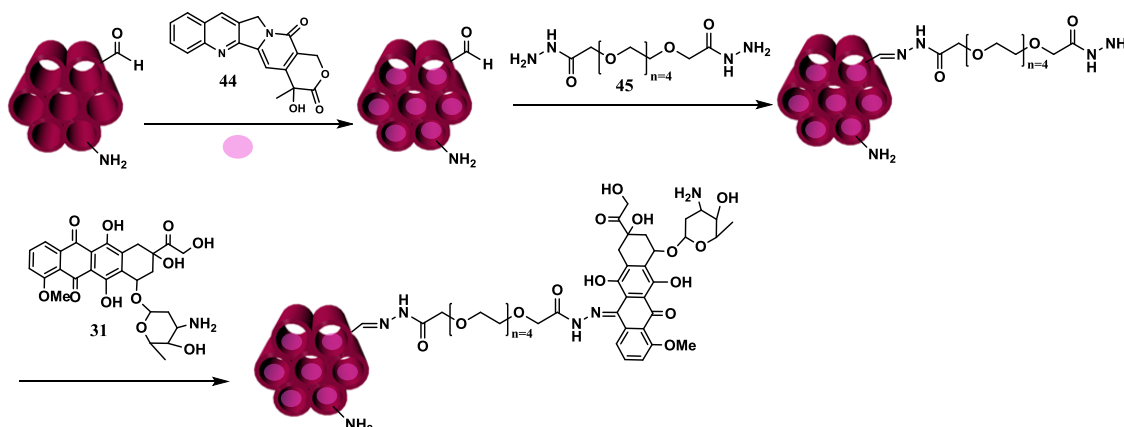
Typically, 9 mg ( $2.4 \cdot 10^{-5}$  mol) of methylene blue (**50**) were added to a solution of 25 mg of bifunctionalized MSNs in a 0.88 M ethanolic/triethylamine. After 24 h, 70 mg (0.2 mmol) of dihydrazide PEG **45** were added in 10 mL of ACN for 24 h. MSNs were washed and centrifuged to remove excess dihydrazide PEG. MB supernatant was measured at 650 nm. Finally, MSNs were suspended in 20 mL of MeOH and 18 mg (0.03 mmol) of DOX (**31**) with 0.5 mL of triethylamine were added. After washing with MeOH, DOX supernatant was measured at 451 nm to assess the loading.

### 7.7.8. CPT loading in amino-aldehyde nanoparticles (MSN-(NH<sub>2</sub>)<sub>i</sub>(CHO)<sub>o</sub>CPT)<sup>18-20</sup>



Typically, 15 mg of MSNs dispersed in 5 mL of EtOH:CHCl<sub>3</sub> (1:4) were added to a solution of 100 mL of 6 mg of CPT ( $1.72 \cdot 10^{-5}$  mol). This solution was left for 24 h at 60 °C. Finally, after washing once with EtOH:CHCl<sub>3</sub> (1:4), CPT supernatant was measured with an UV-Vis absorption spectrophotometer at 354 nm to assess the loading.

### 7.7.9. Dual CPT-DOX nanocarrier



18 mg ( $5.16 \cdot 10^{-5}$  mol) of CPT were dissolved in 35 mL of CHCl<sub>3</sub> by sonicating at 60 °C until total dissolution of the drug was achieved, 30 min. Then, the solution was added to a second solution of 30 mg MSN-(NH<sub>2</sub>)<sub>i</sub>(CHO)<sub>o</sub> dispersed in 25 mL of EtOH previously dispersed. 30 h later, a solution of 0.080 g ( $2.36 \cdot 10^{-4}$  mol) dihydrazide-PEG **45** in 20 mL of EtOH was added. Later, 10 drops ( $4.4 \cdot 10^{-3}$  mol, 20 eq.) of triethylamine were. After 48 h, MSNs were centrifuged and the supernatant was collected and measured at 354 nm to assess the quantity of CPT that was absorbed. Then, to the residual MSNs, 21 mg of DOX ( $3.6 \cdot 10^{-5}$  mol) were added in 20 mL of MeOH in basic medium (10 drops of triethylamine, 0.22M). 48 h later MSNs were washed extensively, until no red supernatant was obtained. Supernatant was collected and measured to assess the quantity of DOX loaded at 490 nm.

## 7.8. Bibliography

- (1) Cheng, S. H.; Lee, C. H.; Yang, C. S.; Tseng, F. G.; Mou, C. Y.; Lo, L. W. *J. Mater. Chem.* **2009**, *19* (9), 1252–1257.
- (2) Lu, F.; Wu, S. H.; Hung, Y.; Mou, C. Y. *Small* **2009**, *5* (12), 1408–1413.
- (3) Grandjean, C.; Boutonnier, A.; Guerreiro, C.; Fournier, J. M.; Mulard, L. a. *J. Org. Chem.* **2005**, *70* (18), 7123–7132.
- (4) Norberg, O.; Deng, L.; Yan, M.; Ramström, O. *Bioconjug. Chem.* **2009**, *20* (12), 2364–2370.
- (5) NANOCS <http://www.nanocs.net/Alkyne-PEG-FITC-3k.htm> 09/15.
- (6) Siegers, C.; Oláh, B.; Würfel, U.; Hohl-Ebinger, J.; Hinsch, a.; Haag, R. *Sol. Energy Mater. Sol. Cells* **2009**, *93* (5), 552–563.
- (7) Suga, Y.; Sunayama, H.; Ooya, T.; Takeuchi, T. *Chem. Commun.* **2013**, *49* (76), 8450–8452.
- (8) Cauda, V.; Argyo, C.; Bein, T. *J. Mater. Chem.* **2010**, *20* (39), 8693–8699.
- (9) Wolfe, A. L.; Duncan, K. K.; Lajiness, J. P.; Zhu, K.; Duerfeldt, A. S.; Boger, D. L. *J. Med. Chem.* **2013**, *56* (17), 6845–6857.
- (10) Kitto, H. J.; Schwartz, E.; Nijemeisland, M.; Koepf, M.; Cornelissen, J. J. L. M.; Rowan, A. E.; Nolte, R. J. M. *J. Mater. Chem.* **2008**, *18* (46), 5615–5624.
- (11) Li, G.; Bhosale, S. V.; Wang, T.; Hackbarth, S.; Roeder, B.; Siggel, U.; Fuhrhop, J. H. *J. Am. Chem. Soc.* **2003**, *125* (35), 10693–10702.
- (12) Park, S.; Hayes, B. L.; Marankan, F.; Mulhearn, D. C.; Wanna, L.; Mesecar, A. D.; Santarsiero, B. D.; Johnson, M. E.; Venton, D. L. *J. Med. Chem.* **2003**, *46* (6), 936–953.
- (13) Tanaka, M.; Yoshioka, K.; Hirata, Y.; Fujimaki, M.; Kuwahara, M.; Niwa, O. *Langmuir* **2013**, *29* (42), 13111–13120.
- (14) Islam, R.; Koizumi, F.; Kodera, Y.; Inoue, K.; Okawara, T.; Masutani, M. *Bioorganic Med. Chem. Lett.* **2014**, *24* (16), 3802–3806.
- (15) Kandil, F.; Chebani, M. K.; Al Zoubi, W. *ISRN Org. Chem.* **2012**, *2012*, 1–8.
- (16) Zhang, Y. C.; Zhang, D. W.; Wang, H.; Zhou, Y.; Li, Z. T. *Polym. Chem.* **2015**, *6* (24), 4404–4408.
- (17) Peng, X.; Huang, D.; Odoom-Wubah, T.; Fu, D.; Huang, J.; Qin, Q. *J. Colloid Interface Sci.* **2014**, *430* (0), 272–282.
- (18) Agostini, A.; Mondragón, L.; Pascual, L.; Aznar, E.; Coll, C.; Martínez-Máñez, R.; Sancenón, F.; Soto, J.; Marcos, M. D.; Amorós, P.; Costero, A. M.; Parra, M.; Gil, S. *Langmuir* **2012**, *28* (41), 14766–14776.
- (19) Bernardos, A.; Mondragón, L.; Aznar, E.; Marcos, M. D.; Martínez-Máñez, R.; Sancenón, F.; Soto, J.; Barat, J. M.; Pérez-Payá, E.; Guillem, C.; Amorós, P. *ACS Nano* **2010**, *4* (11), 6353–6368.
- (20) Agostini, A.; Mondragón, L.; Coll, C.; Aznar, E.; Marcos, M. D.; Martínez-Máñez, R.; Sancenón, F.; Soto, J.; Pérez-Payá, E.; Amorós, P. *Chem. Open* **2012**, *1* (1), 17–20.

## Chapter 8. Conclusions

---





---

**Chapter 8. Conclusions**

1. First, monodispersed aminated MSNs (MSN-(NH<sub>2</sub>)) of 50-100 nm have been synthesized and functionalized with different 4-amine-1.8-naphthalimides for their use as sensors in the detection of protons and fluoride anions. To do so, a general procedure for the introduction of 4-amine-1.8-naphthalimides has been developed by clicking isothiocyanate-naphthalimides into aminated MSNs. This strategy provides the introduction of a thiourea moiety able to act both as linker and as a fluoride receptor. Above all the systems synthesized (MSN-(NaphBr), MSN-(NaphPIP), MSN-(NaphBut) and MSN-(NaphMetProp)), MSN-(NaphBut) presented interesting properties as proton and fluoride sensor, responding as a NOR logic gate (only an output is obtained when all the inputs are 0).
2. A new methodology for the synthesis of regioselective bifunctionalized amino-azido MSNs has been carried out. This procedure permits the correct functionalization of azido moieties in the external surface, while the inner surface is being protected by the surfactant. The resulting MSNs can react with cationic quinoline foldamer allowing their complete functionalization through CuAAC cycloaddition. Foldamer-MSNs synthesized for the first time, present a positive zeta potential, a good solubility in water, are nontoxic at a maximum concentration of 0.16 mgMSN/mL and seems to internalize better in Hela cells than control MSNs. Nevertheless, further experiments need to be carried out in order to quantify foldamer-MSNs uptake. In addition, MSNs with a foldamer moiety and a polyethylene glycol chain were also synthesized (MSN-(FITC)<sub>i</sub>(Fold-PEG-FITC)<sub>o</sub>). These Foldamer-PEG-MSNs showed a positive zeta potential, were nontoxic at a maximum concentration of 0.16 mgMSN/mL and were better internalized in the cells than control MSNs and foldamer-MSN. Furthermore, foldamer-MSNs were used as an intracellular DOX delivery nanocarrier. The study of DOX release with different quantities of foldamer demonstrated that foldamer-MSNs enhance intracellular DOX release, since MSNs with a high concentration of alkyne-foldamer, (MSN-(DOX)(h-Fold)<sub>o</sub>) are more toxic and more quantity of DOX was internalized in the cells, than low alkyne-foldamer MSN-(DOX)(l-Fold)<sub>o</sub> and control MSN(NH<sub>2</sub>)<sub>i</sub>(N<sub>3</sub>)<sub>o</sub>DOX.
3. A protocol to prepare isothiocyanate functionalized MSNs from aminated MSNs has been achieved. With this procedure, new amino-isothiocyanate MSNs (MSN-(NH<sub>2</sub>)<sub>i</sub>(NCS)<sub>o</sub>) have been synthesized for the design of a nanocontainer able to release

the drug Ataluren for the treatment of Duchenne Muscular Dystrophy (DMD). While amino inner moieties enhance Ataluren loading and release, external isothiocyanates have been used for the anchorage of scissile disulfide polyethyleneglycol chains (**41**, **n=3** and **n=15**) in a rich glutathione (GSH) environment. MSN-(NH<sub>2</sub>)<sub>i</sub>(S-PEG)<sub>o</sub>Ata and MSN-(NH<sub>2</sub>)<sub>i</sub>(L-PEG)<sub>o</sub>Ata have been studied demonstrating that the longer the polymer chain, the more controlled is the release, achieving a 44 % release in a rich GSH medium and 10 % when no stimulus is applied.

4. Finally, new regioselective bifunctionalized MSN-(NH<sub>2</sub>)<sub>i</sub>(CHO)<sub>o</sub> nanoparticles have been applied as a nanoplatform, able to release dual synergistic CPT/DOX combination for cancer treatment by using pH stimuli. In this case, DOX is both acting as an active and a capping agent. This system respond to pH stimuli and both CPT and DOX drugs are only released in an acid media (pH=4). This strategy only presents three synthetic steps, avoiding any chemical modification in drug structure, which could damage its active site or activity. DOX quantity release is high enough to use these nanoparticles in cancer applications. Nevertheless, CPT loading and release curves must be enhanced in order to translate this system for *in vivo* experiments. Due to the versatility of this nanoplatform, the system can be used for other drug combinations.

## List of publications and presentations

### Publications:

Llinàs, Maria C; Sánchez-García, David. *Nanopartículas de sílice: preparación y aplicaciones en biomedicina*. *Afinidad* **2014**, *71*,565, 20-31

Maria C. Llinàs, Gabriel Martínez-Edo, Salvador Borrós and David Sánchez-García. *Stable and ready-to-use amino-isothiocyanate bifunctionalized mesoporous silica nanoparticles for the design of nanocarriers* (Submitted to the journal *Microporous and Mesoporous materials*).

### Patents:

Maria C. Llinàs, Salvador Borrós and David Sánchez-García. **Nanopartículas mesoporosas de sílice regioselectivamente bifuncionalizadas con grupos amino en el interior y grupos isotiocianato en el exterior, procedimiento de preparación y uso en la obtención de sistemas de liberación de fármacos**. Spanish patent application 201500862 (2015).

### Congresses:

**Vuitena Trobada de Joves Investigadors dels Països Catalans**, 27-29 of November 2013, Andorra la Vella (Andorra). Oral presentation.

**Fourth International conference of multifunctional, hybrid and nanomaterials**, 9-13 of March 2015, Sitges (Spain). Poster presentation.

**Nanobioapp**, 21-23 of September 2015, organized by ICMA B and *Universitat Autònoma de Barcelona* (UAB), Barcelona (Spain). Poster presentation.

### **Seminars:**

**XIII Conferència Enric Casassas “Teranòstica: Nous reptes del diagnòstic per al tractament clínic”**, 26 of November 2013, *Universitat Autònoma de Barcelona (UAB)*, Barcelona (Spain). Assistant

### **Courses:**

**Curs bàsic sobre microscòpia electrònica de transmissió aplicat a ciència dels materials**, 16-19 of April 2013, *Universitat Autònoma de Barcelona (UAB)*, Barcelona (Spain).

### **Projects:**

IQS and *Vall d’Hebron Research Hospital* was awarded with 25000 € for the project: “Estudio de la eficacia de fármacos con capacidad de restaurar la expresión de distrofina en mioblastos de pacientes afectos de DMD con mutaciones *nonsense*, análisis de las causas que condicionan la variabilidad en la respuesta y evaluación de estrategias destinadas a aumentar esta eficacia en mioblastos humanos y en el ratón mdx” for the study of Duchenne and Becker muscular dystrophy disease.



Esta Tesis Doctoral ha sido defendida el día \_\_\_\_ d \_\_\_\_\_ de 201\_\_

En el Centro \_\_\_\_\_

de la Universidad Ramon Llull, ante el Tribunal formado por los Doctores y Doctoras

abajo firmantes, habiendo obtenido la calificación:

Presidente/a

\_\_\_\_\_

Vocal

\_\_\_\_\_

Vocal \*

\_\_\_\_\_

Vocal \*

\_\_\_\_\_

Secretario/a

\_\_\_\_\_

Doctorando/a

\_\_\_\_\_

(\*): Sólo en el caso de tener un tribunal de 5 miembros